Biomimetic adhesives from natural polymers

Vom Fachbereich Maschinenbau und Verfahrenstechnik der Technischen Universität
Kaiserslautern zur Verleihung des akademischen Grades

Doktor-Ingenieur (Dr.-Ing.)
genehmigte
Dissertation

von
Frau
M.Sc. Charlotte C. Capitain
aus Traben-Trarbach

Dekan:	Prof. Dr.-Ing. Tillmann Beck
Vorsitzende:	Jun.-Prof. Dr.-Ing. Clarissa Schönecker
Berichterstatter:	Prof. Dr. rer. nat. Roland Ulber
	Prof. Dr.-Ing. Nils Tippkötter
	Prof. Dr. Ing. Paul-Ludwig Geiß

Datum der mündlichen Prüfung: 22.03.2021

D 386

Zusammenfassung

Von Muscheln inspirierte catecholhaltige Polymere bieten eine vielversprechende Grundlage für die Entwicklung starker biogener Klebstoffe (siehe **Kapitel 1**). Um einen Klebstoff zu entwickeln, der die Hafteigenschaften der Muschel imitiert, wurden lösungsmittelstabile Laccasen auf ihre Anwendung als biochemische Katalysatoren für die Funktionalisierung natürlicher Polymere (siehe **Kapitel 2**), wie Chitosan und Lignin, mit Catecholen untersucht. Untersuchungen der Laccase-katalysierten Bildung von C-N-Bindungen zwischen primären Aminen und Catecholen, wie beispielsweise Protocatechusäure (PCA) und Dihydrokaffeesäure (DHC), haben gezeigt, dass die Reaktion durch einen niedrigen pKa-Wert des verwendeten primären Amins und einen neutralen oder leicht sauren pH-Wert des Reaktionsgemisches gefördert wird. Da der pKa-Wert der Amingruppen von Chitosan unter 7 liegt, waren spontane Reaktionen mit Catecholen möglich, die zu einem PCA-funktionalisierten Chitosan führten, das auf mit Korund gestrahlten Aluminiumoberflächen eine Zugfestigkeit von 4,56 MPa ± 0,54 MPa erreichte (siehe **Kapitel 3**). Für die Funktionalisierung von Lignin, das im Organosolv (OS)-Prozess extrahiert wurde, war ein zweistufiges Konzept erforderlich, bei dem zunächst L-Lysin und anschließend DHC und PCA an Lignin gebunden wurden. Für DHC-Lignin wurde eine Zugfestigkeit von 169,3 kPa ± 130,6 kPa gemessen (siehe **Kapitel 4**). Da für die Funktionalisierungs- und Aushärtungsprozesse ausschließlich natürlich vorkommende Substanzen verwendet werden, die frei von toxischen Chemikalien sind, wurden hier neuartige und nachhaltige Bioklebstoffe entwickelt.

Die Charakterisierung des muschelinspirierten Chitosan-Klebstoffs erfolgte unter anderem durch die Analyse mittels dynamischer Differenzkalorimetrie (DSC) (siehe **Kapitel 5**). Darüber hinaus wurde eine DSC-basierte Methode zur quantitativen Überwachung von biologischer Abbaubarkeit, unter Verwendung kleiner Probenmengen und einer einfachen Probenvorbereitung, entwickelt. Nur durch die Verwendung von DSC-Messungen war ein quantifizierbarer Nachweis des Abbaufortschritts möglich, während gleichzeitig eine qualitative Beurteilung von Kristallinitätsänderungen möglich war. Die implementierte DSC Methode könnte für die Quantifizierung der biologischen Abbaubarkeit des hier entwickelten PCA-Chitosan-Klebstoffs verwendet werden.

Diese Arbeit stellt neue biobasierte Klebstoffe sowie eine neue Messtechnik zur Messung von biologischer Abbaubarkeit verschiedener Materialien vor.

Abstract

Mussel-inspired catechol-containing polymers provide a promising basis for developing strong biogenic adhesives (see **chapter 1**). In order to develop a biomimetic adhesive, solvent stable laccases were investigated for their application as biochemical catalyst for the functionalization of natural polymers (see **chapter 2**), such as chitosan and lignin, with catechols. Investigation of the laccase-catalysed C–N bond formation between primary amines and catechols, such as protocatechuic acid (PCA) and dihydrocaffeic acid (DHC), suggest that the reaction is promoted by a low pKa value of the primary amine used and a neutral or mildly acidic reaction pH. Since the pKa of chitosan's amine groups is below 7, spontaneous reactions with catechols were possible, resulting in a PCA-functionalized chitosan, which achieved a tensile strength of 4.56 MPa ± 0.54 MPa on aluminum surfaces blasted with corundum (see **chapter 3**). For the functionalization of lignin, which was extracted with the Organosolv (OS) process, a two-step concept was required, where first L-lysine and subsequently DHC and PCA were grafted onto lignin. For DHC-lignin, a tensile strength of 169.3 kPa ± 130.6 kPa was measured (see **chapter 4**). Since the functionalization and curing processes use naturally occurring substances exclusively and are free of toxic chemicals, novel and sustainable bioadhesives were developed.

Moreover, differential scanning calorimetry (DSC) analysis was used to characterize the mussel-inspired chitosan adhesive (see **chapter 5**). Furthermore, DSC measurements were validated for monitoring biodegradation quantitatively using small sample quantities and simple sample preprocessing. Using only DSC measurements, quantifiable detection of degradation progress was possible, while at the same time qualitative assessment of changes in crystallinity (indicating incomplete biodegradation) was obtained. The implemented method is recommended for the quantification of the biodegradability of the PCA-chitosan adhesive.

This work introduces novel bio-based adhesives, as well as a new measuring technique for measuring biodegradability of various material.

List of Figures

Figure 1-1: Schematic overview of the development of mussel mimicking adhesives from natural polymers. Chitosan, which is gained through full or deacetylation of chitin (a main component of shrimp) and OS lignin, a side product of the lignocellulose-biorefinery (a process for converting wood into value-added products), are used as backbones for the adhesives. By functionalizing chitosan and lignin with catechols, the adhesion properties of mussels are imitated, and strong adhesives are developed. Images were taken by author (summer 2019). 3

Figure 1-2: Adhesion-cohesion theory [8]. 4

Figure 1-3: The bond between catechols with metal oxide surfaces depend on the pH value during curing. In an acidic environment (pH 2) catechol groups form hydrogen bonds and in a slightly basic environment (pH 8) coordinative [19]. 6

Figure 1-4: Formation of catechol adhesion, imitating the principle of the mussel [26]. 8

Figure 2-1: Chemical structure of the catechols (A) L-DOPA, (B) PCA, (C) DHC and (D) caffeic acid. 21

Figure 2-2: White-rot fungus on a tree trunk (Ivry-sur-le-Lac, QC, Canada, September 2019). 22

Figure 2-3: Laccase-catalyzed C-C and C-O bond formation using the example of 2-hydroxyphenol [122, 123]. 24

Figure 2-4: Laccase-catalyzed C-N bond formation between a 3,4-hydroquinone (Michael acceptor) and (a) 2-aminobenzamide or (b) H-tyrosine-lysine-OH, functioning as Michael donors [75, 130]. 25

Figure 2-5: The pH-dependent enzyme activity of the purified laccase from *C. unicolor*. Substrate: 0.01 mM syringaldazine; λ=530 nm; 10 vol% McIlvaine buffer; 10 vol% ethanol. The error bars result from triplicates. The protein content was determined to 0.741 g L^{-1} ± 0.001 g L^{-1} by Bradford method. 37

Figure 2-6: Activity of purified laccase from *C. unicolor* on the conversion of PCA. (A) The pH-dependent activity for 10 mM PCA in 0.1 M McIlvaine buffer. (B) Example spectrum for the formation of BQA from PCA over time in 15 s increments. The reaction progress was measured at 400 nm. The protein content was determined to 0.11 g L^{-1} ± 0.02 g L^{-1} by Bradford method. The error bars result from triplicates. 37

Figure 2-7: Solvent stability of laccase from *C. unicolor* towards DMSO (measured at pH 6) and ethanol (measured at pH 5). Substrate: 0.01 mM syringaldazine;

λ = 530 nm; 10 vol% McIlvaine buffer. The error bars result from triplicates. The protein content was determined to 0.741 g L^{-1} ± 0.001 g L^{-1} by Bradford method. 38

Figure 2-8: Chemical structure of the amines donors (A) L-lysine, (B) DAP, (C) NAcDAP and (D) DETA. 39

Figure 2-9: Proposed chemical structures of PCA and DHC and their laccase-catalyzed intermediate products and dimers with NAcDAP. The molar mass of each structure is provided together with the m/z-ratios, which were detected using HPLC-MS analysis. Reaction conditions: 20 mM PCA, 2 mM NAcDAP, purified laccase from *C. unicolor*, 1 mL reaction volume, 10 vol% ethanol, 60 min reaction time for enzyme catalyzed reactions and 24 hours for non-enzymatic reactions, T = 28.5 °C. 41

Figure 2-10: Reaction model for the formation of intermolecular C-N bonds between primary amines and PCA. Laccases initiate the formation of quinone methides by activating the catechol (step 1) [159]. The specific rate constants k_1 and k_{-1} are dependent on the pKa value of the primary amine (step 2). The quinone methides form zwitterionic valence bond structures form aromatic amines as well as amides (step 3). The specific rate constant k_c is temperature dependent. 44

Figure 2-11: Chromatograms of the reaction of NAcDAP and PCA catalyzed by laccase from *C. unicolor* at pH 4, 5, 6 and 7, recorded at 311 nm. Right: mass trace of the dimer at m/z = 295 (ESI-). Reaction conditions: 5 mM PCA, 1 mM NAcDAP, 0.028 g L^{-1} laccase from *C. unicolor*, 1 mL reaction volume, 10 vol% ethanol, 60 min reaction time, T = 25 °C. Note: The selected ratio with an amine excess of 5:1 has been shown in the literature to be the ratio with the largest product formation and the lowest by-product formation [128].. 45

Figure 2-12: Summary of the interaction relationships between the parameters (ethanol concentration, PCA concentration, pH value and temperature) found by the analysis of the nonlinear regression models (#1-#14) for the optimization of NAcDAP and PCA dimerization. The arrows show interactions found between different parameters. The line thickness of the arrows represents the strength of the interaction. A strong relation was found between the PCA concentration and the pH value. 52

Figure 2-13: Results of linear and nonlinear models (see Table 2-3) for the analysis of the relative peak area for the dimerization of PCA and NAcDAP. The predicted values for the relative peak area versus measurement values for the relative peak area (peak area at 311 nm divided by the sum of all peaks around 280 nm) is displayed for A) the linear model #4, B) the two-factor interaction model #8 and C) the Gaussian peak model (#12). D) displays the nonlinear regression of the Gaussian peak model. 53

Figure 2-14: Validation of nonlinear models #7 (two factor interaction between PCA and pH-value) and #12 (Gaussian peak model). The predicted values for the relative peak area versus measurement values for the relative peak area (peak area at 311 nm divided by the sum of all peaks around 280 nm) is displayed for the validation data set. The slope of the linear fit for model #7 and model #12 were calculated to 0.849 ± 0.070 and 0.479 ± 0.108, respectively. 55

Figure 3-1: Deacetylation of chitin to chitosan. 62

Figure 3-2: Michael-type addition and Schiff-base formation between catechols (via o-quinones) with amines [196]. 63

Figure 3-3: pH-dependent solubility of chitosan (10 g L^{-1}) in deionized water in the presence of DHC or PCA at different concentrations. A low absorption indicates partial or complete solubility of the compounds. The absorption of the solution increases when the particles precipitate from the solution. 68

Figure 3-4: FT-IR analysis of (A) chitosan at pH 1,5,6 and 9; (B) chitosan at pH 1, 5 and 9 after PCA addition and (C) chitosan at pH 1, 5 and 9 after DHC addition (t0=reaction start, t2=3 hours). 69

Figure 3-5: pH-dependent PCA absorption onto chitosan. 71

Figure 3-6: Gel formation of a chitosan solution containing DHC at pH 5 after 3 h, 24 h and 48 h. At each point in time, the spontaneous reaction, mild treatment with laccase (0.1 vol%) and strong laccase treatment (1.0 vol%) are shown from left to right. 73

Figure 4-1: Enzymatic synthesis of lignin from the monolignol precursors p-coumaryl alcohol, coniferyl alcohol, and sinapyl alcohol. The phenylpropanoids p-hydroxyphenyl (H), guaiacyl (G), and syringyl (S) are marked with boxes. 80

Figure 4-2: Chemical structures of the G-LMCs A) vanillin B) vanillyl alcohol and C) EROL. 81

Figure 4-3: Two-step extraction of lignin extraction from lignocellulose (beech wood). 82

Figure 4-4: Reaction schemes of condensation reactions. A) Polycondensation reaction of lignin and formaldehyde, B) Mannich reaction of lignin, formaldehyde and dimethylamine. 84

Figure 4-5: Anionic addition of lignin. The reaction is initiated by the formation of a carbanion, which is promoted in a basic environment (A) or by the addition of nucleophilic monomers, such as L-lysine (B). Subsequently, low molecular lignin is added, resulting in the formation of polymerized lignin. 84

Figure 4-6: Two-step functionalization of lignin using a linker molecule. Step 1: The linker molecule L-lysine is bound non-specifically to lignin. Step 2: The catechol group is catalysed by laccases and bound to the terminal amine groups. 85

Figure 4-7: Lignin recovery after OS digestion in relation to the theoretical total mass of lignin, using beech wood as substrate, a liquor ratio of 5:1 with 50 % ethanol and 30 min holding time at the specified maximum temperatures. The lignin was precipitated by dilution to an ethanol concentration of 25 wt%. 95

Figure 4-8: Fibre content (solid) and lignin recovered from the supernatant of beech wood after OS digestion at different temperatures (160 to 200 °C), displayed in relation to the total dry weight of solid (dry matter). Beech wood was used as substrate with a liquor ratio of 5:1 with 50 % ethanol as solvent and 30 min holding time at the specified maximum temperatures. 96

Figure 4-9: Influence of a two-step digestion on the lignin yield in the OS supernatant. In the first step, beech wood was digested by the LHW method (liquor ratio 1:5, addition of catalyst, see column labeling for further information). In the second step the pulp was further treated in an OS digestion (liquor ratio 1:5, 50 wt% ethanol). The temperatures and holding times can be taken from the column labeling. The pH values were measured in the OS supernatant after OS digestion (blue squares)............... 99

Figure 4-10: Precipitation products of amine lignin: A) DETA with OS lignin at 50 °C, B) DETA with OS lignin at 75 °C, C) L-lysine with OS lignin at 50 °C, D) polycondensed L-lysine at 50 °C and E) DAP with OS lignin at 50 °C. Reaction conditions: pH 10.5, holding time: 3 hours, ratio of amine to OS lignin to formaldehyde 5:1:1............... 103

Figure 4-11: Section of a GPC chromatogram of OS lignin (in black), L-lysine-lignin (in blue), L-lysine (light green, dotted line) and polycondenced-L-lysine (dark green). As a reference, the 12 kDa dextran standard is shown in red. The arrows (black)mark the peaks of the polycondenced-L-lysine, which were found as contaminant in the L-lysine-lignine. 103

Figure 4-12: Reaction of vanillin with NAcDAP in 60 % technical ethanol after 24 h incubation time. Reaction preparations depending on the incubation time (from left: room temperature, 40 °C; 75 °C and 100 °C). 108

Figure 4-13: L-lysine reduction during anionic addition of L-lysine to OS lignin. The L-lysine concentration in the supernatant was measured after removal of OS lignin. The assignments of the reaction conditions are listed in Table 4-1. The inserted graph shows the relative L-lysine concentration in the supernatant after anionic addition with OS lignin at a 5-fold substrate concentration. 110

Figure 4-14: Content of primary amines of different lysine-lignins (measured by Ninhydrin assay, see section 4.2.5.1). 113

Figure 4-15: Quantification of primary amines on lysine-lignin (from anionic addition, see section 4.3.2.2) before and after functionalization with the catechols PCA and DHC. The functionalization was performed according to section 4.2.3 and the analysis was conducted using a Ninhydrin assay (see section 4.2.5.1). 117

Figure 4-16: FT-IR spectrograms of functionalized lysine-lignins after 2-step functionalization of OS lignin at pH 5. 118

Figure 4-17: Tensile strength of lignin and various lysine-lignins as a function of the solvent. Lignin derivatives which are soluble in the corresponding solvent are marked with asterisks. 120

Figure 4-18: Flow chart value-added process: from beech wood to catechol lignin adhesive. 125

Figure 4-19: Cost calculation using SuperPro Designer: Process diagram for the synthesis of catechol lignin. 126

Figure 5-1: Processing steps used to prepare samples for biodegradation and subsequent analysis. 136

Figure 5-2: Qualitative analysis of degradation process of PHB over a course of 10 weeks. A) Incubation in water (control) and B) incubation in compost. The table shows the location, width and height averaged over time. The arrows indicate peak 1 (left) and peak 2 (right). 140

Figure 5-3: Characteristic DSC profiles of CA (A) and lignin (B) coated on carrier particles. Incubation type (compost or control), as well as time points (0 weeks to 10 weeks) may vary. Prior to DSC analysis, all samples were dried at 50 °C. Each family of curves show two areas (1 and 2) with characteristic peaks for the coating (CA or lignin). Area 3 marks the characteristic peak for sand. 141

Figure 5-4: Determination of interval between 200 °C and 500 °C in 5 K steps. A) Mean integrated DSC response for non coated-carrier particles, B) Mean integrated DSC response for CA-coated carrier particles. C) Mean of CA coated samples divided by peak area from non-coated carrier particles (SNR). Additional resolution is provided in the box, showing the area around the best interval. The greyscale represents the value of the integral that was calculated between the lower bound and the upper bound temperature (lighter greyscale intensities = small peak areas, darker greyscale intensities = large peak areas; the largest integrals are marked with red). The red arrows and lines indicate ideal search areas for upper and lower bound temperatures and are defined by areas of high signal intensities and low background noise. 143

Figure 5-5: Determination of interval between 200 and 500 °C in 5 K steps. A) Mean integrated DSC response for lignin-coated carrier particles, B) Mean of lignin coated samples divided by AUC of non-coated carrier particles (signal to noise ratio). The arrow indicated where the best interval is found based on the analysis of the opposed graph. The greyscale represents the value of the integral that was calculated between the lower bound and the upper bound temperature (lighter greyscale intensities = small peak areas and darker greyscale intensities = large peak areas). The red arrows and ellipses indicate ideal search areas for upper and lower bound temperatures and are defined by areas of high signal intensities and low background noise.................... 144

Figure 5-6: Calibration of DSC measurements A) DSC-profiles of calibration standards. PHB-coated carrier particles and sea sand were mixed in different ratios to a total of 30 mg. B) Linear regression of PHB and sand “dilutions”. 144

Figure 5-7: Biodegradation with compost: (A) degradation of PHB, (B) degradation of CA (DSC profile was integrated between 260 and 385 °C) and (C) degradation of lignin (DSC profile was integrated between 330 and 420 °C). Vertical bars present the degradation, determined as the change in mass fraction of combustible solids, and curves present the results from DSC analysis. 146

Figure 5-8: DSC profiles of chitosan before (black curve) and after (grey curve) processing. 149

Figure 5-9: DSC profiles of processed chitosan (grey curve), PCA (blue curve) and chitosan-catechol adhesive (light blue curve, dash dotted). The inset graph magnifies the peak interval between 201 °C and 233 °C. 150

Figure 8-1: Cultivation of *C. unicolor* according to section 2.2.1 (no baffles, 20 vol% filling, 25 °C and 50 rpm). Using an initial pH value of (A) 4.5, without a buffer and (B) 7, with CaCO3 buffer. Shown is the time course of glucose concentration (black), the pH value (green) and the enzyme activity (blue). The enzyme activity was determined according to section 2.2.2. 188

Figure 8-2: SDS-page of purified laccase from *C. unicolor*. Left lane: Pierce protein marker, right lane: purified protein. 189

Figure 8-3: Transfer of the HPLC-MS analysis method to the HPLC analysis. Chromatogram of the reaction of PCA and NAcDAP reacted by laccase from *C. unicolor* at pH 6, recorded at 311 nm. Top: recording of an HPLC-MS analysis, Bottom: Picture of HPLC analysis, including peak integration. Reaction conditions: 5 mM PCA, 1 mM NAcDAP, 0.028 g L^{-1} laccase from *C. unicolor*, 1 mL reaction volume, 10 vol% ethanol, 60 min reaction time, T = 25 °C. 190

Figure 8-4: Chromatograms of NAcDAP reacted by laccase from *C. unicolor* at pH 5, recorded at 280 nm. Top: pure substance, bottom: reacted by laccase. Reaction conditions: 1 mM NAcDAP, 0.028 g L^{-1} laccase from *C. unicolor*, 1 mL reaction volume, 10 vol% ethanol, 60 min reaction time, T = 25 °C. 191

Figure 8-5: Chromatograms of PCA reacted by laccase from *C. unicolor* at pH 5, recorded at 280 nm. Top: pure substance, Bottom: reacted by laccase. Reaction conditions: 5 mM PCA, 0.028 g L^{-1} laccase from *C. unicolor*, 1 mL reaction volume, 10 vol% ethanol, 60 min reaction time, T = 25 °C. 192

Figure 8-6: Chromatograms of PCA (top) or PCA and NAcDAP (middle and bottom) reacted by laccase from *C. unicolor* at pH 6, recorded at 280 (top and middle) and 311 nm (bottom). Reaction conditions: 5 mM PCA, 1 mM NAcDAP, 0.028 g L^{-1} laccase from *C. unicolor*, 1 mL reaction volume, 10 vol% ethanol, 60 min reaction time, T = 25 °C. 193

Figure 8-7: Mass trace (m/z = 295, ESI-) of PCA (above) or PCA and NAcDAP (bottom) reacted by laccase from *C. unicolor* at pH 6. Reaction conditions: 5 mM PCA, 1 mM NAcDAP, 0.028 g L^{-1} laccase from *C. unicolor*, 1 mL reaction volume, 10 vol% ethanol, 60 min reaction time, T = 25 °C. 194

List of Tables

Table 1-1: Tensile strength of biogenic and bioinspired adhesives. 15
Table 1-2: Adhesion strength of biogenic and bioinspired adhesives on aluminum surfaces. 16
Table 2-1: Composition of stacking and running gel for SDS-Page......................... 29
Table 2-2: Parameter variations for optimization of laccase-catalyzed Michael-type addition. NAcDAP content: 2 mM, laccase from *C. unicolor* (0.0287 g L^{-1}). Reaction in an open reaction vessel (2mL) in a thermoshaker, reaction time: 60 min................ 31
Table 2-3: Linear and nonlinear models for the analysis of the relative peak area for dimerization of PCA and NAcDAP and the respective coefficients of determination. The influence of the ethanol concentration c(EtOH), the PCA concentration c(PCA), the pH value, temperature (temp) and the shaking speed (rpm) on the relative product formation (dimer area at 311 nm / sum of all peak areas at 280 nm) was investigated. The model parameters pr1 to pr9 are found in the appendix, Table 8-5.................. 50
Table 3-1: Kinematic viscosity (at 30 °C) of chitosan solutions in the presence of DHC or PCA. 72
Table 3-2: Particles size characterization of PCA-chitosan agglomerates after enzyme treatment. (The incubation was completed at 28 °C, at pH 5) 74
Table 3-3: Cost Calculation for catechol-chitosan adhesive. *optimized amount (solid contend of approximately 20 wt%); **rough estimation 76
Table 4-1: Reaction preparations of the anionic addition of OS lignin with L-lysine.. 89
Table 4-2: Reaction parameters for the functionalization of lysine-lignin from anionic addition Add#6 (see section 4.2.2.3). 90
Table 4-3: Mixtures of OS lignin and lysine-lignin (obtained during condensation reaction) for validation of GPC-OPA analysis. 92
Table 4-4: Summary of extraction conditions that are compatible with direct enzymatic conversion of OS lignin. Beech wood with a dry weight of 93.8 wt% was used as substrate for digestion via OS digestion alone or in combination with preceding LHW digestion. The holding times (30 min or 60 min) and the maximum temperatures (160 °C, 180 °C or 200 °C) are specified in first column LHW digestion was completed with a liquor ratio 1:5, without the addition of catalyst. OS digestion was completed with a liquor ratio of 5:1 with 50 % ethanol as solvent.. 101
Table 5-1: Degradation progress after 10 weeks of incubation time. The degradation progress determined as the change in mass fraction of combustible solids. The

degradation progress was calculated as reduction of combustible coating of the carrier particles per the initial sample coating, using equation 5-1. 138
Table 5-2: Results of linear regression of the relative peak area PHB, CA and lignin over the mass fraction. 145
Table 5-3: Decision, detection and determination limits for linear curve fittings, calculated following DIN 32645, 2008 [261]... 145
Table 8-1: List of chemicals 183
Table 8-2: List of equipment and devices 186
Table 8-3: Experimental design and results of the first test series of optimization. (‘-‘: second measurement aborted due to technical problems.) 195
Table 8-4: Experimental design and results of the second test series of optimization. (‘-‘: second measurement aborted due to technical problems.) 196
Table 8-5: Model parameters pr1 to pr9 for model #1-#14 (see Table 2-3) for the analysis of the relative peak area for dimerization of PCA and NAcDAP. 197
Table 8-6: List of supervised seminar papers and theses (2016-2019), who have made a contribution to the dissertation. 200

Abbreviations and Symbols

Abbreviations

Abbreviation	Description
ABTS	2,2′-azino-bis(3-ethylthiazoline-6-sulfonate)
acetovanillone	4-hydroxy-3-methoxyacetophenon
adlerol	1-(3,4-dimethoxyphenyl)-2(2-methoxyphenoxy)-propane-1,3-diol)
AFM	atomic force microscopy
ATR	attenuated total reflection
AUC	area above or under the curve
BQA	1,2-benzoquinone-4-carboxylic acid
C	carbon
C. unicolor	*Cerrena unicolor*
CA	cellulose acetate
$CaCl_2$	calcium chloride
Cl^-	chlorid
$CuSO_4$	copper sulphate
Da	dalton
DAP	diaminopentante or pentane-1,5-diamine
DETA	diethylenetriamine
DHC	3-(3,4-dihydrophenyl) propionic acid or dihydrocaffeic acid
DMP	2,6-dimethoxyphenol
DMSO	dimethyl sulfoxide
dopamine	dopamine hydrochlorid
DSC	differential scanning calorimetry
ECD	1-ethyl-3-(3-dimethylaminopropyl)carbodiimide
EROL	guaiacylglycerol-beta-guaiacyl-ether
ESI	electrospray ionization
ESI-	negative ionization
ESI+	positive ionization
Fe	iron
ferulic acid	3-(4-hydroxy-3-methoxyphenyl)prop-2-enoic acid

Abbreviation	Description
FLD	fluorescence detector
G	guaiacyl (lignin-unit)
GPC	gel permeation chromatography
GPC-OPA	extension of GPC analysis by a precolumn derivatization with OPA
H^+	hydrogen
H	p-hydroxyphenyl (lignin-unit)
H_2O	water
H_2SO_4	sulfuric acid
H_3PO_4	phosphoric acid
HCl	hydrochloric acid
HPLC	high-performance liquid chromatography
KH_2PO_4	potassium dihydrogenphosphate
Lacc I / Lacc II	two isoforms of laccase
L-DOPA	L-3,4-dihydroxyphenylalanine or Levadopa
LHW	Liquid-hot-water
LMC	lignin model compound
lysine-lignin	lignin, which is functionalized with L-lysine
m/z ratio	mass-to-charge ratio
MCE	2-mercaptoethanol
mfp	mussel foot protein
$MgSO_4$	magnesium sulfate
mol%	mole percent
MS	mass spectroscopy
MW	molecular weight
MWCO	molecular weight cut off
N	nitrogen
NAcDAP	N-acetyl diaminopentane
NaCl	sodium chloride
NaOH	sodium hydroxide
$–NH_2$ and NH_3^+	amine group
O	oxygen
$-OCH_3$	methoxy-group

Abbreviation	Description
OH	hydroxyl
OPA	o-phthaldialdehyde
OS	Organosolv
PCA	3,4-dihydroxybenzoic acid or protocatechuic acid
p-coumaric acid	3-(4-hydroxyphenyl)prop-2-enoic acid
PF	phenol-formaldehyde
PHB	polyhydroxybutyrate
pr1 to pr9	model parameters 1 to 9
PTFE	polytetrafluoroethylene
RID	refractive index detector
S	syringyl (lignin-unit)
SDS-PAGE	sodium dodecyl sulfate-polyacrylamide gel electrophoresis
SEM	scanning electron microscopy
sinapic acid	3,5-dimethoxy-4-hydroxycinnamic acid
SNR	signal-to-noise ratio
syringaldehyde	3,5-dimethoxy-4-hydroxybenzaldehyd
T. versicolor	*Trametes versicolor*
TFH	tetrahydrofuran
TGA	thermogravimetric analysis
UV	ultraviolet
UV-vis	ultraviolet–visible
V	volt
vanillin	4-hydroxy-3-methoxybenzaldehyde
vanillin alcohol	4-(hydroxymethyl)-2-methoxyphenol
vol%	volume percent
wt%	mass fraction or weight percent
x g	times gravity

Symbols

Symbol	Description	Unit
$Area_{FLD}$	FLD area (without OPA derivatization)	-
$Area_{FLD,OPA}$	FLD area with OPA derivatization	-
c(EtOH)	ethanol concentration	vol%
c(lignins)	sum of lignins	$g \cdot L^{-1}$
c(lysine-lignin)	concentration of lysine-lignin,	$g \cdot L^{-1}$
c(PCA)	PCA concentration	mM
cd	coating degree of particles	wt%
D0.1	particle diameter, which corresponds to 10 % (cumulative) of the particles of a particle size distribution	µm
D0.5	particle diameter, which corresponds to 50 % (cumulative) of the particles of a particle size distribution	µm
D0.9	particle diameter, which corresponds to 90 % (cumulative) of the particles of a particle size distribution	µm
ε	extinction coefficient	$mM \cdot cm^{-1}$
K	constant for Ubbelohde viscometer	$mm^2 \cdot s^{-2}$
k	*constant for conversion of L-DOPA to dopachrome*	$g \cdot mol^{-1}$ = M
k_1	specific rate constant of the deprotonation step	$g \cdot mol^{-1}$ = M
K_a	ionization constant of the amine group	$g \cdot mol^{-1}$ = M
k_c	specific rate constant for the ring closure (intramolecular 1,4 addition of Michael)	$g \cdot mol^{-1}$ = M
$m_{combustion\ boat\ after\ 100\ °C}$	weight of boat after combustion at 100 °C	g
$m_{combustion\ boat\ after\ 800\ °C}$	weight of boat after combustion at 800 °C	g
$m_{combustion\ boat\ empty}$	weight of empty boat	g
M_n	average molecular weight	Da
MW	molecular weight	kDa
ν	kinematic viscosity	$mm^2 \cdot s^{-1}$

Symbol	Description	Unit
pH	potential of hydrogen (pH value)	-
pKa	acid dissociation constant	-
R^2	coefficient of determination	-
R_f	relative mobility	cm
RI	refractive index	$cm^3 \cdot g^{-1}$
RPM	shaking speed	rpm
RPRI	refractive index	-
T	time	min or hours
Temp	temperature	°C

Table of Contents

Zusammenfassung ..... **I**

Abstract ..... **II**

List of Figures ..... **III**

List of Tables ..... **X**

Abbreviations and Symbols ..... **XII**

Table of Contents ..... **XVII**

1 Introduction **1**

1.1 Project aim 2

1.2 State of the art 4

1.2.1 Adhesion and cohesion theory 4

1.2.2 The mussel's adhesion 5

1.2.3 Biogenic and biodegradable adhesives 10

1.2.4 Mussel inspired synthetic polymers and adhesives 12

1.2.5 Catechol-functionalized chitosan and lignin 13

1.2.6 Comparison of adhesion strength to reported literature values 14

2 Biochemical reactions of catechols for the functionalization of natural polymers **19**

2.1 Theory 20

2.1.1 Catechols 20

2.1.2 Laccases 21

2.1.2.1 Solubility and storage of laccases' substrates 22

2.1.2.2 Laccase-catalyzed homo- and heteromolecular C-C and C-O bond formation 23

2.1.2.3 Laccase-catalyzed Michael-type addition for C-N bond formation.. 24

2.1.3 Kinetic model for the laccase-catalyzed homomolecular Michael-type addition of L-DOPA 25

2.2 Materials and Methods 27
2.2.1 Cultivation and purification of laccases from *C. unicolor* 27
2.2.2 Enzyme characterization 27
2.2.2.1 A colorimetric assay for the determination of enzyme activity 27
2.2.2.2 Stability of laccases towards ethanol (short exposure) 27
2.2.2.3 Long-term stability of laccases towards ethanol 27
2.2.2.4 The pH optimum for laccase-catalyzed conversions 28
2.2.2.5 Laccase stability towards solvents 28
2.2.2.6 Determination of protein content and specific enzyme activity 28
2.2.2.7 Determination of molecular weight using SDS-PAGE 29
2.2.3 Small-scale laccase-catalyzed and spontaneous dimerization reaction 30
2.2.4 Parametric optimization of NAcDAP and PCA dimerization 30
2.2.5 Sample preparation for HPLC and HPLC-MS analysis 31
2.2.6 High-performance liquid chromatography (HPLC) analysis 31
2.2.7 HPLC-MS spectroscopy 32
2.3 Results and Discussion 33
2.3.1 Review of ethanol stable laccases 33
2.3.2 Stability of laccases from *C. unicolor* towards ethanol 34
2.3.3 Expression and purification of laccases from *C. unicolor* 35
2.3.4 Characterization of purified laccases from *C. unicolor* 36
2.3.4.1 Determination of protein size 36
2.3.4.2 Determination of protein content and pH optima of laccase from *C. unicolor* 36
2.3.4.3 Stability towards solvents 37
2.3.5 Laccase-catalyzed reaction with model compounds 39
2.3.6 Influence of the pH value and the primary amine’s pKa for C-N bond formation to catechols 42
2.3.7 Optimization of C-N formation between PCA and NAcDAP 44

2.3.7.1 The pH dependency of PCA and NAcDAP dimerization 45

2.3.7.2 Influence of parameters on pH value.. 46

2.3.7.3 Influences of parameter variations on product formation................ 46

2.3.7.4 Determination of the product-maximizing reaction conditions 50

2.4 Summary and Outlook... 58

3 A novel catechol-adhesive with a chitosan backbone..................................61

3.1 Theory 62

3.1.1 Chitosan.. 62

3.1.2 Methods for chitosan-catechol preparations 62

3.2 Materials and Methods 64

3.2.1 Chitosan.. 64

3.2.2 Determination of PCA concentration in liquid media using spectroscopy 64

3.2.3 Turbidity measurements using spectroscopy....................................... 64

3.2.4 Viscometry analysis 64

3.2.5 Particle size characterization 65

3.2.6 Mid-infrared analysis... 65

3.2.7 Preparation of adhesive and measurement of tensile strength of butt joints 66

3.3 Results and Discussion 67

3.3.1 Spontaneous reaction of chitosan and DHC or PCA............................ 67

3.3.1.1 Solubility of chitosan in the presence of PCA and DHC 67

3.3.1.2 Mid-infrared analysis of spontaneous C-N bond formation............. 68

3.3.1.3 Determination of pH-dependent PCA binding capacity 71

3.3.1.4 Influence of PCA and DHC on the viscosity of chitosan solutions .. 72

3.3.2 Gel formation during spontaneous and enzyme catalyzed functionalization of chitosan with DHC... 72

3.3.3 Formation of chitosan-agglomerates during enzyme catalyzed functionalization with PCA.. 73

3.3.4 Determination of tensile strength of PCA-chitosan using butt joint tests 75

3.3.5 Cost calculation for catechol-chitosan adhesive 76

3.4 Summary and Outlook 77

4 Functionalization of Organosolv (OS) lignin 79

4.1 Theory 80

4.1.1 Structure and production of lignin from biomass 80

4.1.2 Lignocellulose biorefinery concept 81

4.1.3 Reactions of lignin and LMCs 83

4.1.3.1 Condensation reaction 83

4.1.3.2 Anionic addition 84

4.1.4 Two-step concept for lignin functionalization 85

4.2 Materials and Methods 87

4.2.1 Pretreatment and extraction of lignin 87

4.2.2 Amination reaction of OS lignin (1st step) 87

4.2.2.1 Condensation reactions of L-lysine with OS lignin 87

4.2.2.2 Anionic addition of LMCs with amines 88

4.2.2.3 Anionic addition of L-lysine to OS lignin 89

4.2.3 Functionalization of lysine-lignin (2nd step) 89

4.2.4 Chromatographic analysis 90

4.2.4.1 L-lysine detection 90

4.2.4.2 Gel permeation chromatography (GPC) 91

4.2.4.3 Extension of GPC analysis by a precolumn derivatization (GPC-OPA) for the detection of primary amines on lignin 91

4.2.5 Biochemical and optical analysis of functionalization 92

4.2.5.1 Ninhydrin assay 92

4.2.5.2 Mid-infrared analysis 93

4.2.6 Measurement of tensile strength 93

4.2.7 Cost analysis of catechol-lignin adhesives 93

4.3 Results and Discussion 94

4.3.1 Optimization of the lignin extraction in OS digestion 94

4.3.1.1 Optimization of the lignin yield during OS digestion by variation of temperature and catalyst concentration 95

4.3.1.2 Lignin yield in OS digestion after previous LHW digestion (beech wood) 98

4.3.1.3 Consideration of lignin extraction in the OS digestion for direct enzymatic conversion 100

4.3.2 Functionalization of lignin with primary amines (1st step) 101

4.3.2.1 Condensation of OS lignin and amines 102

4.3.2.2 Anionic addition 105

4.3.2.3 Quantification of amine anchors on OS lignin 111

4.3.3 Functionalization of lysine-lignin with catechols (2nd step) 115

4.3.3.1 Quantification of primary amines on lysine-lignin via Ninhydrin assay 116

4.3.3.2 Analysis of functionalized lysine-lignin using FT-IR spectroscopy 118

4.3.4 Tensile strength of lignin and lignin derivates 119

4.3.4.1 Influence of solubility on the tensile strength of lignin derivatives. 119

4.3.4.2 Determination of tensile strength for catechol-lignins 121

4.3.4.3 Evaluation of tensile strength in the presence of iron ions 122

4.3.4.4 Improvement strategies for adhesion of catechol-lignin 123

4.3.5 Cost analysis of catechol-lignin adhesives 124

4.4 Summary and Outlook 127

5 Differential scanning calorimetry (DSC) for characterization of natural polymers and quantification of biodegradability in compost 129

5.1 Theory 130

5.1.1 Degradation of Polymers 130

5.1.2 Techniques for analysis of polymer degradation 130

5.1.3 Differential scanning calorimetry (DSC) 131

5.2 Materials and Methods 132

5.2.1 Coating of carrier particles 132

5.2.2 Biodegradation of coating 132

5.2.3 Analyzing coating 133

5.2.3.1 Sampling and purification of coated carrier particles 133

5.2.3.2 Determination of mass fraction of combustible solids.................. 133

5.2.3.3 DSC measurements for qualitative evaluation of surface coating 134

5.2.3.4 DSC measurements for quantitative analysis of coating degree .. 134

5.2.4 Analysis and validation of DSC results 135

5.2.5 Overview of processing steps for the implementation of a DSC-based method 136

5.2.6 Qualitative evaluation of chitosan and chitosan-derivates using DSC 136

5.3 Results and Discussion 137

5.3.1 Size characterization of pure sand and coated carrier particles.......... 137

5.3.1.1 Polymer coating degree of carrier particles 138

5.3.2 Determination of biodegradation using reference method 138

5.3.3 Determination of biodegradation using DSC analysis 139

5.3.3.1 Analyzing qualitative changes of PHB during incubation using DSC 139

5.3.3.2 Developing a method for quantitative evaluation of DSC profiles. 141

5.3.3.3 Quantification of PHB, lignin and CA biodegradation using quantitative DSC analysis 144

5.3.3.4 Evaluation of DSC-based biodegradation using quantitative monitoring technique... 147

5.3.4 Qualitative analysis of catechol-PCA adhesive using DSC................ 148

5.4 Summary and Outlook.. 151

6 Conclusion 153

6.1 Achievements and comparison to literature.. 154

6.2 Challenges encountered.. 154

6.3 Future work 156

7 Bibliography 157

8 Appendix..183

8.1 Chemicals and Equipment.. 183

8.2 Production and characterization of laccase from *C. unicolor* 188

8.3 Comparison of the chromatograms, resulting from HPLC-MS and HPLC analysis 190

8.4 Example for the analysis of HPLC-MS data 191

8.5 Experimental design and HPLC-MS results for product optimization 195

8.6 Erklärung (Declaration).. 198

8.7 List of author’s peer-reviewed publications... 199

8.8 List of supervised seminar papers and theses 200

8.9 Curriculum Vitae 201

1 Introduction

In view of the steadily growing world population and the associated increase in the consumption of raw materials, the supply of the population with sufficient food, production materials and energy is a challenge. This problem is intensified by the advancing climate change and the scarcity of non-renewable resources, especially fossil fuels such as oil, gas or coal [1]. In order to ensure a long-term and sustainable supply, it is necessary to increasingly substitute the use of conventional, finite resources with renewable raw materials. The trend of recent years has shown an increased use of renewable resources, which has been driven by regional price developments and the availability of fossil fuels due to regulatory requirements, but also by the development of an awareness for climate protection and sustainability among the population [1]. An increased demand from consumers and environmental regulations for environmentally friendly products is pushing manufacturers to produce bio-based products. Those plant-based products, such as paper and packaging, construction, woodworking, personal care, and medical applications has required the development of bio-based adhesives. The global bioadhesive market size in 2019 was USD 5.6 billion, with an expected compound annual growth rate of up to 10 %, underlining the interest of further effort into research and development [2].

Natural polymers (biopolymers) are synthesized in living organisms and form the basic building blocks of organisms. Established concepts for biorefineries offer an excellent use of regenerative raw materials. Analogously to the petroleum refinery, a complex raw material is separated into individual fractions, which are then further processed in subsequent process steps until different intermediate and end products are available. Sugar-, starch- or oil-containing biomass, such as sugar beets, potatoes or rapeseed are used as the starting material in the biorefinery. Residual materials, from forestry and gardening, as well as chitin from insect shells, offer a suitable basis for the second generation biorefinery [3], because these do not compete with food production, are inexpensive and widely available [3].

Chitin, from which chitosan is produced via full or partial deacetylation, belongs to the most abundant organic materials, naturally occurring in the exoskeleton of crustacea, molluscs and as principal fibrillar polymer in certain fungi [4]. Organosolv (OS) lignin, which is often used for thermal use in combined heat and power generation, is a side stream of the lignocellulose biorefinery [5]. So far, lignin is used as an additive in materials, binders and adhesives. However, a lot of potential remains unused, since lignin is able to provide starting materials for the synthesis of many forthcoming high-quality products due to its complex polyphenol structure [3]. For both, chitosan and lignin, a great need for further development of value-added products exists. The goal of this work is to increase the application areas of chitosan and lignin by enhancing it with new functional groups, while avoiding the use of harsh chemicals or special reaction conditions. Biomimetics (composed of "biology" and "mimesis" = imitation) is the application of the findings of biological research. By mimicking the adhesion properties of mussels and combining it with the natural polymers chitosan and lignin as backbone, new biogenic adhesives are developed.

1.1 Project aim

The aim of this work is the functionalization of natural polymers with catechols to develop mussel mimicking adhesives. Catechols play a key role in the adhesion of the mussel to surfaces under water [6]. Furthermore, mussels have the ability to strongly adhere to metals or hydrophobic surfaces such as PTFE [7]. Through the functionalization of natural polymers, such as lignin and chitosan, with catechols, these adhesion properties are imitated. For the functionalization, either spontaneous or enzymatically-catalyzed Michael-type addition between catechol monomers and primary amines are used, while avoiding the use of harsh chemicals or special reaction conditions.

Figure 1-1 shows a graphical overview of two workflows for the development of mussel mimicking adhesives. Workflow 1 shows the development of a catechol-chitosan from chitin, a main component of shrimp shells. By functionalizing chitosan, which is gained through full or partial deacetylation of chitin (step 1A), with catechols, the adhesion properties of mussels are imitated, and a strong adhesive is developed (step 1B). Workflow 2 shows the development of a catechol-lignin from OS lignin via a two-step functionalization. OS lignin is a side stream of the lignocellulose biorefinery, a process for converting wood into value-added products (step 2A). OS lignin is free of sulfurs and consists of long chains of polyphenols, which makes it a great backbone for sustainable products, such as mussel mimicking adhesives. By functionalizing OS lignin first with primary amines (step 2B) and further with catechols (step 2C), the adhesion properties of mussels are imitated.

A further objective of this work is the optimization of the extraction of OS lignin from beech wood and the evaluation of value-added processes for increased competitiveness of the lignocellulose biorefinery.

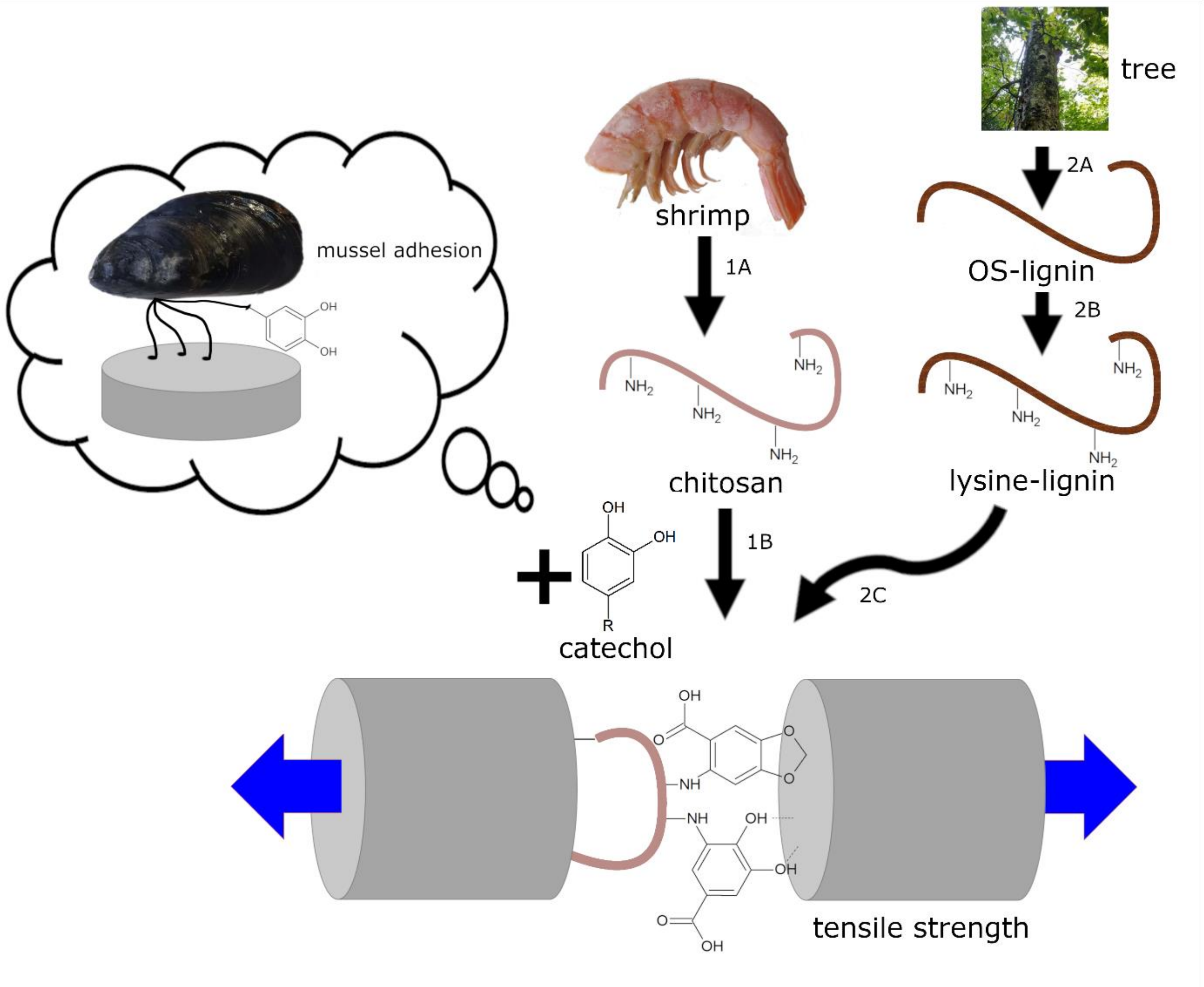
tree
shrimp
mussel adhesion
OH
OH
1A
2A
OS-lignin
2B
NH_2
NH_2
NH_2
NH_2
chitosan
NH_2
NH_2
NH_2
NH_2
lysine-lignin
OH
OH
1B
2C
+
R
catechol
OH
O
O
O
NH
NH
OH
OH
O
OH
tensile strength

Figure 1-1: Schematic overview of the development of mussel mimicking adhesives from natural polymers. Chitosan, which is gained through full or deacetylation of chitin (a main component of shrimp) and OS lignin, a side product of the lignocellulose-biorefinery (a process for converting wood into value-added products), are used as backbones for the adhesives. By functionalizing chitosan and lignin with catechols, the adhesion properties of mussels are imitated, and strong adhesives are developed. Images were taken by author (summer 2019).

The development of sustainable products from renewable resources goes hand in hand with the implementation of suitable biodegradation detection methods. A further goal of this work is the development of a differential scanning calorimetry (DSC)-based method for the detection of the biodegradability of polymers in complex samples. Lastly, DSC is applied for the characterization of the mussel mimicking catechol-chitosan adhesive, developed in this work.

1.2 State of the art

1.2.1 Adhesion and cohesion theory

Bonding strength consists of adhesion and cohesion (see Figure 1-2). Adhesion is the force that holds the substrates and the adhesive together in opposition to stresses which are exerted pulling the substrates apart. Cohesion is the bonding strength of particles within the adhesive (or other material) which holds the adhesive mass together. The combination of adhesion and cohesive strength determines the bonding effectiveness. An adhesive bond fails if either the adhesive separates from the substrate or the adhesive breaks apart.

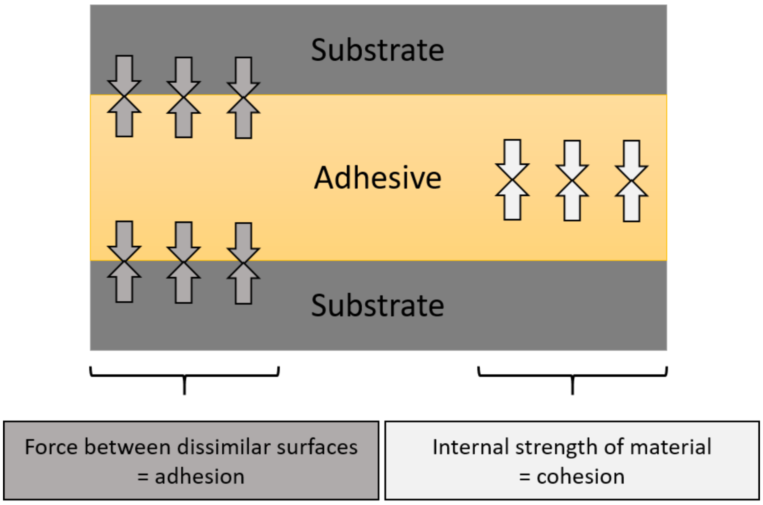
Substrate
Adhesive
Substrate
Force between dissimilar surfaces
= adhesion
Internal strength of material
= cohesion

Figure 1-2: Adhesion-cohesion theory [8].

In general, binding types are differentiated into primary valence bonds and secondary valence bonds [9].

Primary valence bonds are, for example, metal bonds, ion bonds and covalent bonds. Metal bond are characterized by freely moving electrons (delocalized) within the metal grid. Metal bonds are formed during soldering and are therefore not relevant for adhesion binding. Ionic interactions occur between positively (cation) and negatively (anion) charged atoms. The Coulomb force, which describes this heteropolar bonding between two ions, is approximately 600 to 1000 kJ per mol. Ionic bonds have a bonding distance of 0.1 nm to 0.2 nm and are generally water soluble and brittle. A covalent bond is a main valence bond between two atoms (homopolar bond), in which two electrons occupy a binding orbital and the electron density is symmetrically distributed. The force of a covalent bond is approximately 60 to 700 kJ per mol. A special case of covalent bonds are coordinative bonds (metal complexing). While in a covalent bond each atom contributes a single electron to the bond, in a coordinative bond, one electron pair of a ligand interacts with an empty orbital to form a complex. In this complex, one reaction partner will have more reaction partners than its maximal binding capacity [10].

Secondary valence bonds, such as hydrogen bonds and van der Waals interactions are in general weaker than primary valance bonds, because they bond over a longer distance. Hydrogen bonds are formed between partially positively charged hydrogen atoms and electronegative atoms, such as oxygen or nitrogen. The dissociation energy of hydrogen bonds is between 1 to 50 kJ per mol and the length of hydrogen bonds varies depending the molecules. The length between OH and O is approximately 0.177 nm, while the length between NH and O is 0.304 nm [11]. Molecular interactions (van der Waals forces) include the London dispersion force between instantaneously induced dipoles, the Debye force between a permanent dipole and a corresponding induced dipole and the Keesom force between permanent molecular dipoles. Typical energies of intermolecular interactions are between 0.3 and 15 kJ per mol [12].

1.2.2 The mussel's adhesion

Mussels prefer to live in shallow areas of the sea down to a depth of about 50 m. There they cling to surfaces with their byssus threads to withstand strong currents or tides [13]. Their ability to adhere under water and to smooth surfaces is not only highly remarkable from a scientific point of view but is also becoming increasingly important in the context of sustainable resource management.

Functionality of the mussel protein

In the byssus of the mussel, catechols play an essential role in under water adhesion [14, 15]. Six mussel foot proteins (mfps) have been identified, each having different amounts of the catechol-containing amino acid L-DOPA (L-3,4-dihydroxyphenylalanine) [16]. Mfp-3 and mfp-5 play a key role in interfacial adhesion due to their high content of L-DOPA, which was reported to be between 20 mol% (mfp-3) and 25 mol% (mfp-5) [17].

Due to the acidic character of the two hydroxy groups of catechols, the binding process between catechols and surfaces is strongly dependent on the pH value. Sea water has a pH value of approximately 8 and an ionic strength of 0.7 mol L^{-1}. The conditions prevailing in sea water result in numerous surface modifications, such as oxidation. Bonding between catechols and oxidised surfaces change from H-bridge bonds at acidic pH values (such as pH 2) to coordinative bonding in a slightly basic environment (pH 8) (see Figure 1-3). [18]

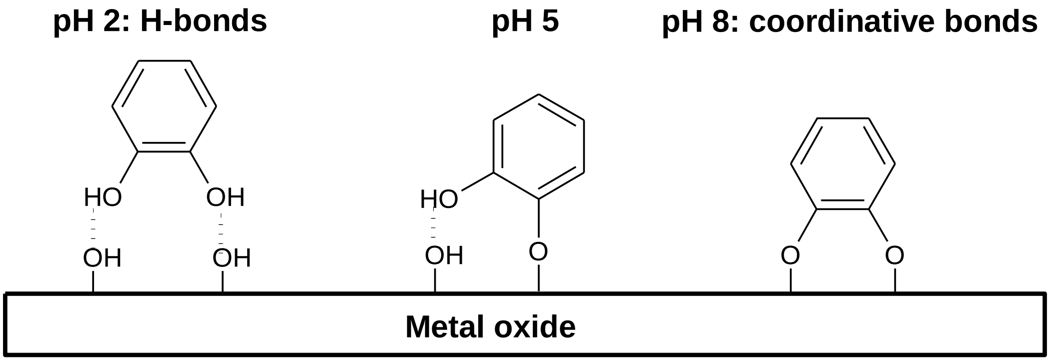

Figure 1-3: The bond between catechols with metal oxide surfaces depend on the pH value during curing. In an acidic environment (pH 2) catechol groups form hydrogen bonds and in a slightly basic environment (pH 8) coordinative [19]**.**

The attachment process of *Mytilus* mussels to a surface in salt water is a sequence of deposition processes that start with the engagement of the mussel foot onto the surface and the formation of a closed space (cavity) between the foot and the surface. Subsequently, the pH value in this cavity is lowered through the addition of acids which both cleans and prepares the surface. The resulting pH value in the cavity is usually between 4 and 6.5 (but can also drop to 2). The mussel adhesive consists of approximately 20 different polypeptides, each containing different amino acids. The ionic strength is reduced to only 0.15 mol L^{-1}, which promotes the formation of secondary bonds between the amino acid side chains and the surface. Furthermore, oxygen is removed to avoid redox processes.

Following the adjustment, the cavity's reaction parameters, catechol-rich proteins are secreted together with antioxidants or reducing agents to establish the adhesion. The interfacial interaction of the mfps with the substrate at an acidic pH value include (1) bidentate H-bonds, (2) electrostatic attraction and (3) hydrophobic interactions, as well as (4) coordinative bonds (the latter only above pH 5). Similar types of forces contribute to cohesion: (1) formation of bidentate intercatechol H-bonding, (2) cation-π interactions, (3) Ca^{2+} salt bridges and (4) hydrophobic interactions. The adhesion proteins mfp-3 or mfp-5 are deposited into the cavity and subsequently bind to the target surface. At low pH values, especially below the pKa of most organic acids, H-bonds are the most common bonds on polar surfaces. As Fe^{3+} or dissolved oxygen leak into the cavity, DOPA is oxidized to DOPA quinone, which is poor in adhesion strength but contributes to cohesion due to cross-linking. DOPA quinone can also be rescued by the reaction with thiolated mfp-6. The protein rich fluid, which was injected into the cavitation, undergoes in further steps coacervation and phase inversion. Further leakage of salt water into the cavity raises the pH value and ion strength, which results in solidification of the mfps and the formation of a plaque, which is a load-bearing porous material. The process is completed by the addition of a protective cuticle over the plaque and the lifting of the foot [19]. Mussels established tensile strength of up to 130 kPa ± 10 kPa under wet conditions on polished aluminum surfaces [20].

In mfps positively charged residues, such as Lys and His, are abundant, but negatively charged residues are rare [17, 21]. These amine groups may contribute in combination with the catechol to the underwater adhesion due to covalent, as well as non-covalent interactions [22, 23]. Catechols linked to polymers are not only able to enable strong adhesion to substrate surfaces, they can additionally provide cohesion through bonding with other catechols [13]. The cohesion can be further improved by Michael addition of L-lysine with oxidized catechols [18].

Lin et al. (2007) have shown that the mussel foot proteins mfp-1 and mfp-6, although they contained similar levels of L-DOPA, had different adhesive forces. It has been theorized that L-lysine has an important influence on the adhesive forces in addition to L-DOPA [24]. Li et al. (2017) have investigated this theory and chemically functionalized PEG polymer with lysine-DOPA, DOPA-lysine, glycerine-DOPA and DOPA-glycerine side chains [18]. The positive influence of L-lysine was confirmed, but the maximum measured force was less than 50 kPa (heavy tensile test: 30 µl 10 % Lys-DOPA-PEG, phosphate buffer pH 8; curing: RT, 90 % moisture, 24 h). The synergistic effects between L-DOPA and L-lysine were attributed to the fact that L-lysine displaced surface water, removed hydrated cations from the adhesive surface and thus improved the interaction of L-DOPA with the surface, so that the catechol group could bind optimally [6]. Positively charged L-lysine contributed to adhesion by binding to negatively charged surfaces.

Oxidation and storage stability

Catechols are susceptible to oxidation. Oxidation progresses in processes are caused, for instance, by sunlight, UV radiation and hydroxyl groups (in basic pH environments). Mussels have various mechanisms to counteract oxidation (see Figure 1-4). For example, reduction by cysteine-containing side chains can restore the functionality of the catechol group. In its semi-oxidized state (semiquinone), the functional group can be used for the bonding of phenols or ligneous plant residues [25]. The oxidation of the catechol group can also be catalyzed by laccases, resulting in covalent bonds which are often C-C or C-O-C-linked [13].

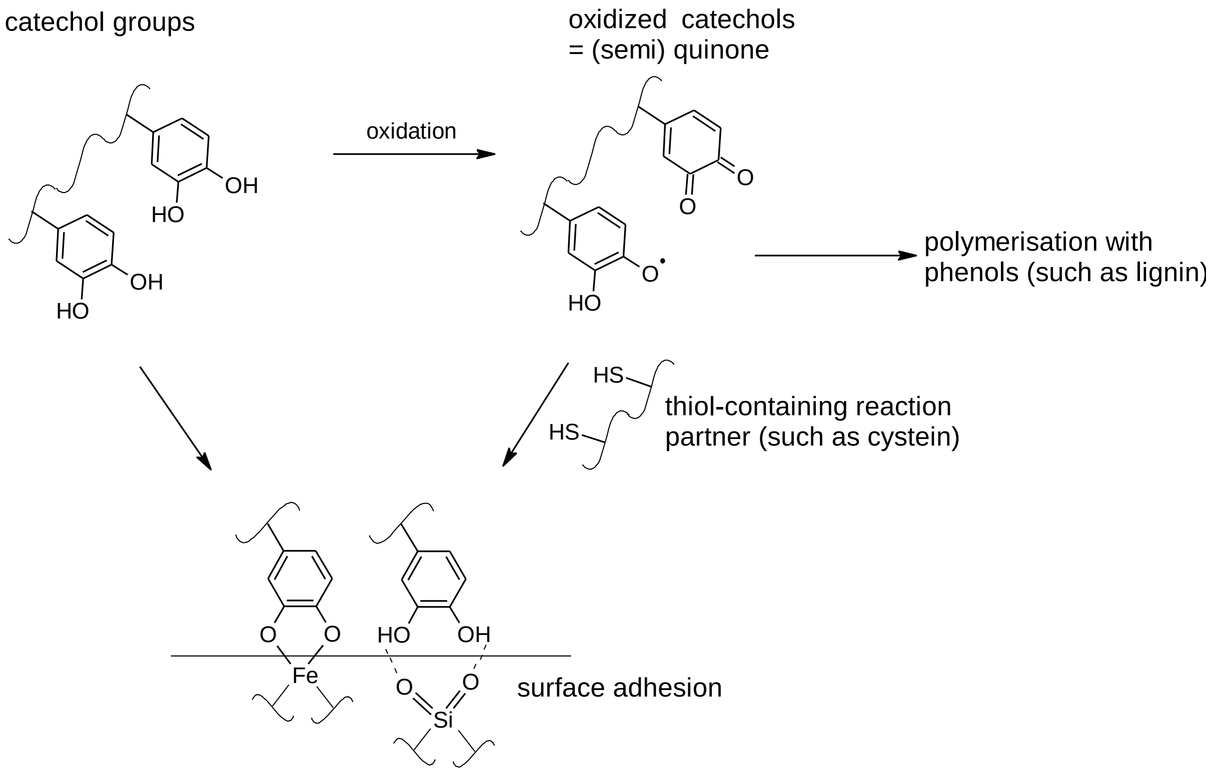
catechol groups
oxidized catechols
= (semi) quinone
oxidation
OH
HO
OH
HO
O
O
O•
HO
polymerisation with
phenols (such as lignin)
HS
HS
thiol-containing reaction
partner (such as cystein)
O
O
Fe
HO
OH
O
O
Si
surface adhesion

Figure 1-4: Formation of catechol adhesion, imitating the principle of the mussel [26].

Several attempts have been made to understand and prevent oxidation of the catechols group. Miller et al. (2015) confirmed the hypothesis, that cysteine-containing proteins are responsible for protecting the DOPA group from oxidation [27], by demonstrating that after 20 days of storage of cysteine-containing proteins, 30 % of the isolated antioxidant properties of the mussel proteins are retained. Mirshafian et al. (2016) have shown by cyclovoltammetric investigations that oxidation of L-DOPA in neutral and basic reaction environments, α, β-dehydro-DOPA was formed, a tautomer of the DOPA quinone, which favored the β-sheet folding of the mfp 3F mussel protein and adhered 20 times stronger to TiO_2 than untreated DOPA [28].

Fullenkamp et al. (2014) have investigated the pH-dependent mechanism of covalent formation of catechol-catechol compounds by oxidation via iron(III) ions. When iron(III) ions were added to catechols, a green coloration was detected at pH 2-3 (not buffered), which was caused by a non-covalent interaction between catechol and iron(III) ions. After one hour, the solution turned yellow and subsequently brown (after approximately

2 days). The coloration was caused by the oxidation of catechols to quinones and was promoted by the reduction of the iron(III) ions to iron(II) ions. In further reactions, quinones formed covalent bonds with catechols, resulting in the lack of catechols for surface adhesion. In contrast, at a pH value of 5 (in acetate buffer) and a pH of 7 (in bis-tris buffer) and a three-fold excess of catechol, dimers complexes, $Fe(DOPA)_2$, were formed. If the pH was raised from acidic to pH 9, after successful complex formation, the dimeric complexes turned into trimer complexes, $Fe(DOPA)_3$, which were resistant to oxidation. In comparison, if a pH value of 9 was set prior to the iron(III) ions addition, catechols were oxidized by the basic environment and the iron(III) ions were not able to form complexes with the oxidized catechols (quinones). In conclusion, iron(III) ion were able to protected the catechols from oxidation in basic environments after successful formation of dimer and trimer catechol-iron(III) complexes at neutral or slightly acidic conditions [29].

Modifications of mussel proteins

Wei et al. (2014) investigated the length and charge of DOPA-functionalized fibers by designing three short, simplified DOPA-containing peptides (15−17 res) and one relatively long peptide (30 res) on the basis of mussel foot protein-5 (mfp-5; length 75 res). It was shown that the peptide adhesion between two mica surfaces was an order of magnitude weaker (adhesion energy $E_{ad} \sim -0.5$ mJ m^{-2}) than full length mfp-5 adhesion and was approximately doubled ($E_{ad} \sim -1$ mJ m^{-2}) upon doubling the peptide length. The conclusion was drawn that the chain length has a significant influence on promoting adhesion between to surfaces [30].

Seo et al. (2015) demonstrate that the ratio of hydrophilic to hydrophobic and cationic to anionic side groups in the mfp-3 protein influenced the stability against oxidation, the distribution on the adhesive surface as well as the adhesive strength [31].

Wei et al. (2016) have produced a selected mussel protein, the mussel foot protein homologue (mfp3S-pep), whose sequence is intended to mimic the pI, polyampholytes and hydrophobic character of the native protein. The native protein and synthetic peptide exhibited similar abilities to self-coacervate, at given pH and ionic strength, which allows thick surface coating and displacement of surface-bound water molecules. Since surface-bound water is the biggest issue for wet adhesion, it was concluded that coacervation is an important property for the development of a bioadhesive in wet environments. [32].

1.2.3 Biogenic and biodegradable adhesives

The development of biogenic adhesives goes hand-in-hand with the development of biogenic and biodegradable plastic products. As nations strive to decrease plastic waste and to increase the biodegradability of products, renewable resources are being seen as an environmentally friendly solution, that provide an alternative to petroleum-based raw materials. The term biogenic addresses the origin of materials, which in this case, derives from renewable resources. The meaning of biodegradability is, that a product capable of undergoing decomposition into carbon dioxide, methane, water, inorganic compounds, or biomass [33]. Biogenic and/or biodegradable use cases are, for example, packaging materials (trash bags, loose fill foams and food containers), consumer goods (egg cartons, toys, straws, utensils) industrial products (planter boxes, compositing bags, fishing nets, mulch films) and hygiene products (flushable sanitary products, diaper inserts) [34, 35]. Common biogenic raw materials for adhesives, resins and coatings from renewable resources are starch, chitosan, casein from milk, linseed oil, hemp oil and soybeans [36].

The advantages of starch-based adhesives are, for example, the ample availability and stable quality, as well as the considerable adhesion properties to cellulose and other porous substrates. Furthermore, starch-based adhesives are insoluble in oils and fats, they are non-toxic, biodegradable and heat resistance. These adhesives are cheap and can be used for making semi-water-resistant plywood, and for coating some types of paper. So far, the use of soy-based adhesives is limited to the production of wood composite materials, such as plywood. A further drawback of bio-based adhesives, such as soybean or casein glues, is often the limited water resistance. [35]

Chitosan-based-adhesives

For films made from 2 % chitosan, which were dissolved in different acidic solutions and subsequently dried for 48 hours, tensile strengths (cohesion) from 2.9 MPa (with lactic acid), 4.0 MPa (with citric acid), 20.0 MPa (with malic acid) to 40.1 MPa (with acetic acid) were obtained [37].

The adhesion of chitosan-based adhesives is dependent on a variety of factors, such as the molecular weight, the degree of deacetylation and chitosan concentration, as well as the solvent, surface treatment and measuring technique used, which makes the comparison of adhesion strength difficult. For plywood adherends, which were glued with glucose-enhanced chitosan, tensile strength up to 2 MPa were reported under dry conditions [38] and up to 1 MPa under wet conditions (warm water immersion at 60 °C for 3 hours, cooling in water and testing in the wet conditions) [39]. Another chitosan-based adhesive, composed of 6 wt% chitosan, 1 % glycerol and 5 mmol L^{-1} trisodium citrate, resulted in 6.0 MPa under dried conditions and 1.6 MPa in wet conditions (specimens immersed for 3 h at 30 °C) in double-lap joint test with adherends made from maritime pine [40]. The same authors obtained a shear strength of 5.7 MPa to 8.8 MPa for a chitosan-based adhesive composed of 6 wt% chitosan and 2 vol% acetic acid using aluminum adherends which were untreated, deep scratched with a metal file, shallow scratched with sandpaper or pressed to obtain small over-shaped grooves [41]. A treatment with 1 mol L^{-1} of NaOH for 1 hour, followed by washing and storage in 1 vol% acetic acid increased the shear strength by more than 3-fold to 31.4 MPa. A further increase in shear strength to 40.8 MPa was observed for 7 wt% chitosan, 2 vol% acetic acid and 1 vol% glycerol. However, these results were obtained after surface treatment with harsh chemicals, which were avoided in this work towards the goal of developing biologically sustainable adhesives. Lastly, Vargas Villanueva et al. (2019) described a chitosan-based bone adhesive which achieved approximately 300 kPa under dry conditions and 30 kPa under wet conditions (tensile strength) [42].

Lignin-based adhesives

In nature, lignin acts, together with hemicellulose, as a cement-like adhesive which bonds together cellulose fibers in wood, where it also serves as a waterproofing and antimicrobial agent. Its highly branched structure and variety of functional groups provide active centers for chemical and biological modifications [43]. More information on the structure of lignin is provided in Chapter 3.

Lignin is a by-product from the pulping industry, where many of the lignin's hydroxyl groups are oxidized by strong alkaline treatment, and the lignocellulose biorefinery, which, in contrast, results in a highly activated lignin [44]. Due to its petrochemical nature, several attempts have been made to replace the phenol in phenol-formaldehyde (PF) adhesives by lignin [45] or tannins [46]. Under alkaline conditions and in the presence of excess formaldehyde, hydroxymethyl lignin and phenols are formed, which are subsequently copolymerized to produce lignin-phenol-formaldehyde resins [47, 48]. However, at most 50 % of the phenol in PF adhesives were replaceable by lignin in exterior grade plywood [48].

The abundance of methyl groups in lignin makes it less reactive and limits its cross-linking properties [49], which makes the production of formaldehyde-free wood adhesives difficult [50]. Demethylation of lignin, either chemically [51] or enzymatically [47] improves the reactivity of lignin. Adhesives from laccase-treated lignin and soy protein exhibited tensile strengths of approximately 1.7 MPa with wood adherends, compared to approximately 0.2 MPa for lignin alone and 2.7 MPa for soy-protein alone [52]. After two cycles of 1h boiling and drying, about 1.2 MPa were retained for the laccase-treated lignin-soy protein blend, which is half of the strength of commercially available polyurethane adhesives. For formulations of lignin with chitosan, tensile strengths of 1.5 MPa were reported, which decline to approximately 0.2 MPa after two rounds of in boiling water [52].

1.2.4 Mussel inspired synthetic polymers and adhesives

Multiple attempts have been made to combine several backbones with catechol groups in order to develop biomimetic adhesives. In this section, some examples of mussel-inspired adhesives are introduced.

Jia et al. (2014) developed a semi-synthetic catechol-containing polyoxetane adhesive polymer which maintained an average lap shear strength of 4.9 MPa on stainless steel after cross-linking with iron(III) ions [53]. Li et al. (2015) described a mussel inspired water-soluble adhesive by grafting catechols and phosphoric acid on a polyoxetane backbone [54]. The highest bonding strength (lap shear test) of 0.35 MPa (under humid conditions) was achieved with 5 mol% catechol and 26 mol% bis-phosphoric acid groups and a molar ratio of Fe^{3+} to catechol of 1 to 1 on aluminum surfaces. Using eigenol (methoxydehydro-DOPA) as functional group, Kang et al. (2016) developed polymer loops inspired by the mussel, which provide surface lubrication and antifouling properties [55]. North et al. (2017) synthesized a poly(catechol-styrene) which achieved a strength of up to 3 MPa in an underwater lap shear test. By dissolving the poly-(catechol-styrene) in chloroform, a hydrophobic, water-insoluble solvent, the hardening of the adhesion and cohesion can be formed even under water between two aluminum plates. The adhesion strength was demonstrated to be higher in salt water than in deionized water [20]. Mu et al. (2017) have also investigated the influence of side chains on the underwater adhesion of catechol adhesives. They compared (1) polystyrene, (2) poly(acryl-co-acrylamide), (3) polyacrylamide and (4) poly-(N-vinylpyrrolidone) (PVP)-based catechol adhesives with similar sizes (12.8 kDa to 14.2 kDa) and catechol contents (20.0 %-21.3 %). For Polymer (1), a lap shear strength of 0.4 MPa and for polymer (2) to (4) lap shear strength of approximately 1 MPa were obtained on glass and aluminum surfaces under dry conditions. In underwater lap shear tests, a linear correlation of the polarity of the side chains was found, obtaining the highest lap shear strength for polymer (4) with glass adherends [56]. Wu et al. (2017) have esterified a polyvinyl alcohol with 3,4-dihydroxybenzoic acid (PCA) and achieved 4 MPa of lap shear strength in adhesive experiments. The curing was performed by adding 10 µl $FeCl_3$ (ratio of catechol to iron(III) ions: 3 to 1) or sodium periodate for 12 hours. An increase in lap shear strength from 2 MPa to 4 MPa was observed when curing was performed at 60 °C instead of room temperature. The adhesion strength in wet or underwater conditions was significantly lower (< 0.5 MPa) [57]. Jenkins et al. (2017) modified a plant-based poly(lactic acid) with catechols and achieved a strong adhesion strength of 2.6 MPa in air and 1.0 MPa under wet conditions to aluminum substrates [58]. Xu et al. (2017) measured an underwater adhesion of 0.65 MPa (lap shear strength on glass surfaces) for a polyester adhesive based on catechol-containing soybean oil [59]. Narkar et al. (2018) reported adhesion strength of a few kPa (against wetted quartz or APTS-functionalized substrates) for hydrogels from dopamine methaceylamide and acrylic acid or N-(-aminopropyl)-methacrylamide hydrochloride [60]. Tang et al. (2019) report a Mussel-inspired cellulose-based adhesive which achieved a lap shear strength of 88 kPa with porcine skin [61].

1.2.5 Catechol-functionalized chitosan and lignin

Several chitosan based gels and adhesives have been described in literature. Peshkova et al. (2003) modified chitosan with phenolic compounds using laccases. Maple veneer strips which were hot-pressed (105 °C, 0.7 MPa for 5 min) with chitosan-phenolic-laccase systems containing catechols, such as caffeic acid, achieved shear strengths of up to 2 MPa [25]. Due to the polymerization reaction with phenolic compounds, after the treatment with laccases, a wet adhesion strength of 1.2 MPa was achieved. Using N-(3-Dimethylaminopropyl)-N’-ethylcarbodiimide hydrochloride (ECD), Xu et al. (2015) developed a genipin cross-linked catechol-chitosan hydrogel which can be used as a drug delivery system [62]. Zeng et al. (2018) developed a surgical adhesive containing 3,4-dihydroxyphenylanine acrylamide, poly (ethylene glycol) diacrylate and thiolated chitosan which cures via ultraviolet (UV) irradiation. For an adhesive containing 41.6 mol% catechol, a lap shear strength of approximately 1 MPa was reached on gelatin coated glass after UV-curing for 15 min and an incubation period of 24 h [63]. Lee et al. (2018) grafted catechol groups derived from 3,4-dihydroxycinnamic acid onto a chitosan backbone via peptide bonds using ECD (1-ethyl-3-(3-dimethylaminopropyl) carbodiimide) chemistry. By adding 10 % vanadyl ions, a 3D printable underwater "bio-ink" was developed which was used to produce well-defined grid shapes [64]. Narkar et al. (2019) developed aggregates between catechol-functionalized chitosan and mucin for biomedical applications [65].

Gan et al. (2019) developed a hydrogel consisting of Ag-lignin nanoparticles, polyacrylic acid and pectin, which was polymerized using ammonium persulfate. Using silver nitrate, the Ag-lignin nanoparticles were synthesized through a redox reaction in an alkaline environment, where the functional groups on lignin (-OCH_3 and -OH) were oxidized by silver ions to quinone/semiquinone free radicals [66]. The authors report long-term and repeatable adhesion, good cell affinity and high antibacterial activity. The application of Ag-lignin nanoparticles for DOPA-mediated adhesion needs further investigation.

1.2.6 Comparison of adhesion strength to reported literature values

The comparison of adhesion is difficult due to various parameters which can be applied, such as the origin of adhesive, the test method (such as tensile strength or lap shear strength), the material of the adherends (such as wood, glass, steel, aluminum), the surface preparation (such as chemical or mechanical pre-treatment), the use of cross-linkers and the curing conditions (such as dry or wet).

In this section, an attempt was made to compare the adhesives, developed in this work, with adhesives reported in literature. In Table 1-1 an overview of the tensile strengths, which were reported for biogenic and bioinspired adhesives is provided. Cohesion testing (no adherend) and testing, which required surface treatment with harsh chemicals (such as NaOH) were not included. Since catechol-containing adhesives were predominantly measured using lap shear test, adhesion results, which were measured using lap shear or lap-joint tests are not included.

The comparison of biogenic adhesives using tensile strength (Table 1-1) shows that the lowest wet adhesion was reported for the mussel itself, with 0.13 MPa ± 0.01 MPa [20]. The tensile strength of butt joints established for DHC-lignin is at the low end of the list with 0.17 MPa ± 0.13 MPa (see chapter 4) and the tensile strength of butt joints of PCA-chitosan with 4.56 MPa ± 0.54 MPa is at the top of the list (see chapter 3). The highest wet adhesion (tensile strength of 1.2 MPa) was reported for a laccase-treated lignin-soy protein with wood adherends [52].

Table 1-1: Tensile strength of biogenic and bioinspired adhesives.

Adhesive	Adherend surface and surface preparation	Conditions	Tensile strength [MPa]	Reference
mussel adhesive (living)	aluminum, polished	wet	0.13 ± 0.01	[20]
DHC-lignin	aluminum, cleaned with an abrasive pad	dry	0.17 ± 0.13	this work (chapter 4)
lignin	wood	dry	0.2	[52]
lignin-chitosan	wood	wet	0.2	[52]
chitosan	aluminum, cleaned with an abrasive pad	dry	0.23 ± 0.13	[67]
chitosan-base bone adhesive	bone	dry	0.3	[42]
dextrin	aluminum, cleaned with an abrasive pad	dry	0.35 ± 0.17	[67]
starch	aluminum, cleaned with an abrasive pad	dry	0.50 ± 0.17	[67]
glucose-enhanced chitosan	plywood	wet	1.0	[39]
laccase-treated lignin-soy protein	wood	wet	1.2	[52]
lignin-chitosan	wood	dry	1.5	[52]
laccase-treated lignin-soy protein	wood	dry	1.7	[52]
glucose-enhanced chitosan	plywood	dry	2.0	[38]
Gummi arabicum	aluminum, cleaned with an abrasive pad	dry	2.10 ± 0.45	[67]
soy-protein	wood	dry	2.7	[52]
PCA-chitosan	aluminum, cleaned with an abrasive pad	dry	3.41 ± 0.12	this work (chapter 3), [67]
PCA-chitosan	aluminum, blasted with corundum	dry	4.56 ± 0.54	this work (chapter 3), [67]

In Table 1-2, an overview of adhesion strength, reported for biogenic and bioinspired adhesives on aluminum surfaces, is provided. These adhesion results were exclusively obtained via lap shear tests. Adhesion testing, which required surface treatment with harsh chemicals (such as NaOH) were, again, not included. Aluminum is of special interest, because it is a relatively soft and easy to process metal, that is also known for its light weight. Due to its barrier properties, it is used as packaging material to protect food or pharmaceuticals. Furthermore, it is interesting for the electrical industry because of its excellent electrical conductivity [68].

The comparison of mussel-inspired adhesives, which were measured using aluminum surfaces using lap shear tests (Table 1-2), shows that the lowest adhesion strength under dry conditions (lap shear strength of 0.42 MPa), was reported for a polystyrene-catechol [56] and the highest adhesion strength of 3.7 MPa for a polyoxetane catechol [53]. The lowest wet adhesion (lap shear strength of 0.18 MPa) was reported for a polystyrene catechol [56] and the highest wet adhesion of 3.0 MPa was reported for a poly(catechol-styrene) [20].

The comparison of adhesion strengths in literature indicates that the PCA-catechol adhesive (chapter 3) is a strong and novel adhesive. In contrast, the DHC-lignin adhesive (chapter 4) requires further improvement. Both adhesives would benefit from increases to their wet adhesion strength.

Table 1-2: Adhesion strength of biogenic and bioinspired adhesives on aluminum surfaces.

Adhesive	cross-linked	Surface preparation	Conditions	Test method	Adhesion strength [MPa]	Reference
polystyrene-catechol	-	polished	wet	lap shear test	0.18	[56]
polyvinyl alcohol (PVA) catechol	iron(III)	grinded, polished	wet	lap shear test	0.18	[57]
polyoxetane catechols and phosphoric acid	iron(III)	sandpaper	wet	lap shear test	0.35	[18]
poly(acryl-co-acrylamide catechol	-	polished	wet	lap shear test	0.36	[56]
polystyrene catechol	-	polished	dry	lap shear test	0.42	[56]
polyester catechol with soybean oil	iron(III)	polished	wet	lap shear test	0.5	[59]

Adhesive	**cross-linked**	**Surface preparation**	**Conditions**	**Test method**	**Adhesion strength [MPa]**	**Reference**
polyacrylamide catechol	-	polished	wet	lap shear test	0.57	[56]
poly(acryl-co-acrylamide catechol	-	polished	dry	lap shear test	0.90	[56]
poly(lactic acid) (PLA) catechol	-	washing with trichloroethylene	wet	lap shear test	1.0	[58]
polyacrylamide catechol	-	polished	dry	lap shear test	1.01	[56]
poly-(N-vinylpyrrolidone) catechol	-	polished	wet	lap shear test	1.02	[56]
poly-(N-vinylpyrrolidone) catechol	-	polished	dry	lap shear test	1.10	[56]
poly(lactic acid) (PLA) catechol	-	washing with trichloroethylene	dry	lap shear test	2.6	[58]
poly(catechol-styrene)	-	polished	wet	lap shear test	3.0	[20]
polyvinyl alcohol (PVA) catechol	iron(III)	grinded, polished	dry	lap shear test	3.2	[57]
polyoxetane catechol	iron(III)	sandpaper	dry	lap shear test	3.7	[53]

2 Biochemical reactions of catechols for the functionalization of natural polymers

In molluscs, such as mussels [14], sandcastle worms [69] or squids [70], catechols play an essential role in adhesion under harsh marine conditions [15]. Mussel-inspired catechol-containing polymers provide a strong basis for the development of biogenic adhesives. The objective of this chapter is to identify biochemical methods for developing a biogenic mussel mimicking adhesive, while avoiding the use of harsh chemicals.

First, catechols and their adhesion properties in nature are introduced in section 2.1.1. Enzymatically catalyzed reactions offer alternatives to the use of toxic chemicals or the requirement of special reaction conditions. Laccases, which provide a low cost and environmentally friendly solution for the functionalization of natural polymers with catechols [71], are described in section 2.1.2. For laccase-catalysed reactions of catechols, various reaction, such as C-C, C-O-C and C-N bond formation have been described [72–74]. The laccase-catalyzed C-N bond formation between a primary amine (as available in chitosan) and a catechol, which is also known as Michael-type addition [75, 76], is identified as the most promising reaction which allows for the functionalization of a backbone with catechols. A kinetic model for the laccase-catalyzed homomolecular Michael-type addition is introduced in section 2.1.3.
As input parameters may change during process development, flexibility of the laccases is required. In this work, the stability towards solvents is identified as a key factor for the development and formulation of adhesives (see section 2.3.1). Therefore, solvent stable laccases are identified, expressed, purified, and characterized (see section 2.3.3 and 2.3.4). Furthermore, the formation of laccase-catalyzed heteromolecular C-N bonds via Michael-type addition is investigated between the catechols 3,4-dihydroxybenzoic acid (PCA) and 3-(3,4-dihydrophenyl) propionic acid (DHC) with the primary amine N-acetyl diaminopentane (NAcDAP) (see section 2.3.5). A model is created and used to investigate the influence of the pH value and the primary amine’s pKa value for the C-N bond formation between the amine and the catechols (see section 2.3.6). Lastly, the reaction is parametrically optimized to identify the most significant reaction parameters (see section 2.3.7).

2.1 Theory

2.1.1 Catechols

Catechols have various functions in plants and animals, such as mediating underwater adhesion in molluscs [14, 69, 70]. Catechol-containing monomeric molecules are widely found in nature, of which this research concentrated on L-DOPA (L-3,4-dihydroxyphenylalanine, Levadopa), PCA and DHC.

L-DOPA is a non-proteinogenic amino acid which derives from the amino acid tyrosine [77]. Its chemical structure is shown in Figure 2-1 A. L-DOPA is a precursor in the biosynthesis of the neuro-transmitters adrenaline, noradrenaline, betaines and dopamine [78]. In mussels, L-DOPA is the main component of the adhesive used to attach mussels to solid surfaces [24]. Incorporated into the protein chain of the adhesive, it increases hydrophilicity through its hydroxyl groups [79]. The drawback to using L-DOPA for industrial products is its high price and low storage stability. Furthermore, polymerization of L-DOPA leads to the formation of the skin pigment melanin [80]. The melanin biosynthesis starts with the formation of dopaquinone-H^+, which is initiated by enzymes (laccases or tyrosinases), as well as UV radiation [76]. Several intermediates, such as dopaquinone, leukodopachrome, dopachrome and 5,6-dihydroxyindol are part of the melanization process, which is highly influenced by pH and temperature [76]. Due to the reaction with itself, heteromolecular dimerization of L-DOPA was found to be difficult (data not shown). Therefore, in this work, L-DOPA was not considered as a catechol donor for mussel mimicking adhesives.

PCA is a phenolic acid which is commonly found in plums [81], gooseberries, grapes [82], olive oil, white wine [83, 84] and plants, such as star anise or melissa [85]. It functions as a fungicide [86] in food processes such as cocoa fermentation [87] and tea preparation [88]. Acai oil, which is obtained from the fruit of the Acai palm and known for its antibacterial [89], antioxidant [90], anticancer [91] and anti-inflammatory [92] activities, contains reported PCA concentrations of 630 mg kg^{-1} ± 36 mg kg^{-1} [93]. PCA’s solubility in water is 18.2 mg ml^{-1} at 14 °C [94] and the pKa constant lies between 4.26 [95] and 4.48 [96] at 25 °C. PCA has a molar mass of 154.12 g mol^{-1}. Its chemical structure is shown in Figure 2-1 B.

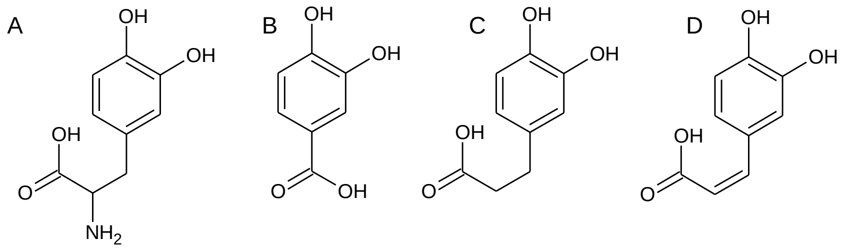

Figure 2-1: Chemical structure of the catechols (A) L-DOPA, (B) PCA, (C) DHC and (D) caffeic acid.

DHC has a molar mass of 182.18 g mol^{-1} and acid dissociation constants of $pKa_1 = 4.56$, $pKa_2 = 9.36$ and $pKa_3 = 11.6$ [97]. Its chemical structure is shown in Figure 2-1 C. Starting from the amino acid L-tyrosine, caffeic acid (see Figure 2-1 D) is an intermediate product in the proposed ferulic acid biosynthesis pathway [98]. L-tyrosine is an intermediate product of the shikimate pathway [99, 100] and can be produced recombinantly in *Corynebacterium glutamicum* [77]. Using the enzyme tyrosine ammonia lyase, L-tyrosine is first converted into 4-coumaric acid [101] which is further converted into caffeic acid and ferulic acid by the enzymes 4-coumarate hydroxylase and caffeic acid methyltransferase [98]. DHC is a degradation product of caffeic acid caused by bacteria found in the gastrointestinal tract [102]. Antioxidant activity has been reported for both DHC and caffeic acid [103].

2.1.2 Laccases

Laccases (EC 1.10.3.2., Benzenediol: oxygen oxidoreductase) are extracellular enzymes which belong to the family of copper-containing polyphenol oxidases [104]. Laccases catalyze the oxidation of phenolic substances and aromatic amines [104]. While the phenol group is being oxidized to form a radical, molecular oxygen, which functions as co-substrate, is transformed into water [105]. Laccases are found in many white-rot fungi (see Figure 2-2), but also occur in plants and bacteria [104]. Furthermore, laccases can catalyze both the initial polymerization of monolignols to oligolignols in plants [106] as well as the cleavage of lignin into monomers and oligomers [107]. While its function in plants is thus the synthesis of lignin, laccases are involved in the biodegradation of lignin by wood-colonizing basidiomycetes [108, 109]. In the presence of suitable redox mediators, laccases are even able to oxidize non-phenolic compounds [110]. Catechols are natural substrates for laccase [111]. Due to their polymerization capability, laccases are well suited enzymes for the functionalization of polymers with catechols.

Figure 2-2: White-rot fungus on a tree trunk (Ivry-sur-le-Lac, QC, Canada, September 2019).

2.1.2.1 Solubility and storage of laccases' substrates

In order to guarantee homogeneous catalysis by enzymes, solubility of the substrate is advantageous. Many substrates of laccases have been reported for their low solubility in water, so that an initial dissolution in organic solvents, such as methanol or ethanol, is necessary. Syringaldazine, for example, is commonly dissolved in ethanol or methanol prior to its addition to an aqueous reaction mixture [112, 113]. Other studies report that monomeric or dimeric phenolic compounds were dissolved by the addition of acetone prior to laccase catalysis. O-hydroxyl phenol, for example, was dissolved in 50 vol% of acetone [72] and 1-(3,4-dimethoxyphenyl)-2(2-methoxyphenoxy)propane-1,3-diol in 10 vol% of acetone [114]. Hence, reaction mixtures can contain various amounts of organic solvents. Furthermore, some laccase substrates, such as catechols, are susceptible to oxidation at a basic pH and in the abundance of oxygen [115]. Therefore, manufacturers often recommend storage in organic solvents over in aqueous solutions [116].

The wood polymer lignin is a complex organic polymer which is composed of cross-linked phenols [117]. Lignin is structurally important for the formation of cell walls, especially in wood and bark, since it acts as a natural glue between the different biomass components [118]. Due to its polyphenolic nature, it is a substrate for enzymatic degradation and polymerization by laccases. In many second generation processes such as the lignocellulose biorefinery, lignin is a side product with a high potential for the development of novel products [119]. Due to its abundance (lignin makes between 15 and 25 % of wooden biomass [118, 119]), it is a great backbone for adhesives made from renewable resources. However, the extraction methods from lignin strongly influence the lignin’s properties such as its water and solvent solubility. The OS process, for example, is an environmentally friendly procedure for the extraction of lignin from wood and plant residues. After a typical extraction of lignin from beech wood (see chapter 4, section 4.2.1), using relatively mild temperatures, such as 160 °C to 200 °C and 15 bar to 25 bar pressure, the lignin is dissolved in 50 wt% ethanol. If the ethanol concentration is reduced, lignin quickly becomes insoluble. Since steric hindrance and surface absorption can decrease the reaction efficiency, dissolved reaction partners are preferred [120]. In order to allow homogeneous transformation of lignin, solvent stable laccases are necessary. Another non-toxic solvent, which showed good solubility of OS lignin is DMSO (dimethyl sulfoxide) [121].

2.1.2.2 Laccase-catalyzed homo- and heteromolecular C-C and C-O bond formation

Enzymatically catalyzed reactions offer alternatives to the use of toxic chemicals or the requirement of special reaction condition. Due to their ability to catalyse the transformation of catechols, such as L-DOPA, PCA and DHC, laccases are suitable catalysts for the development of a catechol-containing adhesive.

The laccase-catalyzed formation of C-C and C-O bonds from 1,4- and 3,4-hydroquinones haven been described in literature [122, 123]. The dimeric products can be homomolecular, consisting of two identical molecules connected via a C-C bond [124] or C-O bond [125]. For products formed between two (or more) different reaction partners (heteromolecular) C-C [126], C-O [123, 127] as well as C-N [75, 128] and C-S [129] bonds are possible. As shown in Figure 2-3, C-C and C-O bonds can form simultaneously in one reaction.

The C-C or C-O bond formation is initiated by the laccase-catalyzed activation of an aromatic hydroxyl group, such as the conversion of hydroquinones (a) into quinones (b), the activated form of the hydroquinones, which is shown in Figure 2-3. A nucleophilic addition is then carried out by a further hydroquinone after deprotonation, whereby an aromatic carbon atom can act as a nucleophile and a C-C bond is formed (c). On the other hand, the nucleophilic attack can be carried out by a hydroxy group of the hydroquinone, resulting in the formation of a C-O bond, as is observed in the lignin biosynthesis [122] (not shown). After a renewed deprotonation of the product (c), there is the possibility that a C-O bond is formed (f) via keto- and enol tautomerism (d,e) in addition to the C-C bond [123, 130].

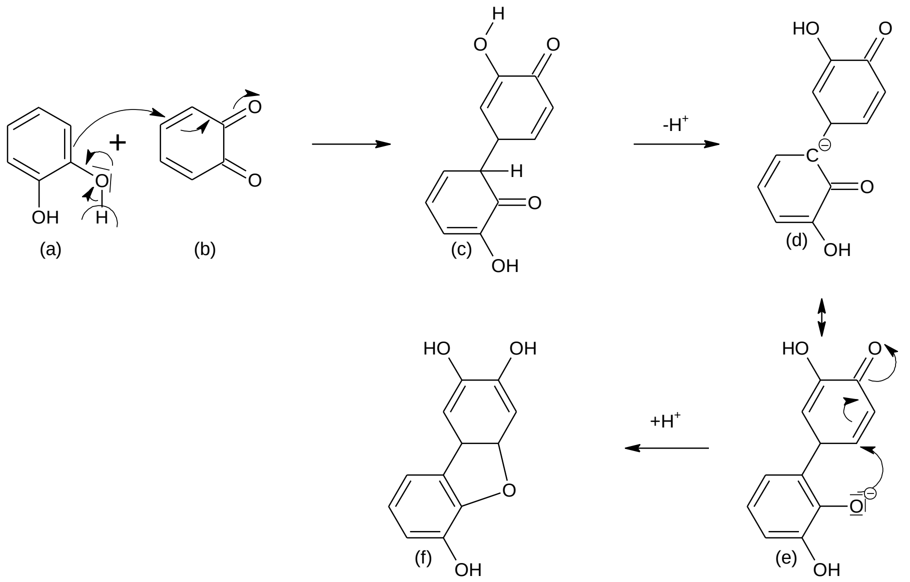

Figure 2-3: Laccase-catalyzed C-C and C-O bond formation using the example of 2-hydroxyphenol [122, 123].

Since the enzymatic reaction of laccases is followed by a subsequent chemical reaction, a large variety of additional products can be produced by Michael-type addition. This named reaction is understood to be a nucleophilic addition of a primary amine (Michael-donor) to a Michael acceptor, which are often α,-β unsaturated carbonyl compounds [128, 131] (see section 2.1.2.3).

2.1.2.3 Laccase-catalyzed Michael-type addition for C-N bond formation

The C-N bond formation between catechols and primary amines (as available in chitosan, see chapter 3), which is referred to as Michael addition [75] or Michael-type addition [65], is another example for laccase-catalyzed reaction. This reaction is, again, initiated by the laccase-catalyzed activation of an aromatic hydroxyl group. In a second step, a nucleophile is added.

The laccase (or tyrosinase) catalyzed formation of a C-N bond between a catechol ring and a primary amine has been widely studied and described [75, 76]. Both the C-N bond formation between 2,3-dihydroxybenzenes and 1,4-dihydroxybezenes are possible [75, 123]. For example, the C-N bond between a 1,4-hydroquinone and an aromatic amine as Michael donor (such as aniline or L-phenylalanine) has been successfully demonstrated [123, 130]. The hydroquinone, which is initially activated by laccases, is attacked by the amino group of the reaction partner, which acts as a nucleophile. Likewise, a laccase-catalyzed bond between the 3,4-hydroquinone and 2-aminobenzamide or H-tyrosine-lysine-OH as amine donors was successfully detected [75] (see Figure 2-4).

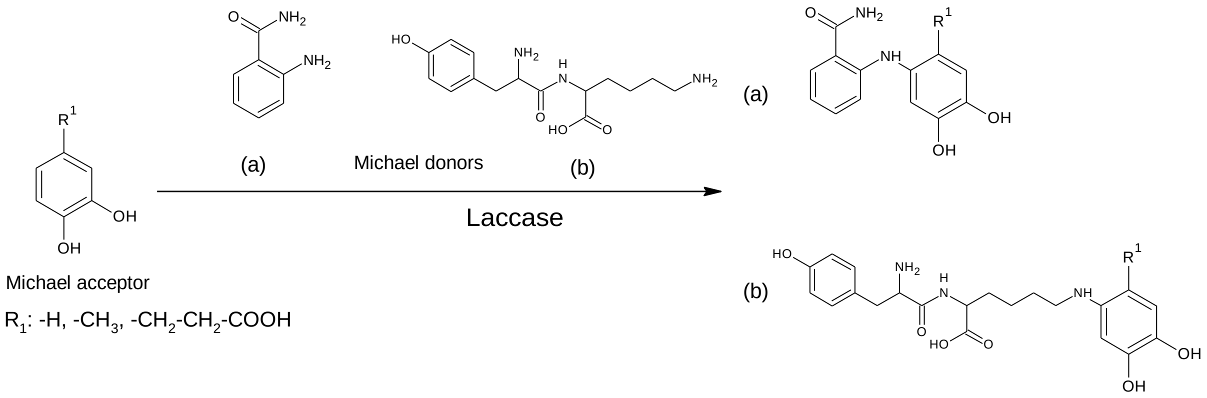

Figure 2-4: Laccase-catalyzed C-N bond formation between a 3,4-hydroquinone (Michael acceptor) and (a) 2-aminobenzamide or (b) H-tyrosine-lysine-OH, functioning as Michael donors [75, 130]**.**

The reaction with H-tyrosine-lysine-OH (see Figure 2-4) has shown that C-N bond formation with aliphatic amine donors, such as L-lysine, is possible and no aromatic amine components are necessary to form a C-N bond with phenolic dihydroxy components.

The Michael-type C-N bond formation between the catechols PCA and DHC with chitosan as amine donor is used in this work to develop a catechol-functionalized chitosan (see chapter 3).

2.1.3 Kinetic model for the laccase-catalyzed homomolecular Michael-type addition of L-DOPA

Garcia-Carmona et al. (1982) created a kinetic model for the formation of melanin from L-DOPA, which plays a key role in interfacial adhesion of mussels [13, 76]. The homomolecular formation of melanin from L-DOPA is disadvantageous for the formation of a mussel mimicking adhesive, however, in this work, the kinetic model is adapted to model heteromolecular reactions between catechol donors and primary amines for the formation of catechol-adhesives (see section 2.3.6).

Based on the mechanism postulated by Lerner et al. (1950), the conversion of L-DOPA to dopachrome is described as an enzymatic-chemical-chemical mechanism [80]. In a first step, the enzyme catalyzes the conversion of L-DOPA to dopaquinone-H$^+$. The second step involves the deprotonation of the amine group of dopaquinone-H$^+$, forming dopaquinone, and the ring closure forming leukodopachrome. In the third step, dopachrome is formed, either enzymatically catalyzed or as a result of the redox reaction involving the reverse reaction of dopaquinone-H^+ to L-DOPA. Dopachrome reacts further to 5,6-dihydroxyindole, which eventually forms melanin. For the conversion rate of dopaquinone-H^+ to leukodopachrome, equation 2-1 was derived, where k_1 is the specific rate constant of the deprotonation step, K_a is the ionization constant of the amino group of dopaquinone-H^+ and k_c is the specific rate constant for the ring closure (intramolecular 1,4 addition of Michael). The K_a value of L-DOPA is $1.91 \cdot 10^{-9}$ M. The specific constant k increases with temperature and pH [76].

$$\frac{1}{k} = \frac{1}{K_a \cdot k_c}[H^+] + \frac{1}{k_1} = \frac{1}{k_c} \cdot 10^{(-pH+pK_a)} + \frac{1}{k_1} \qquad 2\text{-}1$$

with

$[H^+]$ = concentration of H^+ ions/ $g \cdot mol^{-1}$
k = constant for conversion of L-DOPA to dopachrome/ $g \cdot mol^{-1}$
k_1 = specific rate constant of the deprotonation step/ $g \cdot mol^{-1}$
K_a = ionization constant of the amine group/ $g \cdot mol^{-1}$
k_c = specific rate constant for the ring closure/ $g \cdot mol^{-1}$
pH = potential of hydrogen (pH value)/ -
pK_a = acid dissociation constant /-

The study of laccase-, or of a tyrosinase-catalyzed formation of a C-N bond between a catechol ring and a primary amine suggest that the pKa value of the primary amine has a significant impact on the reaction rate [75, 76]. For aromatic amines with a pKa value of 5 to 6, the quinone-aromatic amine adducts form even at an acidic pH [132, 133]. Further investigation of the influence of the pKa and pH on the C-N bond formation is provided in section 2.3.6.However, for catechol-amines used as coating material for nanofiltration membranes, it was shown that catechol-m-phenylenediamine aggregates grow much faster than catechol-piperazine aggregates [134]. According to the authors, secondary amines are less likely to react via a Michael-type addition due to intermolecular pi-pi interactions.

In nature, insect cuticles contain catechol-histidine cross-linked proteins, which are linked via the aromatic amines of histidine (pKa of imidazole groups = 5,97 [97]) [135, 136]. For the sclerotization of insect cuticles via histidine, however, it has been shown that besides the catechol-ring, the side chain of the catecholamines are also used for cross-linking, which suggests that more sophisticated mechanisms are taking place [111, 137].

2.2 Materials and Methods

2.2.1 Cultivation and purification of laccases from *C. unicolor*

The laccase producing white rot fungus *C. unicolor* (PM1070798) obtained from HAMBI Culture Collection, Helsinki, Finland (Hambi No. FBCC 387) was cultivated in a 500 ml baffled flask at 28 °C in 100 ml modified Kirk medium [138, 139], containing 13 g L^{-1} glucose, 2 g L^{-1} KH_2PO_4, 0.5 g L^{-1} $MgSO_4$, 0.1 g L^{-1} $CaCl_2$, 0.1 g L^{-1}, 0.5 g L^{-1} diammonium carbonate, 0.5 g L^{-1} yeast extract and 100 µM Cu^{2+} from $CuSO_4{\cdot}5H_2O$. After 50 days of incubation, the liquid broth was separated from the fungus via decanting and purified using a laboratory crossflow cassette Vivaflow 50 R with a molecular weight cut off (MWCO) of 30.000 Da and a polyethersulfone membrane. The medium components were washed out using a dialysis set up. Afterwards, the broth was concentrated by a factor of 10. In order to prevent growth, the concentrate was filtered through a 0.2 µm nylon filter and stored at 4 °C for several weeks. The activity was measured using colorimetric assay with syringaldazine (see section 2.2.2.1).

2.2.2 Enzyme characterization

2.2.2.1 A colorimetric assay for the determination of enzyme activity

The laccase activity was measured using a colorimetric assay with 10 µM syringaldazine in 10 vol% ethanol (unless stated otherwise) as substrate at a wavelength of 530 nm using an UV-vis spectrometer and an extinction coefficient of $\varepsilon_{530} = 65\ mM\ cm^{-1}$ [140, 141]. One unit of enzyme activity (U) was defined as the amount of enzyme which converts 1 µmol of syringaldazine per minute at 25 °C. Each measurement was performed in triplicates.

2.2.2.2 Stability of laccases towards ethanol (short exposure)

The enzyme activity was measured using colorimetric assay with syringaldazine (see section 2.2.2.1) at 30 °C and pH 6.5 (0.05 M potassium phosphate buffer after Sørenson [142]). The ethanol concentration was varied from 10 vol% to 50 vol%, the volume difference was adjusted by adding water to the final volume of 1 ml and the enzyme concentration was set to 1.5 U ml^{-1}. Measurements were completed as triplicates.

2.2.2.3 Long-term stability of laccases towards ethanol

In order to determine the long-term stability of laccases, the following storage conditions were investigated:

1. pH 4.5 at a temperature of 4 °C
2. pH 6.5 at a temperature of 4 °C
3. pH 6.5, at a temperature of 4 °C and an ethanol concentration of 50 vol%
4. pH 6.5 at room temperature

Over a curse of 47 days, the enzyme activity was measured weekly at an ethanol concentration of 50 vol%, pH 6.5 and 30 °C (see section 2.2.2.2). Measurements were completed as triplicates.

2.2.2.4 The pH optimum for laccase-catalyzed conversions

The optimum pH for enzyme activity is highly dependent on the substrate used [138]. In order to determine the pH optimum of the purified laccase, the enzyme activity was measured using colorimetric assay with syringaldazine (see section 2.2.2.1). McIlvaine buffer from pH 4.5 to 8.5 was used at 10 mM final concentration. Syringaldazine was dissolved in ethanol, therefore, a final ethanol concentration of 10 vol% was present.

In order to determine the optimum pH for the conversion of PCA, 10 mM of PCA were dissolved in 0.1 M McIlvaine buffer at pH 4.0, 4.5, 5.5, 6.5, 7.5 and 8.5. The relative enzyme activity was measured with a colorimetric assay at 400 nm using a laccase solution containing 0.5 % PCA-solution. Measurements were completed as triplicates.

2.2.2.5 Laccase stability towards solvents

The solvent stability of the purified laccase as well as the enzyme activity was measured using a colorimetric assay with syringaldazine (see section 2.2.2.1). McIlvaine buffer was used at 10 mM final concentration. For the determination of the activity in ethanol, the ethanol concentration was varied from 0 vol% to 60 vol% (~50 wt%). Measurement were conduct at a pH of 5 and 25 °C. The enzyme activity in DMSO was determined by varying the DMSO concentration from 0 vol% to 50 vol%. Measurement were conduct at a pH of 6 and 25 °C. The volume difference (caused by the different concentrations of solvent) was adjusted by adding water to the final volume of 1 ml. The enzyme concentration was set to 1.5 U ml^{-1}. Measurements were completed in triplicate.

2.2.2.6 Determination of protein content and specific enzyme activity

The protein concentration was determined using Bradford method with the Pierce Coomassie Protein Assay Kit and a serum albumin as a standard. The specific enzyme activity is defined as enzyme activity in U divided by the amount of protein detected using the Bradford assay. Measurements were completed as triplicates.

2.2.2.7 Determination of molecular weight using SDS-PAGE

Purification degree and molecular weight (MW) of the laccase isoforms was determined by sodium dodecyl sulfate-polyacrylamide gel electrophoresis (SDS-PAGE, 5 % stacking gel and 15 % running gel, see Table 2-1), using an unstained protein marker as reference.

Table 2-1: Composition of stacking and running gel for SDS-Page

Component	5 % Stacking gel	15 % Running gel
Purified water	5.3 ml	2.3 ml
Rotiphorese Gel 30	1.3 ml	5.0 ml
Tris-HCl buffer	2.5 ml of 0.5 M Tris-HCl pH 6.8	2.5 ml of 1.5 M Tris-HCl pH 8.8
10 wt% SDS	0.1 ml	0.1 ml
10 wt% APS	65 µl	65 µl
TEMED	15 µl	15 µl

Prior to purification, samples were denatured at 95 °C for 10 min and mixed with 5x loading buffer (30 vol% glycerol, 10 vol% SDS, 200 mM Tris-HCl pH 6.8, 10 mM 2-mercaptoethanol (MCE), 0.5 wt% bromphenol blue) to a final concentration of 20 vol%. The gels were run in an electrophoresis chamber, which was filled with 1x running buffer (200 mM glycine, 0.5 wt% SDS, 25 mM Tris-HCl pH 8.3), for 60 min under a voltage of 180 V. After electrophoresis, the gel was stained using a staining solution for 15 min (0.1 wt% Coomassie G-250 in 50 vol% methanol and 10 vol% acetic acid). The protein bands were visualized using different destaining solutions (solution 1: 50 vol% methanol and 10 vol% acetic acid; solution 2: 10 vol% methanol and 10 vol% acetic acid) until the bands were clearly visible. The logarithmic molar mass log(MW) of the reference proteins over the relative mobility (R_f) was modeled linearly, resulting in equation 2-2, with a coefficient of determination R^2 of 0.995.

$$\log(MW) = 0.147cm^{-1} \cdot R_f + 1.110 \tag{2-2}$$

with

MW = molecular weight/ kDa

R_f = relative mobility/cm

2.2.3 Small-scale laccase-catalyzed and spontaneous dimerization reaction

The investigation of enzyme mediated reactions and spontaneous reactions were carried out in a reaction vessel with a capacity of 2.0 mL, using a reaction volume of 1.0 mL. The pH value of the reaction system was buffered by citric acid-phosphate buffer, according to McIlvaine [143]. The amine donor, NAcDAP, was diluted in deionized water and transferred into reaction vessel with a final concentration of 5 mM. The catechol donors were dissolved in 100 vol% ethanol at 10 mM and transferred into the reaction vessel with a final concentration of 1 mM, introducing a minimum of 10 vol% of ethanol to the final reaction mixture.

After addition of laccase from *C. unicolor*, the reaction was carried out in a temperature controlled thermoshaker (25 °C). The reaction vessels were kept in the dark to avoid photo-oxidation. Furthermore, the vessels were not closed to allow oxygen to enter the reaction mixture. The enzymatic reaction was stopped with 2 mg mL^{-1} of sodium azide of a stock solution (200 mg mL^{-1}), which as an inhibitor has a negative effect on the electron transport of laccase [144]. Immediate cooling with ice water was intended to suppress possible chemical secondary reactions. The reaction mixture was analyzed using HPLC-MS analysis (see section 2.2.7).

2.2.4 Parametric optimization of NAcDAP and PCA dimerization

In this work, the product concentration during the laccase-catalyzed reaction of PCA with NAcDAP was optimized. The parameters including the selected specifications are summarized in Table 2-2. The selected parameter range of the buffer corresponds to the range in which the laccase from *C. unicolor* is active. The ethanol concentration was varied between 10 vol% and 50 vol%. The lower limit of ethanol is necessary because of PCA solubility and the upper limit reflects the ethanol content in which the lignin fraction of the OS-process is present (see chapter 4, section 4.1.2). The upper limit of temperature variation was chosen because polymerization should take place, if possible, without a large input of energy (such as at room temperature). At a temperature below 15 °C, the activity of laccase from *C. unicolor* is so low that no products are expected after 60 min reaction time, which is the reason for the lower temperature limit. The change in shaking speed allows conclusions to be drawn about the influence of the oxygen input on the product formation. Since the concentration of NAcDAP was kept constant at 2 mM, the influence of the substrate ratio could be investigated by varying the PCA concentration from 1:20 to 5:1.

Table 2-2: Parameter variations for optimization of laccase-catalyzed Michael-type addition. NAcDAP content: 2 mM, laccase from *C. unicolor* (0.0287 g L^{-1}). Reaction in an open reaction vessel (2mL) in a thermoshaker, reaction time: 60 min

Parameter	[unit]	Specifications
pH of citric acid phosphate buffer (300 µL)	[-]	4 / 5 / 6 / 6.5 / 7
PCA concentration	[mM]	0.1 / 1 / 2 / 5 / 10
Ethanol concentration	[vol%]	10 / 20 / 30 / 40 / 50
Temperature	[°C]	15 / 20 / 25 / 30
Shaking speed	[rpm]	0 / 500 / 1000

2.2.5 Sample preparation for HPLC and HPLC-MS analysis

In preparation of HPLC and HPLC-MS analysis, the samples were dilution with methanol in a ratio of 1:1, so that the analyte and the eluents used were in the same solvent. This mixture was then sterile-filtered using a polytetrafluoroethylene (PTFE) filter.

The samples were filtered and analysis was carried out according to section 2.2.6, whereby each sample was analyzed twice in HPLC analysis. The area of the product peak from the HPLC measurement was used as an indicator for product formation. Furthermore, the relative peak area was calculated, which allowed maximizing the product formation while minimizing side product formation.

2.2.6 High-performance liquid chromatography (HPLC) analysis

A Waters HPLC-System was used in combination with a Waters 2996 photodiode array detector between 190 nm to 700 nm. A reversed phase C_{18} column was used at 30 °C with a flow of 0.5 mL min^{-1} (resulting in approximately 190 bar pressure). First, the column was equilibrated for 15 minutes with 80 vol% buffer A (0.1 vol% formic acid in deionized water) and 20 vol% buffer B (0.1 vol% formic acid in methanol). Following, 50 µl of sample was injected into the HPLC. After 10 minutes of isocratic flow, the gradient towards 100 vol% buffer B started. After 20 minutes, 100 vol% buffer B was reached and isocratic flow was continued for 5 minutes.

HPLC analysis was used to quantify product formation by integrating the product peak. Since the product under investigation, a dimer of NAcDAP and PCA, was not isolated and not commercially available, no analytical method with an internal standard could be used for the exact determination of the quantity. Thus, by determining the peak area, only an ordinal quantification was performed.

The area integration of the peaks was software supported by the Empower 2 Software©. Samples were prepared for HPLC analysis in the same way as for HPLC coupled mass spectroscopy (MS) analysis (see section 2.2.6). The retention time of the respective product and educt peaks, as well as the corresponding mass to charge (m/z) ratios, were determined by HPLC-MS analysis (see section 2.2.7). The product peak showed a characteristic maximum at approximately 311 nm (slight variation of the peak maximum when the pH value changes). The comparison of the chromatograms, resulting from an HPLC-MS analysis and an HPLC analysis is shown as an example in the appendix (see Figure 8-3). For analysis the area of the product peak at 311 nm, as well as the total are of all peaks between 10 min and 35 min at 280 nm, were calculated. For product optimization the peak area at 311 nm was analyzed, as well as the relative peak area of the area at 311 nm divided by the sum of all peaks at 280 nm. The data was analyzed using the software Microsoft Excel with the Add-On of XLSTAT by Addinsoft.

2.2.7 HPLC-MS spectroscopy

The HPLC unit (see section 2.2.6) was coupled with an electrospray ionization (ESI) Quattro LC, resulting in an increased retention time of approximately 0.5 min. The molar mass was detected using electrospray ionization (ESI) under a nitrogen flow of 800 L h^{-1}. For positive (ESI+) as well as negative ionization (ESI-), the source block temperature was 100 °C, the desolvation temperature 450 °C, the capillary potential 3.5 V and the cone voltage of 20 V. Fragments between 100 and 1000 g mol^{-1} were analyzed.

HPLC-MS was used to identify the mass of laccase-catalyzed heteromolecular product. Therefore, background measurements of the one-component systems under consideration were carried out without the addition of laccase. Following, the chromatograms of the pure substances, catalyzed by laccase from *C. unicolor,* were used for comparison. The aim was to determine which homomolecular products of the pure substances were formed during the reaction with laccase in the absence of an additional reaction partner. Lastly, heteromolecular products were identified by the comparison of the background data (no laccase), the homomolecular products and the data from the reaction containing two reaction partners. A detailed description of the analysis of the HPLC-MS data for product identification is provided in the appendix (see section 8.4), using the example of PCA and NAcDAP dimerization.

2.3 Results and Discussion

Biochemical reactions offer alternatives to the use of toxic chemicals and the requirement of special reaction conditions. Laccases are versatile catalysis which are well suited for the conversion of catechols for the development of mussel mimicking adhesives and were selected for further analysis.

Many laccase substrates, such as catechols or lignin, require the addition of solvents for facilitated solubility or prolonged storage. Furthermore, adhesives are often formulated using organic solvents [145]. Due to its low toxicity and well studied recyclability [146], ethanol was selected as the preferred solvent in this work. Consequently, solvent stable laccases, with a focus on stability towards ethanol, were investigated and the results are discussed in section 2.3.1. Following, solvent stable laccases were identified, expressed, purified and characterized. These results are discussed in section 2.3.3 and 2.3.4. Thereafter, the laccase-catalysed conversion of catechols is discussed in section 2.3.5, focussing on the laccase mediated C-N bond formation between catechols and primary amines. In section 2.3.6, the model to investigate the influence of the pH value and the primary amine's pKa value for the C-N bond formation between the amine and the catechols is discussed. Lastly, in section 2.3.7, the most significant reaction parameters are outlined.

2.3.1 Review of ethanol stable laccases

Using the online enzyme database BRENDA (www.brenda-enzymes.org), ethanol stable laccases were identified. In order to be able to recycle the enzyme, long-term stability towards solvents was desired. Furthermore, the enzyme, as well as the production host, were supposed to be commercially available and not genetically modified.

Huang et al. (2011) describe the overexpression and characterization of a thermostable, pH-stable and organic solvent-tolerant *Ganoderma fornicatum* 0814 (American Type Culture Collection – ATCC 76536) laccase in Pichia pastoris [147]. Even though the laccase rLac1 retained more than 80 % activity in 50 vol% ethanol after 3 h of incubation at 25 °C, this laccase was not commercially available. For laccases from *T. versicolor* a remaining activity of 40 % was documented after 14 days in 25 vol% ethanol [148, 149]. Chen et al. (2012), however, described 84.8 % of remaining enzyme activity for a laccase form *Cerrena* sp. WR1, an isolate from the botanical garden in Taiwan, after 14 days in 25 vol% ethanol [138, 150]. The fact that this laccase was commercially available and that the non-modified production host was available from the company Jena Bioscience, as well as the reported long-term stability against ethanol made this laccase the most interesting candidate. The laccase from *C. unicolor* was previously described as temperature stable and showed a wide pH stability. The temperature optimum was reported to be 70 °C (with regards to syringol) [149] and 60 °C (with regards to syringaldazine [151] or ABTS (2,2′-azino-bis(3-ethylthiazoline-6-sulfonate)) [138]). Michniewicz et al. (2006) found two isoforms of the laccase (Lacc I and Lacc II). The pH-optima for Lacc I were always lower than those of Lacc II [138]. The activity maxima of Lacc I was 3.5 towards DMP (2,6-dimethoxyphenol [152]) and 4.5 towards syringaldazine, while the pH optima of Lacc II were 4.5 towards DMP and 5.5 towards syringaldazine. The highest activities for ABTS were obtained at the lowest pH values tested (pH 2.5–3); with increasing pH, the activity decreased constantly [138].

2.3.2 Stability of laccases from *C. unicolor* towards ethanol

In order to confirm the laccase’s stability towards ethanol, the short-term (short exposure) and long-term (exposure for several weeks) stability of laccases from *C. unicolor* towards ethanol was investigated here.

In order to investigate the short-term stability towards ethanol, the enzyme activity of laccases from *C. unicolor* and *T. versicolor*, purchased from Jena Bioscience and Sigma Aldrich, were tested for their ethanol stability. The short-term stability towards ethanol was investigated by comparing the enzyme activity at 50 vol% ethanol. It was found that at the laccase from *C. unicolor* remained 40 % ± 1.4 % of its initial activity, while the laccase from *T. versicolor* retained only 5.0 %± 0.3 % of its initial activity. Therefore, the laccase from *C. unicolor* was favoured over the laccase from *T. versicolor* for applications at high ethanol concentrations.

Sustainable processes require the recyclability of the enzyme used. Therefore, the long-term stability of laccases from *C. unicolor* (purchased) was determined in regards to the pH value and storage temperature, as well as the ethanol concentration. No loss of activity was observed for *C. unicolor* laccases when stored for 40 days at pH 6.5 and 4 °C, even in the presence of 50 vol% ethanol. Storage at room temperature or in an acidic environment, however, reduces the activity of the laccase steadily. After 40 days of storage at room temperature (25 °C), pH 6.5 and 50 vol% ethanol, about 15 % of activity remained. After 40 days of storage at pH 4.5 (and 4 °C) and 50 vol% ethanol about 40 % of initial activity remained.

In conclusion, it was shown that laccases from *C. unicolor* are stable towards high ethanol concentrations (up to 50 vol%), even after long-term storage (47 days). Storage at low temperatures and higher pH values (such as pH 6.5) are favoured over storage at room temperature and pH 4.5. Laccases from *C. unicolor* are solvent stable laccase, well suited for processes which use ethanol containing solutions.

2.3.3 Expression and purification of laccases from *C. unicolor*

The availability of solvent stable laccases, non-dependent on a supply chain, was an important topic of this work. Therefore, a cultivation and purification protocol was implemented. The cultivation protocol was adjusted from literature [138, 139] (see section 2.2.1). Since the long-term stability of *C. unicolor* at pH 6.5 was significantly better than at pH 4.5 (see section 2.3.2), the initial pH of the cultivation medium was investigated for optimization of laccase expression. An initial pH of 4.5 (commonly used in literature [139]) was compared to an initial pH of 7. The latter reaction approach was buffered using a calcium carbonate buffer (200 mM), whereby the pH stayed constant at pH 7 throughout the cultivation process. The fermentation curves are shown in the appendix (see Figure 8-1). For the cultivation at pH 4.5, the initial pH dropped from 4.5 to approximately 4 within the first 9 days of cultivation. For the buffered cultivation, the added glucose (13 g L^{-1}) was completely consumed after 28 days of cultivation, whereas the cultivation at pH 4.5 needed 50 days. While the buffered cultivation did not show significant enzyme production, in contrast, for the cultivation with an initial reaction pH of 4.5, the enzyme production and secretion started (measured as activity of the supernatant) after 28 days of fermentation, reaching an enzyme activity of almost 0.06 U ml^{-1} after 50 days of cultivation.

It was previously reported that the pH of the expression medium had a significant influence on the extracellular laccase activity. The optimal pH of the culture medium for the production of laccases from *T. versicolor* was pH 5.2 [153] and 7 for *T. versicolor* expressed in *Pichia pastoris* [154]. The optimal initial pH obtained for *Ganoderma sp.* [155, 156] and *Pleurotus sajorcaju* [157] was pH 6. In section 2.3.1, it was concluded that storage of laccases from *C. unicolor* at low temperatures and higher pH values (such as pH 6.5) is favoured over storage at room temperature and pH 4.5. This is contrary to the findings of the expression experiments, where a pH of 4.5 was found to be superior over a pH of 7 for the expression of laccases from *C. unicolor*. In summary, it was confirmed that the pH of the expression medium had a significant influence on the laccase production, however, further investigation of the pH range (3-7) of the culture medium is suggested. Following, the laccase from *C. unicolor* was purified according to section 2.2.1, after 50 days of cultivation at pH 4.5.

2.3.4 Characterization of purified laccases from *C. unicolor*

The purified laccase from *C. unicolor* was characterized. First, the protein size was determined using SDS gel electrophoresis (see section 2.3.4.1). Second, the pH optima of the purified laccase towards syringaldazine and PCA was investigated (see section 2.3.4.2). Lastly, the stability of the laccases towards ethanol and DMSO was determined in section 2.3.4.3.

2.3.4.1 Determination of protein size

After cultivation of *C. unicolor* and enzyme purification, the purification success was evaluated using a SDS page (see appendix, Figure 8-2). Three protein bands were identified with a size of 1) 62.4 kDa, 2) 57.2 kDa and 3) 45.0 kDa. While protein 1 and 3 seem to have a stronger intensity, protein 1 and 2 are likely attributed to the two isoforms of laccase (Lacc I: 64 kDa and Lacc II: 57 kDa) previously described by Michniewicz et al. (2006). Purified Lacc II was shown to exhibit higher activity towards ABTS, DMP and syringaldazine at higher pH values compared to Lacc I, whose pH optimum was shifted 1 to 2 pH units towards more acidic conditions [138]. A crude enzyme mix of both laccases was therefore expected to show a broad pH optimum.

The protein content was determined to be 0.11 g L^{-1} ± 0.02 g L^{-1}. The specific enzyme activity at pH 5.0 and pH 6.5 was 47.1 U mg^{-1} ± 0.2 U mg^{-1} and 53.8 U mg^{-1} ± 0.2 U mg^{-1} (10 µM syringaldazine at 530 nm and 25 °C), respectively.

2.3.4.2 Determination of protein content and pH optima of laccase from *C. unicolor*

The enzyme activity of purified laccase from *C. unicolor* was measured for the substrate syringaldazine. The pH-dependent detection of the enzyme activity of the purified laccase from *C. unicolor* showed a broad pH optimum of about 5.5 to 6.5 with a maximum at 6.0 (see Figure 2-5).

In preparation for the development of a catechol-chitosan (see chapter 3), the pH optimum of the laccase-catalyzed conversion of PCA was determined. For the conversion of PCA to 1,2-benzoquinone-4-carboxylic acid (BQA) a maximal conversion rate was detected for a pH of 5.5 (see Figure 2-6 A). Since the extinction coefficient was not known, only the relative enzyme activity was measured by comparing the absorption gain at 400 nm (see Figure 2-6 B). For PCA and syringaldazine, a broad pH optimum was shown, suggesting the presence of Lacc I and Lacc II.

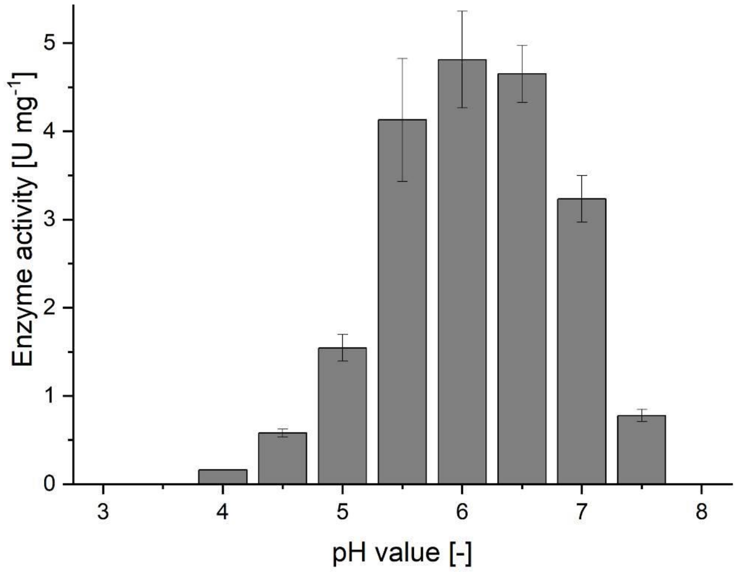

Figure 2-5: The pH-dependent enzyme activity of the purified laccase from *C. unicolor*. Substrate: 0.01 mM syringaldazine; λ=530 nm; 10 vol% McIlvaine buffer; 10 vol% ethanol. The error bars result from triplicates. The protein content was determined to 0.741 g L^{-1} ± 0.001 g L^{-1} by Bradford method.

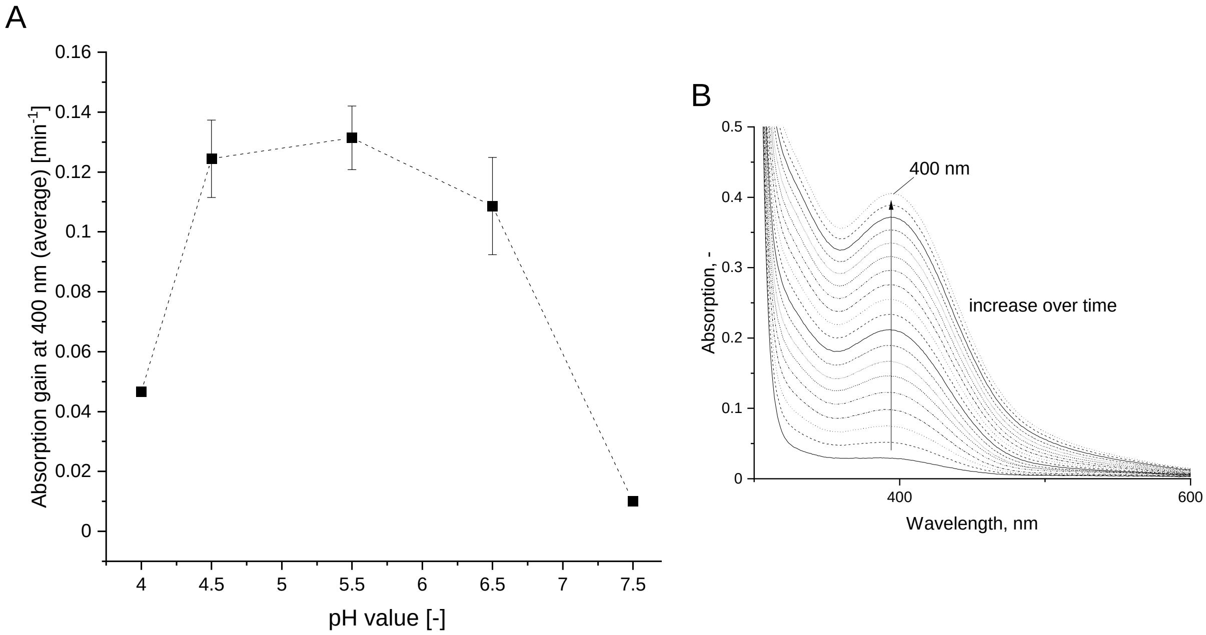

Figure 2-6: Activity of purified laccase from *C. unicolor* on the conversion of PCA. (A) The pH-dependent activity for 10 mM PCA in 0.1 M McIlvaine buffer. (B) Example spectrum for the formation of BQA from PCA over time in 15 s increments. The reaction progress was measured at 400 nm. The protein content was determined to 0.11 g L^{-1} ± 0.02 g L^{-1} by Bradford method. The error bars result from triplicates.

2.3.4.3 Stability towards solvents

The enzyme stability of laccase from *C. unicolor* was measured towards the solvents ethanol and DMSO. The influence of ethanol and DMSO on the enzyme activity of laccase from *C. unicolor* (towards syringaldazine) was measured between 0 vol% and

60 vol% ethanol. Without the use of a solvent (0 vol% ethanol or 0 vol% DMSO), syringaldazine was almost insoluble, whereby enzyme activity of laccase was almost not measurable. The highest enzyme activity was measured at 10 vol% ethanol (2.2 U mg^{-1} ± 0.4 U mg^{-1}). By incremental increasing of the ethanol concentration, the enzymatic activity decreased. At a concentration of 20 vol% ethanol about 86 %, at 30 vol% ethanol 88 %, at 40 vol% ethanol about 63 %, at 50 vol% ethanol 39 % and at 60 vol% ethanol 22 % initial enzyme activity were left.

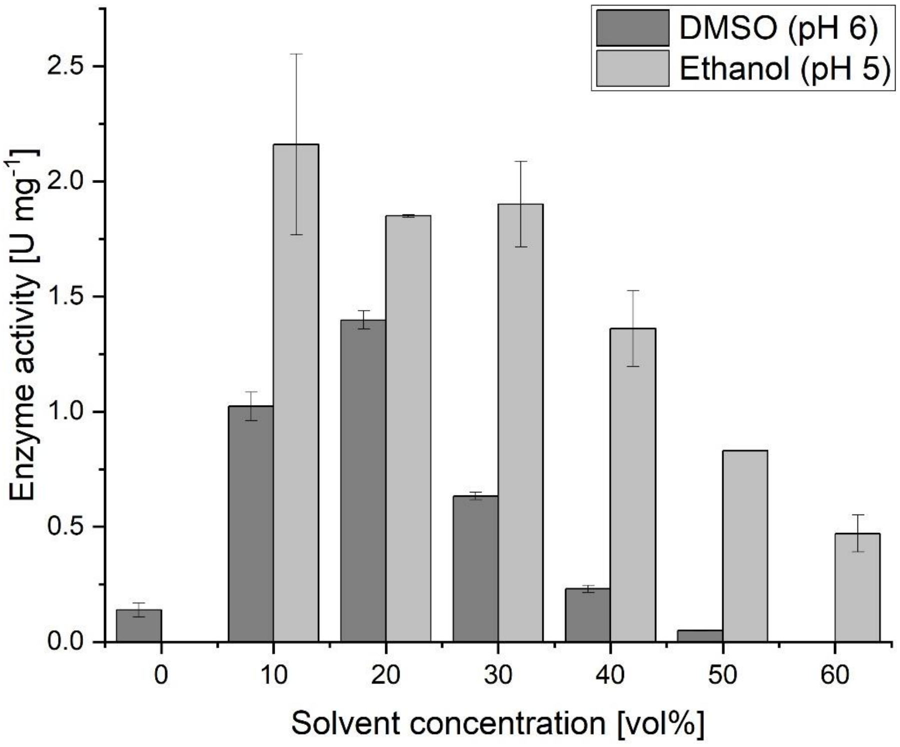

Figure 2-7: Solvent stability of laccase from *C. unicolor* towards DMSO (measured at pH 6) and ethanol (measured at pH 5). Substrate: 0.01 mM syringaldazine; λ = 530 nm; 10 vol% McIlvaine buffer. The error bars result from triplicates. The protein content was determined to 0.741 g L^{-1} ± 0.001 g L^{-1} by Bradford method.

For DMSO, the highest enzyme activity was measured at 20 vol% DMSO (1.40 U mg^{-1} ± 0.04 U mg^{-1}). It was found that at a concentration of 40 vol% a lag phase of approximately 30 s and at 50 vol% of approximately 60 s was present. The presence of lag phases for enzymatic reactions was previously reported for reactions of chloroperoxidases in DMSO [158], where the authors suggested that a first-order degradative process occurred during the lag phase.

In conclusion, laccases from *C. unicolor* were expressed and purified successfully. Using SDS-PAGE, three protein bands were identified between 45 kDa and 62.4 kDa, confirming previous findings [138]. The purified laccase from *C. unicolor* showed a broad pH optimum of about 5.5 to 6.5 with a maximum at 6.0 towards syringaldazine and 5.5 for the conversion of PCA to BQA. The investigation of its solvent stability found that the highest enzyme activity was measured at 10 vol% ethanol (using syringaldazine as substrate) and at 20 vol% DMSO.

2.3.5 Laccase-catalyzed reaction with model compounds

The determination of the reaction progress for the functionalization of natural polymers (such as chitosan or lignin) can be challenging due to their complexity. The use of model compounds is a common method for the investigation of possible reactions and their mechanisms.

Chitosan contains primary amine groups that can function as anchoring sites for catechol groups. In this work, the primary amines L-lysine, diaminopentante (DAP) and NAcDAP (see Figure 2-8) were used as model compounds for the chitosan's primary amine group.

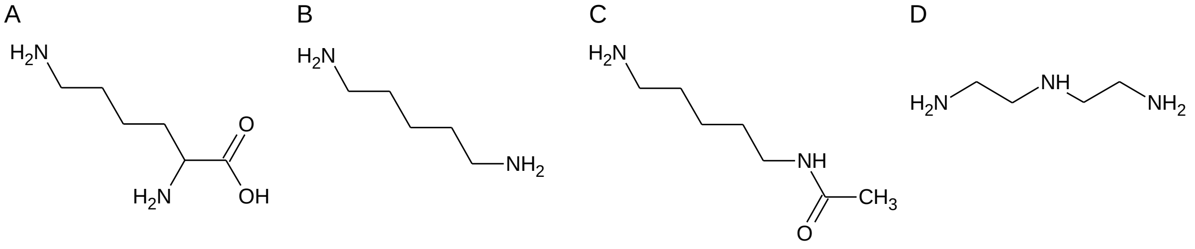

Figure 2-8: Chemical structure of the amines donors (A) L-lysine, (B) DAP, (C) NAcDAP and (D) DETA.

First, the attempt was made to react the primary amine L-lysine with the catechol donors PCA, DHC and caffeic acid (see Figure 2-1 B to D), as well as the lignin model compound vanillyl alcohol (see Figure 4-2 B). L-lysine is a primary amine and hence it can function as a model compound for chitosan, which is used as a backbone in chapter 3. Furthermore, L-lysine is an amino acid which is used as a feed supplement, whereby it is classified as a safe chemical compound which is available in large scale. Therefore, it is a great anchor molecule between a natural polymer such as lignin and a catechol group, forming a catechol-lignin adhesive using a two-step process (see chapter 4, section 4.1.4). The laccase-mediated reactions were conducted at pH 4, 5, 6 and 7 and analyzed using HPLC-MS. For non of the tested compounds the expected dimers were detected (data not shown). However, larger compounds with m/z ratios larger 490 were detected. Hence, it was concluded that both amine groups of the L-lysine react and that L-lysine reacts further with the dimers to form trimers and polymers, as shown in literature [75]. Similar experiments were completed using DAP and PCA. Similarly, to L-lysine, no dimeric products were found, only trimers and polymers (data not shown). In order to avoid the polymer formation, NAcDAP was used as a primary amine instead.

NAcDAP is a derivate of L-lysine, but one amine group is masked by an N-acetyl, making polymer formation less likely. The laccase-catalyzed and spontaneous formation of C-N bonds between a primary amine and a catechol was investigated using the model compounds DHC and PCA as catechol groups together with NAcDAP as primary amine. For the purpose of differentiating between enzyme mediated reactions from spontaneous reactions, single component reactions (without enzyme) were performed and analyzed via HPLC-MS (see section 2.2.7). To identify intermolecular bonds between different molecule types, HPLC-MS analysis of enzyme catalyzed conversions of the single components were conducted and used as comparison. Hence, the reaction mixtures were analyzed prior to and after enzyme incubation, using HPLC-MS analysis. A detailed description of the analysis of the HPLC-MS data for product identification is provided in the appendix, section 8.4. Figure 2-9 gives an overview of the possible molecule structures after the enzymatic reaction. The mass spectroscopy coupled behind the UV-vis detector led to increased retention times of approximated 0.5 min. The UV-vis and mass spectroscopy results were presented in pairs with the retention time from the mass spectrometer presented in parentheses. For NAcDAP, a retention time of 2.51-2.93 min (no mass spectroscopy data recorded), as well as a minor peak at 7.36 min (7.74 min) with a mass of 144 g mol^{-1} (ESI+:145, no ESI-) was found. The enzyme incubation did not notably change the spectra. Hence, it was concluded that NAcDAP was not a substrate for the enzyme.

For the substrate PCA, a peak was found with a retention time of 8.59 min (8.97 min) and a mass of 154 g mol^{-1} (ESI-:153, ESI+: 137). The observed delta of 18 g mol^{-1} in the ESI+ spectra results may have resulted from the cleavage of the OH-group (see Figure 2-9 shows a possible structure). After 60 minutes of PCA incubation with the enzyme, a new peak at 10.56 min (10.95 min) appeared with a mass of 140 g mol^{-1} or 168 g mol^{-1} (ESI+: 141 and 169, no ESI-), the expected quinone structure of 152 g mol^{-1} was only observed in small quantities. Consequently, it was concluded that the quinone reacts further, forming C-C or C-O-C bonds which cleave into fragments of 140 g mol^{-1} or 168 g mol^{-1} during MS analysis. For the laccase-catalyzed reaction of

PCA with NAcDAP at pH 5, a strong peak was found at 17.77 min (18.13 min) with a mass of 296 g mol^{-1} (ESI+: 297, ESI-:295). The structure corresponds well with a C-N connected dimers of PCA and NAcDAP (a possible structure is given in Figure 2-9), forming an aromatic secondary amine, which confirms previous findings [75].

After 24 hours of non-enzyme catalyzed incubation of PCA with NAcDAP at both pH 5 and pH 8, no corresponding dimer peak was detected. Accordingly, no spontaneous reaction was detected between PCA and NAcDAP.

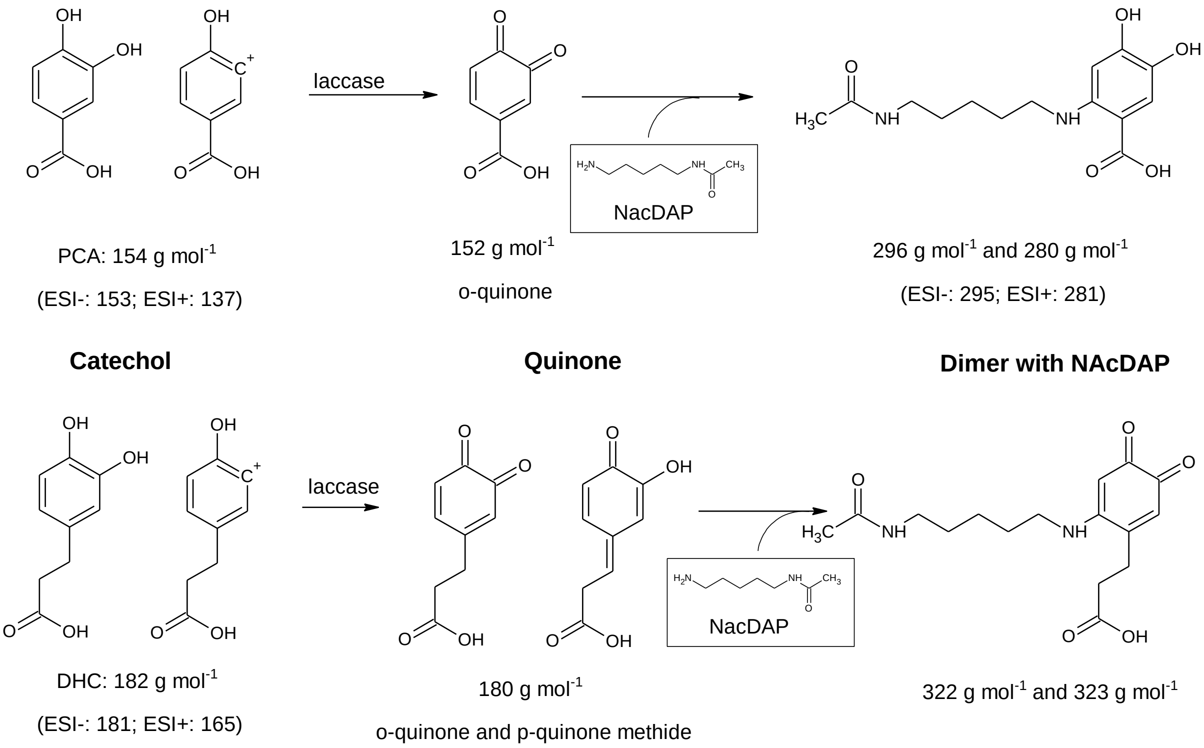
laccase
NacDAP
PCA: 154 g mol-1
(ESI-: 153; ESI+: 137)
152 g mol-1
o-quinone
296 g mol-1 and 280 g mol-1
(ESI-: 295; ESI+: 281)
Catechol
Quinone
Dimer with NAcDAP
laccase
NacDAP
DHC: 182 g mol-1
(ESI-: 181; ESI+: 165)
180 g mol-1
o-quinone and p-quinone methide
322 g mol-1 and 323 g mol-1

Figure 2-9: Proposed chemical structures of PCA and DHC and their laccase-catalyzed intermediate products and dimers with NAcDAP. The molar mass of each structure is provided together with the m/z-ratios, which were detected using HPLC-MS analysis. Reaction conditions: 20 mM PCA, 2 mM NAcDAP, purified laccase from *C. unicolor*, 1 mL reaction volume, 10 vol% ethanol, 60 min reaction time for enzyme catalyzed reactions and 24 hours for non-enzymatic reactions, T = 28.5 °C.

For the substrate DHC, a peak at 14.6 min (15.4 min) with a mass of 182 g mol^{-1} (ESI-:181, ESI+: 165) was detected. After enzymatic incubation, several new peaks were detected: 1) 13.58 min (13.99 min) with a mass of 180 g mol^{-1} (ESI-:179, ESI+: 181); 2) at 20.04 min (20.40 min) and 3) 21.34 min (21.75 min). For peak 2 and 3 various masses were found, which indicate multiple product formation. Identification was not possible via mass spectroscopy. For the laccase-catalyzed reaction of NAcDAP and DHC, again, several new peaks were observed: 1) 12.16 min (12.47 min) with a mass of 180 g mol^{-1}, 2) 16.23 min (16.61 min) and a mass of 322 and 323 g mol^{-1} (ESI+: 323, 324, ESI-:321, 322) and 3) 20.44 min (20.74 min) (no plausible mass detected). Peak 2 likely corresponded to the proposed dimer between DHC and NAcDAP (see Figure 2-9). In contrast to the non-enzymatic incubation of PCA with NAcDAP, for DHC a dimer peak was found which seemed to form spontaneously. The mass of 322 or 323 g mol^{-1} was also found for the non-enzymatic incubation of DHC with NAcDAP at a pH above 5. At pH 5.8, 6.2 and 8.2 increasing amounts of the dimer were detected.

For the laccase-catalyzed reaction of PCA with NAcDAP an aromatic amine with a molar mass of 296 g mol^{-1} was proposed. Both structures suggested a functional catechol group. However, the mass of 322 or 323 g mol^{-1} detected for DHC with NAcDAP, corresponded better with the oxidized form of the catechol, than with the catechol itself.

Even though PCA and DHC have similar compositions (both are catechols with a carboxylic side chain) the product formation was quite different. While PCA only seemed to form C-N bonds with NAcDAP after laccase-catalyzed reaction, for DHC also spontaneous formation of dimers were observed. The catalysis with enzyme led to a broad spectrum of products, which was unfavourable for a specific reaction. DHC was more reactive and less stable. Since the non-oxidized form of the catechol was necessary for the formation of a strong catechol adhesive, DHC appeared to be less suitable as a catechol donor. In section 2.3.6, a model, which was created for homomolecular C-N bond formation (see section 2.1.3), was adapted for the heteromolecular C-N bond formation. The model was applied to investigate the influence of the pH value and the primary amine’s pKa for C-N bond formation to catechols.

2.3.6 Influence of the pH value and the primary amine’s pKa for C-N bond formation to catechols

The HPLC-MS analysis of C-N formation between the model compounds DHC, PCA as catechol groups and NAcDAP as primary amine had shown that the choice of catechol influences the reaction outcome. While DHC was more reactive and able to form spontaneous C-N bonds to NAcDAP, it also produced a large amount of side products. In contrast to DHC, PCA was only able to form C-N bonds to NAcDAP, after enzymatic activation. Next to the origin of the catechol donor, the primary amine used had a major impact on the reaction rate. Based on the model proposed by Garcia-Carmona et al. (1982) (see section 1), in this work an adjusted model for the formation of intermolecular C-N bonds was created.

The pH of the reaction mixture and the pKa of the primary amine played a key role in the formation of intramolecular C-N bonds [76]. Due to the similar molecular structure, it was assumed that pH and pKa also play a key role in intermolecular C-N bond formation between primary amines and catechols. The adjusted model for the intermolecular C-N bond formation is shown in Figure 2-10. The formation of quinones from catechols was catalyzed by the enzyme tyrosinase or laccase as well as due to auto-oxidation (step 1). The specific rate constants k_1 and k_{-1} are dependent on the pKa value of the primary amine (step 2). Kramer et al. (2001) proposed, laccases form o-quinones and p-qinone methides [111]. The quinone methides form zwitterionic valence bond structures explain the formation of aromatic amines as well as amides (step 3).

The rate k_c is the specific rate constant for the intermolecular formation of an aromatic, secondary amine between a catechol and an amine. From equation 2-1 it was established that a high pH of the reaction medium and a low pK_a of the primary amine is favourable for the formation of C-N bonds. For reactions, where the pH value is smaller than the pK_a value of the primary amine, $\frac{1}{k}$ approaches infinity; hence the reaction rate is quite slow. For reaction mixtures with a pH equal to the pK_a of the primary amine, the term $\frac{1}{K_a \cdot k_c}[H^+]$ approaches $\frac{1}{k_c}$. The equation can therefore be simplified to $\frac{1}{k} \approx \frac{1}{k_c} + \frac{1}{k_1}$. Hence, the reaction rate becomes independent of the pH value. If the pH value is larger than the pK_a of the primary amine, the term can be simplified to $\frac{1}{k} \approx \frac{1}{k_1}$.

HPLC-MS analysis of the non-enzymatic incubation of DHC with NAcDAP at a pH above 5 has found a formation of a DHC-NAcDAP dimer. The observation that at pH 5.8, 6.2 and 8.2 increasing amounts of the dimer were detected, are in agreement with this adjusted kinetic model. An increase of the pH led to a decreased concentration of H^+ ions and therefore increased the reaction rate k.

Next to a high pH, a low pK_a value of the primary amine should be favourable for the conversion rate. If a primary amine is used with a K_a value of 10^{-5} to 10^{-7} M (at a neutral pH), the pH of the reaction medium could be more or less neglected. Most primary amines have high pK_a values of 9 or above, contrarily, chitosan has a pK_a value of 6 to 7. Consequently, spontaneous reaction with chitosan was expected at neutral or slightly acidic pH values.

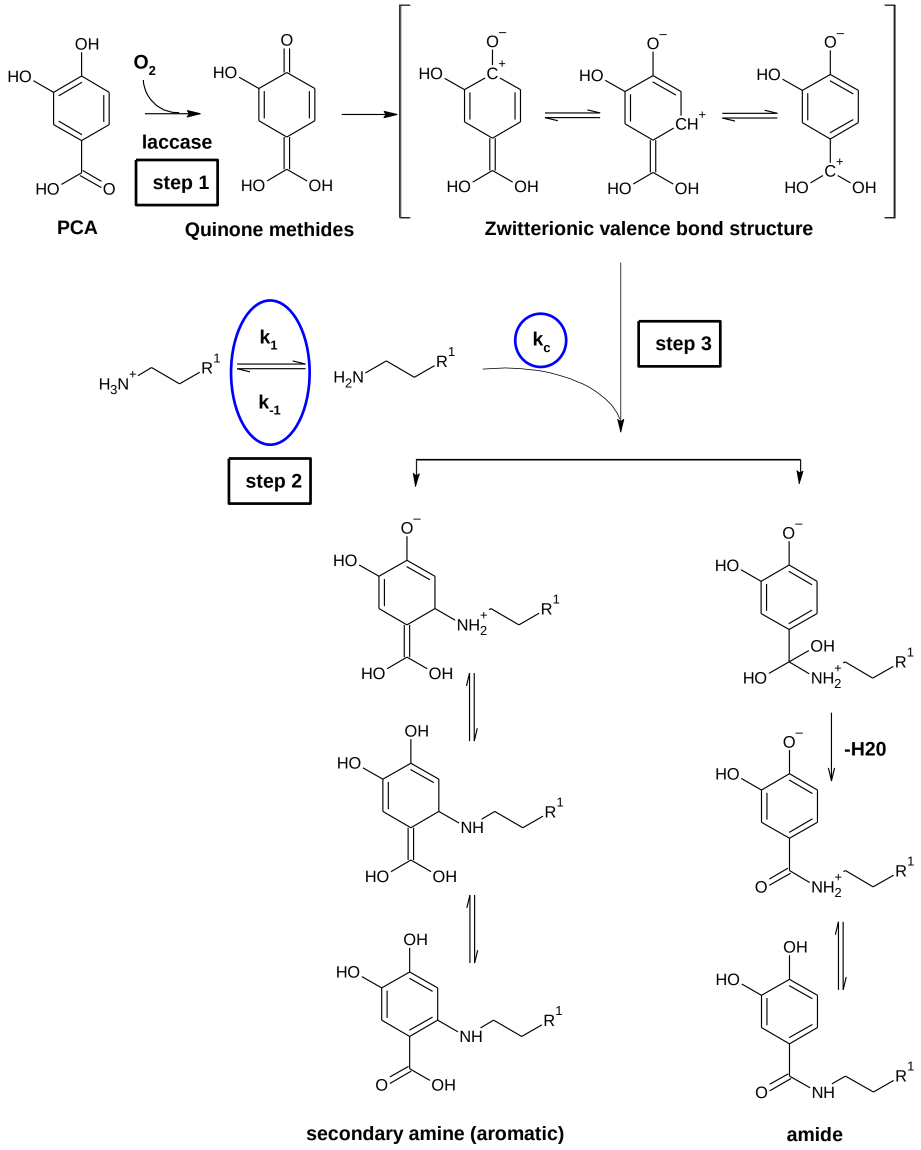

Figure 2-10: Reaction model for the formation of intermolecular C-N bonds between primary amines and PCA. Laccases initiate the formation of quinone methides by activating the catechol (step 1) [159]**. The specific rate constants k_1 and k_{-1} are dependent on the pKa value of the primary amine (step 2). The quinone methides form zwitterionic valence bond structures form aromatic amines as well as amides (step 3). The specific rate constant k_c is temperature dependent.**

2.3.7 Optimization of C-N formation between PCA and NAcDAP

After the investigation of C-N bonds between PCA and DHC with NAcDAP (see section 2.3.5) and the investigation of influence of the pH value and the amine's pKa value (see section 2.3.6), the dimerization of PCA and NAcDAP was further investigated and parametrically optimized. First, the influence of the pH value on the PCA and NAcDAP dimerization was investigated using HPLC-MS analysis (see section 2.3.7.1). It was noted that the ethanol and PCA concentration influenced the effective pH value in the solution, therefore, in section 2.3.7.2, a linear regression for the effective pH value was calculated. Thereafter, the reaction parameters ethanol concentration, PCA concentration, pH value, temperature and shaking speed (which reflects the oxygen availability) were investigated for the product formation of the PCA and NAcDAP dimerization (see section 2.3.7.3). Using linear and nonlinear models, the product-maximizing reaction conditions were investigated in section 2.3.7.4. Two data sets were used to first calculate several linear and nonlinear models and afterwards to validate the different models.

2.3.7.1 The pH dependency of PCA and NAcDAP dimerization

The influence of the pH value on the PCA and NAcDAP dimerization was investigated using HPLC-MS analysis. As shown in section 2.3.5, the laccase-catalyzed Michael-type reaction was dependent on the pH of the reaction medium. For the reaction of PCA and NAcDAP dimer formation, at pH 5, 6 and 7 with a m/z ratio of 295 (ESI-) and an elution time of about 19.38 min, was found, which, however, decreased as the pH value decreased (see Figure 2-11).

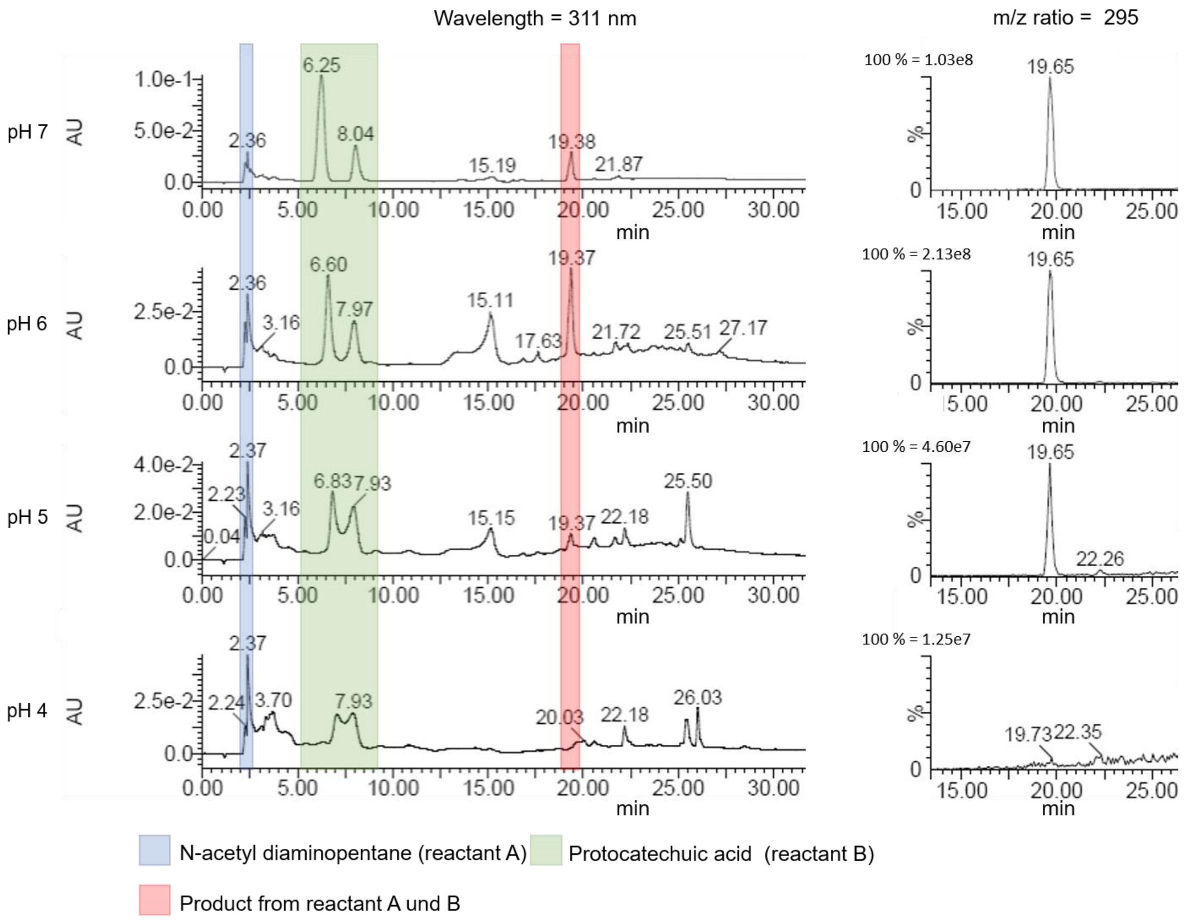

Figure 2-11: Chromatograms of the reaction of NAcDAP and PCA catalyzed by laccase from *C. unicolor* at pH 4, 5, 6 and 7, recorded at 311 nm. Right: mass trace of the dimer at m/z = 295 (ESI-). Reaction conditions: 5 mM PCA, 1 mM NAcDAP, 0.028 g L^{-1} laccase from *C. unicolor*, 1 mL reaction volume, 10 vol% ethanol, 60 min reaction time, T = 25 °C. Note: The selected ratio with an amine excess of 5:1 has been shown in the literature to be the ratio with the largest product formation and the lowest by-product formation [128].

At a pH value of 4, no more dimer formation was observed. One explanation for this is a shorter lifetime of the activated catechol groups due to reduction, which is favoured by the low pH value. A similar effect was observed for the stability of the p-benzoquinone free radical [160].

2.3.7.2 Influence of parameters on pH value

For the optimization of the C-N formation between PCA and NAcDAP, the pH value was set by using 30 vol% of McIlvaine buffer (pH 4 to 7). By adding different concentrations of PCA and ethanol to the solution, however, the resulting pH of the solution varied from the pH value set by the buffer. In order to decrease the effect of the pH shift which is caused by ethanol and PCA, the pH value of the solution (effective pH) was measured (before the addition of laccases) and a regression model was calculated. The effective pH value was correlated with the pH value of the buffer, the ethanol concentration and the PCA concentration. A linear regression with a coefficient of determination $R^2 = 0.9906$ and a confidence level of >99 % was found (see equation 2-3). The equation is valid for the fitted range of 0 vol% to 50 vol% ethanol, 0 mM to 10 mM PCA and a pH value of the McIlvaine buffer of 4 to 7. For further analysis, the effective pH value was used.

$$pH_{effective} = 0.641 + 0.014\,\frac{1}{vol\%}\cdot \mathrm{c(EtOH)} - 0.061\cdot \mathrm{c(PCA)}\,\frac{mol}{mg} + 1.003\cdot \mathrm{pH}_{buffer} \tag{2-3}$$

with

$pH_{effective}$ = effective pH value in dependency of the ethanol and PCA concentration and the pH of the reaction buffer/ -

c(EtOH) = ethanol concentration/ vol%

c(PCA) = PCA concentration/ mM

pH_{buffer} = potential of hydrogen (pH value) of McIlvaine buffer/ -

2.3.7.3 Influences of parameter variations on product formation

The C-N bond formation of PCA and NAcDAP is described as an enzymatic activation followed by a chemical dimerization reaction (see Figure 2-10). In order to investigate the effect of the pH value, the concentration of the catechol donor, the ethanol concentration, the temperature and the oxygen availability on the product formation, a parameter optimization was completed. The reaction of PCA and NAcDAP was completed and quantified using HPLC analysis (see section 2.2.6). The pH value was varied between 4 and approximately 8 (effective pH according to section 2.3.7.2), the PCA concentration between 0.1 mM and 10 mM, the ethanol concentration between 10 vol% and 50 vol%, the temperature between 15 °C and 30 °C and the shaking speed between 0 rpm and 1000 rpm. The specifications are summarized in section 2.2.4.

The aim of this optimization was to evaluate the influence of the selected parameters and to identify the reaction conditions which were optimal for product formation. Based on the parameter variations presented in section 2.2.4, two partial factorial experimental designs were created with the software Visual-Xsel© Version 13.0 (see appendix, section 8.5). The first experimental design consisted of 35 different parameter constellations (Exp. 1 to Exp. 35, see appendix, Table 8-3), whereby three reference experiments were carried out with average parameter values of the influencing variables (pH 5.5, 5.05 mM PCA, 30 vol% ethanol, 22.5 °C and 500 rpm) to evaluate the internal reproducibility. The analysis of the peak area was carried out in in duplicate, which was conducted at least 12 h later.

The initial 35 tests were then extended by a second series of 15 tests (Exp. 36 to Exp. 50, see appendix, Table 8-4), whereby the three reference tests were also carried out with the parameters already mentioned. In addition, the comparability of the two test series was checked by the reference tests. Based on the first test set, different models were calculated using Excel XLSTAT. The second test series (Exp. 36 to Exp. 50) were used to identify the best model. The reaction conditions of the two test series are listed in the appendix, section 8.5.

No product formation was detected after 60 min reaction time for all experimental approaches carried out at a concentration of 0.1 mM PCA or at a set pH value of 4. It was concluded that at a substrate concentration of 0.1 mM PCA, the reaction rate of the enzymatic reaction was so low that the product formation had not yet exceeded the detection limit. NAcDAP is not a substrate for laccase from *C. unicolor* (see appendix, Figure 8-4), whereas only PCA acts as a substrate for the laccase from *C. unicolor* in the present reaction mixture. The lack of product formation at a set pH value of 4 was explained by two possible phenomena. On the one hand, the activity of laccase from *C. unicolor* was reduced at pH 4, since the determined optimal pH for the conversion of PCA was 5.5 (see Figure 2-6). On the other hand, the laccase-activated intermediates of PCA were less stable at acidic pH values (such as 4) compared to a neutral pH value. Due to the protons available at acidic pH values the amount of quinone or semiquinone formed was reduced [160]. Therefore, the enzymatic reaction was not followed by further chemical reactions, and dimer or polymer formation did not occur. This effect also explains the tendency for higher product formation at neutral or slightly basic pH values. The combination of these two effects (low laccase activity and low product stability) explains the lack of product formation at pH 4.

In addition, further trends were identified from the results obtained in the first two test series. First, an increase of the product formation was observed with increasing reaction temperatures. This can be explained with the help of the Van't-Hoff's rule, which states that the reaction rate of a reaction approximately doubles with a temperature increase of 10 °C [161]. However, this rule can only be applied to a limited extent to enzymatic reactions, as the temperature tolerance of the enzymes must be taken into account. The temperature interval under investigation (15 to 30 °C) was within the tolerance range of laccase from *C. unicolor*, and therefore allowed the application of Van't Hoff's rule. In addition to the enzymatic reaction, the chemical reaction was also influenced by the temperature.

A few results showed, contrary to the trend just explained, a comparably high product formation despite a low reaction temperature. Exp. 6, for example, showed a product peak area of approximately 1.6 million units despite a reaction temperature of 15 °C. Here, however, in addition to the temperature, all other test conditions (such as the pH value and the ethanol content) were similar to the optimal conditions for laccases from *C. unicolor*.

Furthermore, higher product formation was observed at higher substrate (PCA) concentrations. This was explained by an increased enzyme activity and thus a faster conversion rate, as well as Le Châtelier's principle [162]. Clear trends regarding the optimal shaking speed and the optimal ethanol content were not directly evident from the results. In addition, it was concluded that control over only one parameter did not lead to high product formation, but always a combination of parameters. In contrast, low or no product formation was observed as soon as one parameter deviated strongly from the laccases' optimal parameters. Due to mutual interactions, a more advanced evaluation was required to determine the optimum parameter combination (see section 2.3.7.4).

For each test series, reference tests were conducted using the average test conditions (30 vol% ethanol, 5.05 mM PCA, 2 mM NAcDAP, 0.0287 g L^{-1} laccase from *C. unicolor*, pH 5.5, temperature of 22.5 °C, shaking speed of 500 rpm). Each test was completed in triplicate. Repeat measurement (also run in triplicate) were completed with a delay of at least 12 h (due to device occupancy). The mean value of the product peak area of the first and second test series were 489,608 ± 39,441 and 514,684 ± 56,826, respectively. The mean value of the product peak area of the repeat measurements for the first and second test services were 725,764 ± 54,521 and 669,550 ± 75,510. Hence, the standard deviation of the reference tests of each test set was between 8 % and 11 %, which indicates similar product peak areas of the respective reference tests of a test series. This indicated a good comparability and reproducibility within a test series. The deviation of the mean values of the product peak areas was 5.1 % for the first measurement sets and 11.3 % for the duplicate measurements, which again indicated good comparability of the two test series. An irregularity, which was seen in these results, is the difference in the product peak areas, which was found between the double determination offset by at least 12 h. The difference was 48 % for the first test set and 30 % for the second test set. These differences in the results of the first and second analytical measurement indicated that cooling down the reaction mixture and stopping the enzymatic reaction with sodium azide was not sufficient to suppress subsequent chemical reactions. It was presumed that the samples continued to react chemically between the two measurements, which was why a double or triple determination with subsequent averaging was not used for the analysis.

Furthermore, it was noticed that the difference between the first and second measurement fluctuated but was not constantly higher or lower. A trend was derived, whereby the reactions which showed a lower product peak in the second analytical measurement than in the first measurement were mainly carried out at temperatures of 25 °C or 30 °C. The reaction conditions of these experimental approaches were also otherwise close to the optimal conditions for laccase from *C. unicolor*. Thus, it was concluded that these reactions were completed after the 60 min reaction time. It was assumed that the resulting product was further chemically converted by degradation or subsequent reactions, which made the first analytical measurement higher than the second. Accordingly, it was assumed that the experimental approaches, in which the first analytical measurement was lower than the second, had not yet completely finished at the time of analysis. It was noticed that at least one experimental parameter deviated significantly from the optimal parameter settings, which explained the incomplete reaction. Accordingly, dimers still formed between the first and second measurement, which meant that a larger product peak area was detected in the second measurement than in the first measurement.

2.3.7.4 Determination of the product-maximizing reaction conditions

The dimerization of PCA and NAcDAP was identified as an enzymatic activation followed by a chemical dimerization reaction (see Table 2-3). The enzymatic activation of PCA, however, also led to the formation of a variety of side products (see appendix, Figure 8-5). For further analysis, the area of the product peak at 311 nm as well as the total area of all peaks between 10 min and 35 min at 280 nm were calculated. In order to minimize side product formation and to optimize product formation, the relative peak area at 311 nm divided by the sum of all peaks around 280 nm was analyzed. An advantage of using the relative peak area was, that the variation between the first and the second measurements (see section 2.3.7.3), is being corrected for. Different linear and nonlinear models were applied for the correlation of the relative peak area with the ethanol concentration, the concentration of PCA, the effective pH value, which was discussed in section 2.3.7.1, the temperature and the shaker speed (oxygen supply). The first dataset (Exp. 1 to Exp. 35) was used to create the model and the second data set (Exp. 36 to Exp. 50) was used to validate the model. The resulting models are shown in Table 2-3. While a more complex model could provide a higher determination coefficient, in this work the focus was set on generating a model that determined the strongest interactions between the different parameters.

Table 2-3: Linear and nonlinear models for the analysis of the relative peak area for dimerization of PCA and NAcDAP and the respective coefficients of determination. The influence of the ethanol concentration c(EtOH), the PCA concentration c(PCA), the pH value, temperature (temp) and the shaking speed (rpm) on the relative product formation (dimer area at 311 nm / sum of all peak areas at 280 nm) was investigated. The model parameters pr1 to pr9 are found in the appendix, Table 8-5.

Model	Function for the relative peak area (dimer peak area at 311 nm / sum of areas at 280 nm)	Determination coefficient (R^2)
#1	=pr6+pr1*c(EtOH)+pr2*c(PCA)+pr3*pH+pr4*Temp+pr5*RPM	0.566
#2	=pr6+pr1*c(EtOH)+pr2*c(PCA)+pr3*pH+pr4*Temp+pr5*RPM+pr7*c(EtOH)*c(PCA)+pr8*c(EtOH)*pH+pr9*c(PCA)*pH	0.780

Model	Function for the relative peak area (dimer peak area at 311 nm / sum of areas at 280 nm)	Determination coefficient (R^2)
#3	=pr6+pr1*c(EtOH)+pr2*c(PCA)+pr3*pH+pr4*Temp+pr5*RPM+pr7*Temp*c(PCA)+pr8*Temp*pH+pr9*c(PCA)*pH	0.811
#4	=pr5+pr1*c(EtOH)+pr2*c(PCA)+pr3*pH+pr4*Temp	0.565
#5	=pr6+pr1*c(EtOH)+pr2*c(PCA)+pr3*pH+pr4*Temp+pr5*RPM+pr7*c(EtOH)*Temp+pr8*c(EtOH)*pH+pr9*Temp*pH	0.578
#6	=pr6+pr1*c(EtOH)+pr2*c(PCA)+pr3*pH+pr4*Temp+pr5*RPM+pr7*c(EtOH)*Temp+pr8*c(EtOH)*c(PCA)+pr9*Temp*c(PCA)	0.638
#7	=pr6+pr1*c(EtOH)+pr2*c(PCA)+pr3*pH+pr4*Temp+pr5*RPM+pr7*c(PCA)*pH	0.745
#8	=pr5+pr1*c(EtOH)+pr2*c(PCA)+pr3*pH+pr4*Temp+pr6*c(EtOH)*c(PCA)+pr7*c(PCA)*pH+pr8*c(PCA)*Temp+pr9*c(EtOH)*pH	0.818
#9	=pr5+pr1*c(EtOH)+pr2*c(PCA)+pr3*pH+pr4*Temp+pr6*c(EtOH)*c(PCA)+pr7*c(PCA)*pH+pr8*c(PCA)*Temp+pr9*Temp*pH	0.800
#10	=pr5+pr1*c(EtOH)+pr2*c(PCA)+pr3*pH+pr4*Temp+pr6*c(EtOH)*c(PCA)+pr7*c(PCA)*pH+pr8*c(PCA)*Temp	0.800
#11	=pr5+pr1*c(EtOH)+pr2*c(PCA)+pr3*pH+pr4*Temp+pr6*c(EtOH)*c(PCA)+pr7*c(PCA)*pH+pr8*c(PCA)*Temp+pr9*c(PCA)^2	0.800
#12	Peak models : Gaussian = pr1*exp(-0.5*((c(EtOH)-pr2)/pr3)^2)	0.739
#13	Peak models : Lorentzian = pr1/(1+((c(EtOH)-pr2)/pr3)^2)	0.763
#14	pr5+pr1*c(EtOH)+pr2*c(PCA)+pr3*pH+pr4*Temp+pr6*c(EtOH)*c(PCA)+pr7*c(PCA)*pH+pr8*c(EtOH)*pH	0.779

Linear and nonlinear models

In Table 2-3 the models applied for the C-N bond formation between PCA and NAcDAP are summarized together with the determinations coefficients which were achieved for each model. First, a linear model without interactions between the parameters was applied (#1). The R^2 of 0.566 was low and it was found that the shaker speed (pr5=0) had little significance in the model (see also #4). Looking at two factor interactions between the ethanol concentration, the concentration of PCA, the effective pH value and the temperature (see model #2, #3, #5 and #6), it was found that model #5 and #6 have low R^2 values of 0.578 and 0.638, model #2 and #3 have higher values of 0.780 and 0.811. The difference of #5 and #6 compared to #2 and #3 was the interaction of the pH value with the PCA concentration. Therefore, it was concluded that the pH and PCA concentration interacted strongly. Model #7, where two factor interactions were excluded (other than the PCA concentration and pH value), confirmed the hypothesis of strong interaction. Model #8 revealed that a mild interaction between the pH value and ethanol concentration existed, model #9 revealed mild interaction between the pH value and temperature. Model #10 had a determination coefficient of 0.800, compared to model #8 which had a determination coefficient of 0.818, which suggested a minor interaction between the ethanol concentration and pH value. The attempt to add the square of the pH value (model #11) could not improve the determination coefficient of the models further. Furthermore, the comparison of model #10 and #14 suggests a minor interaction between the PCA concentration and temperature. A summary of the nonlinear interactions is found in Figure 2-12.

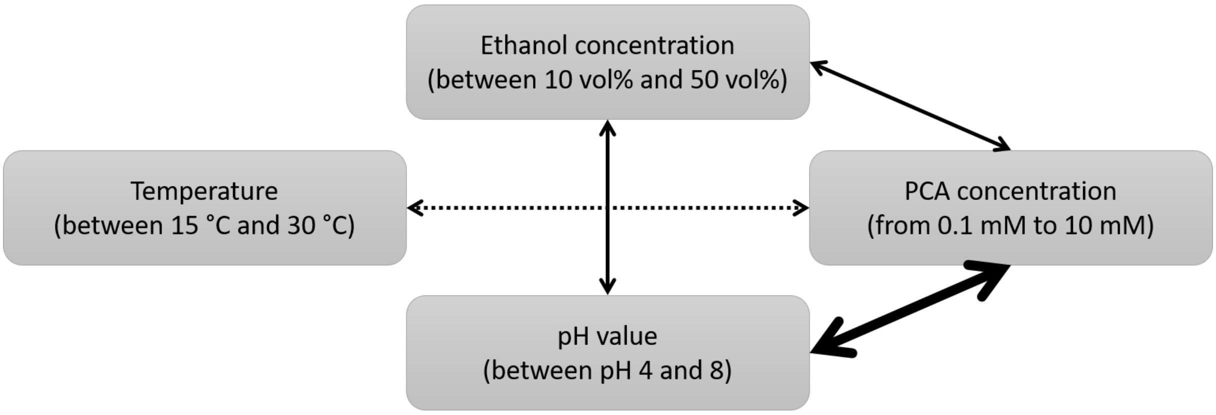

Figure 2-12: Summary of the interaction relationships between the parameters (ethanol concentration, PCA concentration, pH value and temperature) found by the analysis of the nonlinear regression models (#1-#14) for the optimization of NAcDAP and PCA dimerization. The arrows show interactions found between different parameters. The line thickness of the arrows represents the strength of the interaction. A strong relation was found between the PCA concentration and the pH value.

As was discussed, the pH value plays an important role for the product formation (see section 2.3.7.1). The product formation, however, did not correlate with the pH value linearly, which was explained by the pH optimum of the laccase-catalyzed reaction.

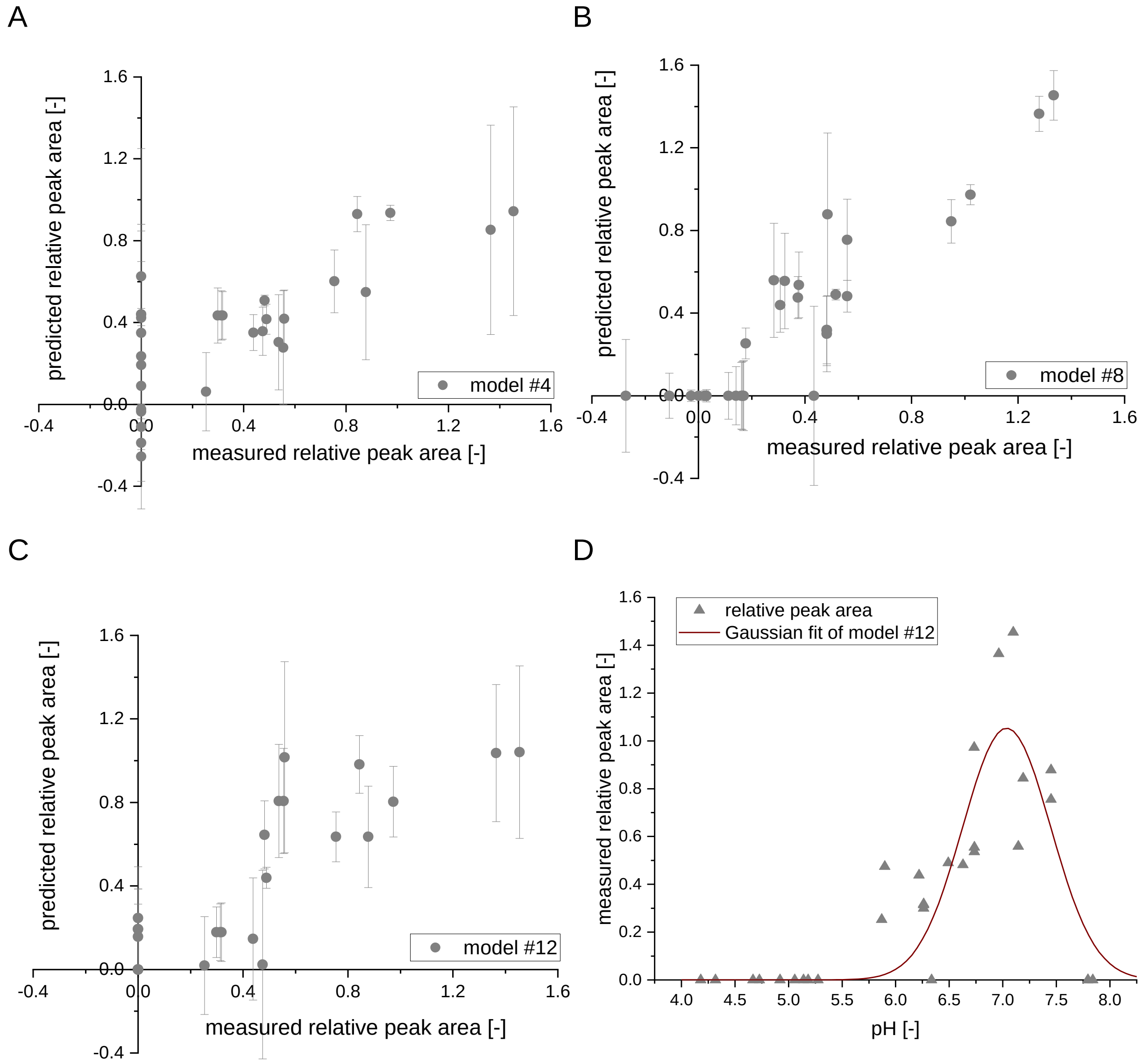

Figure 2-13: Results of linear and nonlinear models (see Table 2-3) for the analysis of the relative peak area for the dimerization of PCA and NAcDAP. The predicted values for the relative peak area versus measurement values for the relative peak area (peak area at 311 nm divided by the sum of all peaks around 280 nm) is displayed for A) the linear model #4, B) the two-factor interaction model #8 and C) the Gaussian peak model (#12). D) displays the nonlinear regression of the Gaussian peak model.

In order to address the nonlinearity and the pH optimum of laccase-catalyzed reactions, two peak models (#12 Gaussian and #13 Lorentzian), which display the effective pH value, were investigated. Other parameters (ethanol concentration, PCA concentration, temperature and shaking speed) were not investigated for these peak models. In doing so, the attempt was made to see if interactions between different factors play an important role or if the pH alone can be used to explain the product formation. Both peak models show good fits with an R^2 of 0.739 and 0.763. Figure 2-13 shows the results of the linear and nonlinear models. The predicted values for the relative peak area versus measurement values for the relative peak area (peak area at 311 nm divided by the sum of all peaks around 280 nm) of the linear model #4 are displayed in A, the two-factor interaction model #8 in B and the Gaussian peak model #12 in C.

Figure 2-13 D shows the nonlinear regression of the Gaussian peak model. The optimum for the Gaussian peak model was found at a pH value of approximately 7. Previously, the pH optimum for laccases from *C. unicolor* for the substrate PCA was found to be 5.5 (see Figure 2-6). This shift of the pH value towards higher value indicated, that the dimerization between NAcDAP and PCA is favorable at higher pH values.

Validation of the models

In a next step, five models were chosen and validated (#4, #7, #8, #12 and #13), using the results of the second set of experimental data (Exp. 36 to Exp. 50). The linear model #4 had a low coefficient of determination of 0.462. While the models #7 and 8 had significantly higher determination coefficients of 0.780 and 0.781, respectively. Surprisingly low were the determination coefficient of 0.176 and 0.154 which were calculated for the peak models #12 and #13. In Figure 2-14 the correlation of the predicted values for the relative peak area versus the measured values for the relative peak area (peak area at 311 nm divided by the sum of all peaks around 280 nm) are displayed for the nonlinear models #7 and #12.

From the validation of the models, it was concluded that the linear model #4 was not able to explain the data well. Furthermore, it was concluded that the 1-factor peak models (#12 and #13) for the effective pH value did not explain the correlations sufficiently. In contrast, both two factor interaction models #7 and #8 were able to predict the product formation of the validation data set. Both models had similar determination coefficients (0.780 and 0.781). While the more complex model (#8) has a slightly higher determination coefficient, the difference of the determination coefficients was not found to be significant and it was concluded that model #7 sufficiently displays the reaction data. Model #7, which only included the interaction between PCA and the pH value was therefore chosen for further analysis (see equation 2-4).

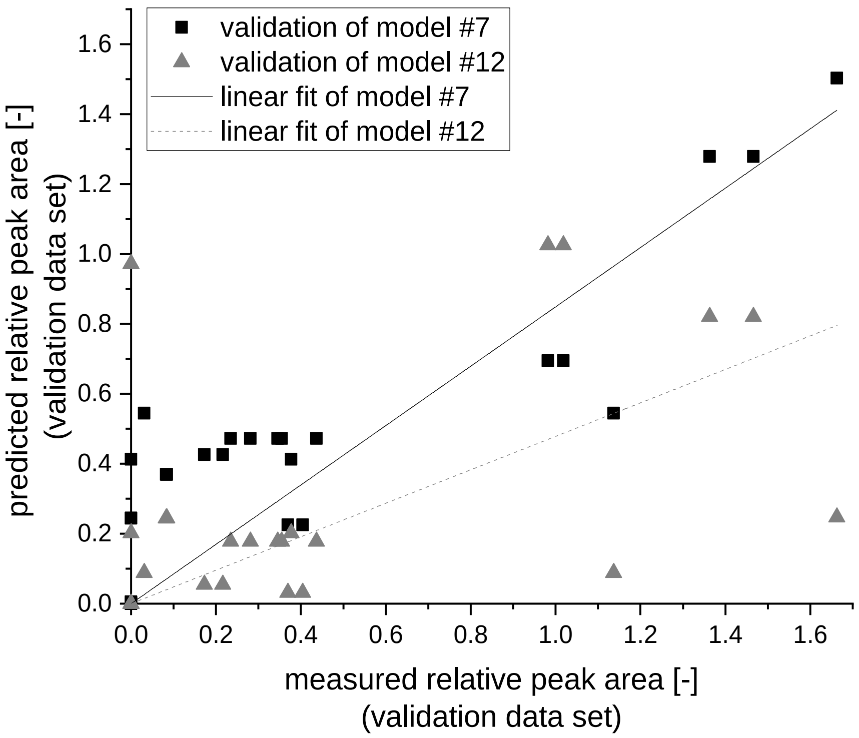

Figure 2-14: Validation of nonlinear models #7 (two factor interaction between PCA and pH-value) and #12 (Gaussian peak model). The predicted values for the relative peak area versus measurement values for the relative peak area (peak area at 311 nm divided by the sum of all peaks around 280 nm) is displayed for the validation data set. The slope of the linear fit for model #7 and model #12 were calculated to 0.849 ± 0.070 and 0.479 ± 0.108, respectively.

$$\begin{aligned} &relative\ area_{dimer} \\ &= -0.4145 + 0.0010 \cdot \frac{1}{vol\%} \cdot \mathrm{c(EtOH)} - 0.1754 \cdot \frac{mol}{mg} \\ &\cdot \mathrm{c(PCA)} + 0.0833 \cdot \mathrm{pH} + 0.0003 \cdot \frac{1}{°C} \cdot \mathrm{Temp} + 0.0001 \\ &\cdot \frac{1}{rpm} \cdot \mathrm{RPM} + 0.0384 \cdot \frac{mol}{mg} \cdot \mathrm{c(PCA)} \cdot \mathrm{pH} \end{aligned} \tag{2-4}$$

with

relative area$_{dimer}$ = nonlinear regression of model #7 for the dimerization of NAcDAP and PCA

c(EtOH) = ethanol concentration/ vol%

c(PCA) = PCA concentration/ mM

pH = effective pH/ -

Temp = temperature/ °C

RPM = shaking speed of thermoshaker for oxygen supply/ rpm

In equation 2-4, the coefficients for the ethanol concentration, the temperature and the shaker speed were positive suggesting that the product formation increased with an increase of these parameters. The increase in temperature and oxygen supply (shaking speed) increased the reaction speed of the enzymatic activation; therefore, the positive effect of the temperature and oxygen supply was well explained by the optimum of the enzymatic reaction. However, for the temperature and shaking speed the maximum increase of the dimer formation was below 1 %, so both parameters were insignificant for the product formation. Contrary to the trends observed for the temperature and shaker speed, it was not possible to explain the trend observed for the ethanol concentration by the enzymatic part of the reaction. For the enzymatic reaction, a decrease of the product formation was expected, for an increasing ethanol concentration (see 2.3.4.3 section). A possible cause for the positive influence of the ethanol concentration could be a more stable intermediate product, as reported for seminquinones in photoreduction processes [163]. However, the impact of the ethanol concentration on the product formation was less than 5 %, which suggests that the impact of the ethanol concentration overall was also low and insignificant for the product formation. After removal of the low significance factors, a simplified equation is found in equation 2-5.

$$\begin{aligned} relative\ area_{dimer} \\ &= -0.4145 - 0.1754 \cdot \frac{mol}{mg} \cdot \mathrm{c(PCA)} + 0.0833 \cdot \mathrm{pH} \\ &+ 0.0384 \cdot \frac{mol}{mg} \cdot \mathrm{c(PCA)} \cdot \mathrm{pH} \end{aligned} \qquad \text{2-5}$$

with

relative area$_{dimer}$ = simplified model #7 for the dimerization of NAcDAP and PCA

c(PCA) = PCA concentration/ mM

pH = effective pH/ -

The simplified equation 2-5 contained a positive prefactor for the pH value, suggesting that the product formation increases with an increasing pH. Furthermore, it was observed that the prefactor for the PCA concentration was negative, suggesting that with an increase of the PCA concentration, the relative product formation decreases. It was concluded that with an increase of the PCA concentration, the side product formation increased as well. Therefore, the use of a fed-batch or continuous reaction set-up is suggested. While the PCA concentration had a negative prefactor, the interaction term (c(PCA)*pH) had a positive prefactor of 0.038, suggesting that the product formation increased with an increasing PCA concentration. It was concluded that the effect of side product formation at high PCA concentrations can be neglected at high pH values. In fact, the simplified equation produced positive values for a pH value > 5. Therefore, high PCA concentrations are in favour of the product formation, but secondary to the pH value. Due to the limitation of the laccase from *C. unicolor*, the optimal pH for the complete reaction is at 7.5. This is the most basic pH which the laccase can operate at (see Figure 2-5 and Figure 2-6). However, using a different laccase, which is more stable at basic pH values, could allow the use of higher pH values and therefore a further increase in the product formation. This interaction, which was found between the pH value and the PCA concentration also explains why the peak models (#12 Gaussian and #13 Lorentzian) had only a low reproducibility in the validation. The reaction optimum is therefore found at a pH value of 7.5, a PCA concentration of 10 mg mol^{1}, a temperature of 30 °C, a shaking speed of 1000 rpm and an ethanol concentration of 50 vol%, which are also the upper boundaries of the chosen system. Most of these boundaries are set by the physiology of the laccase, as such, the use of a laccase which is stable at higher pH values or temperatures, may further increase the reaction rate.

The intercept of equation 2-5 was calculated to be -0.415. This suggests that further optimization of the model is needed. A large number of experiments were found to not produce any NAcDAP-PCA dimers, even though the parameters were in the range of laccases from *C. unicolor* (see section 2.3.7.3). The model could be further improved by focussing the investigation on pH values in the natural and basis pH range.

In conclusion, the investigation of the dimerization of PCA and NAcDAP identified the pH value in combination with the PCA concentration as the two most important parameters for successful binding. It was found that the more basic the reaction pH, the higher the product formation, requiring further research on alkaline laccases. Furthermore, high PCA concentrations were favourable for the product formation, but also increased the side product formation, hence, suggesting the use of a fed-batch process.

2.4 Summary and Outlook

In this chapter, biochemical reactions for the functionalization of natural polymers, which can be developed into biogenic adhesives, were investigated. For this purpose, a laccase-catalyzed approach for bonding primary amines with catechols via Michael-type addition was discussed. An application of the laccase-catalyzed heteromolecular C-N bond formation is found in chapter 3 and chapter 4, where a biogenic adhesive with a chitosan and lignin backbone is described.

In the first part of this chapter, solvent stable laccases were investigated for their application in solvent-rich media and for the production of solvent based adhesives. Ethanol was chosen as the most promising solvent, due to its low toxicity and recyclability [146] and due to its compatibility with many laccase substrates, such as OS lignin, which is dissolved in ethanol after extraction (see chapter 4). It was shown that laccases from *C. unicolor* are stable towards high ethanol concentrations (up to 50 vol%), even after long-term storage (50 days). Storage at low temperatures and less acidic pH values (such as pH 6.5) were favoured over storage at room temperature and pH 4.5.

Furthermore, laccases from *C. unicolor* were expressed using an initial pH of 4.5, instead of 7, due to superior laccase production at pH 4.5. After purification, three proteins (between 45 kDa and 62.4 kDa) were identified, out of which two match previously described laccases from *C. unicolor* [138]. The enzyme activity of purified laccase from *C. unicolor* had a broad pH optimum of about 5.5 to 6.5 with a maximum at 6.0 towards syringaldazine and 5.5 for the conversion of PCA to BQA. The investigation into the solvent stability found, that the highest enzyme activity was measured at 10 vol% ethanol (using syringaldazine as substrate) and at 20 vol% DMSO.

In the second part of this chapter, the laccase-catalyzed Michael-type addition of the catechols PCA and DHC with the primary amine NAcDAP were investigated. While PCA only formed C-N bonds with NAcDAP after the laccase-catalyzed reaction, spontaneous formation of dimers was observed for DHC, thus revealing that DHC was more reactive and less stable. Furthermore, a model originally created for homomolecular C-N bond formation [76], was adapted for the heteromolecular C-N bond formation. The model was applied to investigate the influence of the pH value and primary amine's pKa for C-N bond formation in catechols. It was found that next to a high pH, a low pK_a value of the primary amine led to higher conversion rates.

Lastly, the laccase-catalyzed heteromolecular C-N bond formation was parametrically optimized using the PCA as a catechol donor and NAcDAP as primary amine. The pH value in combination with the PCA concentration were identified as the two most important parameters for successful binding. It was found that the more basic the reaction pH (with respect to the enzyme stability), the higher the product formation, confirming the reaction model (see section 2.3.6). In this work, the optimal pH range was found to be between 5 and 7.5, however, the upper limit can be further increased through the use of alkaline laccase. Furthermore, it was found that high PCA concentrations were favourable for the product formation, but also increased the side product formation, hence, the use of a fed-batch process is recommended. In this work, the product formation was validated for a substrate concentration of up to 10 mM.

The goal of this work was to identify biochemical methods, while avoiding harsh chemicals, for developing biogenic mussel mimicking adhesive. This was achieved by the investigation and optimization of the laccase-catalyzed Michael-type addition of catechols (PCA and DHC) with the primary amine NAcDAP. This biochemical method allows for the functionalization of natural polymers, while avoiding the use of harsh chemicals. Furthermore, a solvent stable laccase from *C. unicolor* was successfully identified for use in up to 50 %wt ethanol.

3 A novel catechol-adhesive with a chitosan backbone

Mussel-inspired catechol-containing polymers provide a strong basis for the development of biogenic adhesives. Chitosan is a suitable backbone for such a biogenic adhesive, as it is a widely used biopolymer which is produced by deacetylation of chitin. The deacetylation process of chitin gives chitosan a defined number of primary amines which can be used for the functionalization with catechols, as was discussed in chapter 2. The objective of this chapter is the development of a novel and sustainably sourced chitosan adhesive, which mimics the mussel’s adhesion mechanism. By grafting catechols onto a chitosan backbone, via spontaneous and laccase-catalyzed Michael-type addition between the catechol monomers and the primary amines of chitosan, a process is investigated for the development of a catechol based adhesive with the intention of avoiding the use of toxic chemicals and the requirement of special reaction conditions.

First, chitosan and methods for the preparation of chitosan-catechols are introduced in sections 3.1.1 and 3.1.2 respectively.

Kinetic models for the C-N bond formation between primary amines and catechols suggested that the reaction is promoted by a low pKa value of the primary amine used and a neutral or mildly acidic reaction pH (see chapter 2). Since the pKa of chitosan is below 7, spontaneous reactions with catechols is proposed and investigated using UV-vis and FT-IR spectroscopy (see section 3.3.1). Following, the gel formation during spontaneous and enzyme catalyzed functionalization of chitosan with dihydrocaffeic acid (DHC) is presented in section 3.3.2. Furthermore, the laccase-catalyzed C-N bond formation between chitosan and protocatechuic acid (PCA) is investigated (see section 3.3.3). Using spontaneous Michael-type addition, a mussel mimicking adhesive is developed by functionalizing chitosan with PCA (see section 3.3.4). Following, the tensile strength is evaluated with a tensile test following DIN EN 15870 using aluminum cylinders. Lastly, a cost analysis is conducted to estimate the production cost of the PCA-chitosan adhesive (see section 3.3.5).

3.1 Theory

3.1.1 Chitosan

Chitin, from which chitosan is derived, belongs to the most abundant organic materials, naturally occurring in the exoskeleton of crustacea, molluscs and as principal fibrillar polymer in certain fungi [4]. With an annual production rate of approximately 10^{11} tons [164], chitin and its derivate chitosan are excellent polymers for use as backbones of biogenic adhesives. Chitosan, the deacetylated derivate of chitin (see Figure 3-1), is a non-toxic, microbial resistant and biodegradable polymer [165].

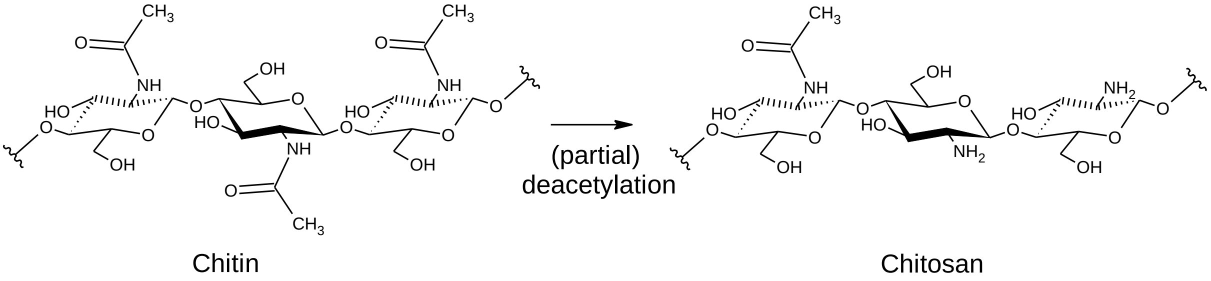

Figure 3-1: Deacetylation of chitin to chitosan.

The conversion of chitin to chitosan is possible by enzymatic or chemical deacetylation, resulting in various degrees of deacetylation [166, 167]. Moreover, chitosan consists of glucosamine and N-acetylglucoseamine monomers which are attached to each other via ß-(1-4) linkages [168, 169]. Due to their low toxicity, chitin and chitosan are used in various applications such as biomedical materials [164], in the food industry [170], for the treatment of pollutants [171] or for various blends of hydrogels [172, 173]. While chitin is nearly insoluble in water, it was found that chitosan with a degree of acetylation of less than 50 mol% is soluble in water at a pH below 6 [132, 174]. Rinaudo et al. (1999) also demonstrated that the concentration of protons needed to solubilize chitosan is at least equal to the concentration of primary amine units involved [174]. The pKa-values of chitosan are reported to be 6.1 [175], 6.2 [176], 6.3 [177] and 6.8 [178]. The pKa value for the monomer of chitosan, D-glucosamine, however, has been reported to be 7.5 [179] and 7.8 [180]. The much lower values obtained for chitosan have been attributed to electrostatic interactions between neighboring NH_3^+ groups [176].

3.1.2 Methods for chitosan-catechol preparations

Three main preparation methods for chitosan-catechols have been described in literature [181]: 1) chemically, 2) electrochemically, and 3) enzymatically. The chemical methods for conjugating catechol moieties onto chitosan backbones can be categorized into three main methods: A) Formation of amide bonds using EDC chemistry [62, 65, 182], B) reductive amination using aldehyde [183, 184], and C) direct formation of catechol-amine adducts [185–187].

The amide formation (A) between carboxylic acid-terminated catechol (such as DHC) and chitosan by EDC coupling resulted in a degree of catechol conjugation between 4 and 30 mol% [188] and 82 mol% after 7 days [189]. The reductive amination (B) is a method, that, in comparison to the amide formation, obtained in a relatively short reaction time (1 to 5 hours) a high degree of catechol-conjugates [190]. In this method, aldehyde-terminated catechols (such as 3,4-dihydroxybenzaldehyde) form reversible imide bonds with the amine groups in chitosan, which are further reduced to an irreversible C-N bond by reducing agents. The formation of catechol-amine adducts (C), which is initiated by the addition of an oxidant (such as sodium periodate) result in catechol cross-linked chitosan films which showed increased tensile properties in wet conditions [185, 186]. The maximum detachment force measured for a DHC-catechol film was, however, only 1.2 kPa (with mucosal tissue) [187].

Electrochemical synthesis (2) [191, 192] and enzymatic synthesis (3) [193–195] of catechol-chitosan conjugates involve the oxidation of the catechol to a semiquinone or quinone. Similarly, to the formation of catechol-amine adducts by a reducing agent, the quinones become subject to nucleophilic attack from the primary amines of chitosan and form covalent C-N bond. Both, Michael-type adducts and Schiff-base formation are possible (see Figure 3-2). The tyrosinase-catalyzed reaction of dopamine and chitosan resulted in a wet adhesion strength of 400 kPa [194].

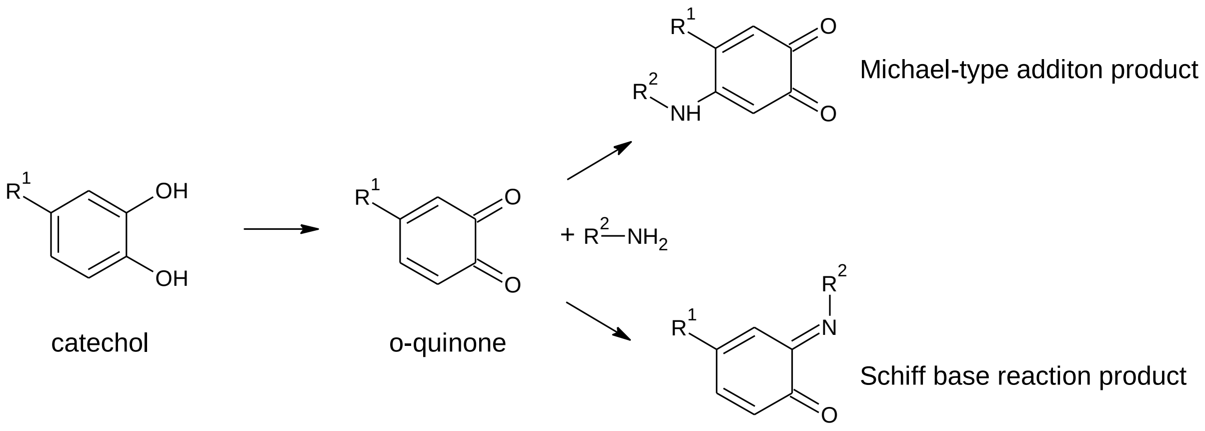

Figure 3-2: Michael-type addition and Schiff-base formation between catechols (via o-quinones) with amines [196]**.**

3.2 Materials and Methods

3.2.1 Chitosan

For this work, low molecular weight chitosan (see appendix, Table 8-1) with a deacetylation degree of 75 mol% to 85 mol%, with an average molar mass of 162.36 g mol^{-1} (per monomer) and an estimated number 4.93 mmol of primary amines per gram of chitosan (at 80 % deacetylation), was used.

3.2.2 Determination of PCA concentration in liquid media using spectroscopy

In an aqueous solution, PCA has two distinct absorption maxima at wavelengths of 252 nm and 290 nm. Using an Agilent Cary 50 UV-vis spectrometer, the extinction coefficient ε was determined to be 0.376 L mol^{-1} cm^{-1} (at 252 nm) and 0.173 L mol^{-1} cm^{-1} (at 290 nm).

In order to determine the pH-dependent absorption changes of PCA on chitosan, a solution of 10 g L^{-1} chitosan was mixed with PCA (solid) to a final molar concentration of 25 mol%, 50 mol% and 100 mol% with respect to chitosan's available amine groups. For each molar concentration of PCA, a solution with a final reaction pH of 5 and 6.5 were prepared. Samples were taken after 15 minutes, 3 hours and 18 hours of incubation; the chitosan was then removed via centrifugation at 16,500 x g. The supernatant was diluted in deionized water and the PCA concentration was measured with UV-vis spectroscopy at a wavelength of 400 nm.

3.2.3 Turbidity measurements using spectroscopy

A 10 g L^{-1} solution of chitosan in deionized water was prepared and left to settle, until a pH of 8 was reached (after approximately 15 minutes). DHC at a molar concentration of 25 mol% or PCA at molar concentrations of either 25 mol% or 50 mol% (with respect to the chitosan's available amine groups) were stirred in and the pH was gradually lowered using 32 vol% hydrochloric acid (HCl). Samples were taken and the turbidity was determined at a wavelength of 680 nm using an UV-vis spectrometer. As a control, no DHC or PCA was added. Each measurement was performed in triplicates.

3.2.4 Viscometry analysis

The kinematic viscosity was measured using an Ubbelohde viscometer at 30 °C. The device constant was determined by the producer to K = 0.3147 mm^2 s^{-2} (according DIN 55 350; capillary number: 501 23/Iic).

3.2.5 Particle size characterization

First, chitosan-catechol agglomerates were formed and subsequently the particle size was analyse using a particle size analyzer.

For the investigation of the effect of enzymes, a solution of 10 g L^{-1} chitosan in 10 vol% McIlvaine buffer was prepared and a pH of 5 was adjusted before adding PCA at a concentration of 100 mol% (in respect to chitosan's available amine groups). To the reaction mixture, 0.1 vol% enzyme was added. As control, a mixture of chitosan and PCA without enzyme was prepared. Samples were taken after 90 min of incubation and 24 hours of incubation at 28 °C. A volume of 1 ml of reaction mixture was centrifuged in a 2 ml reaction vessel at 16,500 x g. The supernatant was discarded and the pellet was washed using deionized water. The pellet was stored at -20 °C for further use. In order to characterize the particle size of the catechol-chitosan agglomerates after 90 minutes or 24 hours of enzyme treatment, the frozen pellet was resuspended in deionized water.

The particle size characterization was conducted using a particle size analyzer (LUMiReader). The extinction profile of the transmitted light through the width of the sample was measured over time. The velocity distribution of the separating particles was calculated via the software SEPView. In order to be able to estimate the particle size from the velocity measurements, the refractive index, the viscosity and density of the medium, as well as the particle density and refractive index of the particle were needed. Measurements were conducted at 30 °C using deionized water as the continuous phase. The material properties of water were used according to the programs specifications: viscosity (30 °C) = 0.7992 mPa s; density (30 °C) = 995.9441 kg m^{-3} [197], RPRI (630 nm) = 1.3308 and RPRI (870 nm) = 1.3259 [198].

The refractive index (RI) for chitosan was previously reported to be between 0.166 and 0.180 cm^3 g^{-1} (measured at 546 nm) [176]. Here, a RI of 0.166 cm^3 g^{-1} and an estimated particle density of 1500 kg m^{-3} was used.

The particle size analysis was validated using an optical microscope (Nikon Eclipse Ni). The particle size was initially determined for the control reaction after 90 minutes and the enzyme catalyzed reaction after 90 minutes and 24 hours using the software NIS-Elements D.

3.2.6 Mid-infrared analysis

Mid-infrared spectra of spontaneous reaction of catechols with chitosan were obtained using an FT-ATR mid-infrared spectrometer 'Spectrum 100' over the range of

4000 cm^{-1} to 650 cm^{-1}. First, a chitosan solution of 100 g L^{-1} was prepared in deionized water and the pH was adjusted using concentrated HCl (32 vol%). Second, the model compounds, DHC or PCA, were added to a concentration of 30 mol% in respect to chitosan's available amine groups. The solution was measured after t0 = 0 min, t1 = 30 min and t2 = 3 hours. Each sample was measured in triplicates. Deionized water was used as background media.

3.2.7 Preparation of adhesive and measurement of tensile strength of butt joints

The adhesive was prepared as follows. 3 g of chitosan were dissolved in 25 ml of water. Following, a solution containing 900 µl concentrated HCl (32 vol%) and 5 ml of water were added to lower the pH from ~9 to ~5. This pH shift was necessary to avoid oxidation of the catechol group. Due to the pH-shift, the chitosan formed a gel, which was advantageous for the application on the adhesion surface (no running off) but limited the maximum concentration of the adhesive. Thereafter, 701 mg of PCA were added and mixed in, using a spatula, and subsequently left to incubate for 30 minutes. The covalent bond between chitosan and PCA formed during the 72 hour curing time, without the use of a catalyst, via spontaneous reaction.

The tensile strength of butt joints was tested with a tensile test according to DIN EN 15870 with aluminum cylinders with a diameter of 20 mm. Therefore, the test surfaces were prepared with an abrasive pad and cleaned using first deionized water then acetone. One surface was covered with adhesive (approximately 1.5 mm high) and gently placed on top of the other. Unless otherwise noted, the curing was conducted at 28 °C for 72 hours. In order to test the influence of pH, NaOH was mixed in prior to PCA. The pH was measured after PCA addition using a pH meter.

Organosolv (OS) lignin used as filler materials in adhesion experiments was provided by the Fraunhofer Center for Chemical-Biotechnological Processes CBP in Leuna, Germany. The OS lignin was extracted from beech wood using ethanol as a solvent (KO74).

3.3 Results and Discussion

Chitosan was identified as a suitable backbone for a mussel-inspired catechol-containing biogenic adhesive, as it contains a defined number of primary amines which can be used for the functionalization via C-N bond formation, as was discussed in chapter 2. In this chapter, measurements from FT-IR and UV-vis spectroscopy were used to evaluate the pH-dependent spontaneous reaction of chitosan and catechols. The results are presented and discussed in section 3.3.1. Following, the results of gel formation during spontaneous and enzyme catalyzed functionalization of chitosan with DHC are presented and discussed in section 3.3.2. Furthermore, the laccase-catalyzed C-N bond formation between chitosan and PCA via Michael-type addition is investigated and the results are presented in section 3.3.3.

Using spontaneous Michael-type addition, a mussel mimicking adhesive is developed by functionalizing chitosan with PCA. An assessment of the adhesion strength is provided in section 3.3.4. Lastly, a cost analysis is conducted to estimate the production cost of the PCA-chitosan adhesive. The results are discussed in section 3.3.5.

3.3.1 Spontaneous reaction of chitosan and DHC or PCA

Chitosan contains a regular structure of glucosamine and N-acetylglucoseamine monomers. The primary amines of the glucosamine units are good anchor points for functionalization with a catechol to form an adhesive mimicking the mussel’s adhesion properties. The formation of the C-N bond between a primary amine and the catechol is favored by a low pK_a value of the primary amine. The pK_a of chitosan is below 7 and therefore significantly lower than most primary amines (such as NAcDAP), which made it susceptible to spontaneous reaction. Following, the spontaneous reaction of chitosan with PCA and DHC was investigated.

3.3.1.1 Solubility of chitosan in the presence of PCA and DHC

For a homogeneous catalysis, complete solubility of chitosan and the catechol donor compounds was sought. The solubility of chitosan was dependent on the pH value and varied with its deacetylation degree and molecular weight. Interestingly, the in presence of PCA and DHC has an effect on the solubility of chitosan as well. The pH-dependent solubility of chitosan in deionized water (10 g L^{-1}) was determined by measuring the turbidity at 680 nm. As shown in Figure 3-3, chitosan became completely soluble at a pH around 5. In the presence of either 25 mol% (data not shown), 50 mol% DHC or 25 mol% PCA, complete solubility was already reached at a pH of 5.2. For a solution containing 50 mol% PCA, complete solubility was only reached at pH 4.5. Overall, PCA as well as DHC had a notable influence on the solubility of chitosan, which indicated spontaneous reactions.

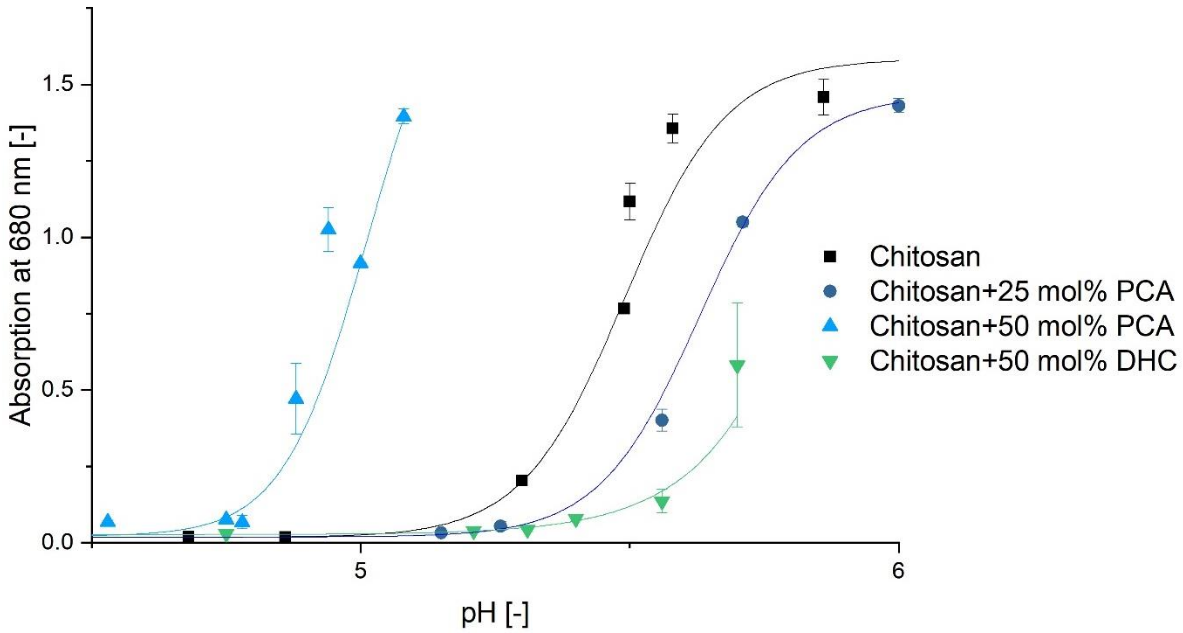

Figure 3-3: pH-dependent solubility of chitosan (10 g L^{-1}) in deionized water in the presence of DHC or PCA at different concentrations. A low absorption indicates partial or complete solubility of the compounds. The absorption of the solution increases when the particles precipitate from the solution.

3.3.1.2 Mid-infrared analysis of spontaneous C-N bond formation

To further evaluate the spontaneous reaction of chitosan with PCA or DHC, FT-IR spectra were recorded directly after mixing, after 30 minutes (t1, data not shown) and after 3 hours (t2). First, a solution of 100 g L^{-1} chitosan was prepared at different pH values. The chitosan dissolved and formed a gel at a pH of 1, 5 and 6, but not at 9, resulting in a suspension of chitosan in deionized water. As shown in Figure 3-4 A, only the gel form of chitosan was detectable using FT-IR measurements. Since PCA did not help to form a chitosan gel at pH 9, the spontaneous reaction was not measurable. At pH 1 and 5 some distinct peaks were formed (see Figure 3-4 B). At pH 5, peaks at 1200 cm^{-1}, 1250 cm^{-1}, 1288 cm^{-1}, 1363 cm^{-1} and 1546 cm^{-1} formed over time. At pH 1, the peaks at 1250 cm^{-1} and 1288 cm^{-1} were shifted to lower and higher wave numbers respectively, while the peaks at 1363 cm^{-1} and 1546 cm^{-1} were no longer present. The peaks at 1250 cm^{-1} and 1288 cm^{-1} were attributed to the C-O vibration bands of the catechol [72]. The absorption at 1363 cm^{-1} was attributed to the aromatic C-N stretch band which is characteristic for secondary amines [199].

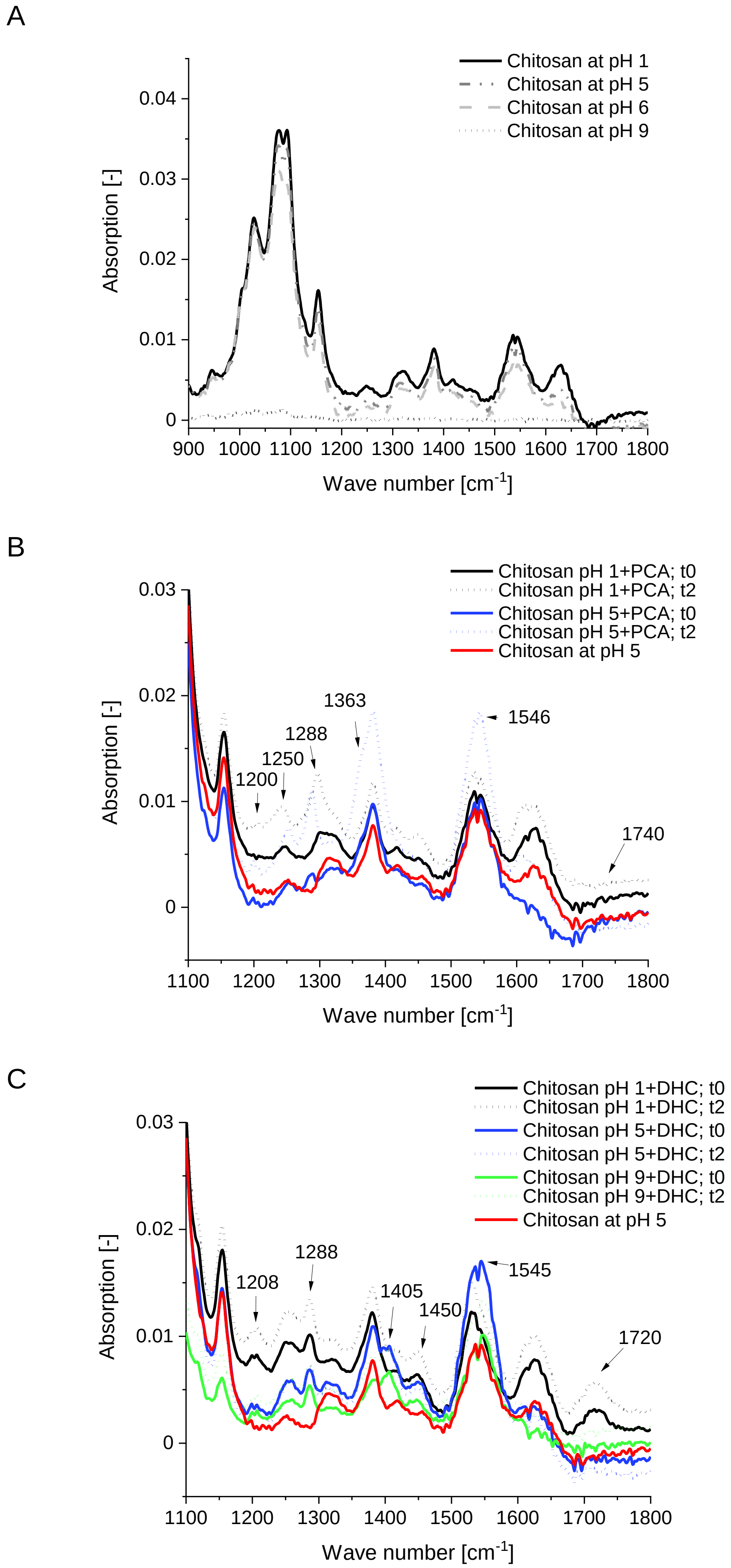

Figure 3-4: FT-IR analysis of (A) chitosan at pH 1,5,6 and 9; (B) chitosan at pH 1, 5 and 9 after PCA addition and (C) chitosan at pH 1, 5 and 9 after DHC addition (t0=reaction start, t2=3 hours).

In contrary, characteristic for amides is a strong characteristic peak (amide II) at around 1510 cm^{-1} to 1550 cm^{-1} which resulted from the N-H deformation band [200]. The peak at 1546 cm^{-1} corresponded well with this area and could represent an amide bond. However, for catechol-functionalized chitosan C=O stretch and N-H bend of the amide bond was found at 1600 cm^{-1} and 1740 cm^{-1} as a result of ECD coupling [65]. Since those peaks were absent in this study, the peak at 1546 cm^{-1} might result from the amine’s N-H bend which is often found between 1580 cm^{-1} and 1650 cm^{-1} [200]. As a result, it was concluded that Michael-type addition was predominant. Hence, the analysis of the FT-IR spectra concluded that aromatic C-N bond were formed during the spontaneous reaction of chitosan and PCA at pH 5. For the reaction of chitosan with PCA, the absorption increased over the course of 3 hours, showing the reaction progress.

DHC mediated the formation of a chitosan gel at pH 9, hence FT-IR analysis was possible for all pH values. At pH 1, 5 and 9, peaks were detected at 1208 cm^{-1}, (1250 cm^{-1}), 1288 cm^{-1}, 1405 cm^{-1} and 1450 cm^{-1}. The peaks at 1250 cm^{-1} and 1288 cm^{-1} were again attributed to the C-O vibration bands of the catechol [72]. Since the peak at 1405 cm^{-1} was particularly strong at pH 9, it was attributed to an oxidation product of DHC [199]. For pH 5 and 9, a strong peak at 1545 cm^{-1} was present (see Figure 3-4 C), which again, corresponds well with either a amide or amine’s N-H bond, however, no peak which correlated well with the aromatic C-N stretch band was observed. Only an absorption peak was found around 1450 cm^{-1} which might result from either C–H bending (scissoring) of a methyl group or an aromatic C=C stretching vibration band. However, analogously to the two peaks of the PCA-catechol (1363 cm^{-1} and 1546 cm^{-1}), the peaks at 1405 cm^{-1} and 1545 cm^{-1} may also result from the formation of an aromatic C-N stretch band. Furthermore, for the reaction pH of 1, peaks were found at 1640 cm^{-1} and 1720 cm^{-1}, which correlated well with the amide bond described for catechol-functionalized chitosan [65]. Since chitosan formed a gel which draws water from the reaction mixture, amide formation might be possible in combination with DHC. Hence, the analysis of the FT-IR spectra concluded that both aromatic C-N bonds, as well as amides were formed during the spontaneous reaction with DHC. In conclusion, the FT-IR analysis of spontaneous C-N bond formation confirmed the kinetic model introduced in chapter 2. While at low pH levels (pH 1), no C-N bond formation was detected with PCA, for both catechols C-N bonds were observed at pH 5.

3.3.1.3 Determination of pH-dependent PCA binding capacity

HPLC-MS analysis have shown that DHC was not stable and auto-catalytically formed quinones (see chapter 2). UV-vis spectra often show the formation of several peaks during the initial oxidation of catechols, which decay over time due to secondary reactions [201]. Furthermore, some peaks have similar UV-vis absorption maxima, but larger extinction coefficients than the corresponding catechols. Therefore, it was concluded that, due to its instability, DHC was not suited for optical analysis. Therefore, the determination of the pH-dependent catechol binding capacity was only conducted using PCA. In order to determine the pH-dependent absorption of PCA onto chitosan, a solution of chitosan in deionized water (10 g L^{-1}) was mixed with 25 mol%, 50 mol% or 100 mol% of PCA (with respect to chitosan's available amine groups) at pH 5 and pH 6.5. After removal of the solid chitosan, the supernatant was analyzed for its PCA concentration. As shown in Figure 3-5, the absorption of PCA at a pH of 5 was preferred over the absorption at pH 6.5. For both pH values, more PCA per gram chitosan was absorbed at higher availability of PCA in the supernatant. The highest PCA absorption was reached after 15 minutes with 100 mol% PCA. 0.45 grams of PCA were absorbed per gram chitosan, which equals 60 mol% of PCA per primary amine of chitosan.

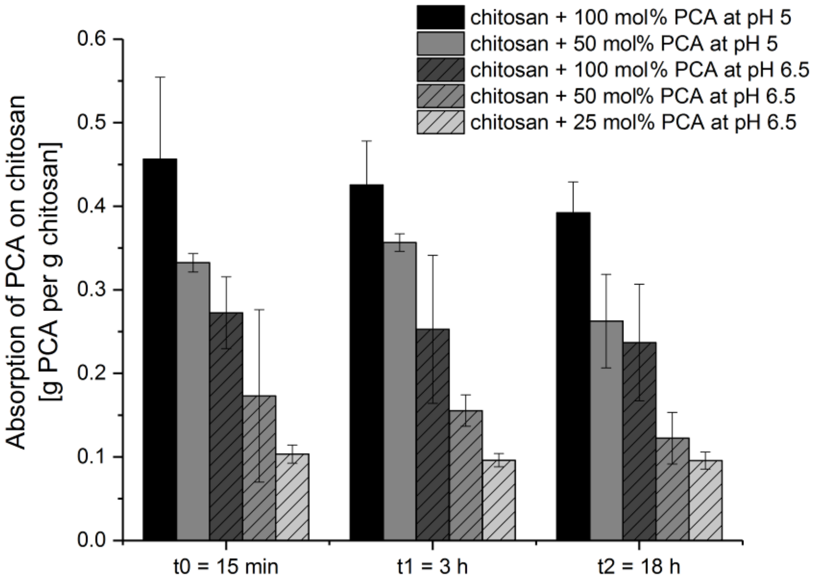

Figure 3-5: pH-dependent PCA absorption onto chitosan.

The absorption of PCA was a fast reaction which occurred within 15 minutes after the PCA dissolved. After 3 hours and 18 hours of incubation, no significant change was detected. Generally, the absorption signal after 18 hours decreased slightly, which may have been caused by a minor instability of PCA. As discussed in section 3.3.1.1, at pH 5 and a molar concentration of 25 mol% PCA, chitosan was completely dissolved and could not be separated by centrifugation. Hence, the absorption experiments confirmed the results of the IR-measurements. A spontaneous reaction occurred between PCA and chitosan.

3.3.1.4 Influence of PCA and DHC on the viscosity of chitosan solutions

The viscosity of the adhesive was an important factor for the proper processing of the adhesive. On the one hand, the lower the viscosity of the adhesive, the easier it was, to wet the material surface. On the other hand, the lower the viscosity, the thinner (more fluid was the adhesive and the higher was the likelihood, that the adhesive flowed away before the curing process was completed.

Table 3-1: Kinematic viscosity (at 30 °C) of chitosan solutions in the presence of DHC or PCA.

Component	pH [-]	Kinematic viscosity ν [mm^2 s^{-1}]
chitosan	4.8	69.9 ± 2.4
chitosan	4.8	55.3 ± 0.6
chitosan (not dissolved)	5.0	14.9 ± 0.4
chitosan+ 25 mol% PCA	5.2	50.0 ± 1.1
chitosan+ 50 mol% PCA	4.5	59.6 ± 1.5
chitosan+ 25 mol% DHC	5.2	57.3 ± 0.3
chitosan+ 50 mol% DHC	5.2	58.8 ± 0.3

Based on the kinetic model for the formation of C-N bonds, a spontaneous reaction of chitosan and catechols was expected, which could lead to more cross-linking of chitosan molecules and therefore an increase of the viscosity. Following, the influence of PCA and DHC on the viscosity of a chitosan solution was investigated.

To determine the kinematic viscosity of the dissolved chitosan, the pH was chosen according to complete solubility as described in section 3.3.1.1. As shown in Table 3-1, while the kinematic viscosity increased as soon as chitosan was soluble, the differences caused by the presence of PCA or DHC were minor.

3.3.2 Gel formation during spontaneous and enzyme catalyzed functionalization of chitosan with DHC

As was shown in section 3.3.1.2, chitosan was able to form a gel on its own at a concentration of 100 g L^{-1} (pH < 7), whereas no gel formation was observed at a concentration of 10 g L^{-1} (see section 3.3.1.4). Even though no effect on the viscosity was found after short-term incubation of chitosan (10 g L^{-1}) with PCA and DHC, it was noted that after 24 to 48 hours of reaction time, DHC was able to cross-link chitosan, resulting in a viscous gel, even at a chitosan concentration of 10 g L^{-1}. Following, the spontaneous reaction (no enzyme) of chitosan and DHC, as well as a mild treatment with laccase (0.1 vol%) and strong laccase treatment (1.0 vol%) were compared.

As shown in Figure 3-6, the solution without laccase turned slightly pink after about three hours of incubation, red with 0.1 % laccase and dark red with 1 % laccase. The solution with 1.0 vol% laccase had already formed a gel at 3 hours of incubation. After further incubation (3 h), a gel had formed with 0.1 vol% laccase as well (data not shown). After a total incubation time of 24 h, a gel was also visible for the spontaneous reaction. However, at this point, the hydrogel catalyzed by 1.0 vol% laccase had solidified and a black residue had formed, which can be attributed to the formation C-O-C' bonds between oxidized catechols (quinones) when forming poly(catechols) [72]. After a further 48 h, the gel of the 0.1 vol% laccase solution had also oxidized. The gel formation is an indicator for cross-links of chitosan molecules via DHC. Hence, the DHC can contribute to cohesion, but lacks the ability to adhere to surfaces. It was shown that the treatment with laccase accelerated the cross-linking of chitosan, but also led to quinone formation, which was undesirable for both cohesion and adhesion.

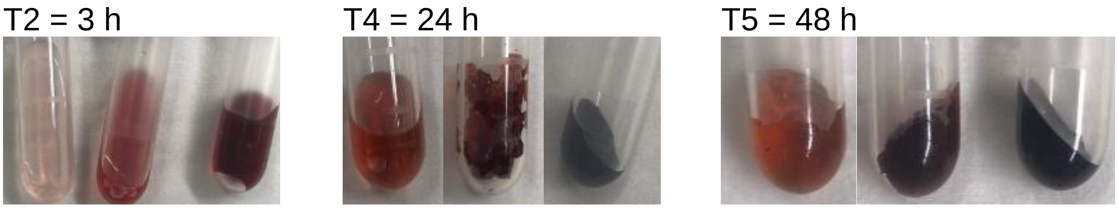
T2 = 3 h

T4 = 24 h

T5 = 48 h

Figure 3-6: Gel formation of a chitosan solution containing DHC at pH 5 after 3 h, 24 h and 48 h. At each point in time, the spontaneous reaction, mild treatment with laccase (0.1 vol%) and strong laccase treatment (1.0 vol%) are shown from left to right.

3.3.3 Formation of chitosan-agglomerates during enzyme catalyzed functionalization with PCA

North et al. (2017) have shown that for poly-catechol-styrene strong adhesion strength (> 2 MPa) required a catechol content of at least 20 mol% [20]. While the cross-linking of chitosan via catechols resulted in a higher polymerization degree, which is usually beneficial for cohesion, in this case the loss of the functionality of the primary catechol group was an issue. The formation of a gel or agglomerates was an indicator for such cross-linking processes.

For chitosan and PCA (with and without enzyme treatment) no gel formation was observed (data not shown). In order to investigate the effect of PCA on the formation of chitosan agglomerates, particle size development over time was investigated. Particle size characterization was conducted via particle sizer (LumiReader) and validated using microscopy imaging. The results are shown in Table 3-2. The comparison of the data obtained for the control experiments (90 minutes, no enzyme) showed a median diameter of 3.8 µm from microscopy imaging and 3.5 µm from the particle sizer. According to the microscopy results, 10 % of particles were smaller than 1.5 µm (D0.1), 90 % of particles were smaller than 11.5 µm (D0.9) and had a span of 2.6 µm. (The span is defined as (D0.1-D0.9)/D0.5 and quantified the distribution width.) Using the particle sizer, 10 % of particles were smaller than 2.4 µm and 90 % of particles were smaller than 11.2 µm, resulting in a span of 2.5 µm. It was clearly shown that the particle size increased significantly due to enzyme incubation.

Table 3-2: Particles size characterization of PCA-chitosan agglomerates after enzyme treatment. (The incubation was completed at 28 °C, at pH 5)

	Sample	**Data points**	**Median [µm]**	**D0.1 [µm]**	**D0.5 [µm]**	**D0.9 [µm]**	**Span [µm]**
microscopy imaging	control (90 min)	132	3.8 ± 5.6	1.5	3.8	11.5	2.6
	enzyme treated (90 min)	100	6.9 ± 54.5	1.4	6.9	75.4	10.8
	enzyme treated (24 h)	105	19.9 ± 64.8	4.0	19.9	107.2	5.2
particle sizer	control (90 min)	3	3.4 ± 5.8	2.2	3.4	12	2.9
	control (90 min)	3	3.5 ± 6.9	2.4	3.5	11.2	2.5
	control (90 min)	2	3.7 ± 6.6	2.3	3.7	11.2	2.4
	enzyme treated (90 min)	2	14.9 ± 18.9	5.9	14.9	53.8	3.2
	enzyme treated (24 h)	3	14.1 ± 15.5	5.4	14.1	40.6	2.5

The particles size of PCA-chitosan agglomerates without addition of the enzyme was analyzed as well. No significant increase of particle size was detected within 90 minutes. The formation of agglomerates was therefore due to the enzyme treatment. Due to laccase treatment, the PCA likely functioned as a linker between two or more chitosan molecules, furthering cohesion, but making it less available for surface adhesion. For surface adhesion on aluminum, where the catechol group was a key element, laccase-treatment was therefore contra productive, resulting in a complete loss of adhesion strength.

3.3.4 Determination of tensile strength of PCA-chitosan using butt joint tests

Using FT-IR and UV-vis spectroscopy, this study has demonstrated that spontaneous reactions occur between chitosan and the catechols PCA or DHC. Furthermore, it was found that DHC was able to cross-link chitosan via spontaneous C-N bond formation, which led to an increase in cohesion, but complete loss of tensile strength (data not shown). Therefore, tensile strength was determined for PCA-chitosan adhesive solely. The tensile strength of butt joints was evaluated by the project partner Naturwissenschaftliches und Medizinisches Institut an der Universität Tübingen, Reutlingen, Germany, NMI. The detailed results are available in Capitain et al. (2020b) [67], an overview of the results are presented here. The use of an adhesion gap, the addition of filler material, the surface preparation of the adherends and the pH value during binding were investigated. Furthermore, the PCA-catechol was compared to other commercially available adhesives from renewable resources.

An adhesion gap is a defined length between the butt joint surfaces. Without the use of an adhesion gap, a tensile strength of 1.79 MPa± 0.36 MPa was measured, which declined to 0.83 MPa ± 0.39 MPa due to the use of a defined 0.5 mm adhesion gap. The novel PCA-chitosan adhesive had a solid content of only 12 wt%, which resulted in a significant loss of mass during the curing process. In order to increase the solid concentration, different filler materials were used. While most filler materials decreased the tensile strength, 2 wt% OS lignin had no negative impact on the tensile strength.

It was found that the surface preparation also had a significant influence on the tensile strength, which was attributed to differences in the aluminum oxide surface layer which formed after the preparation. Grinding of the surface resulted in a tensile strength of only 1.79 MPa ± 0.36 MPa, while a blasting of the surface, using aluminum oxide (corundum), increased the tensile strength to 3.25 MPa ± 0.47 MPa.

Different pH values (1.21; 4.70; 5.03 and 5.41) during binding were tested. The tensile strength achieved with chitosan itself (without PCA) was 0.23 MPa ± 0.13 MPa. For PCA-chitosan at a pH of 1.21, a tensile strength of 0.20 MPa ± 0.13 MPa was measured, which was in agreement with the results of the FT-IR-spectroscopy (see section 3.3.1.2), which suggested that the C-N bond formation did not occur at a pH of 1. The tensile strengths of the PCA-chitosan adhesive at pH 4.70 and 5.03 were similar at 3.40 MPa ± 0.32 MPa and 3.41 MPa ± 0.12 MPa, respectively. At pH 5.41, the tensile strength measured was significantly lower (2.27 MPa ± 0.40 MPa), which was likely due to the partially soluble of chitosan at pH values above 5.

In order to assess the tensile strength obtained, commercially available adhesives from renewable resources (dextrin, starch and Gummi arabicum and chitosan) were tested. Dextrin and starch showed relatively low tensile strengths (0.35 MPa ± 0.17 MPa and 0.50 MPa ± 0.17 MPa after 3 days of curing at 40 °C), while Gummi arabicum was significantly higher with a tensile strength of 2.10 MPa ± 0.45 MPa. The PCA-chitosan adhesive attained a tensile strength of 4.56 MPa ± 0.54 MPa, 2.2 times higher than the tensile strength of Gummi arabicum.

3.3.5 Cost calculation for catechol-chitosan adhesive

A biogenic catechol adhesive based on a chitosan backbone was also developed. For cost estimation, a simple balance of the educts was carried out. Table 3-3 shows a rough cost estimate for this chitosan adhesive. Since chitosan is the main component and thus also forms the main costs, several price scenarios were considered here. The costs for chitosan 1 correspond to the raw material used for this research project. Chitosan 2 is a commercially available chitosan which is available at a much lower cost. The price range for the catechol-chitosan adhesive is thus approximately 7-30 euro per kg.

Table 3-3: Cost Calculation for catechol-chitosan adhesive. *optimized amount (solid contend of approximately 20 wt%); **rough estimation

Ingredient	Amount	Laboratory price	Scale-up price**	Price per unit
chitosan 1	0.14 kg	1870.00 € per kg	187.00 € per kg	25.38 €
chitosan 2		299.00 € per kg	29.98 € per kg	4.07 €
conc. HCl	0.04 L	7.60 € per L	0.76 € per L	0.03 €
PCA	0.03 kg	799.00 € per kg	79.9 € per kg	2.54 €
water*	0.79 L	kA	0.02 € per L	0.02 €
sum	**1 kg**			**27.97 € per kg** **6.66 € per kg**

For the scale-up from laboratory to pilot scale, 10 % of the usual laboratory prices were assumed. The cost extrapolation was based on the power law estimation, also known as six-tenth rule by Williams (1947) [202]. This estimation allows the extrapolation of cost data from one scale to another. It was demonstrated, that the formula is also applicable for the scale-up of whole plant costs [203]. More recently, the six-tenth rule was proposed for the capital cost estimation of biorefinery processes [204].

3.4 Summary and Outlook

In this chapter, chitosan was functionalized with catechols via a Michael-type addition with the aim of developing a mussel-inspired catechol-containing biogenic adhesive. It was demonstrated that spontaneous reactions occur between chitosan and the catechols PCA and DHC, confirming the kinetic models for the C-N bond formation between primary amines and catechols (see chapter 2, section 2.3.6). Due to the relatively low pKa of chitosan, no catalyst was needed and spontaneous reactions were possible at neutral or slightly acidic pH values, as was confirmed using FT-IR and UV-vis spectroscopy, where spontaneous reactions occurred at pH 5 and 6.5. FT-IR spectroscopy further validated the kinetic model by demonstrating that the spontaneous reaction between chitosan and PCA did not occur at a pH of 1.

It was also shown that the spontaneous absorption of PCA and DHC had an impact on the solubility of chitosan in water. In its native form, chitosan (10 g L^{-1}) was soluble in water below a pH of 5. In the presence of 25 % or 50 % DHC or 25 % PCA, the solubility of chitosan in water was achieved at a pH below 5.2 and in the presence of 50 % PCA only at a pH of 4.5.

Laccase-catalyzed C-N bond formation between chitosan and catechols accelerated the reaction and promoted the formation of PCA-chitosan agglomerates and DHC-chitosan hydrogels, as was confirmed by microscopy imaging and particle size analysis. The result for DHC-chitosan was a highly cross-linked chitosan with limited adhesion properties. Moreover, the intense incubation with laccase resulted in the conversion of the catechol to its oxidized form, the quinone, resulting in complete loss of functionality. Therefore, spontaneous reaction C-N bond formation was superior over laccase-catalyzed Michael-type addition for the development of the adhesive.

A mixture of 100 g L^{-1} chitosan and 25 g L^{-1} PCA, cured at a pH of 5, reached a tensile strength of 3.4 MPa. A surface blasted with aluminum oxide (corundum) and an undefined adhesion gap consistently produced the highest tensile strengths. While tested filler materials (cotton and lignin) mostly decreased the tensile strength, 2 wt% OS lignin had no negative impact on the tensile strength. Compared to biogenic adhesives such as dextrin, starch, chitosan and Gummi arabicum, the developed PCA-chitosan adhesive attained a strong tensile strength of 4.56 MPa ± 0.54 MPa, which was 2.2 times higher than the tensile strength of Gummi arabicum, the second strongest biogenic adhesive tested. The production cost for this catechol-chitosan adhesive was estimated to be between 7 and 30 euro per kg.

The water-based nature of chitosan and PCA resulted in a lack of long-term water resistance. In future work, water resistance should be addressed, through laccase treatment, for example. Furthermore, if the concentrations of the components are optimized in order to minimize side product and quinone formation, caused by the laccase treatment, laccases could be used to accelerate the reaction rate.

In this chapter, the development of a mussel mimicking and biogenic adhesive was achieved by functionalizing chitosan with PCA via spontaneous reactions. For a PCA-functionalized chitosan a tensile strength of 4.56 MPa ± 0.54 MPa (on corundum blasted aluminum surfaces) was achieved. Since the functionalization and curing processed use naturally occurring substances exclusively and are free of toxic chemicals, a novel and sustainable bioadhesive has been developed.

4 Functionalization of Organosolv (OS) lignin

Residual materials, from forestry and gardening, offer a suitable basis for biogenic adhesives, as they do not compete with food production and are widely available [3]. The lignocellulose biorefinery is an established concept for the processing of lignocellulosic materials, resulting in fermentable sugars and a lignin side stream (OS lignin), for which further development of value-added products is needed [3]. Its polyphenolic composition makes lignin a remarkable building block for a natural and biogenic adhesive, that can be made available at low cost due to the abundant availability of feedstock. Compared to Kraft lignin, which is the main byproduct of the Kraft pulping process, OS lignin is free of sulfurs and consists of long chains of polyphenols [71]. The objective of this chapter is the development of a novel and sustainably sourced lignin adhesive, which mimics the mussel’s adhesion properties. By subsequently adding L-lysine and catechols (PCA and DHC) onto a lignin backbone, a process is investigated for the development of a lignin based adhesive with the intention of avoiding the use of toxic chemicals and the requirement of special reaction conditions.

First, lignin and its production from biomass is introduced in section 4.1.1. Following, the lignocellulose biorefinery concept and reactions with lignin are described in sections 4.1.2 and 4.1.3, respectively. Furthermore, a two-step concept for the functionalization of lignin is introduced in section 4.1.4.

The extraction of OS lignin via OS digestion was optimized for maximum lignin yield and the use of OS lignin in laccase-catalyzed processes was investigated (see section 4.3.1). As the one-step functionalization of OS lignin with L-DOPA was challenging, a two-step process was implemented. In the 1st step, the amino acid L-lysine is bound to lignin to provide a primary amine for further functionalization (see section 4.3.2). In the 2nd reaction step, the primary amines resulting from the 1st step, are functionalization with a catechol group (PCA and DHC) via a laccase-catalyzed Michael-type addition and spontaneous reaction (see section 4.3.3). Following, the tensile strength was established for OS lignin and its derivates (see section 4.3.4). Lastly, an economical evaluation of lignin-catechol adhesives was performed (section 4.3.5).

4.1 Theory

4.1.1 Structure and production of lignin from biomass

Lignin is, along with cellulose and hemicellulose, one of the three main components of plants. As part of the plant cell wall, lignin forms the structural framework of a plant [205]. Lignin itself consists of a diverse structure of amorphous polyphenols, that is arranged in a complex matrix with cellulose. The resulting lignocellulose is extremely resistant to biological and chemical influences, hence protecting the plant from environmental influences [206].

Despite its complex structure, which varies depending on the type of biomass, lignin consists of three main types of lignols, that all derived from phenylpropane. The three monolignol monomers p-coumaryl alcohol, coniferyl alcohol, and sinapyl alcohol differ in their methoxylation degree at the ortho position [122]. Incorporated into lignin, these lignol precursors are found as the phenylpropanoids p-hydroxyphenyl (H), guaiacyl (G), and syringyl (S), respectively [207]. The phenylpropanoid subunits are crosslinked via a variety of ether and carbon-carbon bonds. The most common type of bond, the β-aryl ether bond (β-O-4 bond), occurs in 50 to 60 % of the linkages (see Figure 4-1).

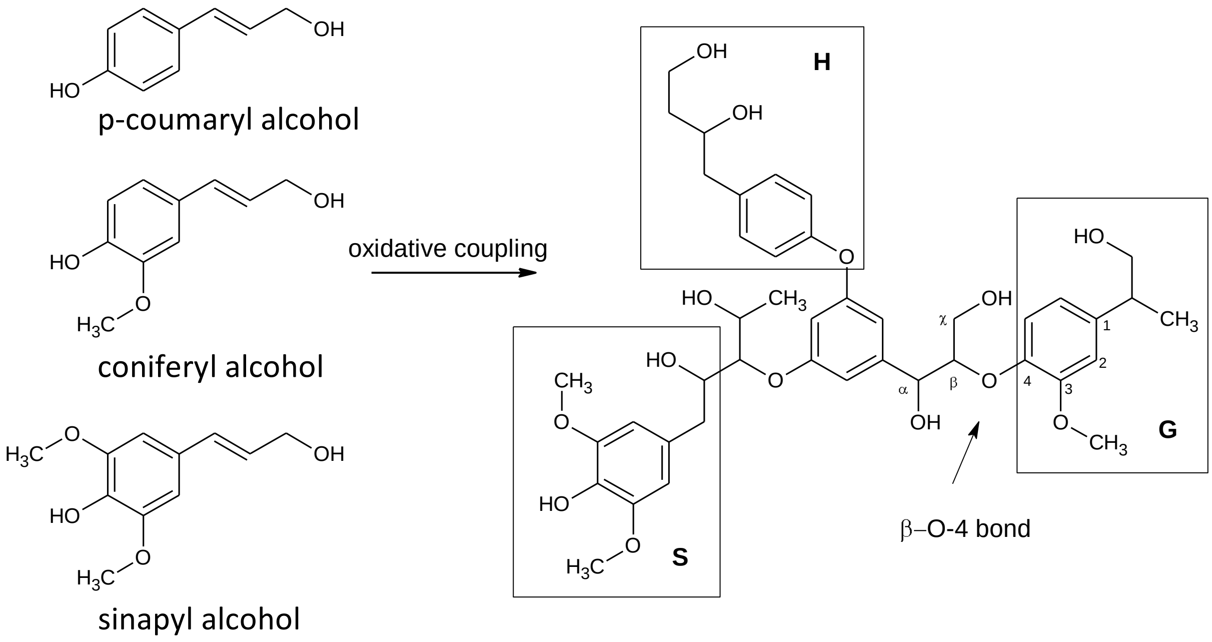

Figure 4-1: Enzymatic synthesis of lignin from the monolignol precursors p-coumaryl alcohol, coniferyl alcohol, and sinapyl alcohol. The phenylpropanoids p-hydroxyphenyl (H), guaiacyl (G), and syringyl (S) are marked with boxes.

Depending on the type of biomass, different proportions of H, G and S occur in the lignin framework. Coniferous woods consist of up to 90 % of G. In contrast, lignin from hardwoods has different compositions of G and S, whereby S varies between 5 % and 65 %. The molar ratio of syringylpropanoid to guaiacylpropanoid units (S/G) in hardwoods was determined to 0.37 and 0.42 for beech wood [208], 0.45 for elm, 0.70 for basswood, 0.70 for oak, 0.85 for maple, 1.00 for cherry, 1.00 for birch and 1.20 for poplar [209]. In general, the lignin of softwood species consists mainly of G, whereas the S content increases with increasing hardness of the wood. Grasses, on the other hand, have a mixture of all three building blocks in different ratios [206].

Monomers, dimers and oligomers, which have the same characteristic functional group as H, G and S subunits of lignin are commonly referred to as lignin model compounds (LMCs). They are used for the investigation of possible reactions of lignin. Common representatives of G-LMCs are vanillin, vanillyl alcohol and EROL, whose structures are provided in Figure 4-2.

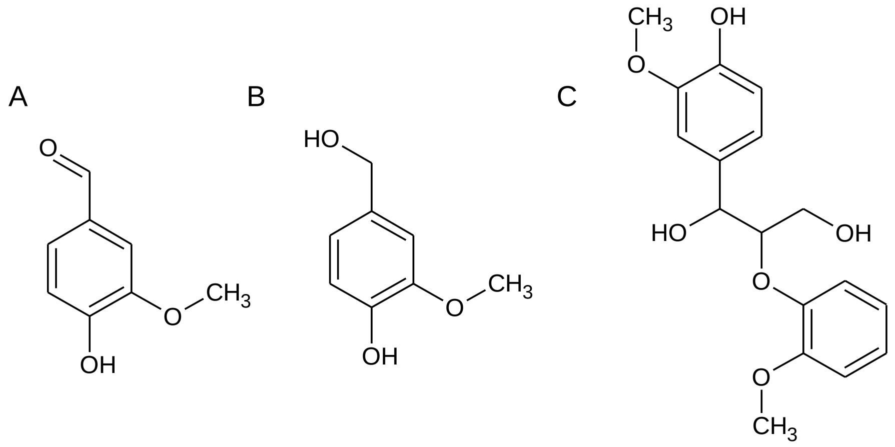

Figure 4-2: Chemical structures of the G-LMCs A) vanillin B) vanillyl alcohol and C) EROL.

4.1.2 Lignocellulose biorefinery concept

Due to the extreme resistance of lignocellulosic material, suitable pretreatment methods are necessary to achieve separation into the three basic components (cellulose, hemicellulose and lignin). Figure 4-3 schematically illustrates the process steps for the lignin extraction, using beech wood as an example. After mechanical disintegration (chipping), further processing of the lignocellulose using Liquid-hot-water (LHW) and Organosolv (OS) digestion is possible. The advantage of these digestion processes is the use of moderate temperatures and pressures, as well as the use of inexpensive, low-toxic solvents, such as ethanol.

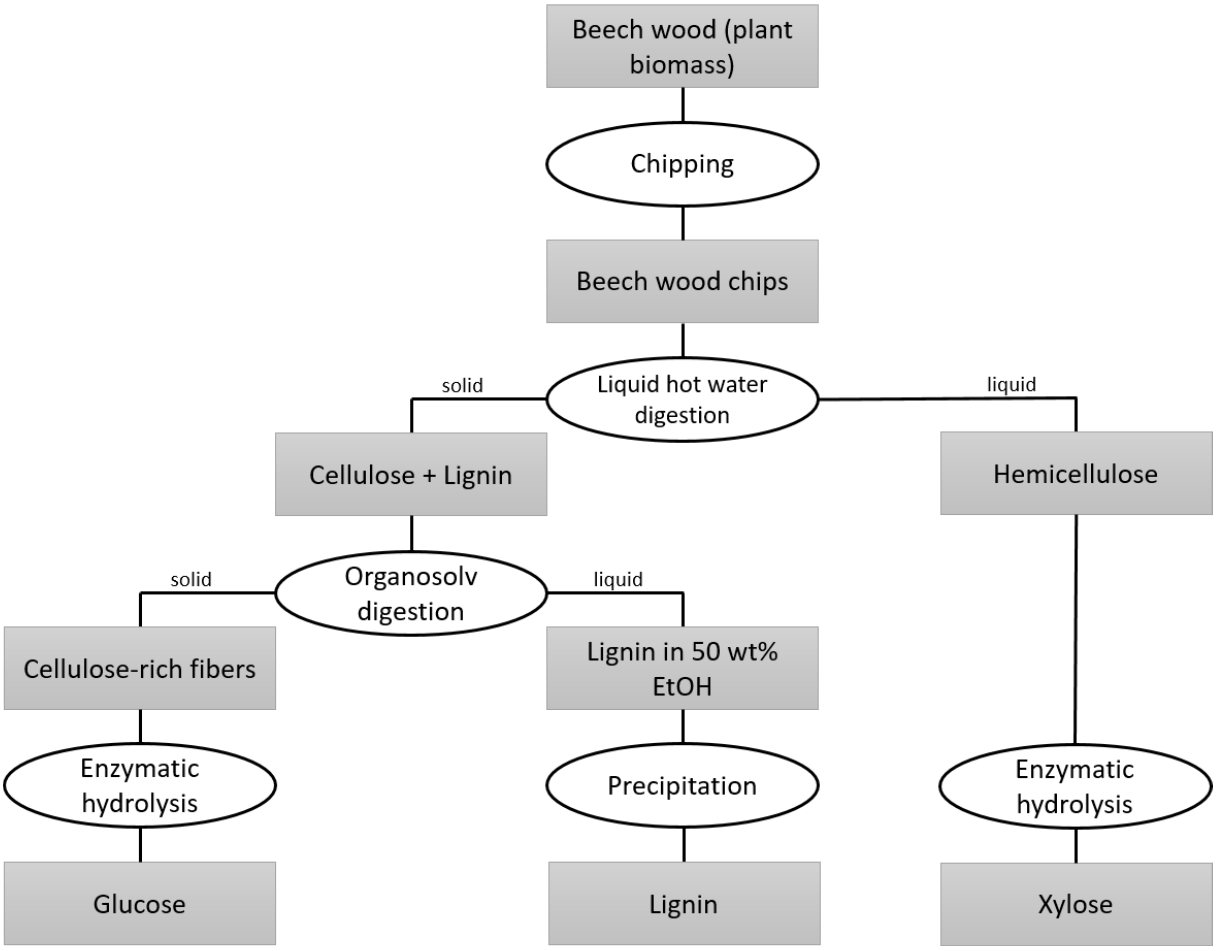
Beech wood (plant biomass)
Chipping
Beech wood chips
Liquid hot water digestion
solid
liquid
Cellulose + Lignin
Hemicellulose
Organosolv digestion
solid
liquid
Cellulose-rich fibers
Lignin in 50 wt% EtOH
Enzymatic hydrolysis
Precipitation
Enzymatic hydrolysis
Glucose
Lignin
Xylose

Figure 4-3: Two-step extraction of lignin extraction from lignocellulose (beech wood).

During LHW digestion, the hemicellulose is extracted using hot water at 160 °C to 180 °C for 15 min to 30 min. Further enzyme treatment of the hemicellulose results in its monomers xylose and arabinose [3]. Using 50 wt% ethanol as solvent, OS treatment of the cellulose-lignin fibers is used to dissolve lignin, resulting in a liquid lignin fraction and solid cellulose-rich fibers. Further enzyme treatment of the cellulose-rich fibers results in glucose. The monosaccharides (glucose from cellulose, as well as xylose and arabinose from hemicellulose) can be either marketed directly or purified and further processed using biological fermentation processes, to produce platform chemicals (such as ethene or butanol), which are the basic building blocks for many chemical syntheses [3].

For optimal economical use, there is a great need for further development of application areas of the lignin fraction, which is dissolved in 50 wt% ethanol after OS digestion [1, 210]. The dissolved lignin can either be directly used or precipitated by lowering the ethanol concentration to 25 wt%. The lignin can be used directly as a polyaromatic polymer or further broken down into its monomer components, using subsequent processes, such as enzyme catalyzed hydrolysis [211]. Compared with other processes, such as the sulphite or sulphate process and other acid-catalysed digestion processes, the OS digestion has the advantage that high yields of sulphur-free, high-quality lignin, dissolved in 50 wt% ethanol, become available [210].

Since lignin is often used for thermal use for combined heat and power generation, a lot of its potential remains unused and there is still a great need for further development of value-added products from lignin. Due to its complex polyphenolic structure, lignin is able to provide starting materials for the synthesis of high-quality products [3]. Value-added products from lignin can increase the competitiveness of the lignocellulose biorefinery.

4.1.3 Reactions of lignin and LMCs

4.1.3.1 Condensation reaction

A condensation reaction is a class of organic addition reaction which is used to produce addition products [212]. Polycondensation is reoccurring sequence of condensation reaction, which converts monomers into polymers (plastics), while eliminating water molecules from the reactants at each polymerizations step. An example for the polycondensation of lignin using formaldehyde, is given in Figure 4-4 A.

One type of condensation reaction is the Mannich reaction, which consists of an amino alkylation of an acidic proton placed next to a carbonyl functional group by formaldehyde and a primary or secondary amine or ammonia. The Mannich reaction with amines is used, for example, to determine the ring positions of lignin which are accessible for crosslinking. Here, dimethylamine is reacted with formaldehyde and lignin. The result is the replacement of the active hydrogen atom on the aromatic ring by an amine methyl group (see Figure 4-4 B). By determining the nitrogen content in the reaction products, the number of reactive ring positions can be calculated [120].

In this work, condensation reactions are used to condensation lignin with diamines and formaldehyde, resulting in lignin functionalized with primary amines.

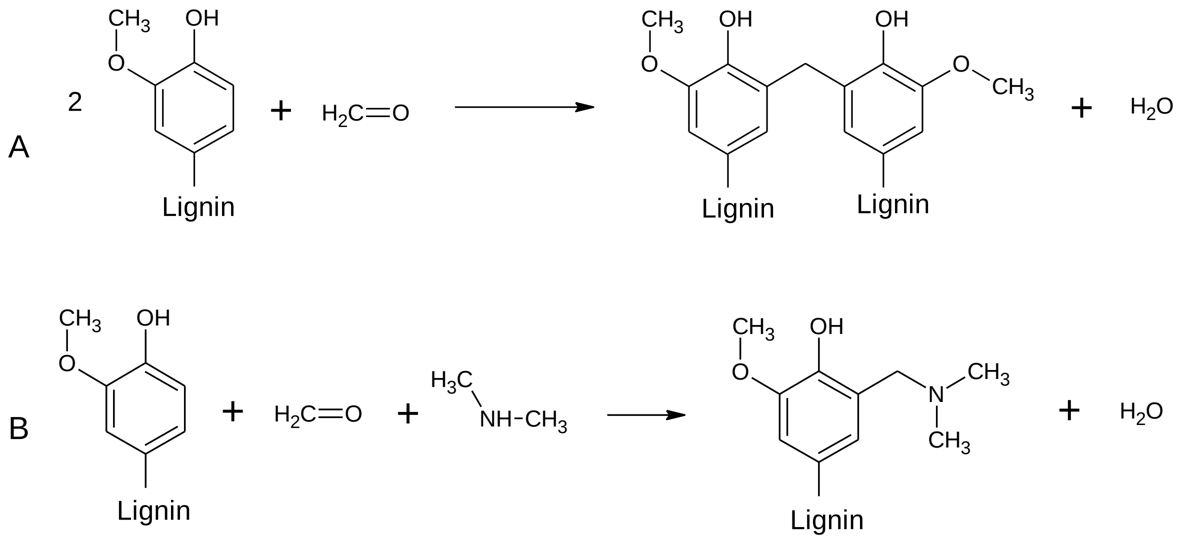

Figure 4-4: Reaction schemes of condensation reactions. A) Polycondensation reaction of lignin and formaldehyde, B) Mannich reaction of lignin, formaldehyde and dimethylamine.

4.1.3.2 Anionic addition

An alternative to the condensation reaction is the anionic addition, which does not require the use of formaldehyde. The reaction is initiated by the formation of a carbanion, which is formed in a basic environment. Subsequently, monomers are added, while retaining the negative center. The reaction ends when no more monomers are available or when the polymerization is chemically stopped. Long reaction times, highly polymerized products and narrow molecular weight distributions are common for anionic addition reactions [213, 214].

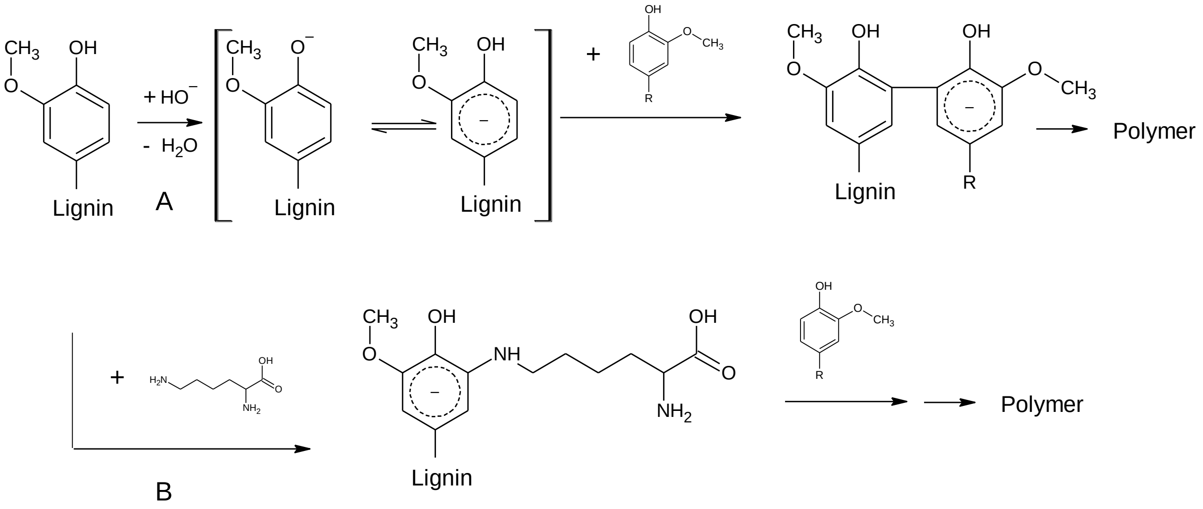

Figure 4-5: Anionic addition of lignin. The reaction is initiated by the formation of a carbanion, which is promoted in a basic environment (A) or by the addition of nucleophilic monomers, such as L-lysine (B). Subsequently, low molecular lignin is added, resulting in the formation of polymerized lignin.

Figure 4-5 shows possible mechanisms for the anionic addition reaction of lignin, which is promoted in a basic environment or by the addition of nucleophilic monomers, such as L-lysine, which is deprotonated at a pH of 9.7. The anionic addition of lignin (with itself) results in polymerized lignin. In comparison, when primary amines (such as L-lysine) are used in combination with lignin, a Mannich-type addition of the amine group to the lignin occurs, resulting in lysine-lignin.

4.1.4 Two-step concept for lignin functionalization

The laccase-catalysed functionalization of lignin with L-DOPA was difficult due to the melanin formation from L-DOPA (see chapter 2). Furthermore, it was observed that L-DOPA suppresses all further reactions with other possible reaction partners due to its substrate properties (data not shown). Therefore, even though L-DOPA is an excellent substrate for laccases, it is not a suitable reaction partner for the formation of a catechol-lignin adhesive.

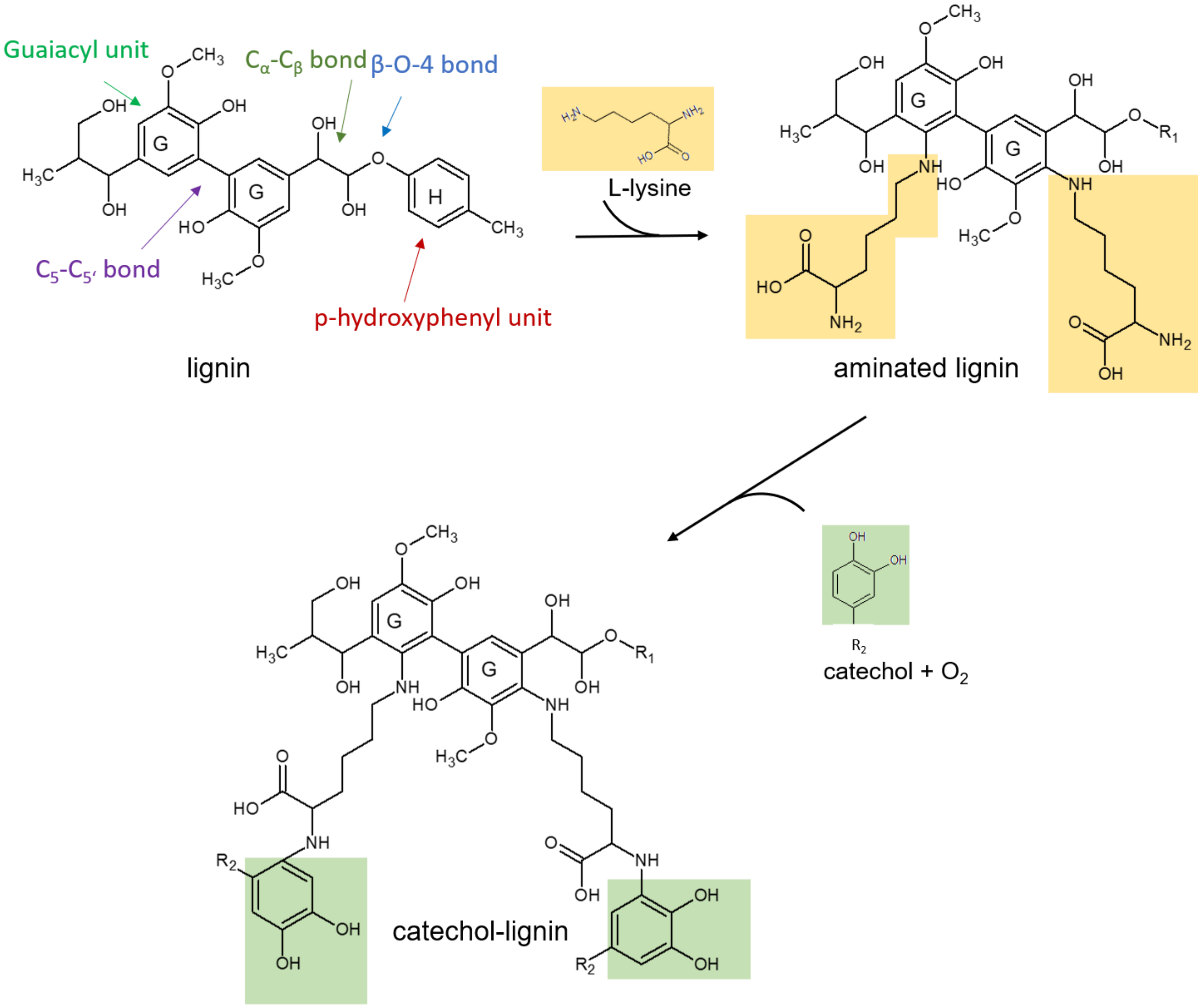

Figure 4-6: Two-step functionalization of lignin using a linker molecule. Step 1: The linker molecule L-lysine is bound non-specifically to lignin. Step 2: The catechol group is catalysed by laccases and bound to the terminal amine groups.

In addition to the challenges faced using L-DOPA, lignin itself varies, depending on its origin, strongly in its composition (see section 4.1.1). The inhomogeneity of lignin [71] makes a specific reaction challenging. In order to circumvent these problems, lignin is functionalized with a L-DOPA-derivate using a two-step reaction process.

In chapter 3, the functionalization of chitosan, which naturally consists amine groups, was introduced. Protocatechuic acid (PCA) was grafted into the primary amines for the development of a biogenic, mussel mimicking adhesive. In order to establish a similar reaction model with lignin, instead of chitosan as backbone, lignin is first functionalized with L-lysine, resulting in lysine-lignin. The amine group of the lysine serves further as linker molecule between lignin and catechol group. The L-lysine introduces a primary amine group to the lignin, which is further available for enzymatic catalyzed C-N formation with catechols, as described in chapter 2 and 3.

L-lysine is an essential amino acid, that is found in various foods, such as fish, meat, eggs and legumes. Furthermore, it is a metabolic product of the genetically modified organism *Corynebacterium glutamicum* and can therefore be produced from renewable resources [215]. As shown in Figure 4-6, in the 1st reaction step, L-lysine is bound to lignin in an undirected manner using condensation reactions (see section 4.1.3.1) or anionic addition (see section 4.1.3.2). Thereby, L-lysine can react once or twice with lignin, promoting either the cross-linking of lignin or providing a free amine group for the subsequent reaction. In the 2nd step of the reaction, the catechol group can react with the free amine group of L-lysine. For this step, the laccase-catalyzed Michael-type addition (see chapter 2) is applied. Monomeric catechols are usually good substrates for laccase, so that they are preferably converted. Besides the directed reaction of the catechol group with L-lysine, the catechol group can also bind non-specifically to lignin. Ideally, all monomers can be bound to lignin and no further purification step is required.

4.2 Materials and Methods

4.2.1 Pretreatment and extraction of lignin

A pressure reactor (Parr Instrument) with a total volume of 7.5 L and a usable volume of approximately 5 L was used for the pretreatment of biomass and extraction of lignin. Beech wood chips with a size of approximately 1 cm^2 (with a thickness of about 1-2 mm) served as substrate for the digestion experiments.

For liquid hot water (LHW) pretreatment of biomass, a liquor ratio of 5:1 (water to biomass) was used and temperatures between 160 °C and 180 °C were applied. In order to increase the digestion efficiency sulphuric acid (1 wt% and 2.5 wt%) and phosphoric acid (5 wt%) were added as a catalyst. The solids were separated from the liquids, which were rich in hemicellulose. The solids, which were rich in cellulose and lignin, were further process in the OS digestion for the extraction of lignin.

For the OS digestions of beech wood a liquor ratio of 5:1 (solvent to solid) was used: 200 g of beech wood chips or LHW pretreated beech wood were digested with 400 g of water and 400 g of ethanol (technical). The digestions took place at temperatures between 160 and 200 °C, which correspond to a steam pressure of up to 25 bar. 50 wt% ethanol (technical) was used as solvent. Phosphoric acid (5 wt% and 7 wt%) were added as catalysts. The solids, which were rich in cellulose, were separated from the liquids, which were rich in lignin (and hemicellulose).

Lignin recovery

After OS digestion, the lignin, which was dissolved in the supernatant (50 wt% technical ethanol), was precipitated by reducing the ethanol concentration to 25 wt%. The lignin was separated by centrifugation at 4000 x g, dried at 50 °C and gravimetrically analyzed.

4.2.2 Amination reaction of OS lignin (1st step)

4.2.2.1 Condensation reactions of L-lysine with OS lignin

Condensation of L-lysine with OS lignin was used to functionalize lignin with amines via Mannich reaction. The amination was carried out according to [216]. OS lignin was dissolved in a mass ratio of 1 to 1.5 with the respective amine (L-lysine or diethylenetriamine (DETA), see Figure 2-8 A and D) in 10-times the amount of deionized water (based on lignin), resulting in 100 g L^{-1} of lignin and 150 g L^{-1} of L-lysine. A pH value of 10.5 was adjusted if this was not automatically achieved by the basicity of the amine. Formaldehyde was then added to the lignin in a mass ratio of 1 to1 and the reaction batch was incubated at 50 °C for 3 hours. The product was precipitated in isopropanol, separated by a filter funnel, and dried.

Purification of precipitated lysine-lignin

To separate the lysine-lignin from unbound lysine, the product was resuspended in distilled water and a pH value of 2 was adjusted. The solids which precipitated at pH 2 were separated by centrifugation. A pH value of 6 was set and the precipitated solids separated first by filtration and then by centrifugation. The lysine-lignins were analyzed by GPC analysis. Repeated GPC analysis showed that precipitation enhanced the product purity (data not shown).

4.2.2.2 Anionic addition of LMCs with amines

The anionic addition of LMCs with NAcDAP was used to investigate and optimize influencing reaction parameters, such as reaction temperature and incubation time.

The screening of LMCs and amine donors was conducted using the LMCs syringaldehyde, sinapic acid, ferulic acid, p-coumaric acid, acetovanillone, vanillin, vanillin alcohol, guaiacylglycerol-beta-guaiacyl-ether (abbreviation: EROL) and 1-(3,4-dimethoxyphenyl)-2(2-methoxyphenoxy)-propane-1,3-diol) (abbreviation: ADLEROL) in combination with the amine donors dopamine, L-DOPA and NAcDAP. Stock solutions of 100 mM LMC or amine donor were prepared in 50 vol% ethanol (p.a.) or water (for sinapic acid and L-DOPA). The LMCs and amine donors were mixed together to a final concentration of 20 mM using deionized water and the pH was measured. The reaction was incubated for 1 hour at 100 °C. As background measurements, LMC and amine donors were dissolved at 20 mM and analyzed separately.

For further investigation of the reaction, the reaction parameters temperature and incubation time were analyzed using the G-LMCs vanillin and EROL in combination with NAcDAP. A final concentration of 20 mM of LMC and NAcDAP was used with either 20 vol% ethanol (p.a.), 50 vol% ethanol (p.a.) or 50 wt% technical ethanol. Different incubation times (1 hour and 24 hours) were compared and different reaction temperatures (RT, 40 °C, 75 °C and 100 °C).

The analysis was conducted via HPLC-MS analysis as described in chapter 2, section 2.2.7.

4.2.2.3 Anionic addition of L-lysine to OS lignin

Anionic addition of OS lignin with L-lysine was used to functionalize lignin. For this purpose, solutions containing different concentrations of OS lignin (20 g L^{-1} and 100 g L^{-1}) and L-lysine (5 g L^{-1}, 10 g L^{-1} and 50 g L^{-1}) were prepared and a pH-value of 11 was adjusted. The solutions were incubated at 50 °C or 25 °C (Add#1). In preliminary tests, the observation was made that in aerobic reactions about 50 % more L-lysine was bound to lignin compared to anaerobic reactions. Therefore, the solutions were incubated under stirring in open reaction vessels. The pH value dropped during the reaction, due to the reaction progress of the anionic addition. In order to investigate the influence of this effect, in some reactions, the pH value was adjusted to pH 11 every 24 hours for a total of 72 hours. The experimental approaches are summarized in Table 4-1. A preparation with 10 g L^{-1} L-lysine serves as a control reaction (Add#7). For sampling, 1 ml solution was taken and the pH value was adjusted to 3 in order to precipitate the lignin from the solution. Afterwards, the lignin was separated by centrifugation at 16,500 x g and the supernatant was analyzed for its L-lysine content. The supernatant was diluted with borate buffer (1:1000) and measured by HPLC analysis (see section 4.2.4.1).

Table 4-1: Reaction preparations of the anionic addition of OS lignin with L-lysine.

	OS lignin [g L $^{-1}$]	**L-lysine [g L $^{-1}$]**	**Adjustment of pH value**	**Temperature [°C]**
Add#1 (25 °C)	20	10	No	25
Add#2 (50 °C)	20	10	No	50
Add#3 (50 °C, pH)	20	10	Yes	50
Add#4 (50 °C)	20	5	No	50
Add#5 (50 °C, pH)	20	5	Yes	50
Add#6 (50 °C, pH, 5x)	100	50	Yes	50
Add#7 (control, no OS lignin)	0	10	No	50

4.2.3 Functionalization of lysine-lignin (2nd step)

The aim of the 2nd reaction step was the functionalization of lysine-lignin with catechols. For this purpose, lysine-lignin from anionic addition reaction (see section 4.2.2.3) was reacted with different catechol donors (PCA and DHC). A saturated lysine-lignin solution (approximately 13 g L^{-1}) was mixed with 10 g L^{-1} catechol and incubated for 24 h at 30 °C in an open reaction vessel, while lightly stirred. Afterwards, the reaction pH of the sample was lowered to 3, in order to precipitate the functionalized lignin from the solution and the liquid was removed by centrifugation. The pellet was analyzed by Ninhydrin assay (see section 4.2.5.1) and FT-IR spectroscopy (see section 4.2.5.2). Subsequently, the tensile strength was tested for selected solvents (see section 4.2.6). In order to investigate the functionalization of lysine-lignin with a catechol, different initial pH values (5 and 6.5), the use of a catalyst (no catalyst or laccase from *C. unicolor*) and different catechols (PCA and DHC) were tested. The reaction preparations are summarized in Table 4-2.

Table 4-2: Reaction parameters for the functionalization of lysine-lignin from anionic addition Add#6 (see section 4.2.2.3).

Name	Initial pH [-]	Catechol	Catalyst used
#7	5.0	-	-
#1	5.0	DHC	-
#2	5.0	PCA	-
#3	5.0	PCA	Laccase from *C. unicolor*
#8	6.5		-
#4	6.5	DHC	-
#5	6.5	PCA	-
#6	6.5	PCA	Laccase from *C. unicolor*

4.2.4 Chromatographic analysis

4.2.4.1 L-lysine detection

The L-lysine concentration was quantified in the supernatant after anionic addition of L-lysine to OS lignin (see section 4.2.2.3). The detection of L-lysine was performed after precolumn derivatization with o-phthaldialdehyde (OPA), which reacts with primary amines of amino acids, peptide and proteins to enable fluorescent detection and quantitation.

For quantification of L-lysine, the samples were filtered and diluted with 0.4 M borate buffer (24.72 g L^{-1} boric acid, pH 10). Subsequently, 30 µl of sample were derivatized with 50 µl of OPA reagent (270 mg OPA in 5 ml ethanol (p.a.), 200 µl MCE and 45 ml 0.4 M borate buffer) and added to the column (Waters Resolve C18, 5 µm, 90 Å, 3.9 x 150 mm). The flow rate was 1 ml min^{-1} and the column temperature was 30 °C using a column oven. L-lysine was eluted using 100 % buffer B (46 vol% deionized water and 54 vol% methanol). The elution time was about 12.5 min.

4.2.4.2 Gel permeation chromatography (GPC)

GPC analysis was used to detect the molecular sizes of lignin. For GPC analysis two columns (Ultrahydrogel 120 and 250, Waters) were connected in series. Since the columns are stable in the pH range of 2 to 12 and lignin is soluble at high pH values, a glycine buffer pH 12 (3.14 g L^{-1} glycine, 2.45 g L^{-1} NaCl, 2 g L^{-1}NaOH) was used as a running buffer. The running buffer with 1 g L^{-1} ethylene glycol as internal standard, served as sample buffer. The temperature of the columns was adjusted to 60 °C, using a column oven. The flow rate was 0.5 mL min^{-1}, resulting in a pressure of about 18 bar. The measuring time for one sample was 45 min, since the internal standard, ethylene glycol, was eluted after about 4 min. After use, columns were stored in distilled water. The analysis of the molecular weight of lignin was performed using a refractive index detector (RID) with dextran standards (5 kDa, 12 kDa, 25 kDa and 50 kDa) at a concentration of 1 g L^{-1} as reference (four measurements each). The best fit was observed for a 4th degree polynomial with the following factors: intercept = 4.51295E7, B1 = 6.2627E6, B2 = 326512.40853, B3 = 7578.26583, B4 = 66.06033.

4.2.4.3 Extension of GPC analysis by a precolumn derivatization (GPC-OPA) for the detection of primary amines on lignin

The GPC analysis, which was established for the size characterization of lignin (see section 4.2.4.2), was extended by a precolumn derivatization with OPA for the analysis of aminated lignins. The precolumn derivatization with OPA is commonly used for the detection of primary amines, such as amino acids [217]. In this work, the aminated lignin samples were derivatized with OPA, in the presence of MCE, in order to detect primary amines which are bound to the lignins. A fluorescence detector (FLD) with an excitation wavelength of 330 nm and extinction wavelength of 450 nm was used to detect the content of primary amines as a function of molecule size, which can be quantified by either the simultaneous detection of the UV signal of lignin (at a wavelength of 280 nm) or by the quantification of the FLD signal of lignin in a second measurement without OPA. A reference was necessary to counteract the variety of solubility of different lignins. Simultaneous use of the FLD and RID was not possible, due to the fact that the OPA reagent produced a large amount of side products. The RID was used to perform a molecular weight analysis in a separate measurement, using dextran standards as reference, as described in section 4.2.4.2.

Sample preparation and measurement

To prepare the samples for GPC-OPA analysis, the lignin pellets were resuspended in sample buffer (10 mM NaOH). Subsequently, the pH of the sample was measured and if necessary adjusted to pH 12. Either 50 µl of borate buffer (reference measurement) or 50 µl of OPA-reagent were added to 30 µl sample and incubated for 1 min. Afterwards 10 µl were measured on a GPC with both a RID and a FLD.

Validation of GPC-OPA analysis

For the quantification of the amination degree of lignin, each sample was measured once after the addition of buffer (reference signal) and once after addition of the OPA-reagent. Afterwards the areas under the FLD signal were integrated.

In order to validate the new measurement different ratios of OS lignin and lysine-lignin from the condensation reaction (see section 4.2.2.1) were mixed (see Table 4-3) and analyzed with and without the addition of OPA.

Table 4-3: Mixtures of OS lignin and lysine-lignin (obtained during condensation reaction) for validation of GPC-OPA analysis.

Concentration of OS lignin [g L-1]	**Concentration of lysine-lignin [g L^{-1}]**	**Sum of lignins (OS lignin + lysine-lignin) [g L^{-1}]**	**Mass fraction of lysine-lignin [g g^{-1}]**
0.5	0	0.5	0
1	0	1	0
2	0	2	0
0	0.1	0.1	1
0	0.5	0.5	1
0	1	1	1
0	2	2	1
1	0.5	1.5	0.34
0.5	1	1.5	0.67
1	1	2	0.5

4.2.5 Biochemical and optical analysis of functionalization

4.2.5.1 Ninhydrin assay

A biochemical method for the detection of primary amines is the Ninhydrin assay, which uses the formation of Ruhemann's purple (absorption maximum at 570 nm) from

Ninhydrin in the presence of primary amines. Ruhemann's purple consists of two Ninhydrin molecules which are linked via a nitrogen molecule. In contrast to the detection of primary amines with OPA (see section 4.2.4.3), Ninhydrin does not bind to the amine, but forms a dimer with itself. This makes the Ninhydrin assay, in contrast to OPA derivatization, also suitable for the analysis of solid samples.

For the analysis of the reaction success of the lignin amination, the lignins were mixed with Ninhydrin reagent (0.50 ± 0.01 g of Ninhydrin were dissolved in 18.75 ml DMSO and 6.25 ml 4M sodium acetate buffer (pH 5.2) were added prior to analysis) and incubated at 95 °C for 10 min. During the incubation a blue-violet dye, the Ruhemann's, purple was formed, leaving deaminated lignin-aldehyde. Afterwards, the lignin was removed from the suspension by centrifugation at 16,500 x g, in order to minimize the background absorption due to the self-coloring of lignin. A solution of 50 vol% ethanol (p.a.) was added as stabilizing agent (ratio 1 to 1). Using an Agilent Cary 50 UV-vis spectrometer, the supernatant was analyzed and the concentration of primary amines was quantified using a wavelength of 595 nm.

4.2.5.2 Mid-infrared analysis

Mid-infrared spectra were obtained using an FT-ATR mid-infrared spectrometer over the range of 4000 cm^{-1} to 650 cm^{-1}. Each sample was measured in triplicates. Water was used as background media.

4.2.6 Measurement of tensile strength

The tensile strength was tested in a butt joint test using aluminum cylinders with a diameter of 20 mm. The test surfaces were prepared with an abrasive pad and cleaned using first distilled water then acetone. One surface was covered with 21 µl of dissolved adhesive (300 g L^{-1}) in the corresponding solvent and gently placed on top of the other. Unless otherwise noted, the curing was conducted at 50 °C for 18 to 40 hours.

4.2.7 Cost analysis of catechol-lignin adhesives

The profitability simulation in the context of this thesis was carried out and evaluated with the help of the software SuperPro Designer© Version 9.0. The simulation was based on a hypothetical process scheme for the production of a bioadhesive from OS lignin, PCA and L-lysine. The aim was to show the framework conditions within which a functioning process must lie in order to be economically feasible and profitable. Based on these framework conditions, a first assessment of the economic efficiency was made.

4.3 Results and Discussion

OS lignin is a side stream of the lignocellulose biorefinery. Since its production is already established at pilot scale level, it is a suitable material for the development of value-added products. In this chapter, the attempt is made to functionalise OS lignin from beech wood with catechol groups to develop a mussel mimicking adhesive with a lignin backbone. First, the lignin extraction during OS digestion is optimized for maximum lignin yield and the use of OS lignin in laccase-catalyzed processes. These results are discussed in section 4.3.1. Furthermore, a two-step concept is applied, where lignin is substituted with new functional groups to increase its application areas. In section 4.3.2, the functionalization of OS lignin with L-lysine is investigated and discussed. The subsequent functionalization with catechols is presented in section 4.3.3. Following, the tensile strength for lignin and its derivates is discussed in section 4.3.4. Lastly, an economic evaluation of lignin-catechol adhesives was performed with the results presented in section 4.3.5.

4.3.1 Optimization of the lignin extraction in OS digestion

The OS digestion, as part of the lignocellulose biorefinery, is a gentle method to extract lignin from biomass (see section 4.1.2). Catalysts can help to better digest biomass and thus increase the yield of the biopolymers hemicellulose, cellulose and lignin [120]. Detailed optimization of the digestion in regards to the extraction of fermentable sugars is found in literature [5, 120], where parameters such as temperature range, stirrer speed, size and moisture content of the wood chips were optimized for beech wood. When using different raw materials, such as pine, bamboo or straw many parameters must be optimized and challenges arise. Pine, for example, is quite sturdy, which makes the production of uniform wood chips challenging. The difficulties in using straw as raw material is, that the long fibers rapped around the stirrer. Therefore, in this work, a focus was set on beech wood as a substrate for lignin extraction.

In this work, different extraction conditions (temperature and use of catalyst) (see section 4.3.1.1), as well as the LHW pretreatment were investigated for the extraction of lignin from beech wood (see section 4.3.1.2). Furthermore, the compatibility of dissolved OS lignin for further functionalization is discussed (see section 4.3.1.3).

4.3.1.1 Optimization of the lignin yield during OS digestion by variation of temperature and catalyst concentration

In this section, the lignin yield from beech wood was optimized in relation to the temperature used in the OS digestion, while adding different concentration of phosphoric acid (5 wt% and 7 wt%) as catalyst. The use of both, sulphuric acid and phosphoric acid, has been shown to increase the digestion efficiency of the OS digestion [5]. Phosphoric acid, however, appears to be more suitable as a catalyst, since it is less corrosive to the steel reactor [5].

Lignin was extracted from beech wood via OS digestion, using 50 wt% ethanol as solvent (see section 4.2.1). Figure 4-7 shows the lignin yield related to the theoretical maximum lignin concentration, which was determined using acid hydrolysis (4 % sulfuric acid) according to the NREL protocol, which was developed by the National Renewable Energy Laboratory [218]. About 12 wt% to 39 wt% of the theoretically available lignin could be recovered from non-catalysed digestions. Lignin precipitation after the use of 5 wt% phosphoric acid in the digestion resulted in a recovery rate of 56 wt% to 73 wt% lignin, showing a strong positive influence of the catalyst phosphoric acid. An increase of the catalyst concentration from 5 wt% to 7 wt% under constant reaction conditions (160 °C, holding time 30 min) did not result in a further increase of the lignin yield. A maximum of 73 wt% of lignin was obtained at 180 °C with 5 wt% phosphoric acid.

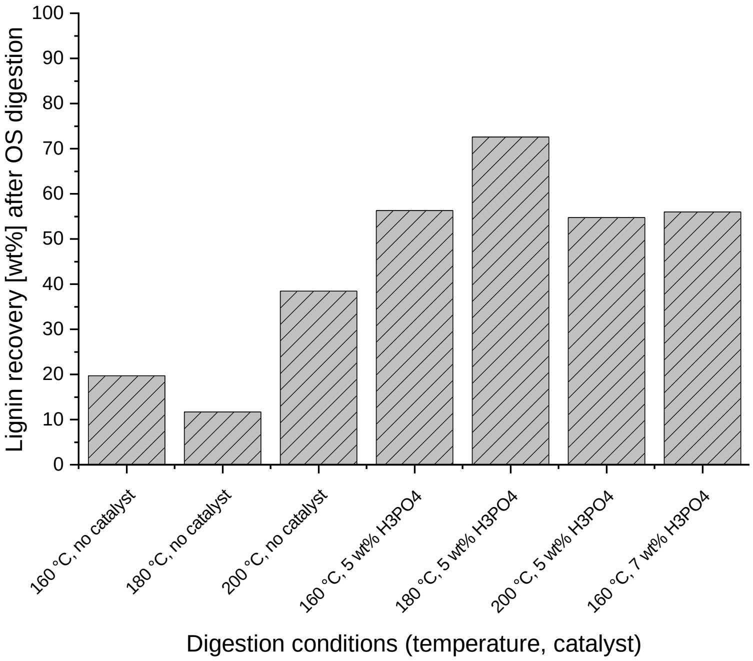

Figure 4-7: Lignin recovery after OS digestion in relation to the theoretical total mass of lignin, using beech wood as substrate, a liquor ratio of 5:1 with 50 % ethanol and 30 min holding time at the specified maximum temperatures. The lignin was precipitated by dilution to an ethanol concentration of 25 wt%.

Influence of the OS digestion conditions on the fiber content and lignin recovery

The solids, which were separated from the lignin-rich OS-supernatant, were further analyzed gravimetrically. This gravimetric evaluation of the solid residues after OS digestions is shown in Figure 4-8. The total amount of solid residue decreased with increasing process temperatures. While 87 wt% of fibers were recovered after digestion at 160 °C, only 52 wt% were recovered after digestion at 200 °C (in relation to the beech wood used in the digestion). For the investigated digestion temperatures 160 °C, 180 °C and 200 °C, the biomass decreased linear with increasing temperature. The decrease in remaining fiber cannot be explained by the increased extraction of lignin alone, since the total yield (remaining fibers and recovered lignin) together decreased as well. It was concluded that at higher temperatures the amount of hemicellulose which was extracted increased as well. Furthermore, NREL analysis (acid hydrolysis according to [218]) showed that the total amount of glucose and xylose remaining in the solid decreased (data not shown). Therefore, it was concluded that not only lignin and hemicellulose, but also cellulose passed into the supernatant at high process temperatures of 180 °C and 200 °C. This corresponds well with previous finding that not only lignin and hemicellulose, but also cellulose are degraded and dissolved at process temperatures above 180°C [5].

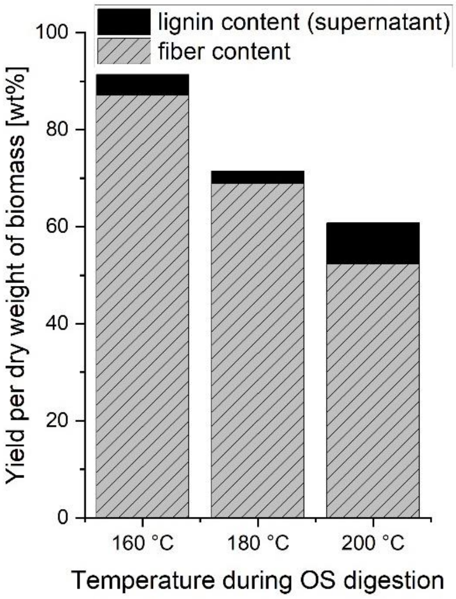

Figure 4-8: Fibre content (solid) and lignin recovered from the supernatant of beech wood after OS digestion at different temperatures (160 to 200 °C), displayed in relation to the total dry weight of solid (dry matter). Beech wood was used as substrate with a liquor ratio of 5:1 with 50 % ethanol as solvent and 30 min holding time at the specified maximum temperatures.

The aim of the thermal pretreatment of lignocellulose was to separate the polymers from each other without damaging them and without producing any by-products, some of which are toxic to microorganisms, therefore making low process temperatures favorable for the lignocellulose biorefinery concept.

Influence of the OS digestion conditions on the molecular weight of OS lignin

North et al. (2017) have shown that the adhesion properties of mussel mimicking adhesives depend significantly on the chain length of the individual molecules: While a lap shear strength of 0.5 MPa was measured at a molecular mass of less than 30,000 g mol^{-1}, a lap shear strength of 2 MPa was determined at a molecular weight of at least 50,000 g mol^{-1} [20].

In literature, the reported molecular weight of OS lignin varied between 600 and 1000 g mol^{-1}, which corresponds to a chain of only 4 to 8 monomers, and 2000 to 6000 g mol^{-1}, which corresponds to about 40 monomers [120]. In both cases, the molar mass reported for lignin was smaller than the optimal molecular weight of 50,000 g mol^{-1} and analysis of the molecular weight was important.

In this section, the molecular sizes of the purified OS lignins, which were produced under varying temperatures and phosphoric acid concentrations (see section 4.3.1.1), were investigated using GPC analysis (see section 4.2.4.2). The mean molecule size (averaged over the molecular weight) of all OS lignins was 5.9 kDa ± 0.3 kDa. None of the determined molecule sizes deviated significantly from this (data not shown). Therefore, no influence of the digestion conditions (temperature and phosphoric acid concentration) on the molecule size of the OS lignins was evident. The molecular weight of the OS lignins correspond well with the molecular weight of 2000 to 6000 g mol^{1}, which was reported in literature [120]. The OS lignins purified in this work had a chain length of approximately 40 molecules.

Influence of the OS digestion conditions on the pH value of dissolved OS lignin

The solvent used for the OS digestion (50 wt% ethanol) had a pH value of 5.55. After the addition of 5 wt% phosphoric acid, the pH value dropped to 1.84 and for 7 wt% phosphoric acid to pH 1.66. In chapter 2, a laccase from *C. unicolor* was presented, which was catalytically active at ethanol concentrations of 50 wt%. The purified laccase from *C. unicolor* showed a broad pH optimum of about 5.5 to 6.5 with a maximum at 6.0 towards syringaldazine and 5.5 for the conversion of PCA to 1,2-benzoquinone-4-carboxylic acid (BQA). A loss of activity was found below a pH of 3.5. The use of phosphoric acid in the OS digestion was therefore only suitable if no direct enzymatic recycling of the supernatant was intended. In contrast, OS lignin from OS digestions without the addition of catalyst, is suitable for direct use as a substrate for enzymatic reactions. Further optimization of lignin extraction was conduction with respect to the resulting pH value.

In summary, it was found that the lignin yield during OS digestion varied on the temperature and phosphoric acid concentrations used in the process: Using 5 wt% phosphoric acid and a temperature of 180 °C about 75 % of the theoretically available lignin was extracted from the beech wood. In contrast, when no catalyst was used and a temperature of 160 °C, only 19.7 wt% of lignin were extracted. The pH of the dissolved OS lignin after OS digestion without the use of a catalyst was approximately 5.55, which was compatible with the solvent stable laccases from *C. unicolor*. In contrast, the pH after OS digestion using phosphoric acid was below 2, hence making direct enzymatic conversion with the laccase less feasible. The adjustment of the pH is counterproductive, due to precipitation of this OS lignin at neutral pH values. Furthermore, it was found that the extraction condition did not have an influence on the molecular weight of the OS lignin.

4.3.1.2 Lignin yield in OS digestion after previous LHW digestion (beech wood)

An alternative to the one-step extraction of lignin from beech wood via OS digestion is a two-step digestion, consisting of a LHW pre-digestion as well as an OS digestion. In the first step (LHW digestion), the water-soluble hemicellulose is removed by boiling hot water, leaving behind a solid consisting of cellulose and lignin. Cellulose and lignin are subsequently separated by OS digestion, resulting in dissolved lignin and remaining cellulose (solid) (reaction scheme see Figure 4-3). The final lignin solution after OS digestion contains less hemicellulose and short sugar molecules, compared to a one-step extraction. This can be advantageous for further processing, especially when the dissolved lignin is used without further purification.

In this section, the use of a catalyst in the LHW digestion was investigation for its influence on the lignin yield after OS digestion. Catalysts were exclusively used during LHW digestion. The influence of the LHW digestion on the lignin yield in the OS process is shown in Figure 4-9. For the control reactions (without LHW pretreatment) an increase of the lignin yield with rising temperature was detected (black columns).

For the two-step extraction of lignin, the holding time of initially 60 min was divided between the two processing steps, resulting in a holding time of 30 min during the LHW digestion and a subsequent holding time of 30 min during the OS digestion. The lignin yield in the OS digestion, after previous LHW digest (see Figure 4-9, hatched columns), showed an increase in the lignin yield at a temperature of 160 °C compared to the process without LHW pretreatment. For a temperature of 170 °C, however, the lignin concentration did not change noticeably when an LHW pretreatment was performed.

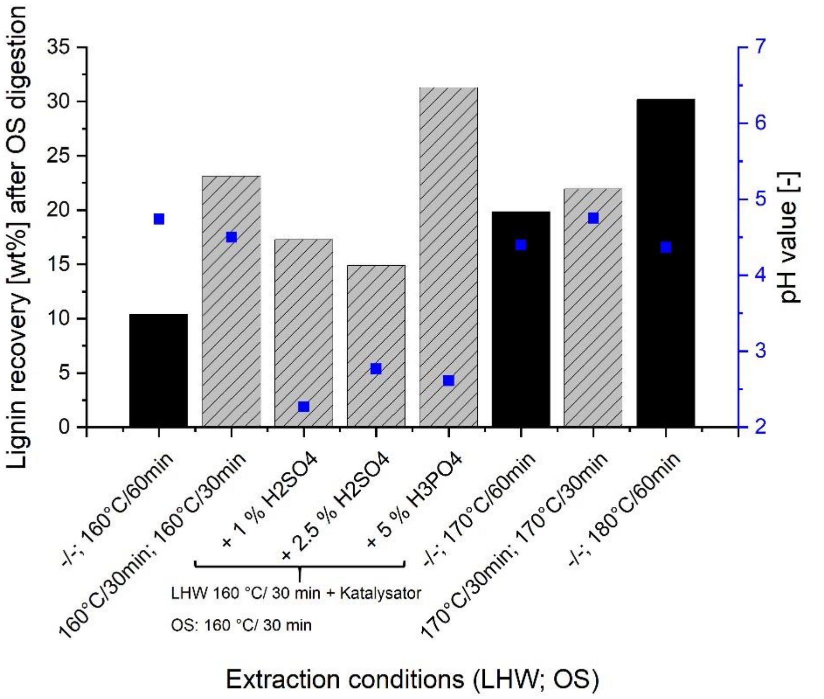

Figure 4-9: Influence of a two-step digestion on the lignin yield in the OS supernatant. In the first step, beech wood was digested by the LHW method (liquor ratio 1:5, addition of catalyst, see column labeling for further information). In the second step the pulp was further treated in an OS digestion (liquor ratio 1:5, 50 wt% ethanol). The temperatures and holding times can be taken from the column labeling. The pH values were measured in the OS supernatant after OS digestion (blue squares).

Without the use of a catalyst, the best results regarding the lignin yield was obtained at temperature of 180 °C (with a holding time of 60 minutes, without preceding LHW process), where 30.2 wt% of the total lignin was extracted. The resulting pH value was 4.37, which was compatible with the laccase from *C. unicolor*. The second best result (when no catalyst was used) was obtained for the two-step process at 160 °C (30 min holding time each). Compared to the 60-minute OS process (without upstream LHW digestion) at 160 °C, the lignin yield was more than doubled from 10.4 wt% to 23.15 wt%. The resulting pH value of 4.5 was also compatible with the catalytic activity of laccase from *C. unicolor*.

Furthermore, the addition of the catalyst sulphuric acid and phosphoric acid during the LHW digestion was investigated. While the addition of sulphuric acid in the LHW process had a negative effect on the lignin yield in the OS process, the addition of phosphoric acid increased the lignin yield (see Figure 4-9). It was concluded that the sulphuric acid in the LHW process caused partial lignin disintegration, whereby the lignin was not available for the OS digestion. A maximum of 31 wt% of lignin (based on the total available lignin content in beech wood of approximately 22.5 wt% [120]) were extracted after LHW and subsequent OS digestion at 160 °C for 30 min, using 5 wt% phosphoric acid as catalyst during LHW treatment. The analysis of the pH of the dissolved lignin after OS digestion found reaction pH values below 3 (see Figure 4-9, blue squares). It was concluded that the washing step after LHW digestion was insufficient to remove the remaining acids. A reaction pH below 3 was outside the catalytically active pH range of laccase from *C. unicolor*.

The pH of the dissolved OS lignin after OS digestion, when using 5 wt% phosphoric acid during LHW pretreatment, was 2.61. Compared to use of a catalyst in the OS digestion (see section 4.3.1.1), where the resulting pH was 1.84, after the use of 5 wt% phosphoric acid, this was a significant advantage towards compatibility with laccases. While the laccase from *C. unicolor* was not active at this pH, other laccases are [105, 219]. Therefore, it was advantageous to use the catalysis during LHW pretreatment, instead of the OS digestion, because the beech wood was broken down, but less catalyst was found in the OS supernatant.

4.3.1.3 Consideration of lignin extraction in the OS digestion for direct enzymatic conversion

The optimization of the lignin yield during OS digestion concluded that the reaction temperature and use of catalyst (phosphoric acid) during OS digestion (see section 4.3.1.1), as well as the use of a catalyst during the LHW digestion (see section 4.3.1.2) had a significant influence on the lignin yield. Furthermore, the resulting pH of the dissolved OS lignin was influenced by the use of a catalyst, hence the use of a catalyst has to be taken into consideration when biochemical conversion of dissolved OS lignin is sought.

The pH of the dissolved OS lignin after OS digestion without the use of a catalyst was about 4.5, which is compatible with the solvent stable laccases from *C. unicolor*. In contrast, the pH after OS digestion using a catalyst in either LHW or OS digestion resulted in a pH below 3, making enzymatic conversion more challenging. In addition to precipitation of the OS lignin due to pH adjustments, washing of the solids is a water consuming process and therefore disadvantageous for the ecobalance. The enzymatic conversion of OS lignin dissolved in 50 wt% ethanol using *C. unicolor* was therefore possible if no catalysts was used during digestion. Table 4-4 lists three digestion methods which can be used for a direct enzymatic conversion of OS lignin without prior precipitation. The maximum lignin concentration in the supernatant was 21.2 g L^{-1} after OS digestion at 200 °C with a holding time of 60 minutes.

Table 4-4: Summary of extraction conditions that are compatible with direct enzymatic conversion of OS lignin. Beech wood with a dry weight of 93.8 wt% was used as substrate for digestion via OS digestion alone or in combination with preceding LHW digestion. The holding times (30 min or 60 min) and the maximum temperatures (160 °C, 180 °C or 200 °C) are specified in first column LHW digestion was completed with a liquor ratio 1:5, without the addition of catalyst. OS digestion was completed with a liquor ratio of 5:1 with 50 % ethanol as solvent.

Digestion conditions (temperature, holding time)	**Lignin yield** [wt% per total lignin]	**Lignin concentration in OS supernatant** [g L^{-1} in 50 wt% ethanol]
200 °C OS, 30 min	38.5	21.2
180 °C OS, 60 min	30.2	16.6
160 °C LHW, 30 min + 160 °C OS, 30 min	23.2	12.7

While the extraction of lignin from straw was not part of this work, a few preliminary experiments found a resulting pH of 5.8 after OS digestion at a temperature of 180 °C and a holding time of 30 minutes (50 wt% ethanol with a liquor ratio of 5:1), hence making further investigation of straw as raw material for direct biochemical conversion interesting.

In order to evaluate the total soluble lignin content, precipitated OS lignin was dissolved. A maximum concentration of 29.1 g L^{-1} ± 2.0 g L^{-1} OS lignin in 50 wt% ethanol was reached. Under the aspect of economic efficiency, the question arises whether a substrate concentration of <30 g L^{-1} lignin is a good basis for a process. Low substrate concentrations often lead to high plant costs, since the plants have to be built accordingly large. The purification of the enzymes from the supernatant, after successful biochemical conversion, is also associated with high costs, as the enzyme concentration is correspondingly low. Furthermore, high transportation cost can occur if the down streaming is not conducted on site. Therefore, it was concluded that, if possible, the production of the adhesive from a solid lignin is the more cost-effective option. Following, the concept of the two-step functionalization of lignin (see section 4.1.4) was investigated.

4.3.2 Functionalization of lignin with primary amines (1st step)

As the one-step functionalization of OS lignin with L-DOPA, which plays a key role for surface adhesion in mussels [26], was challenging, a two-step process was developed.

In the 1st step, an amine group was transferred onto lignin to form an anchor molecule (see section 4.3.2). In a 2nd step, a catechol was grafted to the primary amine anchor (see section 4.3.3).

In section 4.2.2.1 the condensation reaction is investigated for the functionalization of OS lignin with primary amines, such as lysine. In literature, condensation reactions were used for the amination of lignin, but those reactions include the use of toxic co-substrate, such as formaldehyde [51]. Therefore, anionic addition was investigated as an alternative (see section 4.3.2.2). Suitable analytical methods are important for the optimization of the functionalization progress. Since optical and photometric methods often give poor results due to background signals, a chromatographic approach was chosen here. Precolumn derivatization with OPA and subsequent separation using a GPC column provides a promising approach for the detection of primary amines on polymers (see section 4.3.2.3).

4.3.2.1 Condensation of OS lignin and amines

The condensation reaction between amines and OS lignin were previously used to produce aminated lignin [51, 220]. In order to provide an anchor molecule for the laccase-catalyzed binding between catechols and lignin (2nd step), the condensation of lignin and amines was investigated. Three different amines, DETA, L-lysine and DAP (decarboxylation product of L-lysine), were reacted with OS lignin, using formaldehyde as reaction partner in a basic reaction environment (pH 10.5) (see section 4.2.2.1). For DETA a reaction temperature of 50 °C and 75 C were applied. As control reaction, OS lignin was reacted without the presence of amines. Furthermore, L-lysine and DETA were reacted in the absence of OS lignin.

After the completion of the condensation reaction, the reaction products were precipitated. The precipitation products of OS lignin with DETA (at 50 °C and 75 °C), L-lysine (at 50 °C) and DAP (at 50 °C) are shown in Figure 4-10. For the control reactions, when OS lignin was reacted in absence of an amine and when DETA was reacted alone, no product was precipitated. Therefore, it was concluded that the DETA-lignin products were free of non-reacted OS lignin, non-reacted DETA or polycondensed DETA. However, partial reaction cannot be excluded. For the control reaction with L-lysine, in the absence of lignin, a white product was precipitated (see Figure 4-10), which indicated that the precipitation product of L-lysine with OS lignin was a mixture of L-lysine monomers or polycondensated-L-lysine and aminated lignin.

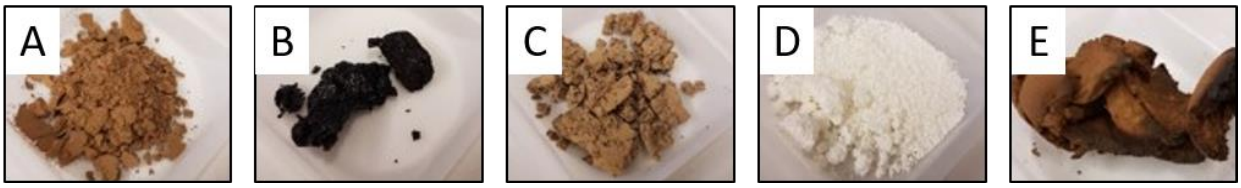

Figure 4-10: Precipitation products of amine lignin: A) DETA with OS lignin at 50 °C, B) DETA with OS lignin at 75 °C, C) L-lysine with OS lignin at 50 °C, D) polycondensed L-lysine at 50 °C and E) DAP with OS lignin at 50 °C. Reaction conditions: pH 10.5, holding time: 3 hours, ratio of amine to OS lignin to formaldehyde 5:1:1.

Investigation of purity and molecular weight of aminated lignin

The precipitated products after successful condensation reaction were analyzed using GPC analysis (see section 4.2.4.2). The molecular weight of untreated OS lignin was determined to approximately 6.2 kDa. The molecular weight of DETA-lignin was significantly larger with 11.8 kDa ± 1.1 kDa (at 50 °C) and 14.3 kDa ± 0.3 kDa (at 75 °C). The molecular weight increased by roughly two, hence suggesting that two OS lignin molecules are condensed with each other. Due to the lack of solubility in the sample buffer, it was not possible to determine the size of DAP-lignin with the method developed for this work.

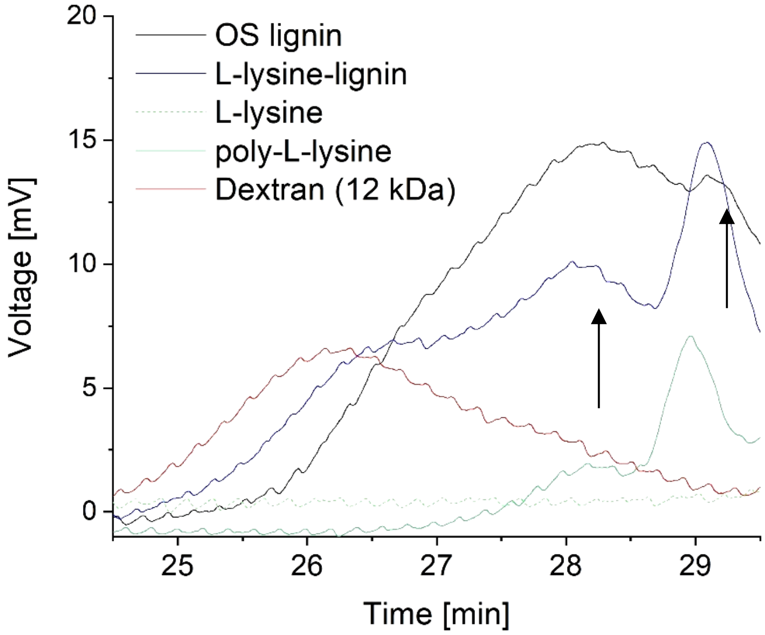

Figure 4-11: Section of a GPC chromatogram of OS lignin (in black), L-lysine-lignin (in blue), L-lysine (light green, dotted line) and polycondenced-L-lysine (dark green). As a reference, the 12 kDa dextran standard is shown in red. The arrows (black)mark the peaks of the polycondenced-L-lysine, which were found as contaminant in the L-lysine-lignine.

The GPC chromatogram of OS lignin, L-lysine, polycondensated-L-lysine and condensated lysine-lignin are shown in Figure 4-11. While the polycondensated-

L-lysine showed two peaks with an average molecular weight of approximately 2.7 kDa ± 0.3 kDa, which was absent in the L-lysine chromatogram, it was concluded that polycondensated-L-lysine (polymerization with itself) was produced due to the condensation reaction. The peak pattern of the GPC chromatogram of lysine-lignin indicated that lysine-lignin was contaminated with polycondensated-L-lysine, hence making purification of lysine-lignin necessary. The molecular weight of lysine-lignin was slightly increased compared to OS lignin, to 7.1 kDa ± 0.2 kDa.

Solubility of precipitation products

In order to confirm amination success, the solubility of the precipitation products in various solvents was investigated qualitatively. The comparison of the two DETA lignins (reaction temperature of 50 °C and 75 °C) showed that DETA lignin (50 °C) tended to be more soluble in solvents with a low relative polarity (Methyl-tert-butylether 0.124, tetrahydrofuran (TFH) 0.207, chloroform 0.259 and DSMO 0.444 [221]). In contrast, DETA lignin, which was produced at a temperature of 75 °C, was more soluble in methanol (relative polarity 0.762) and aqueous solutions.

The comparison of lysine-lignin and DAP-lignin with non-reacted OS lignin found a reduced solubility of lysine-lignin and DPA-lignin in organic solvents. While OS lignin was partially soluble in ethanol (0.789), acetone (0.786) and acetonitrile (0.786), no or little solubility was observed for lysine-lignin. In contrast to DETA lignin, the solubility of lysine-lignin and DAP-lignin in DSMO and THF had strongly decreased compared to OS lignin. The comparison of lysine-lignin and polycondenced L-lysine showed that differences in solubility can only be detected for aqueous solvents.

Solubility of lysine-lignin after purification

The analysis of the GPC chromatograms, as well as FT-IR spectra and DSC profiles (data not shown) suggested that lysine-lignin was precipitated as a mixture with polycondensed-L-lysine. The lysine-lignin was purified (see section 4.2.2.1) and its solubility was analyzed quantitatively. The solubility of physically adherent adhesives depends on the choice of a suitable solvent. Therefore, lysine-lignin was resuspended at different pH-values (pH 1, pH 1.6, pH 2.1, pH 7, pH 9.0, pH 10.7, pH 11.7, pH 12.0) and in different solvents (DMSO, methanol and acetone). Subsequently, non-soluble solids were separated by centrifugation and the solubility was determined in the supernatant. Purified lysine-lignin was insoluble in acidic solutions, but the solubility increases with increasing pH, starting at a pH of 9.0. As of a pH of 12, good solubility was given. Furthermore, lysine-lignin was partially soluble in DMSO, slightly soluble in methanol and not at all in acetone. After the addition of hydrochloric acid to the acetone mixture, a low solubility of lysine-lignin was observed. Hence, for the tested solvents a decrease in solubility of lysine-lignin was detected with an increasing polarity of the solvent. From the reduced solubility in the solvents, compared to the solubility of non-reacted OS lignin in those solvents, it was concluded that OS lignin was successfully aminated with L-lysine, resulting in a change of charge and polarity.

In conclusion, a lysine-lignin was produced via condensation reaction of L-lysine, OS lignin and formaldehyde. After precipitation, the product was contaminated with polycondensated-L-lysine, which needed to be separated. After separation, solubility experiments showed clear distinctions between lysine-lignin and OS lignin confirming successful amination. The comparison of lysine-lignin and DAP-lignin found, on the one hand, an increased solubility in DMSO and TFH, compared to OS lignin, but, on the other hand, some clear distinctions in aqueous solutions. While lysine-lignin was soluble at basic pH value, no solubility was detected for DAP-lignin. Since DAP was the decarboxylation product of L-lysine, it was concluded that the carboxylic acid changed the reactivity of the amine group during the condensation reaction. While both amine groups of DAP may have reacted with OS lignin during the condensation reaction, it was likely that only the ε-amine group of L-lysine reacted, leaving the α-amine group available for functionalization with catechols. Further analysis of the amination success is found in section 4.3.2.3.

4.3.2.2 Anionic addition

The condensation reaction between amines and OS lignin was successfully applied to produce lysine-lignin (see section 4.3.2.1). The disadvantage to using condensation reaction was the use of toxic formaldehyde as reaction partner. An alternative to the condensation reaction is the anionic addition (see section 4.1.3.2). In this section, first, the anionic addition of model compounds was investigated. Afterwards, the anionic addition of L-lysine to lignin was conducted, in order to provide an anchor molecule for the laccase-catalyzed binding between catechols and lignin (2nd step).

Anionic addition of LMCs with amines

The analysis of products from complex heterogeneous substrates (such as OS lignin) was difficult, therefore, in this section, the anionic addition of LMCs with NAcDAP was used to investigate and optimize influencing reaction parameters, such as reaction temperature and incubation time. The screening and optimization reactions were prepared as described in section 4.2.2.2. The analysis was conducted via HPLC-MS analysis as described in chapter 2, section 2.2.7.

For a first screening, the amine NAcDAP was used in combination with the LMCs syringaldehyde, sinapic acid, ferulic acid, p-coumaric acid, acetovanillone, vanillin, vanillin alcohol, EROL and ADLEROL. Furthermore, an attempt was made to use dopamine and L-DOPA as amines, instead of NAcDAP. However, no reaction products were found using an acidic or neutral reaction pH. In a basic environment, dopamine and L-DOPA were highly reactive, forming a black reaction product with itself (data not shown). Hence, the only suitable amine donor was NAcDAP.

Using NAcDAP as amine, dimeric and trimeric reaction products were found with all G-LMCs (ferulic acid, acetovanillone, vanillin, vanillin alcohol, EROL and adlerol), and no products were found for the tested H-LMC (p-coumaric acid) and S-LMCs (syringaldehyde, sinapic) (data not shown). Since under the selected reaction conditions, reaction products were only detected for G-LMCs, it was concluded that the concentration of G-units in lignin mainly influences the reaction success. The molar ratio of guaiacylpropanoid units to syringylpropanoid units (G/S) in beech wood was relatively high (2.4 and 2.7 [208]) compared to other hardwoods, such as elm, oak, maple, birch or poplar (see section 4.1.1), hence making beech wood the better substrate. In general, the lignin of softwood species consists mainly of G-units, therefore, in future work the anionic addition of L-lysine to softwood lignin need to be investigated. The concentration of G units in beech wood was determined to 0.24 and 0.38 mmol g^{-1} [208], which equals roughly 40 to 50 mol% of G units per lignin.

For further investigation of the reaction, the reaction parameters temperature and incubation time were analyzed, using G-LMCs. The monomeric LMC vanillin (see Figure 4-2 A) and the dimeric LMC EROL (see Figure 4-2 C) were selected in combination with NAcDAP. The reaction progress was analyzed using HPLC-MS analysis. As described in chapter 2, section 2.3.5, NAcDAP had a peak at 7.4 min with a mass of 144 g mol^{-1}. Vanillin had a peak at 6.7 min with a mass of 152 g mol^{-1} and EROL has a peak at 22.0 min with a mass of 320 g mol^{-1}.

For the reaction of vanillin with NAcDAP four products were detected. The first product had a peak at 20.0 min (product 1) and a molecular weight of 279 g mol^{-1}, which suggested the formation of a dimer (under the elimination of, for example, water). A second reaction product, which was predominant in all reactions, was found at 22.5 min (product 2) with a mass of 391 g mol^{-1}, suggesting the formation of a trimer which consists of two molecules of NAcDAP and one molecule of vanillin. The theoretical mass of such a trimer was 436 g mol^{-1}. The discrepancy of 45 g mol^{-1} may result from a deacetylation of the NAcDAP either during reaction or analysis via HPLC-MS. Furthermore, two reaction products were found at 24.5 min (product 3) and 25.2 min (product 4) with a mass of approximately 724 g mol^{-1} and 597 g mol^{-1}, suggesting further addition of monomers. However, detailed analysis was not possible due to multiple responses in the MS analysis.

Significant amounts of product were found at either long reaction times (24 hours) or high reaction temperatures (as of 75 °C and 100 °C). At RT and 40 °C after 1 hour of reaction time, almost no product was found. Reaction product 2 was predominant in all reactions. Product 4 only appeared after 24 hours of reaction time and at reaction temperatures above 75 °C. This is in agreement with literature, where high temperatures and long reaction times were identified as the preferred reaction conditions for anionic addition reactions [213].

The reaction between vanillin and NAcDAP was further used to analyze the influence of ethanol on the reaction progress. When using ethanol, the reaction success was decreased and product formation was only observed at temperatures above 75 °C and a reaction time of 24 hours. No product was formed after 1 hour of reaction time or at RT and 40 °C after 24 hours of reaction time. When using 50 vol% ethanol (p.a.) only product 2 and 4 were detected (after 24 h, 75 °C and 100 °C). When using 50 wt% technical ethanol only product 2 and 3 were detected (after 24 h, 75 °C and 100 °C).

The product formation was optically visible by the formation of a red color. Reaction vessels, where no products were identified via HPLC-MS analysis, had a yellow color in comparison (see Figure 4-12). Hence, the reaction success was clearly identified by a color change to red. In literature, it is described that adrenochrom, which had a red color, was formed from intramolecular C-N formation of epinephrine under acidic reaction conditions in the presence of $NaNO_3$ [222]. In contrast, norepinephrine, which did not form intramolecular C-N formation under these conditions, formed a yellow color due to a nitration reaction. The reaction condition between vanillin and NAcDAP were basic and without the presence of $NaNO_3$, hence, a nitration reaction was not confirmed. However, the red coloration due to the product formation between vanillin and NAcDAP suggested the formation of intermolecular C-N bonds. The red reaction product was separated using preparative thin-layer chromatography. Two red products with a R_f of 0.83 and 0.90, which were assigned to product 1 and 2, were separated (data not shown). No clear bands or product 3 and 4 were detected. Further analysis via NMR are needed to identify reaction mechanism and the structure of the products.

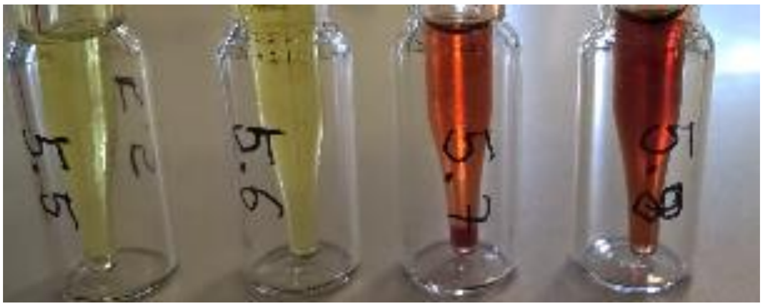

Figure 4-12: Reaction of vanillin with NAcDAP in 60 % technical ethanol after 24 h incubation time. Reaction preparations depending on the incubation time (from left: room temperature, 40 °C; 75 °C and 100 °C).

Furthermore, the reaction of EROL with NAcDAP was analyzed using HPLC-MS analysis. The influence of the reaction conditions temperature (RT, 40 °C, 75 °C and 100 °C) and reaction time (1 h and 24 h) on the dimerization of LMC EROL and NAcDAP was investigated. The reaction was carried out without addition of a catalyst at a pH of 10.3.

For the reaction of EROL with NAcDAP two products were detected using HPLC-MS analysis. The first product had a peak at 24.6 min with a mass of approximately 724 g mol^{-1} and 837 g mol^{-1}, which suggested the formation of a trimer. A second reaction product was found at 25.8 min and a molecular weight of approximately 485 g mol^{-1} to 531 g mol^{-1}, suggesting the formation of a dimeric product. The formation of the dimer and trimer depended primarily on the reaction time and less on the reaction temperature. While after 1 hour of incubation time, mainly the dimeric product was found, after 24 hours the trimer was detected, which was visible by a color change to a slight pink. The analysis of the EROL-NAcDAP products was difficult, because the MS analysis did not result in one clear product, but always in a mix of different ESI+ and ESI- ratios. Hence, the composition (ratio of EROL and NAcDAP) of apparent dimers and timers was speculative.

In conclusion, for the reaction of the G-LMC vanillin and EROL with NAcDAP dimeric and trimeric products were identified via HPLC-MS analysis. No catalyst, other than the basic pH, was added to the reaction, hence, it was suggested that an anionic addition of the LMCs and NAcDAP occurred. As known from anionic addition reaction [213], high temperatures (above 75 °C) and long reaction times (24 hours) were preferred reaction conditions for the addition of NAcDAP to the G-LMCs. Furthermore, it was observed that the reaction efficiency of the reaction of vanillin with NAcDAP decreased after the addition of ethanol.

Anionic addition of L-lysine to OS lignin

The anionic addition, which is free of harsh chemicals, offers an alternative to the condensation reaction (see section 4.3.2.1). In this section, the anionic addition of L-lysine to OS lignin was investigated for the functionalization of OS lignin. Seven different mixtures of OS lignin with L-lysine were reacted in a basic reaction environment at 25 °C or 50 °C (see Table 4-1 for further details) and the L-lysine concentration in the supernatant, after removal of OS lignin, was measured over the course of 72 hours (see section 4.2.4.1). A decrease of the L-lysine concentration was an indicator for successful addition of L-lysine to OS lignin.

Figure 4-13 shows the L-lysine reduction in the reaction medium due to the anionic addition of L-lysine to OS lignin. While the L-lysine concentration stayed constant throughout the control reaction (Add#7_control, no OS lignin present), for all other reaction, the L-lysine concentration decreased after incubation with OS lignin and precipitation of the resulting lysine-lignin (Add#1 to Add#6). After about 70 hours of reaction time, saturation of the L-lysine addition was reached. The reaction temperature of 25 °C versus 50 °C (Add#1_25°C and Add#2_50°C) did not have any influence on the L-lysine addition to OS lignin. The comparison of the reactions with and without pH correction (Add#2_50 °C and Add#3_50 °C, pH adjusted, as well as Add#4_50 °C and Add#5_50 °C, pH adjusted) found that the pH adjustment had a positive effect on the L-lysine addition to the OS lignin. In reaction Add#3 (50 °C, pH adjusted), about 8 g L^{-1} L-lysine were removed from the supernatant, resulting in a functionalization degree of approximately 3 g g^{-1} (~34 mol%). In comparison, the degree of functionalization of Add#5 (50 °C, pH adjusted) was about 24 mol%. Since a higher degree of functionalization was presumed to be better for the 2nd functionalization step, Add#3 (50 °C, pH adjusted) was more suitable. Since the substrate concentration used was relatively low (20 g L^{-1}), in the following, a reaction approach with a 5-fold substrate concentration was investigated. The comparison of the 1-fold concentration (Add#3_50 °C, pH adjusted) and the 5-fold concentration (Add#6_50 °C, pH adjusted, 5x concentration) showed similar reaction progress (see Figure 4-13, inserted graph).

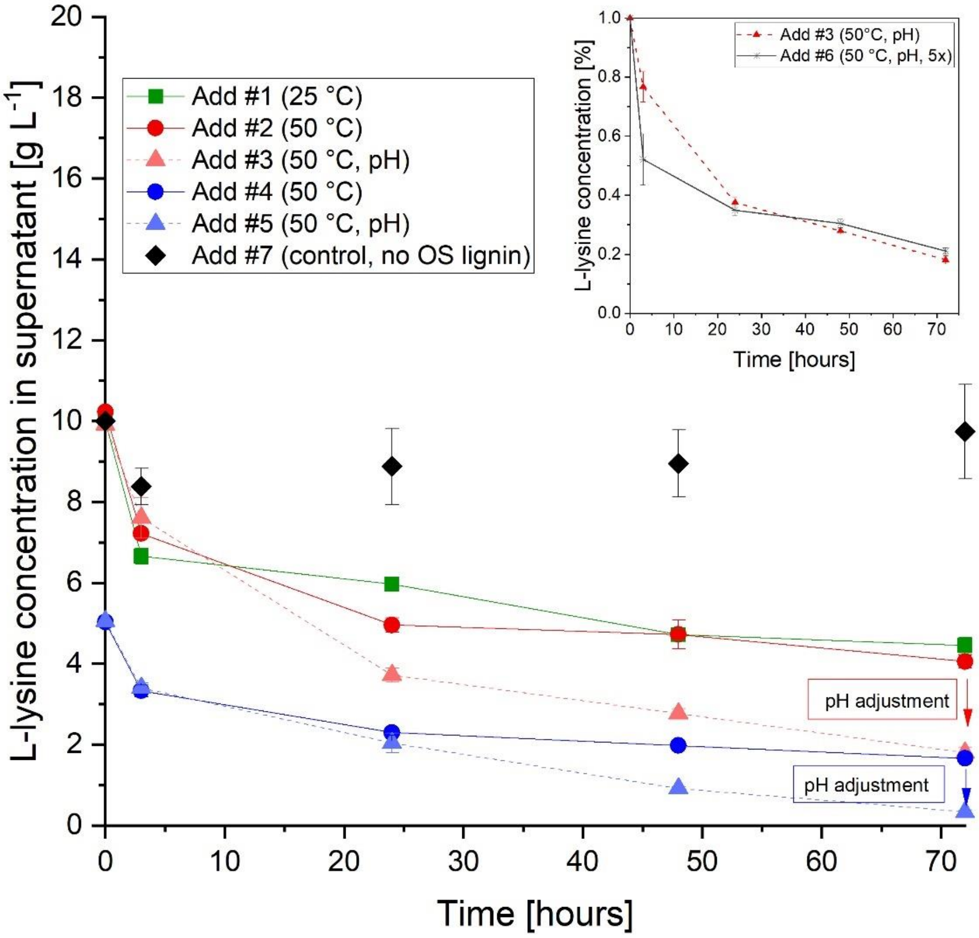

Figure 4-13: L-lysine reduction during anionic addition of L-lysine to OS lignin. The L-lysine concentration in the supernatant was measured after removal of OS lignin. The assignments of the reaction conditions are listed in Table 4-1. The inserted graph shows the relative L-lysine concentration in the supernatant after anionic addition with OS lignin at a 5-fold substrate concentration.

After 24 hours of reaction time, more L-lysine was added to the OS lignin at the 5-fold substrate concentration, compared to the 1-fold concentration. However, after an additional 24 hours of reaction times, no significant difference was observed. Therefore, the higher substrate concentration had no negative effect on the anionic addition reaction. Higher concentrated solutions are preferred, because they are more economical due to the need of smaller reaction vessels and less water. Since no negative effects of the higher substrate concentration were observed, for further functionalization of the OS lignin the 5-fold substrate concentration (Add#6) was used.

Solubility of anionic polymerized lysine-lignin

The solubility in solvents and aqueous solutions had changed after the successful condensation of OS lignin and L-lysine with formaldehyde (see section 4.3.2.1). Therefore, for each newly synthesized lysine-lignin, the solubility had to be analyzed separately.

For this purpose, saturated solutions of lysine-lignin (Add#6) were prepared and insoluble solids separated by centrifugation. The turbidity was measured at 600 nm and the solubility was determined (data not shown). While lysine-lignin was soluble at pH 1, the solubility decreases dramatically with a slight increase in pH to 2. At a pH of 3 almost no solubility was observed. In a basic environment, the solubility of lysine-lignin increased again. At a pH of 8 and above, large amounts of lysine-lignin were dissolved in the solution. For further analysis, lysine-lignin from anionic addition was precipitated at a pH of 3.

Furthermore, the solubility in solvents was determined qualitatively. Lysine-lignin precipitated at pH of 3 was soluble in ethanol, methanol, acetone and DMSO (data not shown). Two phases were formed with chloroform, the lysine-lignin floats on chloroform. Because of their polarity, water and polar solvents can form electrostatic interactions with other polar molecules and ions, resulting in the formation of hydrogen bonds with amines. The increased solubility in very acidic solutions and in slightly basic solutions was attributed to a change of functional groups, such as the addition of primary amines to OS lignin. A good solubility in polar solvents, such as ethanol, methanol and acetone in combination with a bad solubility in the nonpolar solvent chloroform supports the finding of successful amination.

In conclusion, the anionic addition of L-lysine to OS lignin was performed successfully. The best reaction results for the anionic addition of L-lysine with OS lignin were obtained with an initial OS lignin concentration of 100 g L^{-1} and L-lysine of 50 g L^{-1} at 50 °C and repeated adjustment of the pH value to 11. The lysine-lignin from anionic addition was readily soluble in a basic environment ($pH > 7$), at a pH of 1 and in different solvents. Further analysis of the amination success is found in section 4.3.2.3.

4.3.2.3 Quantification of amine anchors on OS lignin

Different lysine-lignins were synthesized via condensation reaction (see section 4.2.2.1) and anionic addition (see section 4.2.2.3). For further functionalization with catechols via two-step reaction (see section 4.1.4), the amine groups from the L-lysine must be available as primary amines on the lignin. A biochemical assay, which is known as Ninyhdrin assay (see section 4.2.5.1), as well as a chromatographic method, which was extended by a precolum derivatization with OPA (see section 4.2.4.3), were used to investigate the functionalization degree the these lysine-lignins.

Quantification of lysine-lignin by Ninhydrin assay

In this section a Ninhydrin assay (see section 4.2.5.1), a standard method for the analysis of primary amines, was used to quantify the primary amines, which were attached to the different lignins.

Chitosan, which naturally contains a high proportion of primary amines (see chapter 3), was used to validate the detection method. The degree of functionalization was determined to 79 mol% ± 24 mol%. The degree of deacetylation of chitosan was specified by the manufacturer to 75-85 mol%. Hence, it was concluded that the accuracy of the Ninhydrin assay was sufficient. From the measuring error, which was relatively high, it was concluded that the precision of the Ninhydrin assay was rather low. Therefore, the number of test samples was increased to five.

Figure 4-14 shows the amount of primary amine in different lysine-lignins, which were investigated via the Ninhydrin assay. Two lignins from the condensation reaction with a mass ration of L-lysine to OS lignin of 1:1 and 1:10, as well as two lignins from anionic addition with a L-lysine to OS lignin ratio (mass) of 1:2 were compared. The lysine-lignin from the condensation reaction with a ratio of lysine to OS lignin of 1:1 resulted in a functionalization of almost 200 mol%. This means, that roughly two molecules of L-lysine were attached to one lignin monomer. If the ratio of L-lysine to OS lignin in the condensation reaction was reduced to 1:10, the content of primary amines decreases to 45 mol% ± 4 mol%, which corresponded to approximately one L-lysine molecule per two lignin monomers. The degree of functionalization after anionic addition of L-lysine to OS lignin was about 26 mol% and 30 mol%, which indicated that roughly every third lignin monomer was functionalized. As already mentioned, the concentration of G units in beech wood was 0.24 and 0.38 mmol g^{-1} [208], which equals roughly 40 to 50 mol% of G units per lignin. It was shown in section 4.3.2.2 that the primary amine NAcDAP only bound to G lignin and did not bind to S or H lignin via anionic addition. The maximum degree of functionalization via anionic additions was therefore 40 mol% to 50 mol%. The achieved functionalization of 26 to 30 mol% (via anionic addition) was therefore a reasonable result. Since a degree larger than 50 mol% was achieved for the functionalization of OS lignin via condensation reaction, it was concluded that the L-lysine did not exclusively bind to G-units here.

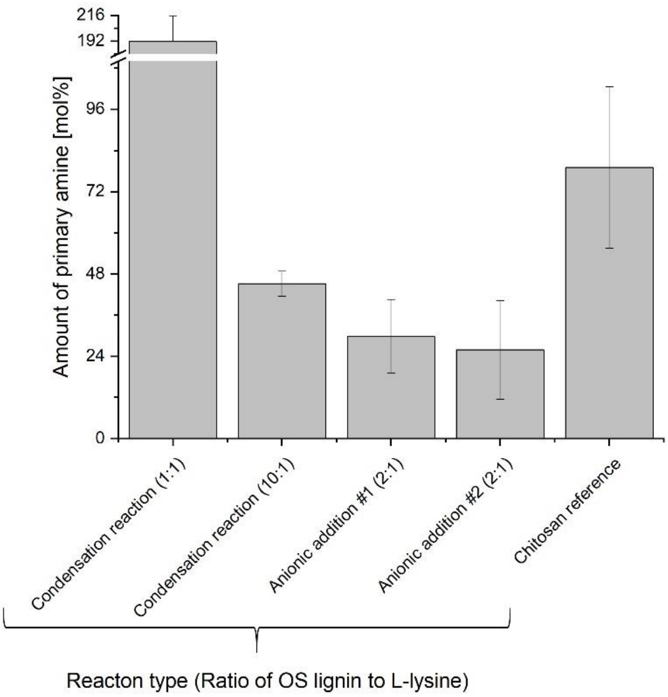

Figure 4-14: Content of primary amines of different lysine-lignins (measured by Ninhydrin assay, see section 4.2.5.1).

The disadvantage of the Ninhydrin assay was, that no distinction was made between covalently bound L-lysine and adherent L-lysine. It was therefore presumed that the sample was perfectly purified and, that no L-lysine monomers were adhering.

Quantification of lysine-lignin by GPC after precolumn derivatization with the fluorophore OPA

An alternative for the detection of primary amines via Ninhydrin assay is the derivatization with OPA reagent, which is commonly used for the quantification of amino acids (see section 4.2.4.1). Similarly, to this analysis, where the amine group of the amino acids was derivatized with OPA reagent, subsequently separated using analytical chromatography and detected by a fluorescence detector, in this work, chromatographic separation in combination with OPA precolumn derivatization was used for the detection of primary amines on lysine-lignins (see section 4.2.4.3: GPC-OPA analysis). Instead of using a C18 column, a GPC column (see section 4.2.4.2) was used to separate small molecular compounds from the functionalized lysine-lignin. Since small molecules such as L-lysine monomers were retained longer in the column and eluted significantly later than OS lignin and lysine-lignin, bound L-lysine could be easily distinguished from unbound L-lysine monomers. The advantage of this method was, that non-bound amine monomers (such as L-lysine) were separated by GPC prior to analysis and were less likely to interfere with the evaluation. Furthermore, the strong self-coloring of lignin, which interfered with photometric assays (see section 4.2.5.1), did not negatively impact the GPC measurements.

In order to validate the new measurement technique, different ratios of OS lignin and lysine-lignin from the condensation reaction (see section 4.2.2.1) were mixed (see Table 4-3) and analyzed with and without the addition of OPA. The correlation of the FLD area (without OPA derivatization), $Area_{FLD}$, over the sum of lignins, c(lignins), found a linear relationship, with a coefficient of determination R^2 of 0.9841 (see equation 4-3). Furthermore, the correlation of the FLD area with OPA derivatization, $Area_{FLD,OPA}$, over the concentration of lysine-lignin, c(lysine-lignin), also found a linear relation, with a coefficient of determination R^2 of 0.9943 (see equation 4-2). Lastly, for the correlation of the ratio of the FLD areas with and without the addition of OPA-reagent over the ratio of lysine-lignin to the sum of lignins a linear relationship was correlated with a linear regression, with a coefficient of determination R^2 of 0.9369 (see equation 4-3).

$$Area_{FLD} = -120.0 + 1040.6 \cdot c(sum\ of\ lignins) \cdot \frac{L}{g} \tag{4-1}$$

$$Area_{FLD,OPA} = 1532.4 + 29021.9 \cdot c(lysine\text{-}lignins) \cdot \frac{L}{g} \tag{4-2}$$

$$\frac{Area_{FLD,OPA}}{Area_{FLD}} = -1.61 + 52.70 \cdot \frac{c(lysine\text{-}lignins)}{c(sum\ of\ lignins)} \tag{4-3}$$

with

$Area_{FLD}$ = FLD area (without OPA derivatization)/ -

$Area_{FLD,OPA}$ = FLD area with OPA derivatization/ -

c(lignins) = concentration of the sum of all lignins/ $g \cdot L^{-1}$

c(lysine-lignin) = concentration of lysine-lignin/ $g \cdot L^{-1}$

From the coefficient of determination for the linear correlation between the FLD-areas with the different concentrations of lignins (equation 4-1 to 4-3), it was concluded that a robust measuring technique was established for the determination of the amination degree of lignin.

After successful validation of the GPC-OPA analysis, the samples from anionic addition of L-lysine to OS lignin (see section 4.2.2.3) were subsequently measured after 72 hours of reaction time. The results corresponded very well with the results for the detection of L-lysine in the supernatant after anionic addition of L-lysine to OS lignin (see section 4.3.2.2). The reaction temperature of 25 °C versus 50 °C (Add#1_25 °C and Add#2_50 °C) did not have a significant influence on the reaction result. The comparison of the reactions with and without pH correction (Add#2_50 °C and Add#3_50 °C, pH adjusted, as well as Add#4_50 °C and Add#5_50 °C, pH adjusted) confirmed that the pH adjustment had a positive effect on the lysine absorption to lignin. Using regression analysis (equation 4-3), a content of primary amines of 26 mol% was calculated for sample Add#3 (50 °C, pH). The highest content of primary amines, 34 mol%, was calculated for the approach with the 5-fold concentration of OS lignin and lysine (Add#6_50 °C, pH, 5x). This corresponded well with the analysis of L-lysine in the supernatant (see section 4.3.2.2) and the Ninhydrin assay, where the functionalization degree was determined to be 34 mol% for Add#3 (50 °C, pH adjusted) and between 26 mol% and 30 mol% for Add#6 (50 °C, pH, 5x).

In conclusion, two methods (Ninhydrin assay and GPC-OPA analysis) were successfully implemented for the analysis of primary amines on functionalized lysine-lignin. While lysine-lignin from condensation reaction had a functionalization degree between 45 mol% and 200 mol%, a functionalization degree of 26 mol% to 34 mol% was found for lysine-lignin from anionic addition. Lysine-lignin from anionic addition was preferred over lysine-lignin from condensation reactions, because its production was possible without the use of formaldehyde, which is toxic.

4.3.3 Functionalization of lysine-lignin with catechols (2nd step)

After successful functionalization of OS lignin with primary amines from L-lysine (1st step, see section 4.3.2), the next step was to examine the C-N bond between lysine-lignin from anionic addition and catechol donors.

In chapter 2, biochemical reactions for the functionalizing of natural polymers were investigated. For this purpose, a laccase-catalyzed approach for bonding primary amines (NAcDAP) with catechols (PCA and DHC), via Michael-type addition, was discussed. While PCA only formed C-N bonds with NAcDAP after enzyme catalysis, spontaneous formation of dimers was observed for DHC, thus revealing that DHC was more reactive or less stable. Furthermore, it was found that next to a high pH, a low pK_a value of the primary amine led to higher conversion rates. The heteromolecular C-N bond formation was parametrically optimized using the PCA as a catechol donor and NAcDAP as primary amine. The pH value and PCA concentration were identified as the two most important parameters for successful binding. Although the enzyme shows an activity at pH of 4 with respect to PCA (see chapter 2, section 2.3.4), no dimer formation was detected at pH of 4, which was presumed to be caused by the availability of protons at an acidic reaction pH. It was found that the more basic the reaction pH (with respect to the enzyme stability), the higher the product formation. The determination of the product-maximizing reaction conditions found an optimal pH value of 7.5, despite the optimum of the pH value of 6.0 for the single-substrate reaction with laccases from *C. unicolor* (see chapter 2, section 2.3.4). Catechols are subject to auto-oxidation in basic reaction milieus. In order to avoid such oxidation, a reaction pH of 6.5 was chosen here for the functionalization of lysine-lignin. A maximum tensile strength of 3.41 MPa ± 0.12 MPa was measured for the catechol-chitosan adhesive, which was introduced in chapter 3, at a reaction pH of approximately 5.0. Since this reaction pH was advantageous over a reaction pH of 5.4, where a significantly lower tensile strength of 2.27 MPa ± 0.40 MPa was measured, it was concluded that the optimal reaction pH for the C-N bond formation and the adhesion formation may be even lower than predicted in chapter 2. Therefore, in addition to a reaction pH of 6.5, which minimized oxidation and maximizes the reaction yield, a reaction pH of 5 is also evaluated for the functionalization of lysine-lignin.

In order to investigate the functionalization of lysine-lignin (from anionic addition, see section 4.3.2.2) with a catechol, different pH value (5 and 6.5), the use of catalyst (no catalyst or laccase from *C. unicolor*) and different catechols (PCA and DHC) were tested (see section 4.2.3). The reaction success was quantified through the analysis of the functionalized lysine-lignin pellet using a Ninhydrin assay (see section 4.2.5.1) and FT-IR spectroscopy (see section 4.2.5.2). The assumption was made that a successful reaction was indicated by a decrease in primary amines on the lignin, which was quantified via Ninhydrin assay, as well as an increase of catechols, which was detected using FT-IR spectroscopy.

4.3.3.1 Quantification of primary amines on lysine-lignin via Ninhydrin assay

A Ninhydrin assay (see section 4.2.5.1) was used to quantify the primary amine groups on lysine-lignin (from anionic addition, see section 4.3.2.2) prior to and after the functionalization with catechols. A reduction of primary amine groups on lysine-lignin was detected due the functionalization with the catechols (DHC and PCA). The content of primary amines at the lysine-lignin before functionalization was about 30 mol%. As shown in Figure 4-15, a decrease of the primary amines was detected after spontaneous reaction with DHC. At a reaction pH of 5, a decrease of primary amines from 30 mol% ± 11 mol% to 5 mol% ± 6 mol% and at pH 6.5 from 26 mol% ± 14 mol%

to 17 mol% ± 7 mol% was observed. This equals a degree of functionalization of 25 mol% ± 17 mol% at pH of 5 and 9 mol% ± 21 mol%. The comparison of the spontaneous reaction with DHC at pH 5 and pH 6.5 showed that more DHC was absorbed at a reaction pH of 5. It was concluded that pH 5 was more suitable for the spontaneous functionalization of lysine-lignin with DHC. This could be due to the fact that DHC is less stable at pH 6.5 and possibly oxidizes faster than it can react. This finding is in agreement with the optimal pH for the spontaneous functionalization of chitosan with DHC (see chapter 3).

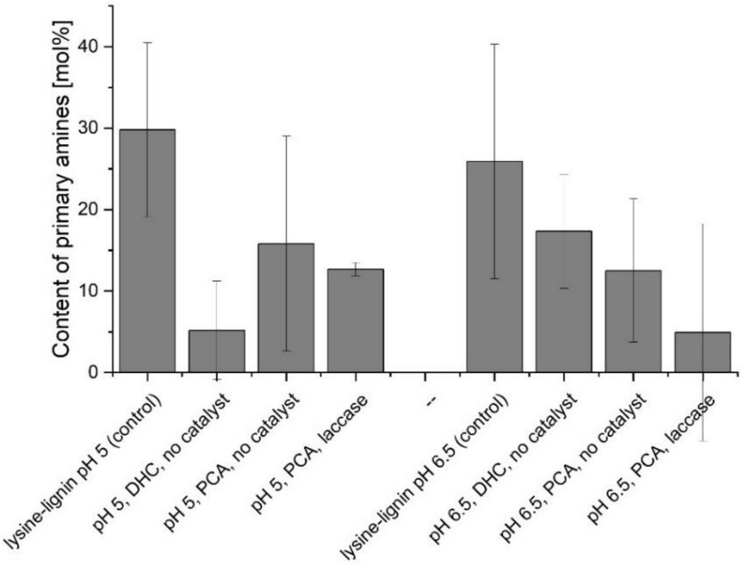

Figure 4-15: Quantification of primary amines on lysine-lignin (from anionic addition, see section 4.3.2.2) before and after functionalization with the catechols PCA and DHC. The functionalization was performed according to section 4.2.3 and the analysis was conducted using a Ninhydrin assay (see section 4.2.5.1).

A decrease of primary amines on lysine-lignin was also detected after the functionalization with PCA. At a reaction pH of 5, the content of primary amines decreased to 16 mol% ± 13 mol% (without the use of enzyme) and to 13 mol% ± 1 mol% (in the laccase-catalyzed reaction). At a reaction pH of 6.5, the content of primary amines decreased to 13 mol% ± 9 mol% without the use of enzyme and to 5 mol% ± 13 mol% in the laccase-catalysed reaction. At a reaction pH of 5, no significant difference was found for spontaneous and enzymatic functionalization with PCA, whereas at pH 6.5 the use of enzyme led to a higher absorption of PCA on the lysine-lignin. It was concluded that the use of enzyme only promotes the binding of PCA at a reaction pH of 6.5. This finding is in agreement with the optimal pH for the enzyme catalysed reaction between the model compounds NAcDAP and PCA (see chapter 2).

4.3.3.2 Analysis of functionalized lysine-lignin using FT-IR spectroscopy

FT-IR spectroscopy (see section 4.2.5.2) was used to quantify the primary amine groups on lysine-lignin prior to and after the functionalization with catechols. The results conducted at a reaction pH of 5 are shown in Figure 4-16. The comparison of the different IR profiles was used to investigate changes to the structure due to the functionalization with catechols. Due to the complex structure of lignin, in depth analysis of the reaction products using IR spectroscopy was not possible.

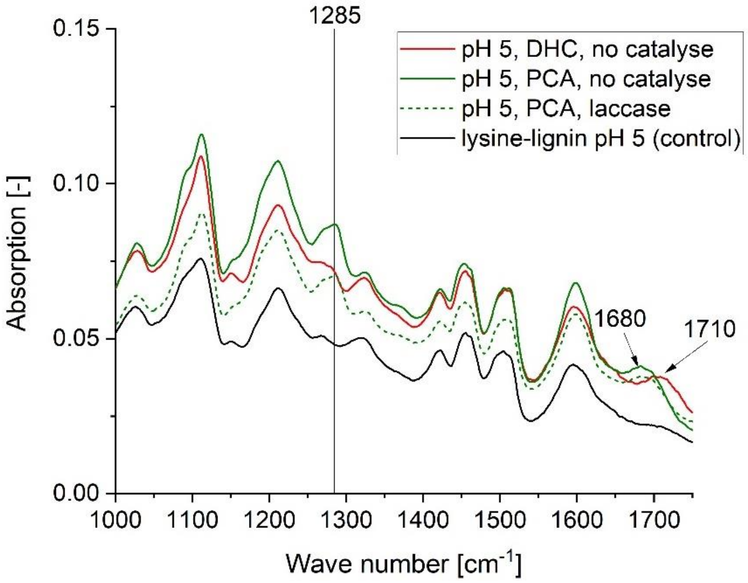

Figure 4-16: FT-IR spectrograms of functionalized lysine-lignins after 2-step functionalization of OS lignin at pH 5.

The analysis of IR profiles for the spontaneous reaction of chitosan with PCA found two main peaks at 1363 cm^{-1} and 1546 cm^{-1} (see chapter 3, section 3.3.1). The absorption at 1363 cm^{-1} was attributed to the aromatic C-N stretch band which is characteristic for secondary amines [199] and the peak at 1546 cm^{-1} to the amine's N-H bend, which is often found between 1580 cm^{-1} and 1650 cm^{-1} [200]. The peak at 1363 cm^{-1} was absent for the spontaneous reaction of chitosan with DHC, but a peak at 1405 cm^{-1} was detected, which might result from a small shift. While peaks at 1700 cm^{-1} were absent for the reaction of chitosan with PCA and DHC at pH 5-9, for the reaction of chitosan and DHC at pH of 1, peaks were found at 1640 cm^{-1} and 1720 cm^{-1}. These peaks correlated well with the amide bond described for catechol-functionalized chitosan [65]. It was concluded that mainly amine bonds are formed, but amide bond might be possible at a pH of 1.

The comparison of the IR profile of lysine-lignin and functionalized lysine-lignin (at pH 5) found two main alterations. At approximately 1285 cm^{-1} and at around 1700 cm^{-1}

(1680 cm^{-1} for PCA and 1710 cm^{-1} for DHC). At a pH of 6.5, the same alterations were found (data not shown). The comparison of PCA with and without the use of enzyme did not find any significant differences in the IR profiles, compared to a pH of 5. The peak at 1285 cm^{-1}, which was found in the functionalized lysine-lignin, might result from the formation of an aromatic C-N stretch band, which was found at 1363 cm^{-1} for PCA and presumably 1405 cm^{-1} for DHC.

Peaks at 1700 cm^{-1} are typically attributed to C=O bonds, resulting from carboxyl groups or amide groups. The peaks at around 1700 cm^{-1} (1680 cm^{-1} for PCA and 1710 cm^{-1} for DHC), which were found for the functionalization of lysine-lignin with DHC and PCA, may result from the formation of an amide due to the functionalization of lysine-lignin with the catechols. Since no peak was found at 1545 cm^{-1}, which was found for the functionalization of chitosan with DHC and PCA, the peaks at 1680 cm^{-1} (for PCA) and 1710 cm^{-1} (for DHC) may be a result of a shift of the amine's N-H bend, which is usually found between 1580 cm^{-1} and 1650 cm^{-1} [200].

The analysis via IR spectroscopy indicated successful bonding of PCA and DHC to lysine-lignin, presumably via amine bond formation. Since the reaction of lysine-lignin with PCA and DHC found reaction products, even when no enzyme was used as catalyst, it was concluded that the reaction between the primary amine and the catechol donor was spontaneous.

4.3.4 Tensile strength of lignin and lignin derivates

The two-step functionalization of OS lignin was successfully completed. First, lysine was bound to the OS lignin by an anionic polymerization (see section 4.3.2) and second, the catechols PCA and DHC were added (see section 4.3.3). After successful completion of the two-step functionalization of OS lignin, in this section, the tensile strength of the synthesis products was tested for selected solvents.

4.3.4.1 Influence of solubility on the tensile strength of lignin derivatives

OS lignin and its derivates were present in a solid form, which needed to be dissolved prior to adhesion testing. Over the course of the two-step functionalization of OS lignin (see section 4.1.4), the solubility of the lignin derivates (intermediates and products) varied. For example, while OS lignin was not soluble in weak acids, it was partially soluble in acetone and very soluble in alkaline solutions (pH >11) (data not shown). In the 1st step of the lignin functionalization, lignin was functionalized with an amine. This reduced its solubility in organic solvents, but increased the solubility in the acidic and alkaline (now soluble as of pH > 7.5) environment (see section 4.2.2). The observation was made that a higher content of amines often correlated with higher solubility in acids. If the lysine-lignin was masked with the catechol group in the 2nd step of the functionalization, a part of the amine groups was shielded and replaced by catechols. Therefore, it was expected that the solubility changed further by adding the catechol group.

In order to establish adhesion, different solvents (organic and aqueous) were used. For this purpose, lignin derivates were dissolved in different solvents and the tensile strength was investigated as described in section 4.2.6. Figure 4-17 shows the lignin derivates and the tested solvents. Lignin derivatives which were highly soluble in the corresponding solvent are marked with asterisks. The majority of the lignin derivates were insoluble in the chosen solvents and subsequently showed little or no adhesive strength.

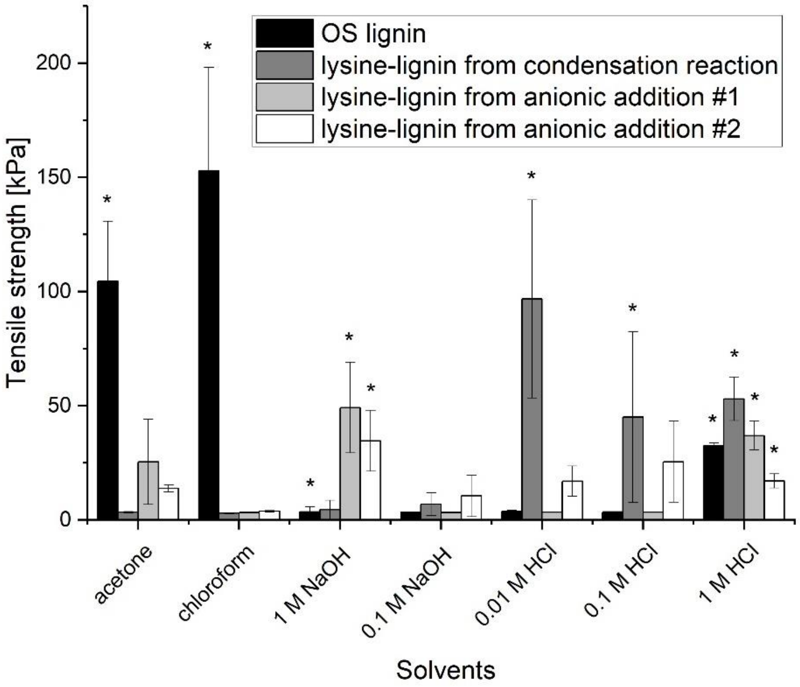

Figure 4-17: Tensile strength of lignin and various lysine-lignins as a function of the solvent. Lignin derivatives which are soluble in the corresponding solvent are marked with asterisks.

OS lignin (prior to functionalization) was soluble in the organic solvents acetone and chloroform and for both solvents a strong tensile strength (on aluminum adherents) was measured (104.5 kPa ± 26.2 kPa and 152.9 kPa ± 45.3 kPa, respectively). In most tested aqueous solvents (0.1 M NaOH, 0.01 M HCl and 0.1 M HCl) OS lignin was neither soluble nor a tensile strength was established. Only in 1 M HCl and 1 M NaOH, lignin was soluble. Using 1 M HCl, a tensile strength of 32.5 kPa ± 1.3 kPa was measured, but at 1 M NaOH no tensile strength was established. All lysine-lignins (from condensation reaction and anionic addition) were neither soluble in the organic solvents tested (acetone and chloroform), nor was a tensile strength established. Lysine-lignin from condensation reaction (see section 4.3.2.1) was soluble the acidic environments of HCl and a tensile strength of 96.7 kPa ± 43.3 kPa (for 0.01 M HCl), 45.1 kPa ± 37.3 kPa (for 0.1 M HCl) and 53.0 kPa ± 9.5 kPa (for 1 M HCl). Lysine-lignin from anionic addition (see section 4.3.2.2) was soluble in 1 M NaOH and 1 M NaOH and insoluble at the other tested aqueous solvents (0.1 M NaOH, 0.01 M HCl and 0.1 M HCl). A tensile strength of 49.2 kPa ± 19.8 kPa (for #1) and 34.7 kPa ± 13.4 kPa was detected using 1 M NaOH as solvent.

It was concluded that the solubility of the lignin derivatives was a requirement for adhesion and that the choice of solvent had a major influence on the formation of the adhesion. Although good solubility was a requirement for strong tensile strength, it did not guarantee adhesion success and therefore did not allow for reverse conclusions. In the following work, unnecessary tests of the adhesive strength were avoided by pre-selecting the solvent for its solubility properties towards the lignin derivative. Only solvents, which were able to solubilise the lignin derivate, were to be considered for adhesion testing.

4.3.4.2 Determination of tensile strength for catechol-lignins

The tensile strength was investigated for the reaction product from the two-step functionalization (see section 4.3.3). The choice of the solvent had a significant influence on the tensile strength (see section 4.3.4.1). In order to establish adhesion for lignin-catechols, a solvent screening was performed. DMSO, water, water together with a pH adjustment to 7, as well as acetone with hydrochloric acid were tested.

The tensile strength measured for the functionalized lignin (catechol-lignin), with DMSO as solvent, was slight. The highest tensile strengths of 73.9 kPa ± 71.3 kPa at pH 5 and 49.6 kPa ± 11.5 kPa at pH 6.5 were measured for the control reactions (lysine-lignin from anionic addition without the addition of catechols). No or very little tensile strength was established for all experiments using water as solvent. When using a combination of acetone and hydrochloric acid as solvent some tensile strength was detected. The tensile strength measured for the lignin derivate from the control reaction at pH 5 was 27.5 kPa ± 11.7 kPa. A significant improvement was found after the functionalization with DHC as catechol donor at pH 5, where a tensile strength of 169.3 kPa ± 130.6 kPa was measured. Compared to the tensile strength of 104.5 kPa and 152.9 kPa on aluminum surfaces, obtained for OS-lignin with acetone and chloroform as a solvents (see section 4.3.4.1), this is an improvement of 62 % and 11 %, respectively. However, compared to other biogenic adhesives (see section 3.3.4), the tensile strength is significantly lower. For dextrin, 350 kPa and for starch 500 kPa were measured on aluminum surfaces, which is a 2 to almost 3 times better performance. Gummi arabicum, with a tensile strength of 2.10 MPa achieved a 12 times better performance. Further development and improvement of the tensile strength is clearly needed. As shown through the use of PCA-chitosan (see chapter 2), where a tensile strength of over 4 MPa was measured, the potential for lignin-catechol adhesives is substantial. The tensile strength of catechol based adhesives was previously improved by the addition of iron(III) ions, which is investigated for different catechol-lignins in the following section.

4.3.4.3 Evaluation of tensile strength in the presence of iron ions

Catechols form complexes with iron(III) ions. Depending on the pH value, mono-complexes ($pH < 5.6$), bis-complexes ($5.6 < pH < 9.1$) and tris-complexes ($pH > 9.1$) are formed, consisting of one mole of catechol and correspondingly one to three moles of iron(III) [223]. It was shown that the supplementation of iron(III) irons can enhance the adhesion strength [54]. Therefore, the influence of iron(III) ions on the adhesive force was investigated. Acetone together with hydrochloric acid was used as a solvent. The resulting pH value was acidic; hence it was presumed that a mono-complex was predominant. The cohesion of the iron complex is a competitive reaction to the adhesion on the surface [223], since catechols which are bond to the iron (III) ions are not available to bind to the surface. Therefore, the iron concentration was varied in the experimental set up. The solid $FeCl_3$ reacted hygroscopic and formed $FeCl_3{\cdot}6H2O$ (red-brown to yellow coloring), which reacted strongly acidic by hydrolysis and $FeOH_3$ precipitated from the solution within a few days [16]. Therefore, the use of freshly prepared Fe(III)-ion solution was necessary.

In the control experiments (without catechol), for which no tensile strength was measured, adhesion was established in the presence of iron(III). For iron(III) concentrations above 0.5 mol per mol catechol neither an influence of the catechol donor source (PCA, DHC and L-DOPA) nor an influence of the reaction time was determined. For an iron(III) concentration of 0.2 mol per mol catechol, an increase in the adhesive force was recorded for all samples. Since this was also the case for the control (without catechol), it was concluded that the supplementation with iron had an influence on the lysine-lignin or lignin backbone. In future work, iron tests could be intensified in combination with different solvents, especially, solvents which allow for the formation of monomer and dimer complexes (pH 5-8).

4.3.4.4 Improvement strategies for adhesion of catechol-lignin

The concept of the two-step functionalization of OS lignin was successfully implemented and a catechol-lignin was formed via anionic addition of L-lysine to OS lignin and subsequent reaction with DHC. The maximum tensile strength achieved was 169.3 kPa ± 130.6 kPa (see section 4.3.4.2). No further improvement of the tensile strength was detected after supplementation with iron (III) ions (see section 4.3.4.3). For many application areas, the tensile strength of the catechol-lignin needs further improvement.

North et al. have shown that a catechol concentration of approximately 20 mol% led to a significant improvement of the adhesion strength, compared to a polymer with a functionalization level of 15 mol% [20]. In order to reach a degree of functionalization higher than 20 mol%, the functionalization of OS lignin with L-lysine in the 1st reaction step via anionic addition (see section 4.2.2.3), should be improved or alternatively, the use of lysine-lignin from condensation reactions (see section 4.3.2.1), which achieves up to 200 mol% functionalization, should be considered. If an increased amount of primary amine groups, which result from the L-lysine, are available for the 2nd reaction step, a higher degree of functionalization with catechols can be achieved. Subsequently, the 2nd reactions step, the functionalization with catechols, needs to be improved. Other catechols (other than PCA and DHC) may be used. The reaction pH, reaction time and the use of catalyst may be further optimized, as well as the curing conditions, such as use of solvent and curing temperature. Furthermore, it was shown that the adhesion of mussel mimicking adhesives depend significantly on the chain length of the individual molecules: While a lap shear strength of 0.5 MPa was measured at a molecular mass of less than 30,000 g mol^{-1}, a lap shear strength of 2 MPa was determined at a molecular weight of at least 50,000 g mol^{-1} [20]. The mean molecule size (averaged over the molecular weight) of all OS lignin samples was 5.9 kDa ± 0.3 kDa, which is significantly lower than 50,000 g mol^{-1}. The molecular weight of lignin is a further point which may need optimization.

Solvent-based wet adhesion is a physical process which comes with certain problems: It can be difficult to bond large areas of impermeable material (such as metal) together, since the solvent must be able to diffuse out of the bonded area. Furthermore, these adhesives often have little resistance to the solvent used. For example, water-based glues, such as glutin (animal glue) or starch glues, often have little resistance to water [224]. Organic solvents, however, are often poisonous, making these adhesives difficult to use in certain workplaces. Since lignin is usually not soluble in water, the catechol-lignin adhesive has a high potential for use in humid environments. Further testing needs to be conducted on the water resistance of the catechol-lignin adhesive. The cost analysis of the catechol-lignin adhesive (see section 4.2.7) estimated the production costs was 33.63 euro per kg of adhesive with a recommended selling price of 55 euro per kg (dry substance). Depending on the application of the catechol-lignin, further reduction of the costs is necessary.

4.3.5 Cost analysis of catechol-lignin adhesives

The aim of this research project was the derivatization of OS lignin with catechol compounds, with the aim of producing a sustainable, biogenic adhesive. Through the extraction with an ethanol-water mixture, an environmentally friendly and sulphur-free lignin was produced as a high-quality polymeric basic structure. The further processing of the dissolved ethanol directly after extraction was possible in principle. However, the transport of liquids with a substrate concentration of about 50 g L^{-1}, as it was observed for OS lignin, is cost-intensive [225]. Therefore, the choice of the location for a production plant for the production of the lignin-catechol adhesive was restricted by the transportation costs. Alternatively, the production plant could be built in proximity of the biorefinery site. Another solution is the use of powdered OS lignin. Previous cost calculation resulted in a price for dried OS lignin of approximately 500 euros per ton [5]. In the course of this research, a two-step process was developed to provide lignin with additional functions (see section 4.1.4). In the 1st step, the amino acid L-lysine was bound non-specifically to lignin by an alkaline catalyzed anionic addition. Derivatization with lysine produced primary amines, which were used as anchor sites for the functionalization with catechols in the 2nd step. Depending on the substrate, the C-N bond between the primary amine and a catechol donor can either occur spontaneously or be catalysed by the enzyme laccase (see chapter 2 and 3). A flow chart for the production of powdered lignin and subsequently a lignin-catechol adhesive is shown in Figure 4-18.

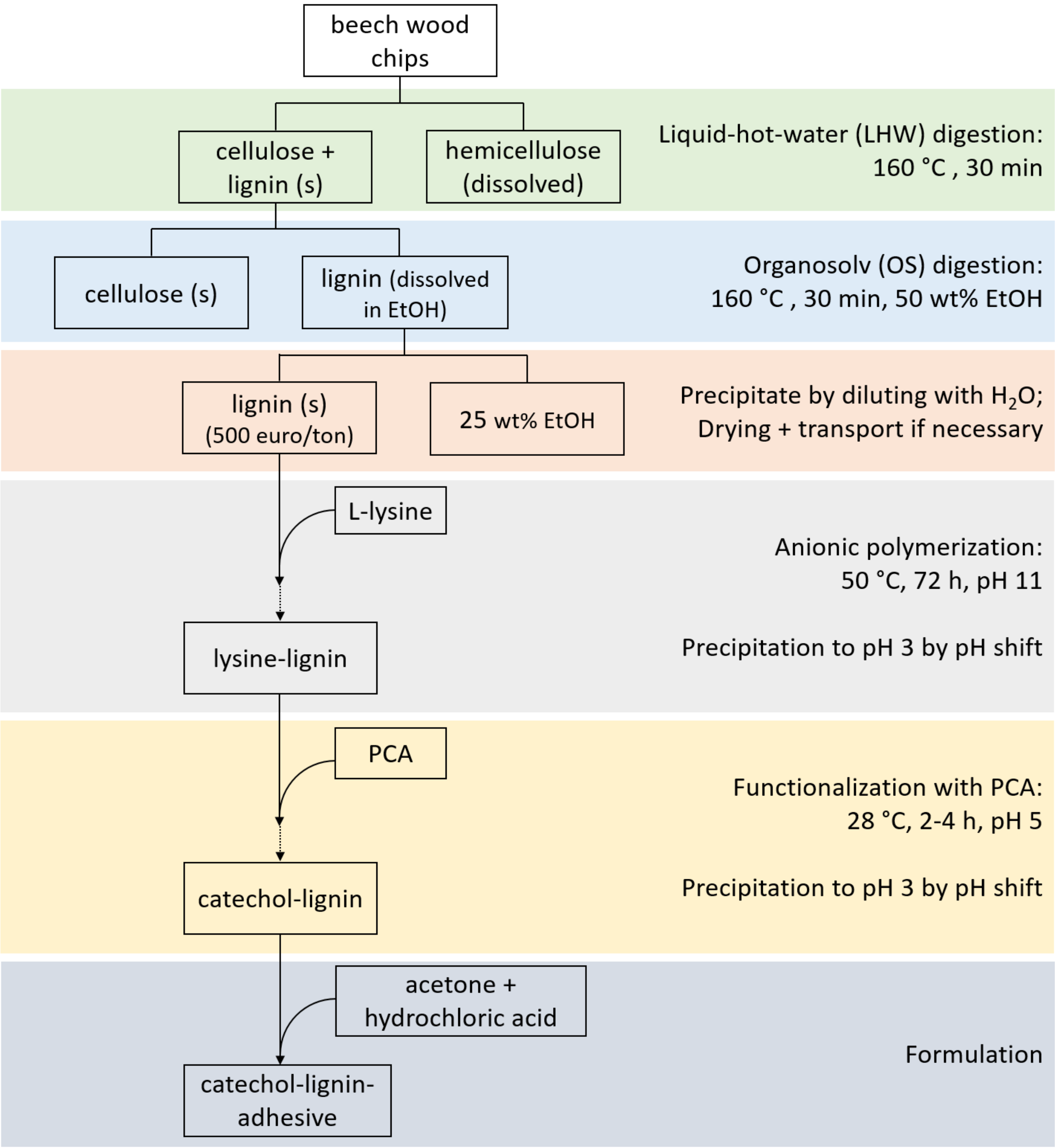
beech wood chips
cellulose + lignin (s)
hemicellulose (dissolved)
Liquid-hot-water (LHW) digestion: 160 °C , 30 min
cellulose (s)
lignin (dissolved in EtOH)
Organosolv (OS) digestion: 160 °C , 30 min, 50 wt% EtOH
lignin (s) (500 euro/ton)
25 wt% EtOH
Precipitate by diluting with H2O; Drying + transport if necessary
L-lysine
Anionic polymerization: 50 °C, 72 h, pH 11
lysine-lignin
Precipitation to pH 3 by pH shift
PCA
Functionalization with PCA: 28 °C, 2-4 h, pH 5
catechol-lignin
Precipitation to pH 3 by pH shift
acetone + hydrochloric acid
Formulation
catechol-lignin-adhesive

Figure 4-18: Flow chart value-added process: from beech wood to catechol lignin adhesive.

The powdered OS lignin was first suspended in water (final concentration 100 g L^{-1}) and a pH value of 11 was adjusted using sodium hydroxide. The amino acid L-lysine is already produced on a large scale by the fermentation of Corynebacterium glutamicum and is thus available at a price of approximately 3,500 euros per ton [215]. The derivatization of the lignin with lysine led to an increase in solubility in a slightly alkaline to neutral milieu. A homogeneous substrate was advantageous for derivatization. In order to achieve a sufficient increase in solubility in the neutral milieu and to provide sufficient primary amines for functionalization with catechols in the 2nd step, a ratio of lignin to lysine of 1 to 0.5 was chosen.

The synthesized lysine-lignin was precipitated by lowering the pH (addition of HCl) and separated from L-lysine monomers by centrifugation. The lysine-lignin was then resuspended in water. Due to the functionalization, a solubility of 200 g L^{-1} was possible already at a pH value of 5. Protocatechuic acid (PCA) (3,4-dihydroxybenzoic acid) was used as catechol donor. A price of 10,000 euros per ton was estimated. North et al. have shown that a catechol concentration of approximately 20 mol% leads to a 5-fold increase in the adhesive power compared to a polymer with a functionalization level of 15 mol% [20]. The ratio of lignin to catechol was therefore chosen as 1 to 0.3. Therefore, 50 g L^{-1} catechol was added.

With an investment of 17,423,000 euros and annual operating costs of 5,664,000 euros, a plant was designed for 170 tonnes of adhesive, generating a profit of around 9,263,000 euros per year. According to the calculation (see Figure 4-19), the production costs was 33.63 euro per kg (dry substance) of adhesive. Wood glues are sold for 10 to 15 euro [226] per kg in hardware stores and special adhesives for approximately 50 to 100 euro per kg [227]. If the adhesive is sold for 55 euro per kg (dry substance), which equals approximately 37 euro per kg wet adhesive, a return on investment (ROI) of 21.33 % can be achieved.

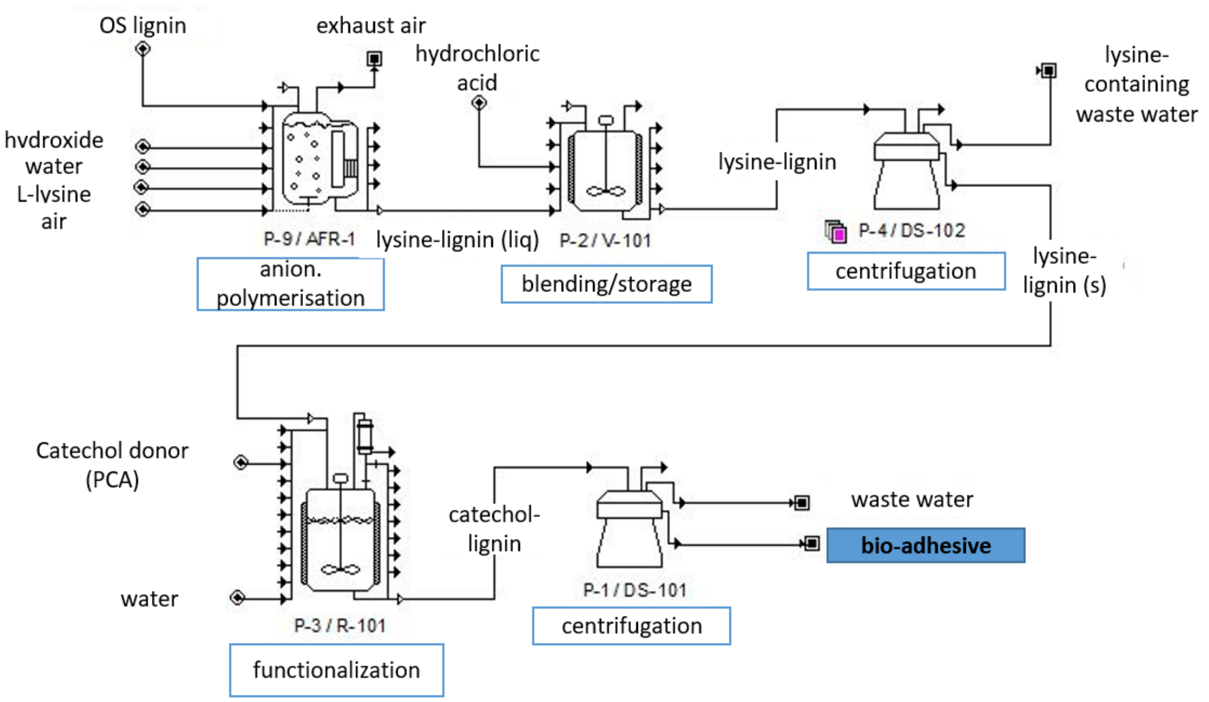
OS lignin
exhaust air
hydrochloric acid
lysine-containing waste water
hydroxide
water
L-lysine
air
lysine-lignin
P-9 / AFR-1
lysine-lignin (liq)
P-2 / V-101
P-4 / DS-102
anion. polymerisation
blending/storage
centrifugation
lysine-lignin (s)
Catechol donor (PCA)
water
catechol-lignin
waste water
bio-adhesive
P-1 / DS-101
P-3 / R-101
centrifugation
functionalization

Figure 4-19: Cost calculation using SuperPro Designer: Process diagram for the synthesis of catechol lignin.

4.4 Summary and Outlook

In this chapter, the OS lignin from beech wood was functionalized with catechol groups via two-step process, in order to develop a mussel mimicking adhesive with a lignin backbone. Prior to the functionalization, the extraction of OS lignin was investigated (see section 4.3.1). The variation on temperature and phosphoric acid concentration during OS digestion, as well as the investigation of a two-step process with LHW pretreatment found either a low yield of OS lignin (below 30 g L^{-1}) and/or an acidic reaction pH, which was outside the active pH range of laccases from *C. unicolor*. It was concluded that direct conversion of lignin from the OS supernatant was not economically feasible and a two-step functionalization was established with purified OS lignin.

In the 1st step, OS lignin was functionalized with the amino acid L-lysine (see section 4.3.2), which provided primary amine groups for further functionalization reactions. The reaction was performed successfully via condensation reaction (see section 4.3.2.1) and anionic addition (see section 4.3.2.2). The degree of functionalization was quantified via a Ninhydrin assay and GPC-OPA analysis (see section 4.3.2.3). While lysine-lignin from condensation reaction had a functionalization degree between 45 mol% and 200 mol%, a functionalization degree of 26 mol% to 34 mol% was found for lysine-lignin from anionic addition.

In the 2nd reaction step, primary amines on lysine-lignin, which resulted from anionic addition of L-lysine to OS lignin, were further functionalization with catechol groups via laccase-catalyzed Michael-type addition or spontaneous reaction (see section 4.3.3). The analysis of the reaction products via IR spectroscopy indicated successful bonding of PCA and DHC to lysine-lignin, presumably via amine bond formation. Since the reaction of lysine-lignin with PCA and DHC found reaction products, even when no enzyme was used as catalyst, it was concluded that the reaction between the primary amine and the catechol donor was spontaneous. The reaction success was evaluated using a Ninhydrin assay, which detected the decrease of primary amines. The best functionalization result was obtained at a reaction pH of 5 with DHC as catechol and without the use of enzymes, with a degree of functionalization of 25 mol% ± 17 mol%. Subsequent to the functionalization of OS lignin, the tensile strength was established for OS lignin and its derivates (see section 4.3.4). The solubility of the lignin derivatives was found to be a requirement for the establishing of adhesion and the choice of solvent had a major influence on the tensile strength. Although good solubility was a requirement for good adhesive strength, it did not guarantee adhesion success and therefore required further investigation. For catechol-lignin, the highest tensile strength was measured when a combination of acetone and hydrochloric acid was used as solvent. For catechol-lignin, which was synthesized at a reaction pH of 5 with DHC as catechol and without the use of enzymes, a tensile strength of 169.3 kPa ± 130.6 kPa was measured, which was about 6 times higher than the control reaction at pH 5 (27.5 kPa ± 11.7 kPa).

Lastly, an economical evaluation of lignin-catechol adhesives was performed (see section 4.3.5). With an investment of 17,423,000 euros and annual operating costs of 5,664,000 euros, a plant was designed for 170 tonnes of adhesive, generating a profit of around 9,263,000 euros per year. The production cost was estimated to be 33.63 euro per kg of adhesive. In order to develop a product from this catechol-lignin, both, the reaction costs and the adhesion characteristics need further development.

The goal of this work was to functionalize OS lignin from beech wood with catechol groups via a two-step process, for the development a mussel mimicking adhesive with a lignin backbone. This was partially achieved, and a catechol-lignin was synthesized. To develop a product from this catechol-lignin, both, the reaction costs, and the adhesion properties need further development.

5 Differential scanning calorimetry (DSC) for characterization of natural polymers and quantification of biodegradability in compost

Biodegradability of polymers and adhesives is an environmental imperative, principally for avoiding ocean pollution and minimizing landfill waste, which is currently increasing yearly [228, 229]. According to the United Nations Environment Programme 2015, UNEP, 6.4 million tons of waste enter into the oceans every year [230, 231]. Biodegradable polymers need to be tailored for their application, performance and lifespan, while at the same time for their biodegradability and environmental impact [232]. Structural changes during biodegradation, such as an increase in brittleness or crystallinity, can be detected by carefully observing characteristic changes in DSC profiles. The objective of this chapter is to validate a DSC based method for monitoring biodegradation quantitatively using small sample quantities and simple sample preprocessing.

First, degradation mechanisms of polymers and techniques for the degradation analysis are introduced in sections 5.1.1 and 5.1.2, respectively. Following, DSC is described in section 5.1.3.

Until now, DSC profiles have not been used to draw quantitative conclusions about biodegradation. Therefore, in this chapter, a DSC-based method for online analysis of the biodegradation of polymers in complex environments is introduced. The proposed method is first applied to evaluate the biodegradation of three polymeric biomaterials: polyhydroxybutyrate (PHB), cellulose acetate (CA) and lignin (see section 5.3.1 and 5.3.2). The method is suitable for the precise quantification of the biodegradability of PHB. For CA and lignin, conclusions regarding their biodegradation can be drawn with lower resolutions (see section 5.3.3).

Furthermore, DSC analysis is applied to characterize chitosan and the mussel mimicking catechol-chitosan adhesive, which was developed in this work (see chapter 3). The DSC profiles give insight into potential structures present in the chitosan adhesive (see section 5.3.4). While distinct peaks in the DSC profiles are detected, making DSC based quantification of biodegradability possible, the degradation studies are not performed for the chitosan adhesive in this work.

5.1 Theory

5.1.1 Degradation of Polymers

Natural polymer degradation process results from changes in physical properties, such as color, shape or tensile strength [233], and is complete when the polymer is fully decomposed into carbon dioxide, water and its mineral components [234]. Literature refers to four different types of polymer degradation, based on the mechanisms responsible for the process: photo-degradation, thermo-oxidative degradation, chemical degradation and biodegradation [235]. The definition of biodegradability has been set by the European Committee for Standardization. The European standard [236] requires achieving a final weight loss (70 wt%) after the set test period (45 days) ([236], Appendix C), or online measurement of carbon dioxide release ([236], Appendix B). While the complete degradation of a polymer can be analyzed quantitatively by measuring the total weight loss or the carbon dioxide emission, both methods are limited in their measurement throughput and require large sample masses (100 Grams).

Cellulose, lignin and PHB are naturally occurring polymers which are widely referred to as biodegradable polymers, since they can be degraded by microbes naturally found in soil [237]. PHB, for example, is a semi-crystalline isotactic polymer. Its degradation is initiated by enzymatic hydrolytic cleavage of ester bonds, resulting in surface erosion [238]. Since most polymers are too large to pass through cellular membranes, most biological degradation processes start with the depolymerization incited by secreted enzymes [239]. Fungi, for example, are known to secrete hydrophobic proteins, (such as laccases and cellulases [240]) which attach to polymer surfaces [235]. Using this ability, fungi play a key role in the degradation of lignocellulosic material.

5.1.2 Techniques for analysis of polymer degradation

Several monitoring technique, such as the quantification of the molecular weight of polymer fragments using either gel permeation chromatography (GPC) or viscometric techniques [241] are provided in literature. HPLC-MS, for example, is used for the isolation and identification of degradation products [242]. The challenge of using chromatographic techniques for measurement analysis is the a priori knowledge of existing molecular structure and composition [241]. Alternatively, surface chemistry is monitored during biodegradation using FT-IR spectroscopy [243] or X-ray photoelectron spectroscopy [244]. Data obtained through optical methods measure changes in the surface composition [245], however, for quantification of the degradation process a large set of calibration data in combination with statistical analysis is needed [246]. Morphology and dimensional changes can be detected using scanning electron microscopy (SEM) [230, 242, 247], and atomic force microscopy (AFM) [248], although both methods lack the ability to quantify biodegradation. Lastly, using NMR spectroscopy, the composition of biodegradable polymers can be determined by calculating the intensity ratio of the assigned peaks [249]. A significant disadvantage to chromatography, SEM, AFM and NMR is the requirement of extensive sample preparation to be performed prior to the analysis, which consequently changes the physical structure of the sample [250, 251]. Recently, non-destructive and wireless detection methods have become the focus of research interest, such as the use of embedded resonance sensors [252] or thermochromic fluorescent molecules [253]. Both methods, however, also require extensive sample preparation.

A technique which does not require extensive sample preparation and is able to monitor changes in weight of inhomogeneous materials, is thermogravimetric analysis (TGA) [230]. TGA monitors the change in weight (due to combustion or pyrolysis) of the polymer along a determined temperature profile, allowing the ratio of the different polymers in a polymer blend to be determined. The disadvantage of this method is that physical or chemical processes such as swelling or hydrolysis are undetectable.

5.1.3 Differential scanning calorimetry (DSC)

An alternative technique for detecting polymers uses DSC, which is also able to detect changes to the polymer’s physical and chemical structure. DSC is a thermo-analytical method in which the difference in the amount of heat required to increase the temperature of a sample and reference, is measured as a function of temperature [254]. DSC analysis for monitoring changes in crystallinity are based on changes in the glass transition temperature, crystallization temperature, melting temperature and heat of fusion [230, 247]. Using these measured values, structural changes such as an increase in brittleness can be detected [255]. As a result, changes in crystallinity of polymers can be detected without prior purification of the sample [256, 257]. Previous research has shown that differences in peak location and width in DSC profiles are indicators of sample degradation [230, 247]. Sample preparation for DSC measurement only requires, that a few milligrams of the non-altered sample be placed in a crucible [254], which provides a significant advantage over the other methods mentioned.

5.2 Materials and Methods

5.2.1 Coating of carrier particles

In order to produce degradation samples, carrier particles (sea sand) were coated with several different polymer materials of interest, by dissolving or melting the respective polymer samples and subsequently precipitating these samples onto the carrier particles in a stir tank. For cellulose acetate and Organosolv (OS) lignin, 30 g of each sample was dissolved in 150 ml of acetone and stirred with an electric stirrer until homogeneous (approximately 2 hours at 25 °C). Subsequently, 200 g of carrier particles were added to the solution. The acetone was evaporated by placing the solution in a drying cabinet at 50 °C for 18 hours. For PHB no solvent was found to dissolve large enough quantities, therefore, 30 g of PHB were melted completely (melting point 160 °C to180 °C [258] in a 200 °C oil bath). Following, 200 g of carrier particles were added and then continuously mixed until room temperature was reached, resulting in 1-2 cm large aggregates, composed of the material of interest and carrier particles. The aggregates were ground in a knife mill and then washed thoroughly with deionized water. After the coated carrier particles had settled, and loose material was removed, the precipitate was dried and separated into four particle size fractions using an analytical sieve shaker: 1) smaller than 100 µm, 2) between 100 and 250 µm, 3) between 250 and 630 µm and 4) above 630 µm. Particles between 100 and 630 µm were used for lignin and PHB degradation analysis, whereas particle sizes between 250 and 630 µm were used for cellulose acetate degradation. The method described above was limited to polymers which can either be dissolved in high concentrations of solvent or melted. An attempt was made to coat carrier particles with chitosan. This attempt failed due to the lack of adhesion to the carrier particles. Despite chitosan being soluble in diluted acetic acid, only 1 wt% of coating remained after the washing.

5.2.2 Biodegradation of coating

In order to decompose the polymer coating of the carrier particles, samples were mixed with compost (Palatihum G from Zentrale Abfallwirtschaft Kaiserslautern, Germany). Therefore, the composting conditions were modified and scaled down from [236] without adverse effects on the study [259]. Since the available sample volumes were small, the volumes of inoculum, dry weight of tested substance and water content were scaled down but the ratios between them were kept constant. The cultivation conditions were aerobic, but samples were not actively oxygenated as suggested in [236]. Biodegradation was performed in 250 mL flasks. 37 g of coated carrier particles (moisture content ~0 %, average coating 8 wt% or equivalent to 3 g of coating), were mixed with either compost equal to 18 g of dry weight (ratio 1:6, as described in [236]). The moisture content was determined using a moisture balance. Sterile water was added to a final moisture content of 50 wt%. For reference, the coated carrier particles were mixed with sterile water to a final concentration of 50 wt%. Gas exchange was allowed using 0.2 µm PTFE-filters. Where PHB and cellulose are used as reference materials, samples were cultivated at 25 °C in an universal oven, as suggested in [236], Triplicates of samples were taken at the start of the incubation process and again after five and ten weeks of incubation. The mean was calculated and used for further analysis.

5.2.3 Analyzing coating

Prior to sample analysis, the coated carrier particles were purified and dried. Afterwards, the degree of surface coating was measured by determining the mass fraction of combustible solids. DSC measurements of the coated particles before and after composting were used for qualitative analysis of biodegradation as described previously [247]. Lastly, by using the characteristic signal of sand as an internal standard in the DSC measurements, a new method was developed for quantifying the degradation progress using DSC data.

5.2.3.1 Sampling and purification of coated carrier particles

For sample analysis, 4 g of a homogeneous mix of culture were taken from the composting culture. The sample was washed with water four times. The compost was separated from the coated carrier particles through sedimentation. The coated carrier particles were then dried at 50 °C. In order to even out “diluting” effects due to sand naturally occurring in the compost, the amount of sand in the compost was determined prior to use.

5.2.3.2 Determination of mass fraction of combustible solids

The degradation progress over time was determined as the change in mass fraction of combustible solids, using a tube furnace. In preparation for the measurements, empty combustion boats were dried and weighed using an analytical balance. Approximately 350 mg of pre-dried coated carrier particles were transferred into the combustion boats and heated to 100 °C for 2 h to remove any remaining water. After cooling, the dry weight of the sample was measured. In a second heating phase, the coated samples were heated to 800 °C with a heating gradient of 10 K per minute. During a holding period of 4 hours, the coating was burned off entirely. After cooling, the final weight was measured. The coating degree was the fraction volatile at or below 800 °C, which was determined gravimetrically, using equation 5-1.

$$\begin{aligned} &coating\ degree\ of\ particles \\ &= \frac{m_{combustion\ boat\ after\ 800\ °C} - m_{combustion\ boat\ after\ 100\ °C}}{m_{combustion\ boat\ after\ 100\ °C} - m_{combustion\ boat\ empty}} \end{aligned} \tag{5-1}$$

with

$m_{combustion\ boat\ after\ 100\ °C}$ = *weight of boat after combustion at 100 °C/ g*

$m_{combustion\ boat\ after\ 800\ °C}$ = *weight of boat after combustion at 800 °C/ g*

$m_{combustion\ boat\ empty}$ = *weight of empty boat/ g*

5.2.3.3 DSC measurements for qualitative evaluation of surface coating

Degradation was monitored using DCS. In preparation for the DSC measurements, 30 mg of pre-dried coated carrier particles and sand was weighed into standard 100 µl aluminum crucibles. The polymer to sand ratio of coated carrier particles was between 6 % and 10 %, the polymer sample weight being 1.8 mg to 3.0 mg. Subsequently, each crucible was sealed with a lid, which was then automatically perforated by the auto sampler. To detect the thermal influence of the coating, the samples were heated in a nitrogen atmosphere. A differential scanning calorimeter DSC 1 was used to perform the calorimetric measurement. The heat flux was measured for both the reference and sample crucibles as a temperature profile was applied, consisting of two phases. In the initial phase of 10 minutes, a constant temperature of 25 °C was applied. In the second phase, the crucibles were heated from 25 °C to 600 °C with a heating rate of 10 °C per minute. All peaks of a temperature profile were detected using the pre existing Matlab (from Mathworks Inc.) function "findpeaks()", which finds local extrema with their corresponding values, location (temperature) and width of each peak found. It was found that the location of each peak remained relatively stationary for each sample.

5.2.3.4 DSC measurements for quantitative analysis of coating degree

To evaluate the amount of biomaterial remaining on the samples, the DSC results were analyzed using Matlab. The data was exported from STARe as a plain text file and reformatted into a matrix of DSC responses. Iterating through each curve, the area above or under the curve (AUC) for particular temperature regions was calculated. For each polymer, the temperature range of the thermal response was initially chosen manually, later this was automated to minimize the signal-to-noise ratio (SNR). Interpolating between the start and ending temperatures of the interval provided a baseline. The measured values were interpolated using the Matlab function “trapz()”. The difference between the area under the baseline and the area under the sampled curve provided the peak area. For exothermic and endothermic responses, the integrated peak areas were positive and negative, respectively. Two peak areas were calculated, one for pure sand and a second, which was characteristic for the coating. Sand showed a thermal response in the range between 568 °C and 582 °C. This endothermic peak occurs due to the phase transformation of quartz [260]. The temperature ranges for the coating changed according to the chemical and physical characteristics of the sample analyzed. The polymer’s degradation was evaluated by comparing the ratio of a sample’s peak area to sand’s peak area throughout the process.

5.2.4 Analysis and validation of DSC results

To validate the data obtained in section 5.2.3.4, a calibration curve was created using different mixtures of pure sand and coated carrier particles. The resulting curves were used to analyze the absolute degradation progress of the coating analyzed. A linear regression between the relative peaks and the mass fraction was calculated from the calibration sets. As the peak analysis was found to be appropriate for analyzing the data, the decision, detection and determination limits of the regression were calculated according to norm [261]. These results were then used as initial criteria for the validation of the proposed method to analyze the successful polymer degradation degree of the particles. Specifically, the determination limit should be lower than the degradation degree. In this case, for the successful detection of coating degradation, the detection limit should be less than 10 mg per g (1 % of coating).

A second validation step was performed through comparison against a reference method (determination of mass fraction), whereby the degradation calculated using DSC measurements would need to be proportional to the degradation degree detected by the reference method.

5.2.5 Overview of processing steps for the implementation of a DSC-based method

In this work, a DSC-based method for monitoring biodegradation quantitatively using small sample quantities and simple sample preprocessing is developed. Figure 5-1 provides an overview of the processing steps (section 5.2.1 to 5.2.4), that were used to prepare samples for biodegradation and subsequent analysis.

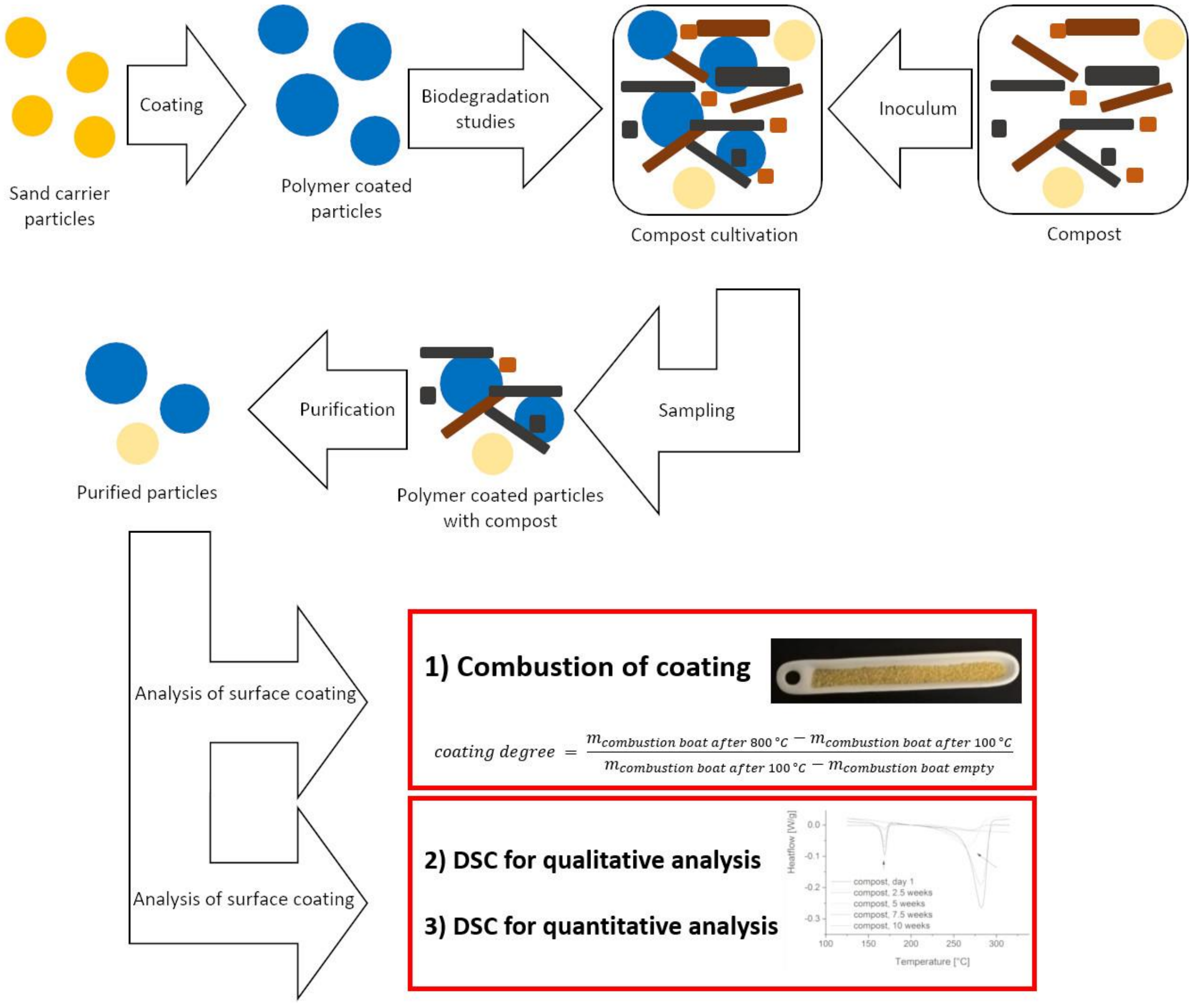
Sand carrier particles
Coating
Polymer coated particles
Biodegradation studies
Compost cultivation
Inoculum
Compost
Purified particles
Purification
Polymer coated particles with compost
Sampling
Analysis of surface coating
Analysis of surface coating
1) Combustion of coating
$coating\ degree = \frac{m_{combustion\ boat\ after\ 800\,°C} - m_{combustion\ boat\ after\ 100\,°C}}{m_{combustion\ boat\ after\ 100\,°C} - m_{combustion\ boat\ empty}}$
2) DSC for qualitative analysis
3) DSC for quantitative analysis
Heatflow [W/g]
0.0
-0.1
-0.2
-0.3
compost, day 1
compost, 2.5 weeks
compost, 5 weeks
compost, 7.5 weeks
compost, 10 weeks
100
150
200
250
300
Temperature [°C]

Figure 5-1: Processing steps used to prepare samples for biodegradation and subsequent analysis.

5.2.6 Qualitative evaluation of chitosan and chitosan-derivates using DSC

Approximately 7 mg of chitosan-catechol adhesive (see chapter 3), 5 mg of low molecular weight chitosan or 2 mg of PCA were weighed into standard 100 µl aluminum crucibles. Subsequently, each crucible was sealed with a lid, which was then automatically perforated by the auto sampler. A differential scanning calorimeter DSC 1 was used to perform the calorimetric measurement. The heat flux was measured for both the reference and sample crucibles as the crucibles were heated from 25 °C to 600 °C with a heating rate of 10 °C per minute under a nitrogen atmosphere.

5.3 Results and Discussion

In this chapter, a DSC based method for monitoring biodegradation quantitatively using small sample quantities and simple sample preprocessing was developed. First, carrier particles were coated with three biodegradable polymers (PHB, cellulose acetate (CA) and lignin). The size characterization of the coated particles, which was determined by identifying the change in mass fraction of combustible solids, is discussed in section 5.3.1. Following, the biodegradability of the coated carrier particles was determined in compost. The results, which were obtained using a reference method (measurement of combustible solids after composting), are discussed in section 5.3.2 and further used for validation of the DSC based quantification of biodegradability. Following, the degradation progress was determined using DSC and the results are discussed in section 5.3.3. In section 5.3.3.1, qualitative changes in the DSC profiles were analyzed as a result of biodegradation. In section 5.3.3.2, a method for quantitative evaluation of the DSC profiles is developed. In section 5.3.3.3 and 5.3.3.4, the DSC based quantification of biodegradability is evaluated and validated.

Lastly, in section 5.3.4, the analysis of the DSC profiles of chitosan and the mussel mimicking catechol-chitosan adhesive, which was developed in this work (see chapter 3), is discussed.

5.3.1 Size characterization of pure sand and coated carrier particles

For an initial evaluation of the coating progress, non-coated and coated carrier particles were classified into four size fractions: 0 to 100 µm, 100 to 250 µm, 250 µm to 630 µm and above 630 µm. Size classification of non-coated carrier particles (prior to polymer coating) determined that almost all particles were evenly distributed between 100 and 250 µm or between 250 and 630 µm with significantly fewer carrier particles sized below 100 µm and above 630 µm. To deal with these marginal outsize fractions two assumptions were made; specifically, 1) the particle fraction smaller than 100 µm were remains of polymer powder which had not been coated onto the carrier particles and 2) the particle fraction larger than 630 µm were polymer-sand aggregates, which varied in the different batches of polymers, which may have resulted from different processing intensities and mixing times in the knife mill. Consequently, both of these outsized fractions were not included in the biodegradation studies and were discarded. A successful homogeneous coating of carrier particles was confirmed by a decrease in the mass fraction of particles between 100 and 250 µm and by an increase in the mass fraction of particles between 250 and 630 µm, which is what was measured in a secondary size classification.

5.3.1.1 Polymer coating degree of carrier particles

The coating degree was determined as the change in mass fraction of combustible solids of the coated carrier particles. The PHB-coating of particles between 100 and 630 µm, measured as the mass fraction of coating to total mass, was determined to be 7.7 wt%. For CA, the coating success, was found to be highest for particles between 250 and 630 µm (8.0 wt%). For lignin, the coating success for particles from 100 to 250 µm was 7.5 wt%, and for particles between 250 and 630 µm 5.7 wt%. Since the mass fraction of lignin coated particles in the smaller fraction (100 to 250 µm) was only about 30 wt%, the combined fractions (particles between 100 and 630 µm) were used for lignin degradation studies.

5.3.2 Determination of biodegradation using reference method

In order to evaluate the composting environment used for biodegradation experiments and to exclude inhibitory effects which may result from the preprocessing of the polymers, the degradation progress was analyzed using a reference method, measurement of combustible solids [262]. Therefore, the coating degree after biodegradation was measured in a combustion furnace. The degradation process was quantified through comparison of the coating degree before and after 10 weeks of incubation. In order to correct for non-biological degradation, such as abrasion, erosion or swelling, a control experiment was performed without inoculum. Biodegradation was estimated using the reduction of volatile substances per initial sample coating (equation 5-1). Non-biological degradation was evaluated through comparison of inoculated samples and control samples (results are shown in Table 5-1).

Table 5-1: Degradation progress after 10 weeks of incubation time. The degradation progress determined as the change in mass fraction of combustible solids. The degradation progress was calculated as reduction of combustible coating of the carrier particles per the initial sample coating, using equation 5-1.

Coating\ Degradation method	Weight loss of control [wt%]	Weight loss of compost [wt%]
PHB	3.0	96.3
Lignin	13.0	21.2
CA	-0.3	32.4

The determination of the mass fraction of combustible solids showed degradation of the coating of almost 100 wt% of the initial PHB-coating during compost incubation, which agrees with previous findings [259]. No degradation was observed for the PHB-coating in the control trials. CA is a naturally occurring polymer and previous reports found CA to be degraded by soil microbes [263]. Determination of combustible solids showed partial biodegradability of the CA-coating (32.4 wt%), confirming biodegradability. The controls showed no degradation of the CA-coating. For lignin, the treatment with compost showed a degradation progress of 21.2 wt% of initial lignin coating. However, the control showed a loss of coating of 13.0 wt%. Since no fungal or bacterial growth was visible on the lignin control, it was concluded that the loss of coating of the control samples occurred due to abrasion of the brittle coating during composting or during preparation of the samples for the combustion analysis. The biodegradability of lignin, which has also been reported in previous work [237], was confirmed. A second reference method, total weight loss, was provided in Capitain et al. (2020a) [264].

5.3.3 Determination of biodegradation using DSC analysis

DSC is a thermo-analytical method [254] which has been used for monitoring qualitative changes of a polymer structure due to biodegradation [230, 247]. In this work, DSC profiles were first analyzed qualitatively for degradation progress monitoring. Following, a method was developed for quantification of biodegradation using DSC temperature profiles.

5.3.3.1 Analyzing qualitative changes of PHB during incubation using DSC

The DSC analysis results on a PHB sample are presented in Figure 5-2, where the specific heat flow of the PHB coating is shown over the course of 10 weeks of microbial degradation. In order to differentiate biodegradation from mechanical or chemical degradation, evaluation against control samples was necessary, as was done for the combustion experiments.

Figure 5-2 A shows PHB incubated in water (control) and Figure 2 B shows PHB incubated in compost. PHB incubated in water had two distinct peaks with local minima at 169.7 °C ± 0.2 °C and 284.8 °C ± 1.9 °C (average over all control samples). While the control samples showed very little variation, the average peak locations of PHB incubated in compost had a higher standard deviation and the peaks shifted towards lower temperatures when biodegradation occurred (peak 1: 169.1 °C ± 0.2 °C and

peak 2: 274.6 °C ± 9.3 °C). Evaluation of the peak width revealed that peak 2 widens after biodegradation, from 120.7 ± 2.2 to 124.6 ± 6.2.

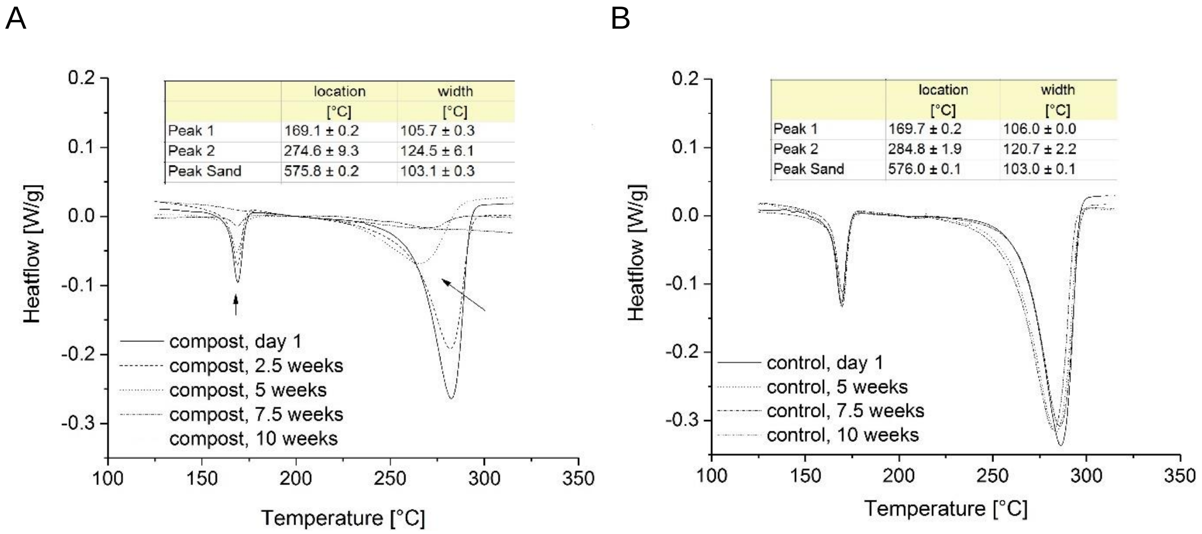

A

	location [°C]	width [°C]
Peak 1	169.1 ± 0.2	105.7 ± 0.3
Peak 2	274.6 ± 9.3	124.5 ± 6.1
Peak Sand	575.8 ± 0.2	103.1 ± 0.3

B

	location [°C]	width [°C]
Peak 1	169.7 ± 0.2	106.0 ± 0.0
Peak 2	284.8 ± 1.9	120.7 ± 2.2
Peak Sand	576.0 ± 0.1	103.0 ± 0.1

Figure 5-2: Qualitative analysis of degradation process of PHB over a course of 10 weeks. A) Incubation in water (control) and B) incubation in compost. The table shows the location, width and height averaged over time. The arrows indicate peak 1 (left) and peak 2 (right).

In order to exclude peak widening as being caused by the decreasing degree of coating, a third set of data was created, whereby PHB-coated carrier particles were mixed with sand in different ratios, analyzed using DSC, and the local minimum and peak width were calculated. The average local minimum of peak 2 was 291.2 °C ± 0.4 °C and the width 114.5 °C ± 0.6 °C.

The peak location and width of the DSC-profiles of PHB-coated particles before and after incubated in compost were compared to a PHB-control (incubated in sterile water). While the control samples showed very little variation in the location and width of PHB peak 2, the peak locations of PHB peak 2 incubated in compost had a higher standard deviation, the peaks shifted towards lower temperatures and grew wider after biodegradation occurred. While it was noted that the peak width of non-composted PHB-coated carrier particles did not show an area increase of peak 2, the compost incubated samples did. Therefore, the observed increase of peak width was likely an effect caused by the biodegradation due to the treatment with compost. PHB is a semi-crystalline isotactic polymer [265] whose degradation was initiated by enzymatic hydrolytic cleavage of ester bonds, resulting in surface erosion [238]. Since depolymerization initiated by secreted enzymes was found to start biodegradation [239], both effects (movement of peak location and growth of peak width) were attributed to biodegradation by compost which was saliently detected using qualitative DSC analysis.

5.3.3.2 Developing a method for quantitative evaluation of DSC profiles

Analysis of the DSC profiles revealed that the area under (exothermic) or over the curve (endothermic) at a polymer's characteristic peak was proportional to the amount of polymer remaining on the carrier particles. For this purpose, the identification of temperature interval for integration was indispensable for proper analysis.

Identifying the integration interval manually

Sand had a characteristic peak in a DSC profile [260], starting at 568 °C and ending at 582 °C (see Figure 5-3 A and B, area 3). The peak size and location of the polymer, however, shifted depending on the polymer used for coating. Additionally, reviewing the DSC profiles of the model substrates PHB, lignin and CA, revealed that the polymers had more than one characteristic peak (see Figure 5-2 and Figure 5-3).

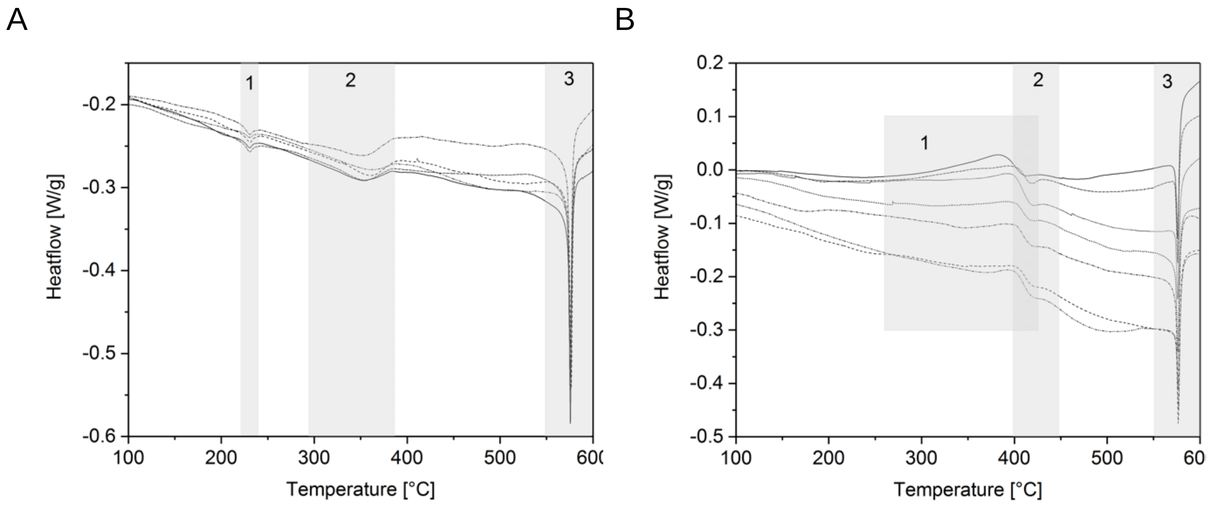

Figure 5-3: Characteristic DSC profiles of CA (A) and lignin (B) coated on carrier particles. Incubation type (compost or control), as well as time points (0 weeks to 10 weeks) may vary. Prior to DSC analysis, all samples were dried at 50 °C. Each family of curves show two areas (1 and 2) with characteristic peaks for the coating (CA or lignin). Area 3 marks the characteristic peak for sand.

The first PHB peak extended from 150 °C to 180 °C and the second peak from 230 °C to 310 °C. Both, PHB peaks were suitable for establishing calibration curves. While PHB had a large response area in the DSC profile, CA and lignin had much narrower peaks. The first peak for CA extended from 220 °C to 255 °C and the second peak from around 300 °C to 400 °C. Narrower peaks were advantageous since wider temperature ranges result in increased background noise. Small peak areas, however, were challenging, since the absolute error increased. For lignin, peak detection was especially challenging, since the DSC profile indicated that an exothermic (peak 1) was followed closely by an endothermic peak (peak 2), with some overlap. Choosing the optimal interval for each DSC profile is further discussed the next section.

Advanced peak detection by reducing signal to noise ratio

Data collection was challenging given extraneous circumstances which confounded results. Following are descriptions of challenges encountered. Samples such as lignin or CA produced less distinct peaks as compared to PHB, which made selecting the start and ending temperatures for peak integration challenging. A temperature range for integration of DSC peaks was well chosen when it provided a large area for integration while minimizing background noise. Samples extracted from a compost matrix contained interfering contaminations. Lignin was a particularly challenging substance to analyzed because samples frequently over boiled during DSC analysis. From the manual evaluation of the characteristic DSC profiles for CA and lignin (see Figure 5-3), it was concluded that the DSC response areas for CA and lignin are within the range of 200 °C to 500 °C. To determine the optimal SNR interval, for every polymer, each DSC-profile (all controls and initial samples of compost of one polymer) was integrated over every interval between 200 °C to 500 °C in 5 °C steps. For every interval, the mean of the relative peak areas of the different DSC-curves was calculated and stored. The integral that was calculated between the lower bound temperature and the upper bound temperature was visualized using a greyscale intensity (see Figure 5-6 A to C and Figure 5-7 A and B), with darker greyscale intensities representing higher peak areas. Figure 5-4 B shows the result for the systematic integration of the DSC response curves for CA, where larger peak areas are desired. The background signals were obtained using the non-coated carrier particles. Similar to the coated-carrier particles, the non-coated carrier particles were incubated and processed according to the procedure described in section 5.2. The peak area from the non-coated particles was used to characterize the background signal (shown in Figure 5-4, A), which included the quantification of the noise caused by the instrument as well as the remaining compost or fibers. Conversely, for the background signal, low peak areas, displayed in lighter greyscale, are desired. The mean over the interval for both samples increased with increasing temperature range intervals (shown in Figure 5-4 A and B). The SNR was then calculated by dividing the mean values of the polymer coated carrier particles by the mean value of the non-coated carrier particles over all calculated intervals. A higher SNR corresponded to a larger peak area divided by a smaller background signal. As shown in Figure 5-4 C, the SNR analysis revealed suitable intervals for quantitative analysis. According to the SNR plot, the optimal range for CA detection was between 260 °C and 385 °C, where the SNR was highest.

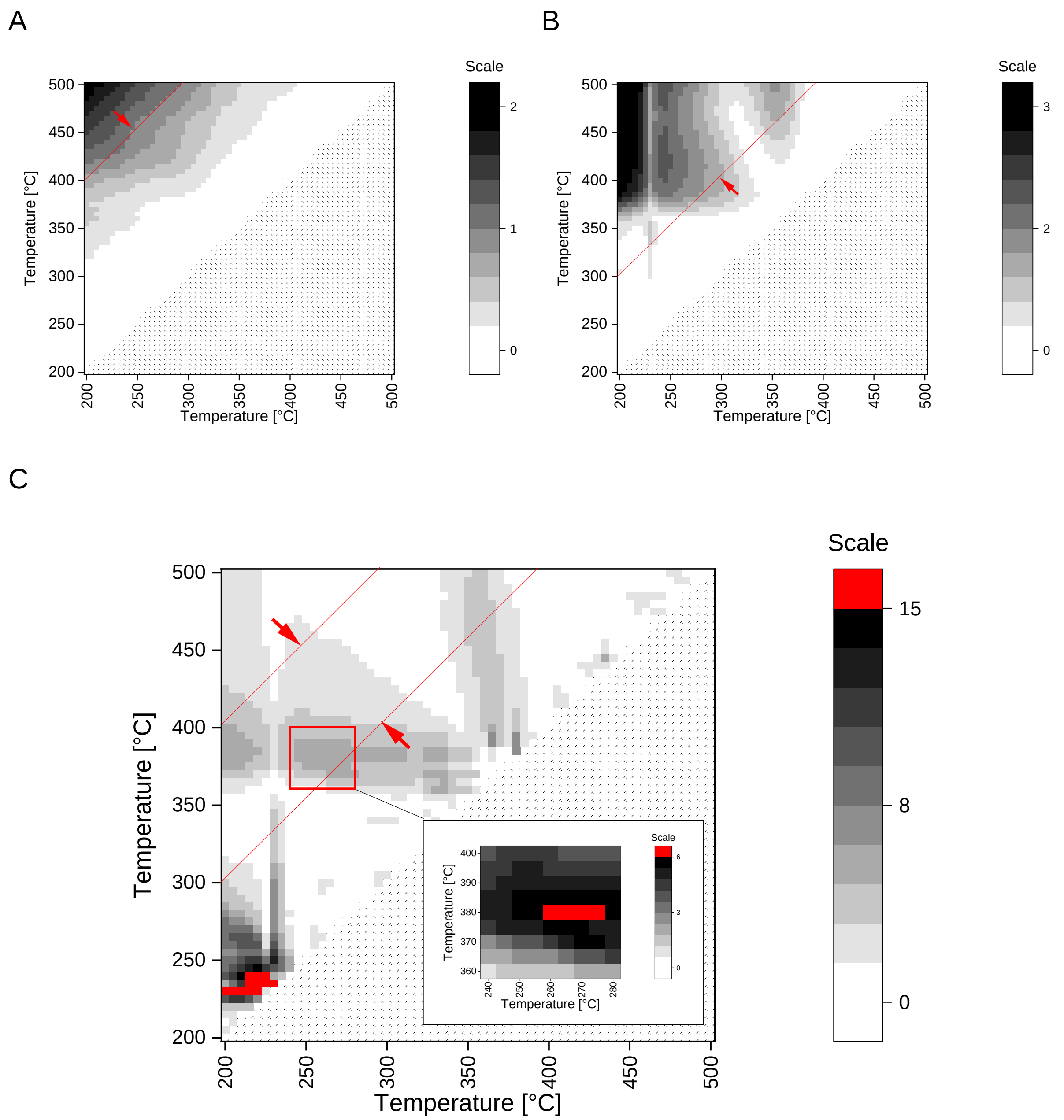

Figure 5-4: Determination of interval between 200 °C and 500 °C in 5 K steps. A) Mean integrated DSC response for non coated-carrier particles, B) Mean integrated DSC response for CA-coated carrier particles. C) Mean of CA coated samples divided by peak area from non-coated carrier particles (SNR). Additional resolution is provided in the box, showing the area around the best interval. The greyscale represents the value of the integral that was calculated between the lower bound and the upper bound temperature (lighter greyscale intensities = small peak areas, darker greyscale intensities = large peak areas; the largest integrals are marked with red). The red arrows and lines indicate ideal search areas for upper and lower bound temperatures and are defined by areas of high signal intensities and low background noise.

The same analysis was conducted for lignin. While many intervals were found with high SNR, when 420 °C was set as an upper temperature limit, the lower border seemed to be more variable (250 °C to 370 °C) (see Figure 5-5 A). The highest SNR was obtained for small temperature ranges, such as from 400 °C to 420 °C (see Figure 5-5 B). However, as previously described, the relative peak area was also small, which made this a less favorable interval. More robust intervals with smaller SNR's were identified having larger absolute peak areas. Using this approach, suitable intervals for lignin had an approximate lower limit of 350 °C and an upper limit at 420 °C.

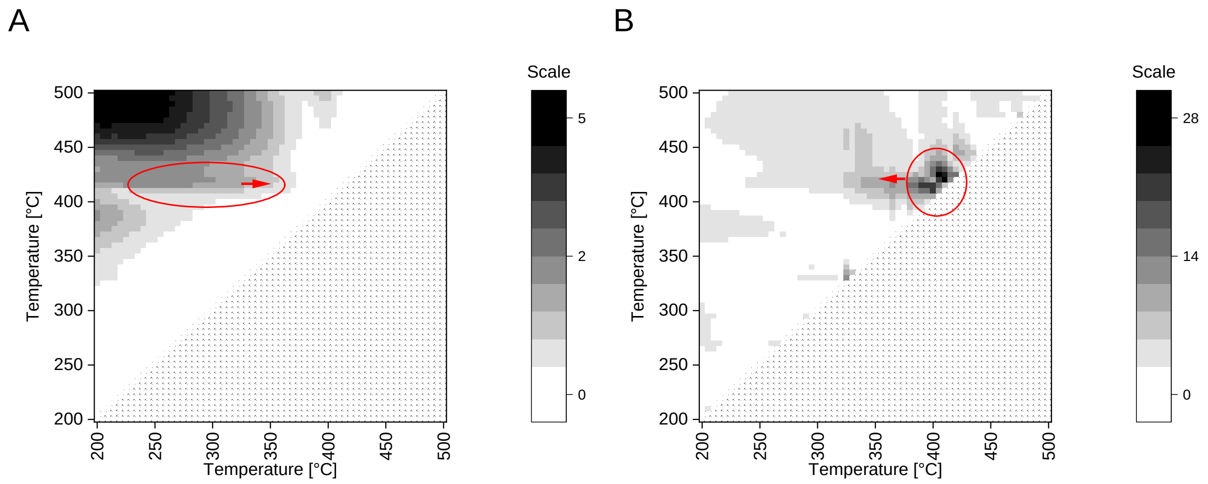

Figure 5-5: Determination of interval between 200 and 500 °C in 5 K steps. A) Mean integrated DSC response for lignin-coated carrier particles, B) Mean of lignin coated samples divided by AUC of non-coated carrier particles (signal to noise ratio). The arrow indicated where the best interval is found based on the analysis of the opposed graph. The greyscale represents the value of the integral that was calculated between the lower bound and the upper bound temperature (lighter greyscale intensities = small peak areas and darker greyscale intensities = large peak areas). The red arrows and ellipses indicate ideal search areas for upper and lower bound temperatures and are defined by areas of high signal intensities and low background noise.

5.3.3.3 Quantification of PHB, lignin and CA biodegradation using quantitative DSC analysis

To evaluate the suitability of the described DSC method for quantitative analysis, linear regressions between the relative peaks and the mass fraction were calculated using a calibration data set (see Figure 5-6).

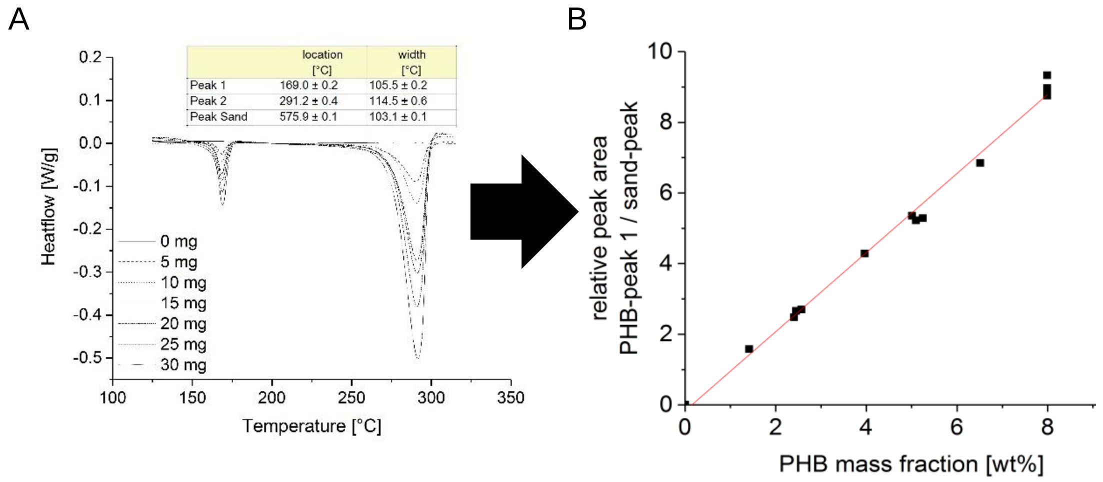

	location [°C]	width [°C]
Peak 1	169.0 ± 0.2	105.5 ± 0.2
Peak 2	291.2 ± 0.4	114.5 ± 0.6
Peak Sand	575.9 ± 0.1	103.1 ± 0.1

Figure 5-6: Calibration of DSC measurements A) DSC-profiles of calibration standards. PHB-coated carrier particles and sea sand were mixed in different ratios to a total of 30 mg. B) Linear regression of PHB and sand "dilutions".

For PHB and CA, peaks 1 and 2 were used for analysis. For lignin the optimized peak area (as described in section 5.3.3.2) was used. For all measurements, a linear relation was found between the sample weight and the peak area and consequently, a linear regression fit was appropriate for analyzing the data. The slope, y-axis and the coefficient of determination of each regression curve for PHB, CA and lignin are provided in Table 5-2. Since an exothermic reaction occurred in the interval chosen for lignin, the regression had a negative slope.

Table 5-2: Results of linear regression of the relative peak area PHB, CA and lignin over the mass fraction.

Polymer	y-axis	slope	coefficient of determination
PHB 1	-0.167	112.01	0.992
PHB 2	-0.041	15.53	0.991
Cellulose-Acetate 1	0.022	1.450	0.469
Cellulose-Acetate 2	0.140	22.768	0.888
Lignin	0.456	-18.673	0.985

For PHB and CA, endothermic peaks were used, and hence, the regression had positive slopes. Table 5-3 summarizes the decision, detection and determination limits of the regression calculated following DIN 32645, 2008 [261]. The determination limit for PHB was 13.6 mg per g sand for peak 1 and 14.5 mg per g sand for peak 2. Since the initial PHB-coating (77 mg per g sand) was more than 5 times higher than the calculated determination limit, high resolution determination was possible. The determination limits for lignin and CA were much higher, resulting in a quantification of lower resolution.

Table 5-3: Decision, detection and determination limits for linear curve fittings, calculated following DIN 32645, 2008 [261].

Polymer (start and end temperature of peak)	Decision limit [mg g^{-1} Sand]	Detection limit [mg g^{-1} Sand]	Determine. limit [mg g^{-1} Sand]
PHB (150 °C-180 °C)	4.5	9.0	13.6
PHC (230 °C – 310 °C)	4.8	9.7	14.5
Lignin (350 °C – 420 °C)	28.9	57.9	86.8
CA (220 °C – 255 °C)	55.8	111.6	167.4
CA (260 °C – 385 °C)	19.5	39.0	58.5

By applying the linear regressions to the extracted peak areas from the DSC profiles, the samples from the degradation experiments were analyzed (results see Figure 5-7). For PHB, the coating degree of the control (sterile water) was steady over the course of 10 weeks of incubation, remaining constant at 81 mg g^{-1} ± 6 mg g^{-1}. The coating degree of PHB incubated in compost decreased from 61 mg g^{-1} (day 1) to 2 mg g^{-1}

(after 10 weeks of incubation). For CA, the coating degree of the control (sterile water) was steady over the course of 10 weeks of incubation, remaining constant at 70 mg g^{-1} ± 1 mg g^{-1}. The coating degree of CA incubated in compost decreased from 53 mg g^{-1} (day 1) to 25 mg g^{-1} (after 10 weeks of incubation). For lignin, the coating degree of the control (sterile water) was steady over the course of 10 weeks of incubation, remaining constant at 105 mg g^{-1} ± 5 mg g^{-1}. The coating degree of lignin incubated in compost decreased from 98 mg g^{-1} (day 1) to 24 mg g^{-1} (after 10 weeks of incubation).

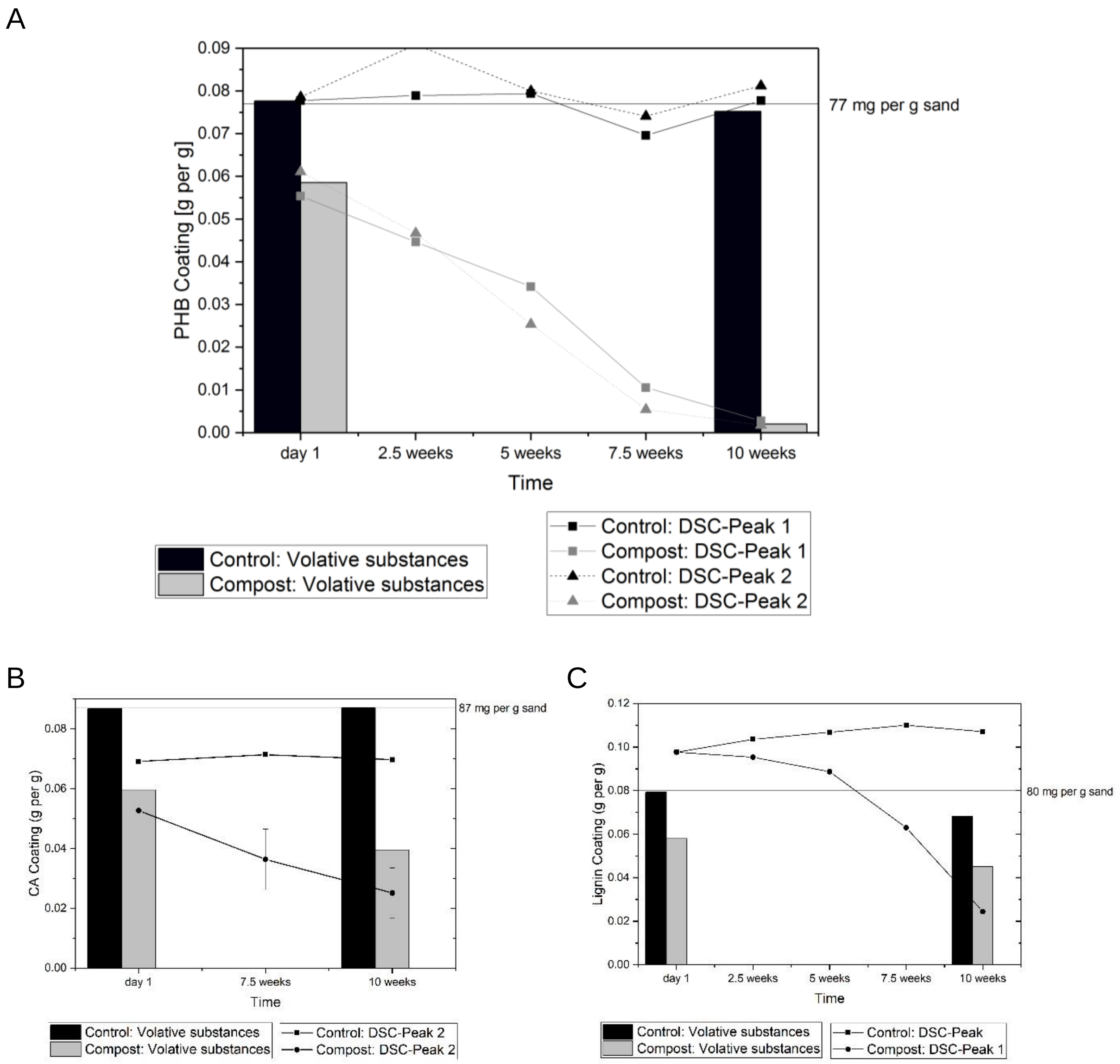

Figure 5-7: Biodegradation with compost: (A) degradation of PHB, (B) degradation of CA (DSC profile was integrated between 260 and 385 °C) and (C) degradation of lignin (DSC profile was integrated between 330 and 420 °C). Vertical bars present the degradation, determined as the change in mass fraction of combustible solids, and curves present the results from DSC analysis.

5.3.3.4 Evaluation of DSC-based biodegradation using quantitative monitoring technique

In this work, a quantitative method was developed for the evaluation of DSC profiles. It was found that the area under (exothermic) or over the curve (endothermic), at a polymer's characteristic peak [254], is proportional to the amount of polymer on the carrier particles. This relationship made the choice of a characteristic temperature interval for integration of great importance. While PHB showed two distinct peaks which could be manually selected, CA and lignin had more complicated DSC profiles. Therefore, an advanced method for peak detection was developed by reducing the SNR. It was shown that by using the proposed advanced technique for peak detection, even samples with non-optimal DSC profiles could be analyzed. Linear calibration curves were successfully calculated for each material (see section 5.3.3.3).

By applying these linear curves from section 5.3.3.3 to the DSC profiles, the samples from the degradation experiments were analyzed. In order to complete the quantitative analysis of the surface coating of carrier particles using DSC measurements, results were compared to the combustion experiment results (section 5.3.2). Both methods (quantitative DSC analysis and combustion experiments) were able to detect loss of surface coating due to abrasion.

Compost naturally contains sand [266, 267]. By adding compost to the PHB-coated carrier particles, a “dilution” of the internal sand standard occurred which was visible in the reduction of the PHB coating of the compost samples after 1 day, from 0.077 to 0.059 g per g. Both methods showed a coating of 77 mg per gram sand and no degradation or loss of surface coating in the control. Both methods showed 100 wt% degradation of PHB due to compost. Therefore, it was concluded that the DSC-based method was suitable for the quantification of the biodegradability of PHB.

The degradation progress of CA-coated carrier particles was also analyzed with DSC alongside the combustion experiments. Compost growth was compared to a control trial. The “sand dilution” effect due to the addition of compost was observed as well. DSC-based evaluation of degradation progress and the combustion experiments showed comparable degradation results. The control trial showed no degradation or loss of coating due to abrasion. The data obtained by DSC were, however, up to 20 wt% lower than the data obtained with combustion experiments. It was concluded that CA underwent non-chemical or non-biological alterations, such as swelling [268], causing a temperature shift in the DSC peak. The standard curve for DSC analysis was conducted using dry material which was only exposed to water during initial production. The DSC results would likely be improved by using particles which underwent the same pretreatment. The results showed that the DSC-based method was suitable for measuring biodegradation of CA, however, quantification of the degradation required a calibration to include polymer swelling effects.

Lastly, the degradation of lignin was analyzed using DSC. In contrast to CA, the data obtained with the DSC started 20 wt% higher and ended 20 wt% lower as compared to the combustion experiments. As described previously, peaks can move during incubation towards lower or higher temperatures [247]. In the case of lignin, this was likely due to an overlap of endothermic and exothermic peaks [210]. The method was therefore not applicable for the quantification of biodegradation of lignin.

5.3.4 Qualitative analysis of catechol-PCA adhesive using DSC

In order to analyze the effect of chitosan dissolution on its thermal properties, first, chitosan powder was analyzed using DSC. Second, chitosan was dissolved in water and the pH was adjusted to 5-6 using concentrated hydrochloric acid. Due to the addition of the acid, chitosan formed a gel, which was dried at room temperature for 24 hours (further referred to as processed chitosan) and analyzed using DSC. The DSC profiles of non-processed and processed chitosan are shown in Figure 5-8. The non-processed chitosan powder exhibited two distinct peaks: A minimum (endothermic) at 92 °C and a maximum (exothermic) at 305 °C. For the processed chitosan a minimum was also detected at 92 °C, but with lower intensity. Furthermore, two distinct peaks were detected, an exothermic peak at 214 °C followed by a smaller endothermic peak at 226 °C.

The endothermic peak at around 92 °C was attributed to water evaporation occurring during the DSC measurement. In a solid state, polysaccharides have disordered structures which easily hydrate due to their strong affinity for water [269, 270]. It was shown that for chitin and chitosan the endothermic peak area increased with increasing N-deacetylation [271]. The resulting increase in the content of polar groups (amines) together with an observed increase in amorphous regions caused an increase in water retention capacity which was reflected in the DSC profiles [272]. The lower intensity of the endothermic peak at 92 °C of processed chitosan was therefore attributed to a decrease of water binding capacity.

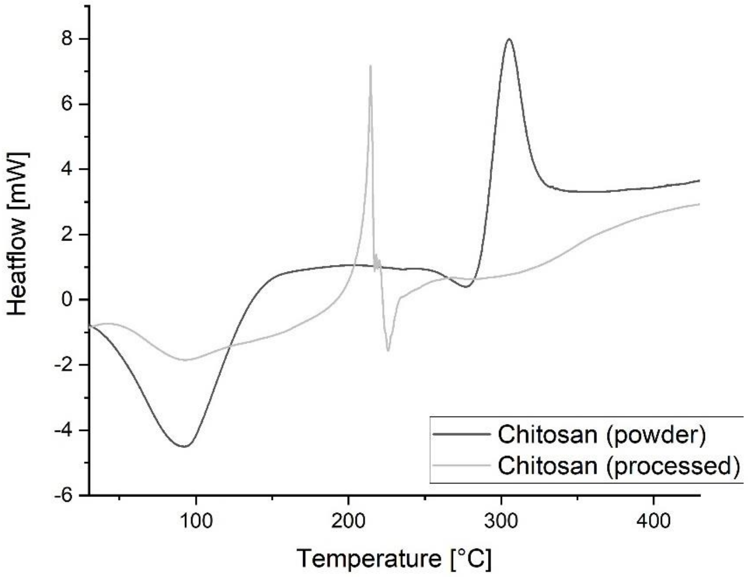

Figure 5-8: DSC profiles of chitosan before (black curve) and after (grey curve) processing.

The exothermic peak at around 305 °C was credited to the depolymerization of chitosan. While chitin and chitosan with a deacetylation degree as low as 25 % showed exothermic peaks between 390 and 430 °C [271], TGA analysis showed that depolymerization of chitosan occurred between 260 °C and 380 °C [273]. This shift towards lower temperatures was attributed to a decrease of molecular weight which occurred as a side effect of deacetylation as well as the decrease in acetyl content [271]. For the processed chitosan, the exothermic depolymerization peak was detected at a lower temperature (214 °C) compared to the non-processed chitosan. During chitosan processing, the pH decreased from about 9 to 6, affecting the ionization of the amine groups. Therefore, it was concluded that the polarization of the amine group ($–NH_2$ to NH_3^+) decreased the depolymerization temperature, confirming the results presented in chapter 3. The decrease of water binding capacity and the previously described formation of a gel suggest that intermolecular water bonds were displaced by intramolecular bonds of chitosan.

Chitosan was used as the backbone for a mussel mimicking adhesive (see chapter 3). Here, DSC is used to evaluate the adhesive and its components. Distinct peaks from the DSC profiles were observed for the individual components (see Figure 5-9). PCA (solid) showed three endothermic peaks: A minuscule peak at 131 °C, a sharp endothermic peak with a minimum at 206 °C and a broader endothermic peak with a minimum at 259 °C. The two latter endothermic peaks correlate well with the melting temperature of 221 °C [85]. For benzoic acid, 4-Hydroxybenzoic acid and for shikimic acid sharp peaks were detected at 140 °C [274], 215 °C [275], 185 °C [276], respectively. Since benzyl derivates which lack the carboxylic group also lack this characteristic sharp peak, it was concluded that the sharp endothermic peak at 206 °C was characteristic of the carboxylic group. The three endothermic peaks are followed by an exothermic peak, which was identified as decomposition of chitosan [276].

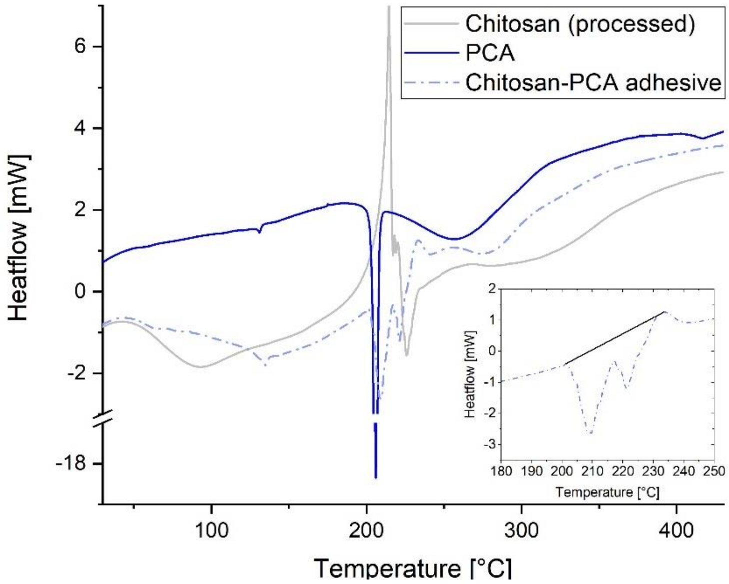

Figure 5-9: DSC profiles of processed chitosan (grey curve), PCA (blue curve) and chitosan-catechol adhesive (light blue curve, dash dotted). The inset graph magnifies the peak interval between 201 °C and 233 °C.

The chitosan-catechol adhesive showed a wide peak with a minimum at 134 °C, two sharp peaks with a minimum at 209 °C and 221 °C (see Figure 5-9, magnified graph) and a wider peak with a minimum at 276 °C, followed by an exothermic decomposition. Due to the similarity of shape and temperature, the first peak (134 °C) was attributed to PCA (bound or free). The endothermic peak at around 92 °C, however, which was detected for chitosan and processed chitosan was not observed for the PCA-chitosan adhesive, suggesting limited water absorption capacity. The sharp characteristic melting peak of PCA (206 °C) and the exothermic depolymerization peak of processed chitosan (214 °C) were both absent in the DSC profile of the PCA-chitosan adhesive. In their place, two new endothermic peaks at 209 °C and 221 °C were detected. This finding suggests that the carboxylic group of PCA and the amine group of chitosan had reacted in order to form the PCA-chitosan adhesive. This finding is coherent with chapter 3, where it was concluded that the carboxyl group reacted with the amine group. However, due to the proximity of the PCA and chitosan peaks it is unclear whether the new peaks detected for the catechol-PCA adhesive may be a result from a thermal overlap of the endothermic and exothermic effects. Further analysis is needed.

In order to adequately address polymer waste in the environment, their complete biodegradation is indispensable [277] and a finished product, with all of its components, must be completely biodegradable. The development of biodegradable adhesives goes therefore hand-in-hand with the development of suitable biodegradation methods.

The DSC profiles give insight into potential structures present in the catechol-chitosan adhesive. The distinct endothermic peaks at 209 °C and 221 °C, which were detected in the DSC profiles of the catechol-chitosan adhesive, are in principle suitable for the DSC based quantification of biodegradation. While the DSC based analysis of biodegradability is possible, the degradation studies are not performed for the chitosan adhesive in this work and are suggested for future work.

5.4 Summary and Outlook

The proposed DSC-based method provided quantifiable detection of degradation progress while at the same time providing qualitative assessment of changes in crystallinity. Both pieces of information could be acquired using only DSC measurements. The method successfully detected biodegradability of PHB, but needed manual tuning when used to detect biodegradation of CA and lignin. While the automated detection of the temperature ranges to be used for the peak detection allowed improved detection of CA and lignin, quantitative analysis using DSC should still be improved further. Due to its linear chain structure, PHB was highly crystalline and had a defined melting point as well as a distinct decomposition temperature [265]. In contrast, for CA and lignin, the melting and decomposition temperatures were found to have a wide range and reaction peaks were partially overlapping. This difference made the analysis of CA and lignin unfavorable.

The developed adhesive (see chapter 3) displayed two characteristic endothermic peaks at 209 °C and 221 °C (see section 5.3.4). These peaks can be used to quantify the biodegradability of the PCA-chitosan adhesive using DSC. In order to verify that the developed adhesive retains its biodegradable properties, it is suggested that the DSC-based method be used to evaluate qualitative biodegradation of the adhesive. To tailor adhesives properties according to specific applications, field experiments should be performed.

In this chapter, DSC measurements were validated for monitoring biodegradation quantitatively using small sample quantities and simple sample preprocessing. Using only DSC measurements, quantifiable detection of degradation progress was possible, while simultaneously qualitative assessment of changes in crystallinity (indicating incomplete biodegradation) were obtained. The developed PCA-chitosan adhesive (see chapter 3) was characterized using DSC. It is proposed to use the implemented method for the quantification of the biodegradability of this PCA-chitosan adhesive.

6 Conclusion

In this work, natural polymers were functionalized with catechols to develop mussel mimicking adhesives. Biochemical methods, which avoid the use of harsh chemicals, were investigated for this purpose. The laccase-catalyzed formation of C-N bonds between primary amines and catechols via Michael-type addition were identified as most promising. The model reactions between the catechols, PCA and DHC, and the primary amine NAcDAP were parametrically optimized for their product yield. A solvent stable laccase from *C. unicolor* for use in up to 50 %wt ethanol was successfully identified and characterized for use in OS supernatants.

Thereafter, the catechols PCA and DHC were grafted onto a chitosan backbone via spontaneous and laccase-catalyzed Michael-type reaction towards mimicking the mussel’s adhesion properties. A strong and biogenic adhesive was obtained by functionalizing chitosan with PCA via spontaneous reactions, achieving a tensile strength of butt joints of 4.56 MPa ± 0.54 MPa (on aluminum surfaces blasted with corundum). Since the functionalization and curing processes use naturally occurring substances exclusively and are free of toxic chemicals, a novel and sustainable bioadhesive has been developed.

Furthermore, the extraction of OS lignin from beech wood was optimized for direct conversion using laccases from *C. unicolor.* Value added products for increased competitiveness of the lignocellulose biorefinery were also investigated. For the functionalization of OS lignin, a two-step concept was required, where first L-lysine and subsequently DHC and PCA were grafted onto lignin. For DHC-lignin, a tensile strength of 169.3 kPa ± 130.6 kPa was measured.

Lastly, a DSC-based method for the detection of biodegradability of polymers in complex samples was developed. DSC measurements were validated for monitoring biodegradation quantitatively, using small sample quantities and simple sample preprocessing. Using only DSC measurements, quantifiable detection of degradation progress was demonstrated, while simultaneously qualitative assessment of changes in crystallinity (indicating incomplete biodegradation) were obtained.

This work provides suitable tools for the functionalization of natural polymers towards the development of mussel mimicking adhesives and subsequent analysis of biodegradability via DSC.

6.1 Achievements and comparison to literature

In this work, two biogenic and mussel mimicking adhesives were developed, a PCA-catechol and a DHC-lignin. To evaluate the tensile strength of the adhesives developed in this work, both were compared to adhesives reported in literature (see section 1.2.6). Direct comparison of adhesion is difficult due to variations in the test parameters, such as test method, material of the adherends, and the curing conditions (such as dry or wet) among others. In this work, the tensile strength was used as the comparative parameter. The tensile strength comparison of biogenic adhesives (results, see Table 1-1) showed that the lowest wet adhesion was reported for the mussel itself, with 0.13 MPa ± 0.01 MPa [20]. The tensile strength measured for DHC-lignin under dry conditions, is at the low end of the list with 0.17 MPa ± 0.13 MPa, while the tensile strength of PCA-chitosan with 4.56 MPa ± 0.54 MPa is at the top of the list. The highest wet adhesion (tensile strength of 1.2 MPa) was reported for a laccase-treated lignin-soy protein with wood adherends [52].

The comparison of tensile strengths obtained in this work to literature reported values demonstrates that the PCA-chitosan adhesive is a strong and novel biobased adhesive which was produced without the use of harsh chemicals. The DHC-lignin, while being biobased and providing valorization to a side stream of the lignocellulose biorefinery, demonstrated weaker adhesion and requires further improvement.

6.2 Challenges encountered

The following challenges are highlights of those which were encountered during the course of this work and can be considered the main achievements.

- For various reasons, such as homogeneous catalysis and substrate solubility, the stability of laccases towards solvents was identified as a key factor in adhesive development. Using the BRENDA enzyme database, a solvent stable laccase from *C. unicolor* was identified for the use in up to 50 wt% ethanol.
- The commercial availability of the solvent stable laccase from *C. unicolor* was limited and production was stopped throughout the course of this work. To become independent from suppliers, a fermentation and purification protocol was implemented and optimized in order to produce the laccase.
- The determination of the reaction progress for the functionalization of natural polymers (such as chitosan or lignin) was challenging due to the substrate complexity. To overcome these challenges, model reactions were used to investigate suitable reaction mechanisms. For qualification of the reaction products, HPLC-MS protocols needed to

be developed and for quantification purposes HPLC protocols needed to be implemented.

- The identification of a biochemical method for developing biogenic mussel mimicking adhesives, which avoid the use of harsh chemicals, was a challenge. Several methods were investigated and success was obtained through the use of laccase-catalyzed Michael-type addition of catechols with the primary amines.
- Another challenge encountered was the determination of reaction progress during the functionalization of chitosan. This was addressed through the implementation and development of suitable optical analysis methods, based on FT-IR and UV-Vis spectroscopy. UV-Vis spectroscopy was used for solubility measurements and the detection of the chitosan binding capacity to detect the functionalization of chitosan with catechols.
- The establishment of adhesion of the PCA-chitosan was difficult due to solubility issues, changes in the viscosity and the reaction pH during chitosan functionalization. Through careful adjustment of the reaction pH during the curing process, strong tensile strength was established while avoiding damage to the catechol group.
- Through use of laccases from *C. unicolor*, direct conversion of OS lignin from the OS supernatant is, despite high ethanol concentrations, theoretically possible. However, the resulting reaction pH after OS digestion is often below the capable range of laccase from *C. unicolor* and needed to be addressed. Therefore, the extraction method of OS lignin was tuned in order to obtain a pH value, which allows for direct conversion using laccases from *C. unicolor*.
- A one-step functionalization, as was demonstrated for chitosan, was not achieved for lignin, due to the lack of binding sites. Therefore, to attain functionalization, a two-step process was implemented, including an amination reaction before functionalization with the catechol.
- To avoid the use of harsh chemicals, condensation reactions and anionic addition were investigated for the amination of lignin. Due to the complex structure of lignin and its low solubility, optical analysis of the reaction progress was challenging. Therefore, several alternatives were investigated. The amount of primary amines on precipitated aminated lignin was measured using a Ninhydrin assay. The remaining L-lysine content in the supernatant, after successful functionalization, was measured for the indirect determination of the functionalization degree. Lastly, a GPC method was extended by an OPA precolumn derivatization for the quantification of the lignin's amination degree.
- Obtaining adhesion using DHC-lignin was challenging due to solubility issues. The tensile strength was slightly improved through the investigation of different solvents, as well as the addition of iron(III) ions and acids during the curing process.

- During the development of the DSC-based quantification of biodegradability, several challenges were encountered. For quantification, a method to correlate the remaining mass of polymer after biodegradation to the measured DSC peak areas was needed. This was achieved using sand, which functions as an inert standard, coated with the polymer to be investigated.
- A further challenge encountered during DSC-based quantification was the specification of the DSC-interval used for analysis. A computer-based method was developed for improving measurement accuracy.

6.3 Future work

Building upon this work, the following topics are interesting future project ideas. These ideas have been described further in the relevant chapters and have been summarized here. Please refer to the discussion chapter of the corresponding topic for further details.

Both adhesives, PCA-chitosan and DHC-lignin, would benefit from increases to their wet adhesion strength. The water-based nature of chitosan and PCA resulted in a lack of long-term water resistance. The water resistance may be addressed through laccase treatment. Furthermore, through optimization of the substrate concentrations to minimize side product and quinone formation, caused by the laccase treatment, the laccases could also be used to accelerate the reaction rate.

To develop a commercial product from DHC-lignin, both, the reaction costs and the adhesion characteristics need further development. In order to reduce the number of required processing steps and thus reducing process cost for production of a lignin adhesive, a laccase from *C. unicolor*, which withstands 50 %wt ethanol was identified and the production of OS supernatant was optimized for conversion using this laccase. The implementation of a production process, however, has not yet been implemented and is suggested for further investigation.

Lastly, while the DSC-based analysis of biodegradability has been demonstrated, degradation studies have not been performed for the PCA-chitosan and DHC-lignin adhesives. Both of these studies are suggested for future investigations.

7 Bibliography

[1] WAGEMANN, K.: *Roadmap Bioraffinerien*, 2012

[2] *Bioadhesives Market by Type (Plant Based, Animal Based)*. URL https://www.marketsandmarkets.com/Market-Reports/bioadhesive-market-16386893.html. - retrieved 2020-09-28. — Market research report

[3] KAMM, B. ; KAMM, M.: Principles of biorefineries. In: *Applied Microbiology and Biotechnology* vol. 64 (2004), Nr. 2, pp. 137–145

[4] ROBERTS, G.A.F.: *Chitin Chemistry*. London : Macmillan Education UK, 1992 — ISBN 978-1-349-11547-1

[5] TIPPKÖTTER, N.: *Lokale Vorbehandlung nachwachsender Rohstoffe für Bioraffinerien (BioSats)*. Kaiserslautern, 2018

[6] MAIER, G.P. ; RAPP, M. V. ; WAITE, J.H. ; ISRAELACHVILI, J.N. ; BUTLER, A.: Adaptive synergy between catechol and lysine promotes wet adhesion by surface salt displacement. In: *Biological adhesives* (2015), p. 628

[7] WILKER, J.J.: Biomaterials: Redox and adhesion on the rocks. In: *Nature Chemical Biology* vol. 7, Nature Publishing Group (2011), Nr. 9, pp. 579–580

[8] EBNESAJJAD, S.: *Handbook of Adhesives and Surface Preparation*. 1st. ed. : Elsevier, 2011 — ISBN 9781437744613

[9] JANIAK, C.: Chemie —einfach alles. VonP. W. Atkins undJ. A. Beran. VCH Verlagsgesellschaft, Weinheim, 1996, 993 S., geb. 98.00 DM.—ISBN 3–527–29259–4. In: *Angewandte Chemie* vol. 109 (1997), Nr. 12, pp. 1413–1414

[10] MÜLLER, H.: Prinzipien der Chemie. Von R. E. Dickerson, H. B. Gray und G. P. Haight Jr. Aus dem Englischen übersetzt und bearbeitet von H.-W. Sichting. Walter de Gruyter &amp; Co., Berlin, New York 1978. XXVII, 965 S., zahlr. Abb., Tab., geb. DM 78,-. In: *Chemie in unserer Zeit* vol. 13 (1979), Nr. 6, pp. 197–197

[11] EMSLEY, J.: Very strong hydrogen bonding. In: *Chemical Society Reviews* vol. 9 (1980), Nr. 1, p. 91

[12] TSCHUMPER, G.S.: Reliable Electronic Structure Computations for Weak Noncovalent Interactions in Clusters. In: , 2009, pp. 39–90

[13] WAITE, J.H.: Adhesion a la moule. In: *Biochemistry* vol. 1180 (2002), Nr. June, pp. 1172–1180

[14] FLORIOLLI, R.Y. ; VON LANGEN, J. ; WAITE, J.H.: Marine surfaces and the expression of specific byssal adhesive protein variants in Mytilus. In: *Marine*

Biotechnology vol. 2 (2000), Nr. 4, pp. 352–363 — ISBN 1436-2228

[15] WAITE, J.H. ; TANZER, M.L.: Polyphenolic Substance of Mytilus edulis: Novel Adhesive Containing L-Dopa and Hydroxyproline. In: *Science* vol. 212 (1981), Nr. 4498, pp. 1038–1040

[16] LEE, B.P. ; MESSERSMITH, P.B. ; ISRAELACHVILI, J.N. ; WAITE, J.H.: Mussel-Inspired Adhesives and Coatings. In: *Annual Review of Materials Research* vol. 41 (2011), Nr. 1, pp. 99–132

[17] WAITE, J.H. ; QIN, X.: Polyphosphoprotein from the adhesive pads of Mytilus edulis. In: *Biochemistry* vol. 40 (2001), Nr. 9, pp. 2887–2893 — ISBN 0006-2960

[18] LI, Y. ; LIANG, C. ; GAO, L. ; LI, S. ; ZHANG, Y. ; ZHANG, J. ; CAO, Y.: Hidden complexity of synergistic roles of Dopa and lysine for strong wet adhesion. In: *Materials Chemistry Frontiers* vol. 1, Royal Society of Chemistry (2017), Nr. 12, pp. 2664–2668

[19] WAITE, J.H.: Mussel adhesion – essential footwork. In: *The Journal of Experimental Biology* vol. 220 (2017), Nr. 4, pp. 517–530

[20] NORTH, M.A. ; DEL GROSSO, C.A. ; WILKER, J.J.: High Strength Underwater Bonding with Polymer Mimics of Mussel Adhesive Proteins. In: *ACS Applied Materials & Interfaces* vol. 9 (2017), Nr. 8, pp. 7866–7872

[21] WAITE, J.H. ; HOUSLEY, T.J. ; TANZER, M.L.: Peptide repeats in a mussel glue protein: theme and variations. In: *Biochemistry* vol. 24 (1985), Nr. 19, pp. 5010–5014

[22] YU, M. ; HWANG, J. ; DEMING, T.J.: Role of <scp>l</scp> -3,4-Dihydroxyphenylalanine in Mussel Adhesive Proteins. In: *Journal of the American Chemical Society* vol. 121 (1999), Nr. 24, pp. 5825–5826

[23] LIU, B. ; BURDINE, L. ; KODADEK, T.: Chemistry of Periodate-Mediated Cross-Linking of 3,4-Dihydroxylphenylalanine-Containing Molecules to Proteins. In: *Journal of the American Chemical Society* vol. 128 (2006), Nr. 47, pp. 15228–15235

[24] LIN, Q. ; GOURDON, D. ; SUN, C. ; HOLTEN-ANDERSEN, N. ; ANDERSON, T.H. ; WAITE, J.H. ; ISRAELACHVILI, J.N.: Adhesion mechanisms of the mussel foot proteins mfp-1 and mfp-3. In: *Proceedings of the National Academy of Sciences* vol. 104 (2007), Nr. 10, pp. 3782–3786

[25] PESHKOVA, S. ; LI, K.: Investigation of chitosan-phenolics systems as wood adhesives. In: *Journal of Biotechnology* vol. 102 (2003), Nr. 2, pp. 199–207

— ISBN 0168-1656

[26] WILKER, J.J.: Redox and adhesion on the rocks. In: *Nature Chemical Biology* vol. 7 (2011), Nr. 9, pp. 579–580

[27] MILLER, D.R. ; SPAHN, J.E. ; WAITE, J.H. ; WAITE, J.H.: The staying power of adhesion-associated antioxidant activity in Mytilus californianus (2015), Nr. pH 8

[28] MIRSHAFIAN, R. ; WEI, W. ; ISRAELACHVILI, J.N. ; WAITE, J.H.: α,β-Dehydro-Dopa: A Hidden Participant in Mussel Adhesion. In: *Biochemistry* vol. 55 (2016), Nr. 5, pp. 743–750

[29] FULLENKAMP, D.E. ; BARRETT, D.G. ; MILLER, D.R. ; KURUTZ, J.W. ; MESSERSMITH, P.B.: PH-dependent cross-linking of catechols through oxidation via Fe 3+ and potential implications for mussel adhesion. In: *RSC Advances* vol. 4 (2014), Nr. 48, pp. 25127–25134

[30] WEI, W. ; YU, J. ; GEBBIE, M.A. ; TAN, Y. ; MARTINEZ RODRIGUEZ, N.R. ; ISRAELACHVILI, J.N. ; WAITE, J.H.: Bridging adhesion of mussel-inspired peptides: Role of charge, chain length, and surface type. In: *Langmuir* vol. 31 (2015), Nr. 3, pp. 1105–1112

[31] SEO, S. ; DAS, S. ; ZALICKI, P.J. ; MIRSHAFIAN, R. ; EISENBACH, C.D. ; ISRAELACHVILI, J.N. ; WAITE, J.H. ; AHN, B.K.: Microphase Behavior and Enhanced Wet-Cohesion of Synthetic Copolyampholytes Inspired by a Mussel Foot Protein. In: *Journal of the American Chemical Society* vol. 137 (2015), Nr. 29, pp. 9214–9217

[32] WEI, W. ; PETRONE, L. ; TAN, Y. ; CAI, H. ; ISRAELACHVILI, J.N. ; MISEREZ, A. ; WAITE, J.H.: An Underwater Surface-Drying Peptide Inspired by a Mussel Adhesive Protein. In: *Advanced Functional Materials* vol. 26 (2016), Nr. 20, pp. 3496–3507

[33] KARLSSON, S. ; ALBERTSSON, A.: Biodegradable polymers and environmental interaction. In: *Polymer Engineering & Science* vol. 38 (1998), Nr. 8, pp. 1251–1253

[34] AZLAN, M. ; DAVID, N..: Biodegradable material options for industrial and goods packaging. In: *2011 IEEE Colloquium on Humanities, Science and Engineering* : IEEE, 2011 — ISBN 978-1-4673-0020-9, pp. 23–27

[35] HABENICHT, G.: *Kleben*, *VDI-Buch*. 5. ed. Berlin/Heidelberg : Springer-Verlag, 2006 — ISBN 3-540-26273-3

[36] MATHIAS, J.-D. ; GRÉDIAC, M. ; MICHAUD, P.: Bio-based adhesives. In: *Biopolymers and Biotech Admixtures for Eco-Efficient Construction Materials* : Elsevier, 2016, pp. 369–385

[37] PARK, S.Y. ; PARK, H.J. ; LIN, X.Q. ; SANO, Y.: Characterization of chitosan film and structure in solution. In: *Hydrocolloids* : Elsevier, 2000, pp. 199–204

[38] UMEMURA, K. ; INOUE, A. ; KAWAI, S.: Development of new natural polymer-based wood adhesives I: dry bond strength and water resistance of konjac glucomannan, chitosan, and their composites. In: *Journal of Wood Science* vol. 49 (2003), Nr. 3, pp. 221–226

[39] UMEMURA, K. ; MIHARA, A. ; KAWAI, S.: Development of new natural polymer-based wood adhesives III: effects of glucose addition on properties of chitosan. In: *Journal of Wood Science* vol. 56 (2010), Nr. 5, pp. 387–394

[40] PATEL, A.K. ; MICHAUD, P. ; PETIT, E. ; DE BAYNAST, H. ; GRÉDIAC, M. ; MATHIAS, J.-D.: Development of a chitosan-based adhesive. Application to wood bonding. In: *Journal of Applied Polymer Science* vol. 127 (2013), Nr. 6, pp. 5014–5021

[41] PATEL, A.K. ; MICHAUD, P. ; DE BAYNAST, H. ; GRÉDIAC, M. ; MATHIAS, J.-D.: Preparation of chitosan-based adhesives and assessment of their mechanical properties. In: *Journal of Applied Polymer Science* vol. 127 (2013), Nr. 5, pp. 3869–3876

[42] VARGAS VILLANUEVA, J.G. ; SARMIENTO HUERTAS, P.A. ; GALAN, F.S. ; ESTEBAN RUEDA, R.J. ; BRICEÑO TRIANA, J.C. ; CASAS RODRIGUEZ, J.P.: Bio-adhesion evaluation of a chitosan-based bone bio-adhesive. In: *International Journal of Adhesion and Adhesives* vol. 92 (2019), pp. 80–88

[43] LIN, S. Y. ; DENCE, C. W. (eds.): *Methods in Lignin Chemistry*, *Springer Series in Wood Science*. Berlin, Heidelberg : Springer Berlin Heidelberg, 1992 — ISBN 978-3-642-74067-1

[44] MAITY, S.K.: Opportunities, recent trends and challenges of integrated biorefinery: Part I. In: *Renewable and Sustainable Energy Reviews* vol. 43 (2015), pp. 1427–1445

[45] KHAN, M.A. ; ASHRAF, S.M. ; MALHOTRA, V.P.: Development and characterization of a wood adhesive using bagasse lignin. In: *International Journal of Adhesion and Adhesives* vol. 24 (2004), Nr. 6, pp. 485–493

[46] HOONG, Y.B. ; PARIDAH, M.T. ; LOH, Y.F. ; JALALUDDIN, H. ; CHUAH, L.A.: A new source of natural adhesive: Acacia mangium bark extracts co-polymerized with phenol-formaldehyde (PF) for bonding Mempisang (Annonaceae spp.) veneers. In: *International Journal of Adhesion and Adhesives* vol. 31 (2011), Nr. 3, pp. 164–167

[47] NASIR, M.I.M. ; ZAKARIA, N. ; SIPAUT, C.S. ; SULAIMAN, O. ; HASHIM, R.: Chemical and thermal properties of lignins from oil palm biomass as a substitute for phenol in a phenol formaldehyde resin production. In: *Carbohydrate Polymers* vol. 86 (2011), Nr. 1, pp. 112–119

[48] ZHANG, W. ; MA, Y. ; XU, Y. ; WANG, C. ; CHU, F.: Lignocellulosic ethanol residue-based lignin–phenol–formaldehyde resin adhesive. In: *International Journal of Adhesion and Adhesives* vol. 40 (2013), pp. 11–18

[49] OKAMOTO, T. ; TAKEDA, H. ; FUNABIKI, T. ; TAKATANI, M. ; HAMADA, R.: Fundamental studies on the development of lignin-based adhesives, I. Catalytic demethylation of anisole with molecular oxygen. In: *Reaction Kinetics & Catalysis Letters* vol. 58 (1996), Nr. 2, pp. 237–242

[50] LI, K. ; GENG, X.: Formaldehyde-Free Wood Adhesives from Decayed Wood. In: *Macromolecular Rapid Communications* vol. 26 (2005), Nr. 7, pp. 529–532

[51] LIU, Y. ; LI, K.: Preparation and Characterization of Demethylated Lignin-Polyethylenimine Adhesives. In: *The Journal of Adhesion* vol. 82 (2006), Nr. 6, pp. 593–605

[52] IBRAHIM, V. ; MAMO, G. ; GUSTAFSSON, P.J. ; HATTI-KAUL, R.: Production and properties of adhesives formulated from laccase modified Kraft lignin. In: *Industrial Crops and Products* vol. 45, Elsevier B.V. (2013), pp. 343–348

[53] JIA, M. ; LI, A. ; MU, Y. ; JIANG, W. ; WAN, X.: Synthesis and adhesive property study of polyoxetanes grafted with catechols via Cu(I)-catalyzed click chemistry. In: *Polymer (United Kingdom)* vol. 55, Elsevier Ltd (2014), Nr. 5, pp. 1160–1166

[54] LI, A. ; JIA, M. ; MU, Y. ; JIANG, W. ; WAN, X.: Humid bonding with a water-soluble adhesive inspired by mussels and sandcastle worms. In: *Macromolecular Chemistry and Physics* vol. 216 (2015), Nr. 4, pp. 450–459

[55] KANG, T. ; BANQUY, X. ; HEO, J. ; LIM, C. ; LYND, N.A. ; LUNDBERG, P. ; OH, D.X. ; LEE, H. ; ET AL.: Mussel-Inspired Anchoring of Polymer Loops That Provide Superior Surface Lubrication and Antifouling Properties. In: *ACS Nano* vol. 10 (2016), Nr. 1, pp. 930–937

[56] MU, Y. ; WU, X. ; PEI, D. ; WU, Z. ; ZHANG, C. ; ZHOU, D. ; WAN, X.: Contribution of the Polarity of Mussel-Inspired Adhesives in the Realization of Strong Underwater Bonding. In: *ACS Biomaterials Science and Engineering* vol. 3 (2017), Nr. 12, pp. 3133–3140

[57] WU, Z. ; LI, L. ; MU, Y. ; WAN, X.: Synthesis and Adhesive Property Study of a

Mussel-Inspired Adhesive Based on Poly(vinyl alcohol) Backbone. In: *Macromolecular Chemistry and Physics* vol. 218 (2017), Nr. 16, pp. 1–9

[58] JENKINS, C.L. ; SIEBERT, H.M. ; WILKER, J.J.: Integrating Mussel Chemistry into a Bio-Based Polymer to Create Degradable Adhesives. In: *Macromolecules* vol. 50 (2017), Nr. 2, pp. 561–568

[59] XU, Y. ; LIU, Q. ; NARAYANAN, A. ; JAIN, D. ; DHINOJWALA, A. ; JOY, A.: Mussel-Inspired Polyesters with Aliphatic Pendant Groups Demonstrate the Importance of Hydrophobicity in Underwater Adhesion. In: *Advanced Materials Interfaces* vol. 4 (2017), Nr. 22, p. 1700506

[60] NARKAR, A.R. ; KELLEY, J.D. ; PINNARATIP, R. ; LEE, B.P.: Effect of Ionic Functional Groups on the Oxidation State and Interfacial Binding Property of Catechol-Based Adhesive. In: *Biomacromolecules* vol. 19 (2018), Nr. 5, pp. 1416–1424

[61] TANG, Z. ; ZHAO, M. ; WANG, Y. ; ZHANG, W. ; ZHANG, M. ; XIAO, H. ; HUANG, L. ; CHEN, L. ; ET AL.: Mussel-inspired cellulose-based adhesive with biocompatibility and strong mechanical strength via metal coordination. In: *International Journal of Biological Macromolecules* vol. 144 (2020), pp. 127–134

[62] XU, J. ; STRANDMAN, S. ; ZHU, J.X.X. ; BARRALET, J. ; CERRUTI, M.: Genipin-crosslinked catechol-chitosan mucoadhesive hydrogels for buccal drug delivery. In: *Biomaterials* vol. 37, Elsevier Ltd (2015), pp. 395–404 — ISBN 1878-5905 (Electronic)r0142-9612 (Linking)

[63] ZENG, Z. ; WANG, H. ; MORSI, Y. ; MO, X.: Synthesis and characterization of incorporating mussel mimetic moieties into photoactive hydrogel adhesive. In: *Colloids and Surfaces B: Biointerfaces* vol. 161, Elsevier B.V. (2018), pp. 94–102

[64] LEE, D. ; PARK, J.P. ; KOH, M.Y. ; KIM, P. ; LEE, J. ; SHIN, M. ; LEE, H.: Chitosan-catechol: A writable bioink under serum culture media. In: *Biomaterials Science* vol. 6, Royal Society of Chemistry (2018), Nr. 5, pp. 1040–1047 — ISBN 2047-4849 (Electronic)2047-4830 (Linking)

[65] NARKAR, A.R. ; CANNON, E. ; YILDIRIM-ALICEA, H. ; AHN, K.: Catechol-Functionalized Chitosan: Optimized Preparation Method and Its Interaction with Mucin. In: *Langmuir* vol. 35 (2019), Nr. 48, pp. 16013–16023

[66] GAN, D. ; XING, W. ; JIANG, L. ; FANG, J. ; ZHAO, C. ; REN, F. ; FANG, L. ; WANG, K. ; ET AL.: Plant-inspired adhesive and tough hydrogel based on Ag-Lignin nanoparticles-triggered dynamic redox catechol chemistry. In: *Nature*

Communications vol. 10 (2019), Nr. 1, p. 1487

[67] CAPITAIN, C. ; WAGNER, S. ; HUMMEL, J. ; TIPPKÖTTER, N.: Investigation of C–N Formation Between Catechols and Chitosan for the Formation of a Strong, Novel Adhesive Mimicking Mussel Adhesion. In: *Waste and Biomass Valorization* (2020)

[68] STARKE, E.A. ; STALEY, J.T.: Application of modern aluminum alloys to aircraft. In: *Progress in Aerospace Sciences* vol. 32 (1996), Nr. 2–3, pp. 131–172

[69] ZHAO, H. ; SUN, C. ; STEWART, R.J. ; WAITE, J.H.: Cement proteins of the tube-building polychaete Phragmatopoma californica. In: *Journal of Biological Chemistry* vol. 280 (2005), Nr. 52, pp. 42938–42944 — ISBN 8058932817

[70] MISEREZ, A. ; SCHNEBERK, T. ; SUN, C. ; ZOK, F.W. ; HERBERT, J.: NIH Public Access vol. 319 (2009), Nr. 5871, pp. 1816–1819

[71] ROTH, S. ; SPIESS, A.C.: Laccases for biorefinery applications: a critical review on challenges and perspectives. In: *Bioprocess and Biosystems Engineering* vol. 38, Springer Berlin Heidelberg (2015), Nr. 12, pp. 2285–2313

[72] AKTAŞ, N. ; ŞAHINER, N. ; KANTOĞLU, Ö. ; SALIH, B. ; TANYOLAÇ, A.: Biosynthesis and Characterization of Laccase Catalyzed Poly(Catechol). In: *Journal of Polymers and the Environment* vol. 11 (2003), Nr. 3, pp. 123–128 — ISBN 1566-2543

[73] LAHTINEN, M. ; KRUUS, K. ; HEINONEN, P. ; SIPIL, J.: On the reactions of two fungal laceases differing in their redox potential with lignin model compounds: products and their rate of formation. In: *Journal of Agricultural and Food Chemistry* vol. 57 (2009), Nr. 18, pp. 8357–8365 — ISBN 3589191503

[74] ROTH, S. ; SPIESS, A.C.: Laccases for biorefinery applications: a critical review on challenges and perspectives. In: *Bioprocess and Biosystems Engineering* vol. 38, Springer Berlin Heidelberg (2015), Nr. 12, pp. 2285–2313 — ISBN 1615-7605

[75] MIKOLASCH, A. ; HAHN, V. ; MANDA, K. ; PUMP, J. ; ILLAS, N. ; G??RDES, D. ; LALK, M. ; GESELL SALAZAR, M. ; ET AL.: Laccase-catalyzed cross-linking of amino acids and peptides with dihydroxylated aromatic compounds. In: *Amino Acids* vol. 39 (2010), Nr. 3, pp. 671–683 — ISBN 1438-2199 (Electronic) 0939-4451 (Linking)

[76] GARCIA-CARMONA, F. ; GARCIA-CÁNOVAS, F. ; IBORRA, J.L. ; LOZANO, J.A.: Kinetic study of the pathway of melanizationn between l-dopa and dopachrome. In: *BBA - General Subjects* vol. 717 (1982), Nr. 1, pp. 124–131

[77] IKEDA, M. ; KATSUMATA, R. ; TIJSSELING, L. ; HOEFNAGEL, M.H.N. ; HUGENHOLTZ, J.: Metabolic Engineering To Produce Tyrosine or Phenylalanine in a Tryptophan-Producing Corynebacterium glutamicum Strain. In: *Applied and environmental microbiology* vol. 58 (1992), Nr. 3, pp. 781–5

[78] BROMBERG-MARTIN, E.S. ; MATSUMOTO, M. ; HIKOSAKA, O.: Dopamine in Motivational Control: Rewarding, Aversive, and Alerting. In: *Neuron* vol. 68 (2010), Nr. 5, pp. 815–834

[79] WAITE, J.H. ; TANZER, M.L.: The bioadhesive of Mytilus byssus: a protein containing L-dopa. In: *Biochemical and biophysical research communications* vol. 96 (1980), Nr. 4, pp. 1554–61

[80] LERNER, A.B. ; FITZPATRICK, T.B.: BIOCHEMISTRY OF MELANIN FORMATION. In: *Physiological Reviews* vol. 30 (1950), Nr. 1, pp. 91–126

[81] KAYANO, S.I. ; KIKUZAKI, H. ; FUKUTSUKA, N. ; MITANI, T. ; NAKATANI, N.: Antioxidant activity of prune (Prunus domestica L.) constituents and a new synergist. In: *Journal of Agricultural and Food Chemistry* vol. 50 (2002), Nr. 13, pp. 3708–3712 — ISBN 0021-8561

[82] MAITI, B. ; THOMAS, P. ; NAIR, P.M.: High-Performance Liquid Chromatography Determination of Phenolic Acids in Potato Tubers (Solanum tuberosum) during Wound Healing (1992), pp. 569–572

[83] MASELLA, R. ; CANTAFORA, A. ; MODESTI, D. ; CARDILLI, A. ; GENNARO, L. ; BOCCA, A. ; CONI, E.: Antioxidant activity of 3,4-DHPEA-EA and protocatecuic acid: a comparative assessment with other olive oil biophenols. In: *Redox Report* vol. 4 (1999), Nr. 3, pp. 113–121

[84] MASELLA, R. ; VARI, R. ; ARCHIVIO, M.D. ; BENEDETTO, R. DI ; MATARRESE, P. ; MALORNI, W. ; SCAZZOCCHIO, B. ; GIOVANNINI, C. ; ET AL.: Nutrient-Gene Interactions Extra Virgin Olive Oil Biophenols Inhibit Cell-Mediated Oxidation of LDL by Increasing the mRNA Transcription of Glutathione-Related Enzymes 1 (2004), Nr. October 2003, pp. 785–791

[85] KAKKAR, S. ; BAIS, S.: A Review on Protocatechuic Acid and Its Pharmacological Potential. In: *ISRN Pharmacology* vol. 2014 (2014), pp. 1–9 — ISBN 0141-0229

[86] VITAGLIONE, P. ; DONNARUMMA, G. ; NAPOLITANO, A. ; GALVANO, F. ; GALLO, A. ; SCALFI, L. ; FOGLIANO, V.: Protocatechuic Acid Is the Major Human Metabolite of Cyanidin-Glucosides. In: *The Journal of Nutrition* vol. 137 (2007), Nr. 9, pp. 2043–2048 — ISBN 0022-3166 (Print)r0022-3166 (Linking)

[87] HOLDEN, M.: Processing of raw cocoa. III.—Enzymic aspects of cocoa fermentation. In: *Journal of the Science of Food and Agriculture* vol. 10 (1959), Nr. 12, pp. 691–700

[88] CHANDRA, S. ; DE MEJIA, E.G.: Polyphenolic compounds, antioxidant capacity, and quinone reductase activity of an aqueous extract of Ardisia compressa in comparison to mate (Ilex paraguariensis) and green (Camellia sinensis) teas. In: *Journal of Agricultural and Food Chemistry* vol. 52 (2004), Nr. 11, pp. 3583–3589 — ISBN 0021-8561 (Print)

[89] CHAO, C.-Y. ; YIN, M.-C.: Antibacterial Effects of Roselle Calyx Extracts and Protocatechuic Acid in Ground Beef and Apple Juice. In: *Foodborne Pathogens and Disease* vol. 6 (2009), Nr. 2, pp. 201–206 — ISBN 1535-3141

[90] XICAN, L. ; WANG, X. ; CHEN, D. ; CHEN, S.: Antioxidant Activity and Mechanism of Protocatechuic Acid in vitro. In: *Functional Foods in Health and Disease* vol. 1 (2011), Nr. 7, pp. 232–244

[91] TANAKA, T. ; TANAKA, T. ; TANAKA, M.: Potential Cancer Chemopreventive Activity of Protocatechuic Acid. In: *Journal of Experimental & Clinical Medicine* vol. 3, Elsevier Taiwan LLC (2011), Nr. 1, pp. 27–33

[92] LENDE, A.B. ; KSHIRSAGAR, A.D. ; DESHPANDE, A.D. ; MULEY, M.M. ; PATIL, R.R. ; BAFNA, P.A. ; NAIK, S.R.: Anti-inflammatory and analgesic activity of protocatechuic acid in rats and mice. In: *Inflammopharmacology* vol. 19 (2011), Nr. 5, pp. 255–263

[93] PACHECO-PALENCIA, L. A ; MERTENS-TALCOTT, S. ; TALCOTT, S.T.: Chemical composition, antioxidant properties, and thermal stability of a phytochemical enriched oil from Acai (Euterpe oleracea Mart.). In: *Journal of agricultural and food chemistry* vol. 56 (2008), pp. 4631–4636 — ISBN 0021-8561

[94] DANNENFELSER, R.M. ; YALKOWSKY, S.H.: Data base of aqueous solubility for organic non-electrolytes. In: *Science of the Total Environment, The* vol. 109–110 (1991), Nr. C, pp. 625–628

[95] SERJEANT, E. ; DEMPSEY, B.: *Ionisation constants of organic acids in aqueous solution*, *IUPAC chemical data series* : Pergamon Press, 1979

[96] DAWSON, R.M.C. ; DAWSON, R. M. C. (ed.): *Data for Biochemical Research*, *Data for Biochemical Research* : Clarendon Press, 1989 — ISBN 9780198552994

[97] FUGMANN, B. ; ADAM, G. ; ANKE, H. ; BOLAND, W. ; FRANCKE, W.: *Römpp Lexikon Naturstoffe*. 1st editio. Stuttgart : Thieme, 2014 — ISBN 9783131792914

[98] KANG, S.-Y.Y. ; CHOI, O. ; LEE, J.K. ; HWANG, B.Y. ; UHM, T.-B.B. ; HONG, Y.-S.S.: Artificial biosynthesis of phenylpropanoic acids in a tyrosine overproducing Escherichia coli strain. In: *Microbial Cell Factories* vol. 11 (2012), Nr. 1, p. 153 — ISBN 1475-2859

[99] SRINIVASAN, P.R. ; SHIGEURA, H.T. ; SPRECHER, M. ; SPRINGSON, D.B. ; DAVIS, B.D.: The biosynthesis of shikimic acid from D-glucose. In: *The Journal of biological chemistry* vol. 220 (1956), Nr. 1, pp. 477–97

[100] HERRMANN, K.M. ; WEAVER, L.M.: THE SHIKIMATE PATHWAY. In: *Annual Review of Plant Physiology and Plant Molecular Biology* vol. 50 (1999), Nr. 1, pp. 473–503

[101] LOUIE, G. V. ; BOWMAN, M.E. ; MOFFITT, M.C.C. ; BAIGA, T.J. ; MOORE, B.S.S. ; NOEL, J.P.: Structural Determinants and Modulation of Substrate Specificity in Phenylalanine-Tyrosine Ammonia-Lyases. In: *Chemistry and Biology* vol. 13 (2006), Nr. 12, pp. 1327–1338 — ISBN 1074-5521 (Print)r1074-5521 (Linking)

[102] PEPPERCORN, M.A. ; GOLDMAN, P.: Caffeic acid metabolism by bacteria of the human gastrointestinal tract. In: *Journal of Bacteriology* vol. 108 (1971), Nr. 3, pp. 996–1000

[103] MOON, J. ; TERAO, J.: Antioxidant Activity of Caffeic Acid and Dihydrocaffeic Acid in Lard and Human Low-Density Lipoprotein †. In: *Journal of agricultural and food chemistry* vol. 46 (1998), pp. 5062–5065

[104] THURSTON, C.F.: The structure and function of fungal laccases. In: *Microbiology* vol. 140 (1994), Nr. 1, pp. 19–26

[105] KURNIAWATI, S. ; NICELL, J.A.: Characterization of Trametes versicolor laccase for the transformation of aqueous phenol. In: *Bioresource Technology* vol. 99 (2008), Nr. 16, pp. 7825–7834 — ISBN 0960-8524 (Print)r0960-8524 (Linking)

[106] KUHAD, R.C. ; SINGH, A. ; ERIKSSON, K.-E.L.: Microorganisms and enzymes involved in the degradation of plant fiber cell walls. In: *Advances in biochemical engineering/biotechnology*. vol. 57, 1997, pp. 45–125

[107] LEONOWICZ, A. ; MATUSZEWSKA, A. ; LUTEREK, J. ; ZIEGENHAGEN, D. ; WOJTAŚ-WASILEWSKA, M. ; CHO, N.S. ; HOFRICHTER, M. ; ROGALSKI, J.: Biodegradation of lignin by white rot fungi. In: *Fungal Genetics and Biology* vol. 27 (1999), Nr. 2–3, pp. 175–185

[108] HATAKKA, A.: Biodegradation of Lignin. In: STEINBÜCHEL, A. ; HOFRICHTER, M. (eds.): *Biopolymers Online*. Weinheim, Germany : Wiley-VCH Verlag GmbH &

Co. KGaA, 2005

[109] MAYER, A.M. ; STAPLES, R.C.: Laccase: New functions for an old enzyme. In: *Phytochemistry* vol. 60 (2002), Nr. 6, pp. 551–565

[110] LI, K. ; XU, F. ; ERIKSSON, K.E.L.: Comparison of fungal laccases and redox mediators in oxidation of a nonphenolic lignin model compound. In: *Applied and Environmental Microbiology* vol. 65 (1999), Nr. 6, pp. 2654–2660

[111] KRAMER, K.J. ; KANOST, M.R. ; HOPKINS, T.L. ; JIANG, H. ; ZHU, Y.C. ; XU, R. ; KERWIN, J.. ; TURECEK, F.: Oxidative conjugation of catechols with proteins in insect skeletal systems. In: *Tetrahedron* vol. 57 (2001), Nr. 2, pp. 385–392

[112] RIDE, J.P.: The effect of induced lignification on the resistance of wheat cell walls to fungal degradation. In: *Physiological Plant Pathology* vol. 16 (1980), Nr. 2, pp. 187–196

[113] HARKIN, J.M. ; LARSEN, M.J. ; OBST, J.R.: Use of syringaldazine for detection of laccase in sporophores of wood rotting fungi. In: *Mycologia* vol. 66 (1974), Nr. 3, pp. 469–476

[114] RITTSTIEG, K. ; SUURNAKKI, A. ; SUORTTI, T. ; KRUUS, K. ; GUEBITZ, G. ; BUCHERT, J.: Investigations on the laccase-catalyzed polymerization of lignin model compounds using size-exclusion HPLC. In: *Enzyme and Microbial Technology* vol. 31 (2002), Nr. 4, pp. 403–410 — ISBN 4331641015

[115] MAIER, G.P. ; BERNT, C.M. ; BUTLER, A.: Catechol oxidation: Considerations in the design of wet adhesive materials. In: *Biomaterials Science* vol. 6, Royal Society of Chemistry (2018), Nr. 2, pp. 332–339

[116] LCD, N.L. ; LIGHT, B.: *Cayman-Chemicals; Product Information*. URL https://www.caymanchem.com/pdfs/14916.pdf

[117] LEBO, S.E. ; GARGULAK, J.D. ; MCNALLY, T.J.: Lignin. In: *Kirk-Othmer Encyclopedia of Chemical Technology*. Hoboken, NJ, USA : John Wiley & Sons, Inc., 2001, pp. 1–32

[118] ZAKZESKI, J. ; BRUIJNINCX, P.C.A. ; JONGERIUS, A.L. ; WECKHUYSEN, B.M.: The catalytic valorization of lignin for the production of renewable chemicals. In: *Chemical Reviews* vol. 110 (2010), Nr. 6, pp. 3552–3599

[119] PERLACK, R.D. ; WRIGHT, L.L. ; TURHOLLOW, A.F. ; GRAHAM, R.L.: Biomass as Feedstock for Bioenergy (2005), pp. 1–78

[120] MICHELS, J.: "Lignocellulose-Bioraffinerie" Aufschluss lignocellulosehaltiger Rohstoffe und vollständige stoffliche Nutzung der Komponenten (Phase 2)

(2014), Nr. Phase 2, pp. 1–397

[121] CYBULSKA, I. ; BRUDECKI, G. ; ROSENTRATER, K. ; JULSON, J.L. ; LEI, H.: Comparative study of organosolv lignin extracted from prairie cordgrass, switchgrass and corn stover. In: *Bioresource Technology* vol. 118 (2012), pp. 30–36

[122] WENG, J.-K. ; CHAPPLE, C.: The origin and evolution of lignin biosynthesis. In: *New Phytologist* vol. 187 (2010), Nr. 2, pp. 273–285

[123] HAJDOK, S.: *Laccase-katalysierte Dominoreaktionen von Brenzcatechinen und Hydrochinonen mit 1 , 3- Dicarbonylverbindungen*. Stuttgart, Hohenheim, 2012

[124] CIECHOLEWSKI, S. ; HAMMER, E. ; MANDA, K. ; BOSE, G. ; NGUYEN, V.T.H. ; LANGER, P. ; SCHAUER, F.: Laccase-catalyzed carbon–carbon bond formation: oxidative dimerization of salicylic esters by air in aqueous solution. In: *Tetrahedron* vol. 61 (2005), Nr. 19, pp. 4615–4619

[125] JONAS, U. ; HAMMER, E. ; SCHAUER, F. ; BOLLAG, J.-M.: Transformation of 2-hydroxydibenzofuran by laccases of the white rot fungi Trametes versicolor and Pycnoporus cinnabarinus and characterization of oligomerization products. In: *Biodegradation* vol. 8 (1997), Nr. 5, pp. 321–327

[126] ANYANWUTAKU, I.O. ; PETROSKI, R.J. ; ROSAZZA, J.P.N.: Oxidative coupling of mithramycin and hydroquinone catalyzed by copper oxidases and benzoquinone. Implications for the mechanism of action of aureolic acid antibiotics. In: *Bioorganic & Medicinal Chemistry* vol. 2 (1994), Nr. 6, pp. 543–551

[127] BOLLAG, J.-M. ; LIU, S.-Y.: Copolymerization of halogenated phenols and syringic acid. In: *Pesticide Biochemistry and Physiology* vol. 23 (1985), Nr. 2, pp. 261–272

[128] NIEDERMEYER, T.H.J. ; MIKOLASCH, A. ; LALK, M.: Nuclear Amination Catalyzed by Fungal Laccases: Reaction Products of p -Hydroquinones and Primary Aromatic Amines. In: *The Journal of Organic Chemistry* vol. 70 (2005), Nr. 6, pp. 2002–2008

[129] WELLINGTON, K.W. ; BOKAKO, R. ; RASEROKA, N. ; STEENKAMP, P.: A one-pot synthesis of 1,4-naphthoquinone-2,3-bis-sulfides catalysed by a commercial laccase. In: *Green Chemistry* vol. 14 (2012), Nr. 9, p. 2567

[130] HAHN, V. ; MIKOLASCH, A. ; KUHLISCH, C. ; SCHAUER, F.: Laccase-mediated multi-step homo- and heteromolecular reactions of ortho -dihydroxylated aromatic

compounds and mono- or diaminated substances resulting in C C, C O and C N bonds. In: *Journal of Molecular Catalysis B: Enzymatic* vol. 122 (2015), pp. 56–63

[131] MATHER, B.D. ; VISWANATHAN, K. ; MILLER, K.M. ; LONG, T.E.: Michael addition reactions in macromolecular design for emerging technologies. In: *Progress in Polymer Science* vol. 31 (2006), Nr. 5, pp. 487–531

[132] SOGIAS, I.A. ; KHUTORYANSKIY, V. V. ; WILLIAMS, A.C.: Exploring the factors affecting the solubility of chitosan in water. In: *Macromolecular Chemistry and Physics* vol. 211 (2010), Nr. 4, pp. 426–433 — ISBN 1022-1352

[133] MASON, H.S. ; PETERSON, E.W.: Melanoproteins I. reactions between enzyme-generated quinones and amino acids. In: *Biochimica et Biophysica Acta (BBA) - General Subjects* vol. 111 (1965), Nr. 1, pp. 134–146

[134] QIU, W.Z. ; WU, G.P. ; XU, Z.K.: Robust Coatings via Catechol-Amine Codeposition: Mechanism, Kinetics, and Application. In: *ACS Applied Materials and Interfaces* vol. 10 (2018), Nr. 6, pp. 5902–5908

[135] MERRITT, M.E. ; CHRISTENSEN, A.M. ; KRAMER, K.J. ; HOPKINS, T.L. ; SCHAEFER, J.: Detection of intercatechol cross-links in insect cuticle by solid-state carbon-13 and nitrogen-15 NMR. In: *Journal of the American Chemical Society* vol. 118 (1996), Nr. 45, pp. 11278–11282 — ISBN 0002-7863

[136] SCHAEFER, J. ; KRAMER, K.J. ; GARBOW, J.R. ; JACOB, G.S. ; STEJSKAL, E.O. ; HOPKINS, T.L. ; SPEIRS, R.D.: Aromatic cross-links in insect cuticle: detection by solid-state 13C and 15N NMR. In: *Science (New York, N.Y.)* vol. 235 (1987), Nr. 4793, pp. 1200–4

[137] XU, R. ; HUANG, X. ; HOPKINS, T.L. ; KRAMER, K.J.: Catecholamine and histidyl protein cross-linked structures in sclerotized insect cuticle. In: *Insect Biochemistry and Molecular Biology* vol. 27 (1997), Nr. 2, pp. 101–108 — ISBN 0965-1748

[138] MICHNIEWICZ, A. ; ULLRICH, R. ; LEDAKOWICZ, S. ; HOFRICHTER, M.: The white-rot fungus Cerrena unicolor strain 137 produces two laccase isoforms with different physico-chemical and catalytic properties. In: *Applied Microbiology and Biotechnology* vol. 69 (2006), Nr. 6, pp. 682–688 — ISBN 0025300500159

[139] KIRK, T.K. ; SCHULTZ, E. ; CONNORS, W.J. ; LORENZ, L.F. ; ZEIKUS, J.G.: Influence of culture parameters on lignin metabolism byPhanerochaete chrysosporium. In: *Archives of Microbiology* vol. 117 (1978), Nr. 3, pp. 277–285

[140] SONDHI, S. ; SHARMA, P. ; SAINI, S. ; PURI, N. ; GUPTA, N.: Purification and Characterization of an Extracellular, Thermo-Alkali-Stable, Metal Tolerant Laccase from Bacillus tequilensis SN4. In: DUHALT, R. V. (ed.) *PLoS ONE* vol. 9 (2014), Nr. 5, p. e96951

[141] HERTER, S. ; SCHMIDT, M. ; THOMPSON, M.L. ; MIKOLASCH, A. ; SCHAUER, F.: Study of enzymatic properties of phenol oxidase from nitrogen-fixing azotobacter chroococcum. In: *AMB Express* vol. 1 (2011), Nr. 1, p. 14

[142] BUSSLER, W.: Romeis, B.: Mikroskopische Technik. 16., neubearbeitete u. verbesserte Auflage. R. Oldenbourg Verlag, München 1968. XVI, 757 Seiten, 21 Abbildungen, 16 Tabellen, 2 Anhänge. Gr.-8°, Leinen DM 98,—. In: *Zeitschrift für Pflanzenernährung und Bodenkunde* vol. 121 (1968), Nr. 1, pp. 78–79

[143] MCILVAINE, T.C.: A buffer solution for colorimetric comparison. In: *J. Biol. Chem.* vol. 49 (1921), Nr. 1, pp. 183–186

[144] PATEL, H. ; GUPTE, S. ; GAHLOUT, M. ; GUPTE, A.: Purification and characterization of an extracellular laccase from solid-state culture of Pleurotus ostreatus HP-1. In: *3 Biotech* vol. 4 (2014), Nr. 1, pp. 77–84

[145] KIM, H.-J. ; LIM, D.-H. ; HWANG, H.-D. ; LEE, B.-H.: Composition of Adhesives. In: *Handbook of Adhesion Technology*. Berlin, Heidelberg : Springer Berlin Heidelberg, 2011, pp. 291–314

[146] TAPANI, E. ; TAAVITSAINEN, M. ; LINDROS, K. ; VEHMAS, T. ; LEHTONEN, E.: Toxicity of Ethanol in Low Concentrations. In: *Acta Radiologica* vol. 37 (1996), Nr. 6, pp. 923–926

[147] HUANG, W. ; TAI, R. ; HSEU, R. ; HUANG, C.: Overexpression and characterization of a thermostable , pH-stable and organic solvent-tolerant Ganoderma fornicatum laccase in Pichia pastoris. In: *Process Biochemistry* vol. 46, Elsevier Ltd (2011), Nr. 7, pp. 1469–1474

[148] KOSCHORRECK, K. ; RICHTER, S.M. ; SWIERCZEK, A. ; BEIFUSS, U. ; SCHMID, R.D. ; URLACHER, V.B.: Comparative characterization of four laccases from Trametes versicolor concerning phenolic C – C coupling and oxidation of PAHs vol. 474 (2008), pp. 213–219

[149] CHEN, S. ; WU, P. ; SU, Y. ; WEN, T. ; WEI, Y. ; WANG, N. ; HSU, C. ; WANG, A.H. ; ET AL.: Biochemical characterization of a novel laccase from the basidiomycete fungus Cerrena sp . WR1 † vol. 25 (2012), Nr. 11, pp. 761–769

[150] BRYJAK, J. ; REKUĆ, A.: Effective purification of cerrena unicolor laccase using

microfiltration, ultrafiltration and acetone precipitation. In: *Applied Biochemistry and Biotechnology* vol. 160 (2010), Nr. 8, pp. 2219–2235 — ISBN 1559-0291 (Electronic) 0273-2289 (Linking)

[151] AL-ADHAMI, A.J.H. ; BRYJAK, J. ; GREB-MARKIEWICZ, B. ; PECZYŃSKA-CZOCH, W.: Immobilization of wood-rotting fungi laccases on modified cellulose and acrylic carriers. In: *Process Biochemistry* vol. 37 (2002), Nr. 12, pp. 1387–1394

[152] DE JONG, E. ; DE VRIES, F.P. ; FIELD, J.A. ; VAN DER ZWAN, R.P. ; DE BONT, J.A.M.: Isolation and screening of basidiomycetes with high peroxidative activity. In: *Mycological Research* vol. 96 (1992), Nr. 12, pp. 1098–1104

[153] TAVARES, A.P.M. ; COELHO, M.A.Z. ; AGAPITO, M.S.M. ; COUTINHO, J.A.P. ; XAVIER, A.M.R.B.: Optimization and Modeling of Laccase Production by Trametes versicolor in a Bioreactor Using Statistical Experimental Design. In: *Applied Biochemistry and Biotechnology* vol. 134 (2006), Nr. 3, pp. 233–248

[154] LI, Q. ; PEI, J. ; ZHAO, L. ; XIE, J. ; CAO, F. ; WANG, G.: Overexpression and characterization of laccase from Trametes versicolor in Pichia pastoris. In: *Applied Biochemistry and Microbiology* vol. 50 (2014), Nr. 2, pp. 140–147

[155] R. SIVAKUMAR ; R. RAJENDRAN ; C. BALAKUMAR ; TAMILVENDAN, M.: Isolation, Screening and Optimization of Production Medium for Thermostable Laccase Production from Ganoderma sp. In: *International Journal of Engineering Science and Technology* vol. 2 (2010)

[156] TEERAPATSAKUL, C. ; PARRA, R. ; BUCKE, C. ; CHITRADON, L.: Improvement of laccase production from Ganoderma sp. KU-Alk4 by medium engineering. In: *World Journal of Microbiology and Biotechnology* vol. 23 (2007), Nr. 11, pp. 1519–1527

[157] PATRICK, F. ; MTUI, G. ; MSHANDETE, A. ; KIVAISI, A.: Optimization of laccase and manganese peroxidase production in submerged culture of Pleurotus sajorcaju. In: *African Journal of Biotechnology* vol. 10 (2011), Nr. 50

[158] COONEY, C.L. ; HUETER, J.: Enzyme catalysis in the presence of nonaqueous solvents using chloroperoxidase. In: *Biotechnology and Bioengineering* vol. 16 (1974), Nr. 8, pp. 1045–1053

[159] TOTEVA, M.M. ; RICHARD, J.P.: The generation and reactions of quinone methides. In: , 2011, pp. 39–91

[160] BLOIS, S.: Observation of the Semiquinone of Benzoquinone. In: *The Journal of Chemical Physics* vol. 23 (1955), Nr. 7, pp. 1351–1351

[161] DEHNICKE, K.: Hollemann-Wiberg, Lehrbuch der Anorganischen Chemie. 101. Auflage. VonNils Wiberg. Walter de Gruyter, Berlin/New York, 1995. 2033 S., geb. 158.00 DM. ISBN 3–11–012641–9. In: *Angewandte Chemie* vol. 108 (1996), Nr. 21, pp. 2696–2696

[162] CAMPBELL, J.A.: Le Châtelier's principle, temperature effects, and entropy. In: *Journal of Chemical Education* vol. 62 (1985), Nr. 3, p. 231

[163] RENNERT, J. ; MAYER, M. ; LEVY, J. ; KAPLAN, J.: STABILIZATION OF SEMIQUINONE INTERMEDIATES IN THE PHOTOREDUCTION OF PHENANTHRENEQUINONE BY COMPLEX FORMATION. In: *Photochemistry and Photobiology* vol. 10 (1969), Nr. 4, pp. 267–271

[164] ELIEH-ALI-KOMI, D. ; HAMBLIN, M.R.: Chitin and Chitosan: Production and Application of Versatile Biomedical Nanomaterials. In: *International journal of advanced research* vol. 4. Cham, Springer International Publishing (2016), Nr. 3, pp. 411–427 — ISBN 0000000000000

[165] JOSHI, M. ; PURWAR, R. ; WAZED ALI, S. ; RAJENDRAN, S.: Antimicrobial Textiles for Health and Hygiene Applications Based on Eco-Friendly Natural Products. In: *Medical and Healthcare Textiles* : Elsevier, 2010, pp. 84–92

[166] KAFETZOPOULOS, D. ; MARTINOU, A. ; BOURIOTIS, V.: Bioconversion of chitin to chitosan: purification and characterization of chitin deacetylase from Mucor rouxii. In: *Proceedings of the National Academy of Sciences* vol. 90 (1993), Nr. 7, pp. 2564–2568 — ISBN 0027-8424 (Print)r0027-8424 (Linking)

[167] AIBA, S. ICHI: Preparation of N-acetylchitooligosaccharides by hydrolysis of chitosan with chitinase followed by N-acetylation. In: *Carbohydrate Research* vol. 265 (1994), Nr. 2, pp. 323–328 — ISBN 0008-6215 (Print)0008-6215 (Linking)

[168] PARK, B.K. ; KIM, M.M.: Applications of chitin and its derivatives in biological medicine. In: *International Journal of Molecular Sciences* vol. 11 (2010), Nr. 12, pp. 5152–5164 — ISBN 1422-0067 (Electronic) 1422-0067 (Linking)

[169] SHAHIDI, F. ; ARACHCHI, J.K.V. ; JEON, Y.J.: Food applications of chitin and chitosans. In: *Trends in Food Science and Technology* vol. 10 (1999), Nr. 2, pp. 37–51 — ISBN 0924-2244

[170] KRAJEWSKA, B.: Application of chitin- and chitosan-based materials for enzyme immobilizations: A review. In: *Enzyme and Microbial Technology* vol. 35 (2004), Nr. 2–3, pp. 126–139 — ISBN 0141-0229

[171] SONGKROAH, C. ; NAKBANPOTE, W. ; THIRAVETYAN, P.: Recovery of silver-thiosulphate complexes with chitin. In: *Process Biochemistry* vol. 39 (2004), Nr. 11, pp. 1553–1559

[172] HIRANO, S. ; NAKAHIRA, T. ; NAKAGAWA, M. ; KIM, S.K.: The preparation and applications of functional fibres from crab shell chitin. In: *Progress in Industrial Microbiology* vol. 35 (1999), Nr. C, pp. 373–377 — ISBN 0168-1656

[173] HIRANO, S.: Wet-spinning and applications of functional fibers based on chitin and chitosan. In: *Macromolecular Symposia* vol. 168 (2001), Nr. 1, pp. 21–30

[174] RINAUDO, M. ; PAVLOV, G. ; DESBRIE, J. ; DESBRIÈRES, J.: Influence of acetic acid concentration on the solubilization of chitosan. In: *Polymer* vol. 40 (1999), pp. 7029–7032 — ISBN 0032-3861

[175] KATCHALSKY, A. ; SPITNIK, P.: Potentiometric titrations of polymethacrylic acid. In: *Journal of Polymer Science* vol. 2 (1947), Nr. 4, pp. 432–446

[176] MUZZARELLI, R.A.A.: *Chitin Chemistry*, 1977 — ISBN 9780333524176

[177] NOGUCHI, J. ; ARATO, K. ; KOMAI, T.: Chitosan-Epichlorohydrin Anion Exchange Resin with Primary Amine as Absroption Site. In: *The Journal of the Society of Chemical Industry, Japan* vol. 72 (1969), Nr. 3, pp. 796–799

[178] MUZZARELLI, R.A.A. ; TANFANI, F. ; SCARPINI, G.: Chelating, film-forming, and coagulating ability of the chitosan–glucan complex from Aspergillus niger industrial wastes. In: *Biotechnology and Bioengineering* vol. 22 (1980), Nr. 4, pp. 885–896

[179] TAMURA, Z. ; MIYAZAKI, M. ; SUZUKI, T.: METAL COMPLEXES OF D-GLUCOSAMINE AND ITS DERIVATIVES. 3. DETERMINATIONS OF ACID DISSOCIATION CONSTANTS OF D-GLUCOSAMINE AND ITS THREE O-METHYL DERIVATIVES. In: *Chemical & pharmaceutical bulletin* vol. 13 (1965), pp. 330–2

[180] DOMARD, A.: Determination of N-acetyl content in chitosan samples by c.d. measurements. In: *International Journal of Biological Macromolecules* vol. 9 (1987), Nr. 6, pp. 333–336 — ISBN 0887-6266

[181] RYU, J.H. ; HONG, S. ; LEE, H.: Bio-inspired adhesive catechol-conjugated chitosan for biomedical applications: A mini review. In: *Acta Biomaterialia* vol. 27 (2015), pp. 101–115

[182] RYU, J.H. ; JO, S. ; KOH, M.-Y. ; LEE, H.: Bio-Inspired, Water-Soluble to Insoluble Self-Conversion for Flexible, Biocompatible, Transparent, Catecholamine

Polysaccharide Thin Films. In: *Advanced Functional Materials* vol. 24 (2014), Nr. 48, pp. 7709–7716

[183] NI, K. ; ZHOU, X. ; ZHAO, L. ; WANG, H. ; REN, Y. ; WEI, D.: Magnetic Catechol-Chitosan with Bioinspired Adhesive Surface: Preparation and Immobilization of ω-Transaminase. In: NEVES, N. M. (ed.) *PLoS ONE* vol. 7 (2012), Nr. 7, p. e41101

[184] OSHITA, K. ; TAKAYANAGI, T. ; OSHIMA, M. ; MOTOMIZU, S.: Adsorption Properties of Ionic Species on Cross-linked Chitosans Modified with Catechol and Salicylic Acid Moieties. In: *Analytical Sciences* vol. 24 (2008), Nr. 5, pp. 665–668

[185] OH, D.X. ; HWANG, D.S.: A biomimetic chitosan composite with improved mechanical properties in wet conditions. In: *Biotechnology Progress* vol. 29 (2013), Nr. 2, pp. 505–512

[186] PRAJATELISTIA, E. ; LIM, C. ; OH, D.X. ; JUN, S.H. ; HWANG, D.S.: Chitosan and hydroxyapatite composite cross-linked by dopamine has improved anisotropic hydroxyapatite growth and wet mechanical properties. In: *Engineering in Life Sciences* vol. 15 (2015), Nr. 2, pp. 254–261

[187] XU, J. ; SOLIMAN, G.M. ; BARRALET, J. ; CERRUTI, M.: Mollusk Glue Inspired Mucoadhesives for Biomedical Applications. In: *Langmuir* vol. 28 (2012), Nr. 39, pp. 14010–14017

[188] KIM, K. ; RYU, J.H. ; LEE, D.Y. ; LEE, H.: Bio-inspired catechol conjugation converts water-insoluble chitosan into a highly water-soluble, adhesive chitosan derivative for hydrogels and LbL assembly. In: *Biomaterials Science* vol. 1 (2013), Nr. 7, p. 783

[189] ZVAREC, O. ; PURUSHOTHAM, S. ; MASIC, A. ; RAMANUJAN, R. V. ; MISEREZ, A.: Catechol-Functionalized Chitosan/Iron Oxide Nanoparticle Composite Inspired by Mussel Thread Coating and Squid Beak Interfacial Chemistry. In: *Langmuir* vol. 29 (2013), Nr. 34, pp. 10899–10906

[190] YAVVARI, P.S. ; SRIVASTAVA, A.: Robust, self-healing hydrogels synthesised from catechol rich polymers. In: *Journal of Materials Chemistry B* vol. 3 (2015), Nr. 5, pp. 899–910

[191] BEN-YOAV, H. ; WINKLER, T.E. ; KIM, E. ; KELLY, D.L. ; PAYNE, G.F. ; GHODSSI, R.: Catechol-modified Chitosan System as a Bio-amplifier for Schizophrenia Treatment Analysis. In: *MRS Proceedings* vol. 1572 (2013), pp. mrss13-1572-ss05-03

[192] WINKLER, T.E. ; BEN-YOAV, H. ; CHOCRON, S.E. ; KIM, E. ; KELLY, D.L. ; PAYNE, G.F. ; GHODSSI, R.: Electrochemical Study of the Catechol-Modified Chitosan System for Clozapine Treatment Monitoring. In: *Langmuir* vol. 30 (2014), Nr. 48, pp. 14686–14693

[193] CHEN, T. ; VAZQUEZ-DUHALT, R. ; WU, C.-F. ; BENTLEY, W.E. ; PAYNE, G.F.: Combinatorial Screening for Enzyme-Mediated Coupling. Tyrosinase-Catalyzed Coupling To Create Protein−Chitosan Conjugates. In: *Biomacromolecules* vol. 2 (2001), Nr. 2, pp. 456–462

[194] YAMADA, K. ; CHEN, T. ; KUMAR, G. ; VESNOVSKY, O. ; TOPOLESKI, L.D.T. ; PAYNE, G.F.: Chitosan Based Water-Resistant Adhesive. Analogy to Mussel Glue. In: *Biomacromolecules* vol. 1 (2000), Nr. 2, pp. 252–258

[195] LIU, Y. ; ZHANG, B. ; JAVVAJI, V. ; KIM, E. ; LEE, M.E. ; RAGHAVAN, S.R. ; WANG, Q. ; PAYNE, G.F.: Tyrosinase-mediated grafting and crosslinking of natural phenols confers functional properties to chitosan. In: *Biochemical Engineering Journal* vol. 89 (2014), pp. 21–27

[196] YANG, J. ; COHEN STUART, M.A. ; KAMPERMAN, M.: Jack of all trades: versatile catechol crosslinking mechanisms. In: *Chem. Soc. Rev.* vol. 43 (2014), Nr. 24, pp. 8271–8298

[197] LINDE, D.R. ; WEAST, R. C. (ed.): *CRC HANDBOOK OF CHEMISTRY AND PHYSICS*. 81. ed. : CRC Press, Inc. Boca Raton, 1980 — ISBN 978-0849304811

[198] XU, R. ; SCARLETT, B. (ed.): *Particle Characterization: Light Scattering Methods*, *Particle Technology Series*. vol. 13. 1. ed. Dordrecht : Springer Netherlands, 2002 — ISBN 0-7923-6300-0

[199] SCHWEDT, G. ; SCHMIDT, T.C. ; SCHMITZ, O.J.: *Analytische Chemie*. 3. ed. Weinheim : Wiley-VCH, 2016 — ISBN 978-3-527-34082-8

[200] BELLAMY, L.J.: *The Infra-red Spectra of Complex Molecules*. Dordrecht : Springer Netherlands, 1975 — ISBN 978-94-011-6019-3

[201] LEE, B.P. ; DALSIN, J.L. ; MESSERSMITH, P.B.: Synthesis and Gelation of DOPA-Modified Poly(ethylene glycol) Hydrogels. In: *Biomacromolecules* vol. 3 (2002), Nr. 5, pp. 1038–1047

[202] WILLIAMS, R.: Six-tenths factor aids in approximating costs. In: *Chemical Engineering* vol. December (1947), Nr. 54, pp. 124–125

[203] CHILTON, C.H.: Six-tenths factor applies to complete plant costs. In: *Chemical*

Engineering vol. April (1950), Nr. 57, pp. 112–114

[204] TSAGKARI, M. ; COUTURIER, J.-L. ; KOKOSSIS, A. ; DUBOIS, J.-L.: Early-Stage Capital Cost Estimation of Biorefinery Processes: A Comparative Study of Heuristic Techniques. In: *ChemSusChem* vol. 9 (2016), Nr. 17, pp. 2284–2297

[205] RICO, A. ; RENCORET, J. ; DEL RÍO, J.C. ; MARTÍNEZ, A.T. ; GUTIÉRREZ, A.: Pretreatment with laccase and a phenolic mediator degrades lignin and enhances saccharification of Eucalyptus feedstock. In: *Biotechnology for Biofuels* vol. 7 (2014), Nr. 1, p. 6

[206] WAGENFÜHR, A.; SCHOLZ, F.: *Taschenbuch der Holztechnik*. 1. ed. : Carl Hanser Verlag GmbH&Co. KG, 2008 — ISBN 9783446228528

[207] BOERJAN, W. ; RALPH, J. ; BAUCHER, M.: LIGNIN BIOSYNTHESIS. In: *Annual Review of Plant Biology* vol. 54 (2003), Nr. 1, pp. 519–546

[208] HANSEN, B. ; KUSCH, P. ; SCHULZE, M. ; KAMM, B.: Qualitative and Quantitative Analysis of Lignin Produced from Beech Wood by Different Conditions of the Organosolv Process. In: *Journal of Polymers and the Environment* vol. 24 (2016), Nr. 2, pp. 85–97

[209] MANDERS, W.F.: Solid-State 13 C NMR Determination of the Syringyl/Guaiacyl Ratio in Hardwoods. In: *Holzforschung* vol. 41 (1987), Nr. 1, pp. 13–18

[210] WULFHORST, H. ; DUWE, A.-M. ; MERSEBURG, J. ; TIPPKÖTTER, N.: Compositional analysis of pretreated (beech) wood using differential scanning calorimetry and multivariate data analysis. In: *Tetrahedron* vol. 72 (2016), Nr. 46, pp. 7329–7334

[211] BUGG, T.D.H. ; AHMAD, M. ; HARDIMAN, E.M. ; RAHMANPOUR, R.: Pathways for degradation of lignin in bacteria and fungi. In: *Natural Product Reports* vol. 28 (2011), Nr. 12, pp. 1883–1896 — ISBN 0265-0568

[212] FAKIROV, S.: Condensation Polymers: Their Chemical Peculiarities Offer Great Opportunities. In: *Progress in Polymer Science* vol. 89 (2019), pp. 1–18

[213] LAURICHESSE, S. ; AVÉROUS, L.: Chemical modification of lignins: Towards biobased polymers. In: *Progress in Polymer Science* vol. 39, Elsevier Ltd (2014), Nr. 7, pp. 1266–1290

[214] GONÇALVES, A.R. ; BENAR, P.: Hydroxymethylation and oxidation of Organosolv lignins and utilization of the products. In: *Bioresource Technology* vol. 79 (2001), Nr. 2, pp. 103–111

[215] RAZAK, M.A. ; VISWANATH, B.: Optimization of fermentation upstream parameters and immobilization of Corynebacterium glutamicum MH 20-22 B cells to enhance

the production of l-lysine. In: *3 Biotech* vol. 5 (2015), Nr. 4, pp. 531–540

[216] LIU, J. ; LIU, H.F. ; DENG, L. ; LIAO, B. ; GUO, Q.X.: Improving aging resistance and mechanical properties of waterborne polyurethanes modified by lignin amines. In: *Journal of Applied Polymer Science* vol. 130 (2013), Nr. 3, pp. 1736–1742

[217] LEE, K.S. ; DRESCHER, D.G.: Fluorometric amino-acid analysis with o-phthaldialdehyde (OPA). In: *International Journal of Biochemistry* vol. 9 (1978), Nr. 7, pp. 457–467

[218] SLUITER, A. ; HAMES, B. ; RUIZ, R. ; SCARLATA, C. ; SLUITER, J. ; TEMPLETON, D. ; CROCKER, D.: Determination of structural carbohydrates and lignin in Biomass-Laboratory Analytical Procedure (LAP). In: *National Renewable Energy Laboratory (NREL), Technical Report NREL/TP-510-42618* (2012), Nr. August, p. 17 — ISBN NREL/TP-510-42618

[219] JUNGHANNS, C. ; PECYNA, M.J. ; BÖHM, D. ; JEHMLICH, N. ; MARTIN, C. ; VON BERGEN, M. ; SCHAUER, F. ; HOFRICHTER, M. ; ET AL.: Biochemical and molecular genetic characterisation of a novel laccase produced by the aquatic ascomycete Phoma sp. UHH 5-1-03. In: *Applied Microbiology and Biotechnology* vol. 84 (2009), Nr. 6, pp. 1095–1105

[220] YUE, X. ; CHEN, F. ; ZHOU, X.: Improved interfacial bonding of pvc/wood-flour composites by lignin amine modification. In: *BioResources* vol. 6 (2011), pp. 2022–2034

[221] REICHARDT, C.: *Solvents and Solvent Effects in Organic Chemistry*. 3. ed. Weinheim : Wiley-VCH, 2003 — ISBN 978-3-527-60567-5

[222] ELSINGHORST, P.W.: *Farbreaktionen und Nachweise für DC Analyse*. URL http://pwe.no-ip.org/pharma/chemie/docs/farbrkt.pdf

[223] HOLTEN-ANDERSEN, N. ; HARRINGTON, M.J. ; BIRKEDAL, H. ; LEE, B.P. ; MESSERSMITH, P.B. ; LEE, K.Y.C. ; WAITE, J.H.: pH-induced metal-ligand cross-links inspired by mussel yield self-healing polymer networks with near-covalent elastic moduli. In: *Proceedings of the National Academy of Sciences* vol. 108 (2011), Nr. 7, pp. 2651–2655

[224] BIRENDRA B. ADHIKARI, M.C. AND D.C.B.*: Utilization of Slaughterhouse Waste in Value-Added Applications: Recent Advances in the Development of Wood Adhesives. In: *Polymers* vol. 10 (2018), Nr. 2, p. 176

[225] LIMAO, N.: Infrastructure, Geographical Disadvantage, Transport Costs, and Trade. In: *The World Bank Economic Review* vol. 15 (2001), Nr. 3, pp. 451–479

[226] BAUHAU: *Wood glue*. URL www.bauhaus.info. - retrieved 2020-07-01

[227] CONRAD: *Special adhesives*. URL www.conrad.de. - retrieved 2020-07-01

[228] KUMAR, A. ; HOLUSZKO, M. ; ESPINOSA, D.C.R.: E-waste: An overview on generation, collection, legislation and recycling practices. In: *Resources, Conservation and Recycling* vol. 122 (2017), pp. 32–42

[229] MARKOWICZ, F. ; KRÓL, G. ; SZYMAŃSKA-PULIKOWSKA, A.: Biodegradable Package – Innovative Purpose or Source of the Problem. In: *Journal of Ecological Engineering* vol. 20 (2019), Nr. 1, pp. 228–237

[230] SAFFIAN, H.A. ; ABDAN, K. ; HASSAN, M.A. ; IBRAHIM, N.A. ; JAWAID, M.: Characterisation and Biodegradation of Poly(Lactic Acid) Blended with Oil Palm Biomass and Fertiliser for Bioplastic Fertiliser Composites. In: *BioResources* vol. 11, Nr. 1

[231] MOHEE, R. ; UNMAR, G.: Determining biodegradability of plastic materials under controlled and natural composting environments. In: *Waste management (New York, N.Y.)* vol. 27 (2007), Nr. 11, pp. 1486–1493

[232] ZHANG, Z. ; ORTIZ, O. ; GOYAL, R. ; KOHN, J.: Biodegradable Polymers. In: *Principles of Tissue Engineering* : Elsevier, 2014 — ISBN 9780123983589, pp. 441-473 TS-CrossRef

[233] SEIDEL, W.W. ; THODEN, B. ; HAHN, F.: *Werkstofftechnik*. 7., aktual. München : Hanser, 2007 — ISBN 978-3-446-40789-3

[234] GÖPFERICH, A.: Mechanisms of polymer degradation and erosion. In: *Biomaterials* vol. 17, Nr. 2, pp. 103–114

[235] SHAH, A.A. ; HASAN, F. ; HAMEED, A. ; AHMED, S.: Biological degradation of plastics: A comprehensive review. In: *Biotechnology Advances* vol. 26 (2008), Nr. 3, pp. 246–265

[236] 148551, D.I.N.E.N.I.S.O.: Bestimmung der vollständigen aeroben Bioabbaubarkeit von Kunststoff-Materialien unter den Bedingungen kontrollierter Kompostierung –Verfahren mittels Analyse des freigesetzten Kohlenstoffdioxides. Berlin, DIN Deutsches Institut für Normung e. V. — ISBN DIN EN ISO: 14855-1:2012

[237] VIKMAN, M. ; KARJOMAA, S. ; KAPANEN, A. ; WALLENIUS, K. ; ITÄVAARA, M.: The influence of lignin content and temperature on the biodegradation of lignocellulose in composting conditions. In: *Applied Microbiology and Biotechnology* vol. 59 (2002), Nr. 4–5, pp. 591–598 — ISBN 0025300210

[238] ZINN, M. ; WITHOLT, B. ; EGLI, T.: Occurrence, synthesis and medical application of bacterial polyhydroxyalkanoate. In: *Advanced Drug Delivery Reviews* vol. 53, Nr. 1, pp. 5–21

[239] BANERJEE, A. ; CHATTERJEE, K. ; MADRAS, G.: Enzymatic degradation of polymers. In: *Materials Science and Technology* vol. 30, Nr. 5, pp. 567–573

[240] ZAHRA, S. ; ABBAS, S.S. ; MAHSA, M. ; MOHSEN, N.: Biodegradation of low-density polyethylene (LDPE) by isolated fungi in solid waste medium. In: *Waste Management* vol. 30, Elsevier Ltd (2010), Nr. 3, pp. 396–401

[241] CROMPTON, T.R.: *Polymer reference book*. Shawbury : Rapra Technology Limited, 2006 — ISBN 1-85957-526-9

[242] AZEVEDO, H. ; REIS, R.: Understanding the Enzymatic Degradation of Biodegradable Polymers and Strategies to Control Their Degradation Rate. In: REIS, R. ; SAN ROMÁN, J. (eds.): *Biodegradable Systems in Tissue Engineering and Regenerative Medicine* : CRC Press TS - CrossRef, 2004 — ISBN 978-0-8493-1936-5

[243] MAROIS, Y. ; ZHANG, Z. ; VERT, M. ; DENG, X. ; LENZ, R. ; GUIDOIN, R.: Mechanism and rate of degradation of polyhydroxyoctanoate films in aqueous media: A long-termin vitro study. In: *Journal of Biomedical Materials Research* vol. 49 (2000), Nr. 2, pp. 216–224

[244] KAILAS, L. ; NYSTEN, B. ; AUDINOT, J.-N. ; MIGEON, H.-N. ; BERTRAND, P.: Multitechnique characterization of thin films of immiscible polymer systems. In: *Surface and Interface Analysis* vol. 37 (2005), Nr. 5, pp. 435–443

[245] MUKHERJEE, S. ; GOWEN, A.: A review of recent trends in polymer characterization using non-destructive vibrational spectroscopic modalities and chemical imaging. In: *Analytica chimica acta* vol. 895. School of Biosystems Engineering, University College Dublin, Belfield, Dublin 4, Co. Dublin, Ireland. Electronic address: sindhuraj.mukherjee@ucdconnect.ie. School of Biosystems Engineering, University College Dublin, Belfield, Dublin 4, Co. Dublin, Irel (2015), pp. 12–34

[246] KEESSLER, W.: *Multivariate Datenanalyse in der Bio- und Prozessanalytik*. Weinheim : Wiley-VCH, 2005 — ISBN 978-3-527-31262-7

[247] IOVINO, R. ; ZULLO, R. ; RAO, M.A. ; CASSAR, L. ; GIANFREDA, L.: Biodegradation of poly(lactic acid)/starch/coir biocomposites under controlled composting conditions. In: *Polymer Degradation and Stability* vol. 93, Nr. 1, pp. 147–157

[248] KANE, S.R. ; ASHBY, P.D. ; PRUITT, L.A.: ATR-FTIR as a thickness measurement technique for hydrated polymer-on-polymer coatings. In: *Journal of biomedical materials research. Part B, Applied biomaterials* vol. 91 (2009), Nr. 2, pp. 613–620

[249] NAKAYAMA, A. ; YAMANO, N. ; KAWASAKI, N.: Biodegradation in seawater of aliphatic polyesters. In: *Polymer Degradation and Stability* vol. 166 (2019), pp. 290–299

[250] TANEM, B.S. ; KAMFJORD, T. ; AUGESTAD, M. ; LØVGREN, T.B. ; LUNDQUIST, M.: Sample preparation and AFM analysis of heterophase polypropylene systems. In: *Polymer* vol. 44 (2003), Nr. 15, pp. 4283–4291

[251] ECHLIN, P.: *Handbook of sample preparation for scanning electron microscopy and x-ray microanalysis*. New York : Springer TS - The British Library M4 - Citavi, 2009 — ISBN 978-0-387-85730-5

[252] SALPAVAARA, T. ; HÄNNINEN, A. ; ANTNIEMI, A. ; LEKKALA, J. ; KELLOMÄKI, M.: Non-destructive and wireless monitoring of biodegradable polymers. In: *Sensors and Actuators B: Chemical* vol. 251, pp. 1018–1025

[253] TOIVOLA, R. ; HOWIE, T. ; YANG, J. ; LAI, P.-N. ; SHI, Z. ; JANG, S.-H. ; JEN, A.K.-Y. ; FLINN, B.D.: Highly sensitive thermal damage sensors for polymer composites. In: *Smart Materials and Structures* vol. 26 (2017), Nr. 8, p. 85039

[254] FRICK, A. ; STERN, C.: *DSC-Prüfung in der Anwendung*. 2., aktual. München : Hanser, 2013 — ISBN 978-3-446-43692-3

[255] LV, S. ; LIU, X. ; GU, J. ; JIANG, Y. ; TAN, H. ; ZHANG, Y.: Microstructure analysis of polylactic acid-based composites during degradation in soil. In: *International Biodeterioration & Biodegradation* vol. 122 (2017), pp. 53–60

[256] RICHERT, A. ; OLEWNIK-KRUSZKOWSKA, E. ; ADAMSKA, E. ; TARACH, I.: Enzymatic degradation of bacteriostatic polylactide composites. In: *International Biodeterioration & Biodegradation* vol. 142 (2019), pp. 103–108

[257] STEPCZYŃSKA, M. ; RYTLEWSKI, P.: Enzymatic degradation of flax-fibers reinforced polylactide. In: *International Biodeterioration & Biodegradation* vol. 126 (2018), pp. 160–166

[258] POUTON, C.W. ; AKHTAR, S.: Biosynthetic polyhydroxyalkanoates and their potential in drug delivery. In: *Advanced Drug Delivery Reviews* vol. 18, Nr. 2, pp. 133–162

[259] WENG, Y.-X. ; WANG, Y. ; WANG, X.-L. ; WANG, Y.-Z.: Biodegradation behavior of

PHBV films in a pilot-scale composting condition. In: *Polymer Testing* vol. 29 (2010), Nr. 5, pp. 579–587

[260] MERADI, H. ; ATOUI, L. ; BAHLOUL, L. ; BOUBENDIRA, K. ; BOUAZDIA, A. ; ISMAIL, F.: Characterization by Thermal Analysis of Natural Kieselguhr and Sand for Industrial Application. In: *Energy Procedia* vol. 74, pp. 1282–1288

[261] 32645, D.I.N.: Chemical analysis –Decision limit, detection limit and determination limit under repeatability conditions –Terms, methods, evaluation. Berlin, DIN Deutsches Institut für Normung e. V. — ISBN DIN 32645

[262] SHEN, D.K. ; GU, S. ; LUO, K.H. ; BRIDGWATER, A.V. ; FANG, M.X.: Kinetic study on thermal decomposition of woods in oxidative environment. In: *Fuel* vol. 88 (2009), Nr. 6, pp. 1024–1030

[263] NAIR, L.S. ; LAURENCIN, C.T.: Biodegradable polymers as biomaterials. In: *Progress in Polymer Science (Oxford)* vol. 32 (2007), Nr. 8–9, pp. 762–798

[264] CAPITAIN, C. ; ROSS-JONES, J. ; MÖHRING, S. ; TIPPKÖTTER, N.: Differential scanning calorimetry for quantification of polymer biodegradability in compost. In: *International Biodeterioration & Biodegradation* vol. 149 (2020), p. 104914

[265] GOEBEL, L. ; BONTEN, C.: Crystallization behavior of polyhydroxybutyrate (PHB). In: GEOBEL, L. ; BONTON, C. (eds.) *Crystallization Behavior of Polyhydroxybutyrate (PHB)*, *AIP Conference Proceedings TS - CrossRef*. (2016)

[266] SCHWAB, B.: Characterization of Compost from a Pilot Plant-scale Composter Utilizing Simulated Solid Waste. In: *Waste Management & Research* vol. 12 (1994), Nr. 4, pp. 289–303

[267] SHARMA, A. ; GANGULY, R. ; GUPTA, A.K.: Spectral characterization and quality assessment of organic compost for agricultural purposes. In: *International Journal of Recycling of Organic Waste in Agriculture* vol. 8 (2019), Nr. 2, pp. 197–213

[268] RHIM, J.W. ; HWANG, H.S. ; KIM, D.S. ; PARK, H.B. ; LEE, C.H. ; LEE, Y.M. ; MOON, G.Y. ; NAM, S.Y.: Aging effect of poly(vinyl alcohol) membranes crosslinked with poly(acrylic acid-co-maleic acid). In: *Macromolecular Research* vol. 13 (2005), Nr. 2, pp. 135–140

[269] KAČURÁKOVÁ, M. ; BELTON, P.S. ; WILSON, R.H. ; HIRSCH, J. ; EBRINGEROVÁ, A.: Hydration properties of xylan-type structures: an FTIR study of xylooligosaccharides. In: *Journal of the Science of Food and Agriculture* vol. 77

(1998), Nr. 1, pp. 38–44

[270] PHILLIPS, G.O. ; TAKIGAMI, S. ; TAKIGAMI, M.: Hydration characteristics of the gum exudate from Acacia senegal. In: *Food Hydrocolloids* vol. 10 (1996), Nr. 1, pp. 11–19

[271] KITTUR, F.S. ; HARISH PRASHANTH, K.V. ; UDAYA SANKAR, K. ; THARANATHAN, R.N.: Characterization of chitin, chitosan and their carboxymethyl derivatives by differential scanning calorimetry. In: *Carbohydrate Polymers* vol. 49 (2002), Nr. 2, pp. 185–193

[272] RUEDA, D.: Differences in the interaction of water with starch and chitosan films as revealed by infrared spectroscopy and differential scanning calorimetry. In: *Carbohydrate Polymers* vol. 40 (1999), Nr. 1, pp. 49–56

[273] DHAWADE, P.P. ; JAGTAP, R.N.: Characterization of the glass transition temperature of chitosan and its oligomers by temperature modulated differential scanning calorimetry. In: *Advances in Applied Science Research* vol. 3 (2012), Nr. 3, pp. 1372–1382

[274] BABASAKI, Y. ; IIZUKA, Y. ; MIYAKE, A.: Influence of organic acid on the thermal behavior of dimethyl sulfoxide. In: *Journal of Thermal Analysis and Calorimetry* vol. 121 (2015), Nr. 1, pp. 295–301

[275] Purity using DSC and HPLC, 4-Hydroxybenzoic Acid and its Esters. In: *Thermal Analysis Application* : Mettler Toledo TA Application Handbook Pharmaceuticals, 2019

[276] RABELO, T.K. ; ZEIDÁN-CHULIÁ, F. ; CAREGNATO, F.F. ; SCHNORR, C.E. ; GASPAROTTO, J. ; SERAFINI, M.R. ; DE SOUZA ARAÚJO, A.A. ; QUINTANS-JUNIOR, L.J. ; ET AL.: In Vitro Neuroprotective Effect of Shikimic Acid Against Hydrogen Peroxide-Induced Oxidative Stress. In: *Journal of Molecular Neuroscience* vol. 56 (2015), Nr. 4, pp. 956–965

[277] SWIFT, G.: Biodegradable Polymers in the Environment: Are They Really Biodegradable? In: GEBELEIN, C. G. ; CARRAHER, C. E. (eds.): *Biotechnology and Bioactive Polymers*. vol. 18. Boston, MA : Springer US, 1994 — ISBN 978-1-4757-9521-9, pp. 161-168 TS-CrossRef

8 Appendix

8.1 Chemicals and Equipment

The chemicals used in this work are listed in Table 8-1. The devices and equipment used for this work are listed in Table 8-2.

Table 8-1: List of chemicals

IUPAC name	Other names/ Short form	Molecular formula	CAS-No./batch	Manu-facturer	Application
2,2′-azino-bis(3-ethylthiazoline-6-sulfonate)	ABTS	$C_{18}H_{24}N_6O_6S_4$	30931-67-0	Sigma Aldrich	Assay
Acetic acid	acetic acid	$C_2H_4O_2$	64-19-7	Sigma Aldrich	Basic chemical
Propan-2-one	acetone	C_3H_6O	Lot # 16G28420	VWR	Solvent
4-Hydroxy-3-methoxyacetophenon 98 %	acetovanillone	$C_9H_{10}O_3$	498-02-2	Sigma Aldrich	LMC
1-(3,4-dimethoxyphenyl)-2(2-methoxyphenoxy)-propane-1,3-diol)>95 %	ADLEROL	$C_{18}H_{22}O_6$	10535-17-8	Flouorochem Ltd.	LMC
Ammonium persulfate	APS	(NH4)2S2O8	7727-54-0	Carl Roth	SDS page
Sodium azide	azium	NaN_3	26628-22-8	Sigma-Aldrich	Termination of enzymes
3′,3′′,5′,5′′-Tetrabromophenolsulfonephthalein	Bromphenol blue	$C_{19}H_{10}Br_4O_5S$	115-39-9	Sigma-Aldrich	SDS page
Calcium chloride dihydrate	calcium chloride	$CaCl_2{\cdot}H_2O$	10035-04-8	Honeywell	Basic chemical
2,6-di-O-acetyl-beta-D-gluco-hexopyranose	cellulose acetate	average molecular weight Mn ~ 30 kDa by GPC	Lot # MKBZ3084V	Sigma-Aldrich	Degradation studies
poly(D-glucosamine)	chitosan (ow molecular weight) deacetylation degree of 75-85 mol%		9012-76-4	Sigma Aldrich	Adhesive backbone
2-Hydroxypropane-1,2,3-tricarboxylic acid	citric acid	$C_6H_8O_7 \cdot H_2O$	5949-29-1	Sigma-Aldrich	Buffer component

IUPAC name	Other names/ Short form	Molecular formula	CAS-No./batch	Manu-facturer	Application
Palatihum G, plant residues from gardening and agriculture	compost	particle size 0-20 mm		Zentrale Abfallwirtschaft Kaiserslautern	Degradation studies
Laccase from Cerrena unicolor	*C. unicolor*		80498-15-3	Jena Bioscience	laccase
Pentane-1,5-diamine	DAP	$C_5H_{14}N_2$	462-94-2	TCI	Amine donor
Diethylenetriamine	DETA	$C_4H_{13}N_3$	111-40-0	Roth	Amine donor
3-(3,4-dihydroxyphenyl) propionic acid	DHC	$C_9H_{10}O_4$	1078-61-1	Alfa Aesar	Catechol donor
Sodium hydrogen phosphate	disodium phosphate	Na_2HPO_4	7558-79-4	Sigma Aldrich	Buffer component
Dopamine hydrochlorid 99 %	dopamine	$C_8H_{11}NO_2$	62-31-7	TCI	Catechol donor
Guaiacylglycerol-beta-guaiacyl-ether	EROL	$C_{17}H_20O$	7382-59-4	Sigma-Aldrich	LMC
Ethanol absolute, reag. ISO, reag. Ph. Eur., ≥99.8 %	ethanol, p.A.	C_2H_5OH	66-17-5	Geyer	Solvent
Ethanol 99.8 vol%, with 1 % Petroleumbenzin	ethanol, technical	C_2H_5OH	66-17-5	Brenntag	Solvent
3-(4-hydroxy-3-methoxyphenyl)prop-2-enoic acid	ferulic acid	$C_{10}H_{10}O_4$	537-98-4	Sigma Aldrich	LMC
Formaldehyde	formaldehyde	CH_2O	50-00-0	Sigma-Aldrich	Synthesis
Methanoic acid	formic acid	HCOOH	64-18-6		HPLC analysis
Dextrose	glucose	$C_6H_{12}O_6$	50-99-7	Sigma-Aldrich	Basic chemical
Glycerol	glycerol	$C_3H_8O_6$	56-81-5	Honeywell	Basic chemical
Glycine	glycine	$C_2H_5NO_2$	56-40-6	AppliChem GmbH	Buffer agent
Hydrochloric acid	HCl	HCl	7647-01-0	Chemsolute	Acid
3,4-Dihydroxy-L-phenylalanine	L-DOPA	$C_9H_{11}NO_4$	53587-29-4	Sigma Aldrich	Catechol donor
2,6-Diaminohexanoic acid	L-lysine	$C_6H_{14}N_2O_2$	56-87-1	Sigma-Aldrich	LMC
Magnesium heptahydrate	magnesium heptahydrate	$MgSO_4 \cdot 7H_2O$	10034-99-8	Bernd Kraft GmbH	Basic chemical
Methanol	MeOH	H_3COH	67-56-1	VWR	LMC

IUPAC name	Other names/ Short form	Molecular formula	CAS-No./batch	Manu-facturer	Application
N-Acetyl-Diaminopentan	NAcDAP	$C_7H_{16}N_2O$	32343-73-0	TCI	Amine donor
Sodium hydroxide	NaOH	NaOH	1310-73-2	Sigma-Aldrich	Base
Organosolv lignin (powdered)	OS lignin	-	batch KO 74	Pilot plant in Leuna (Fraunhofer CBP)	Adhesive backbone
3,4-Dihydroxybenzoic acid	PCA	$C_7H_6O_4$	99-50-3	Alfa Aesar	Catechol donor
(R)-3-Hydroxybutyric acid polymerized	PHB		29435-48-1	Sigma-Aldrich	Degradation studies
3-(4-Hydroxyphenyl)prop-2-enoic acid	p-coumaric acid	$C_9H_8O_3$	501-98-4	Sigma Aldrich	LMC
Rotiphorese Gel 30 30 % acrylamide and bisacrylamide at a ratio of 37.5:1	Rotiphorese (acrylamide)		79-06-1	Carl Roth	SDS page
Sodium dodecyl sulfate	SDS	$C_{12}H_{25}NaO_4S$	151-21-3	AppliChem GmbH	SDS page
Carrier particles	sea sand	batch no. 1786080	14464-46-1	KB Bern Kraft	Carrier particles
Silicon oil	silicon oil M100	Medium viscous	68083-14-7	Grussig	Oil bath
3,5-Dimethoxy-4-hydroxycinnamic acid	sinapic acid	$C_{11}H_{12}O_5$	530-59-6	Sigma Aldrich	LMC
Sea salt	sodium chloride	NaCl	7647-14-5	Sigma-Aldrich	Basic chemical
3,5-Dimethoxy-4-hydroxybenzaldehyd 98 %	syringaldehyde	$C_9H_{10}O_4$	134-96-3	Sigma-Aldrich	LMC
4-Hydroxy-3,5-dimethoxybenzaldehyde azine	syringaldazine	$HOC_6H_2(OCH_3)_2CH{=}N\text{-}]_2$	14414-32-5	Sigma-Aldrich	Assay
N,N,N',N'-Tetramethylethylendiamin, 1,2-Bis-(dimethylamino)-ethan	TEMED	$C_6H_{16}N_2$	110-18-9	Carl Roth GmbH	SDS page
2-Amino-2-(hydroxymethyl)propane-1,3-diol)	Tris Pufferan	$C_4H_{11}NO_3$	77-86-1	Carl Roth GmbH	Buffer agent

IUPAC name	Other names/ Short form	Molecular formula	CAS-No./batch	Manu-facturer	Application
Laccase from Trametes versicolor	*T. versicolor*		80498-15-3	Sigma Aldrich	laccase
4-Hydroxy-3-methoxybenzaldehyde	vanillin	$C_8H_8O_3$	121-33-5	Sigma-Aldrich	LMC
4-(Hydroxymethyl)-2-methoxyphenol	vanillin alcohol	$C_8H_{10}O_3$	498-00-0	Sigma-Aldrich	LMC
Water-Soluble part of autolyzed yeast	Yeast extract			AppliChem GmbH	Biological nutrient

Table 8-2: List of equipment and devices

Type	Model	Manufacturer
Aluminum crucibles	Art. No. 51119872	Mettler Toledo, Germany
Aluminum crucibles lid	Art. No. 51119873,	Mettler Toledo, Germany
Analytical balance	XS105	Toledo, Germany
Centrifuge	Z383K	Hermle, Germany
Centrifuge	5418/5418 R	Eppendorf, Germany
Centrifuge	1-14K	Sigma, Japan
Combustion boats	unglazed porcelain, 44 mm x 12 mm x 10 mm,	Labsolute, Germany
Coomassie Protein Assay Kit		Thermo Fisher Scientific, USA
Drying cabinet	universal oven UNE 500	Memmert, Germany
Differential scanning calorimetry	DSC 1	Mettler Toledo, Germany
Electric stirrer	RZR 2052	Heidolph, Germany
Electrophoresis chamber	Mini Protean Tetra Cell	Bio-Rad Laboratories Inc.
Electrophoresis device	PowerPac 3000 Power Supply	Bio-Rad Laboratories Inc.
Flasks	250 ml Duran	VWR International GmbH, Germany
FT-ATR mid-infrared spectrometer	Spectrum 100	Perkin Elmer, USA
GPC column	Ultrahydrogel 120	Waters, USA
GPC column	Ultrahydrogel 250	Waters, USA
High-resolution balance	ABS 220-4	Kern and Sohn GmbH, Germany
HPLC Reversed phase column	RP C_{18} Eurospher II, 100-5	Knauer, Germany
HPLC column	Waters Resolve C_{18}, 5 µm, 90 Å, 3.9 x 150 mm	Waters, USA

Type	Model	Manufacturer
HPLC Separation module	Alliance 2695	Waters, USA
HPLC System (Alliance)	2695	Waters, USA
HPLC Photodiode Array Detector	2996	Waters, USA
Knife mill	GRINDOMIX GM 300	Retsch, Germany
Mass spectrometer	Quattro LC	Waters Micromass, USA
Moisture balance	MLB 50-3	Kern, Germany
Optical microscope	Nikon Eclipse Ni	Nikon, Japan
Particle size analyzer	LUMiReader	LUM GmbH, Germany
pH-Meter	pH 211	HANNA Instruments Deutschland GmbH, Germany
Polyethersulfone membrane	PSE	Satorius, Germany
Polytetrafluoroethylene filter	PTFE pore size 0.45 µm	WICOM, Germany
Pressure reactor		Parr Instrument, Germany
Protein marker, unstained	Pierce	Thermo Fisher, USA
Sieve shaker	AS 300 control	Retsch, Germany
Thermoshaker	TS-100	Biosan, Latvia
Tube furnace	MTF 12/38/250/E301	Carbolite, UK
Ubbelohde viscometer		SI Analytics, Germany
Universal oven	UNE 500	Memmert, Germany
UV-vis Spectrophotometer	Cary 60	Agilent Technologies, USA

8.2 Production and characterization of laccase from *C. unicolor*

A cultivation and purification protocol was implemented for the production of laccases from *C. unicolor* (see section 2.2.1). The initial pH of the cultivation medium was investigated for optimization of laccase expression. The fermentation curves are shown in Figure 8-1. An initial pH of 4.5 (see Figure 8-1 A) was compared to an initial pH of 7 (Figure 8-1 B).

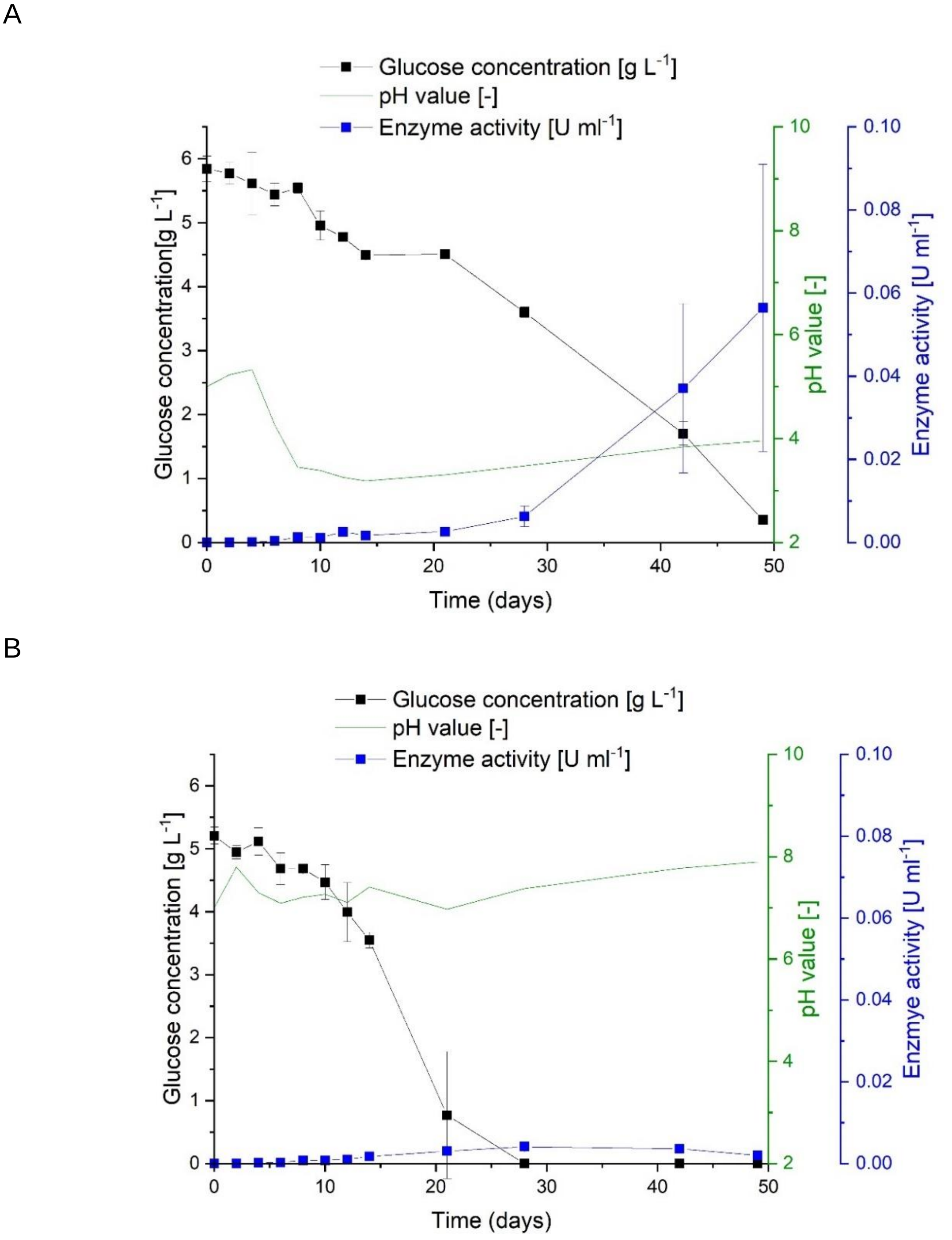

Figure 8-1: Cultivation of *C. unicolor* according to section 2.2.1 (no baffles, 20 vol% filling, 25 °C and 50 rpm). Using an initial pH value of (A) 4.5, without a buffer and (B) 7, with CaCO3 buffer. Shown is the time course of glucose concentration (black), the pH value (green) and the enzyme activity (blue). The enzyme activity was determined according to section 2.2.2.

After cultivation of *C. unicolor* and enzyme purification, the purification success was evaluated using a SDS page, the results are shown in Figure 8-2.

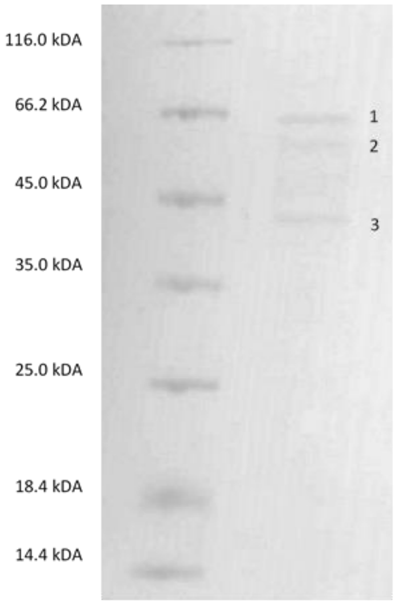
116.0 kDA
66.2 kDA
45.0 kDA
35.0 kDA
25.0 kDA
18.4 kDA
14.4 kDA
1
2
3

Figure 8-2: SDS-page of purified laccase from *C. unicolor*. Left lane: Pierce protein marker, right lane: purified protein.

8.3 Comparison of the chromatograms, resulting from HPLC-MS and HPLC analysis

The retention time of the respective product and educt peaks varied slightly between HPLC and HPLC-MS analysis. The comparison of the chromatograms, resulting from an HPLC-MS analysis and an HPLC analysis is shown as an example in Figure 8-3.

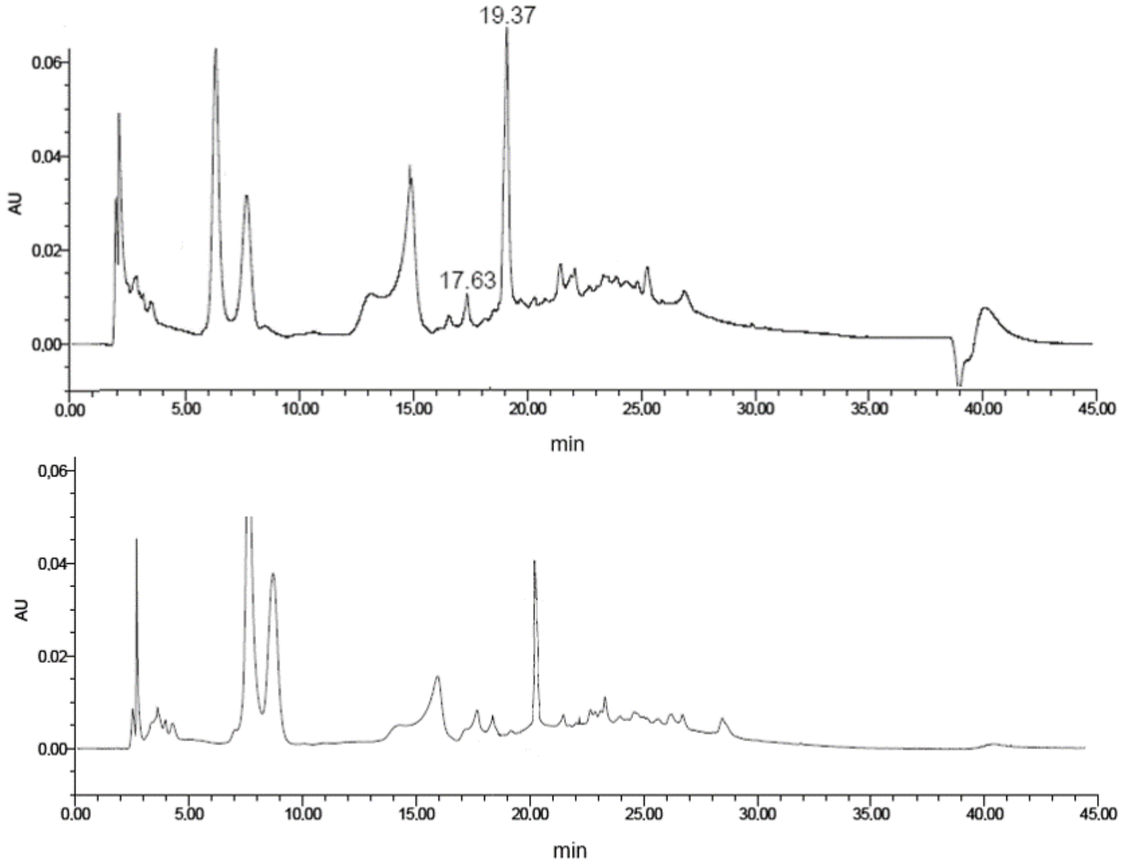

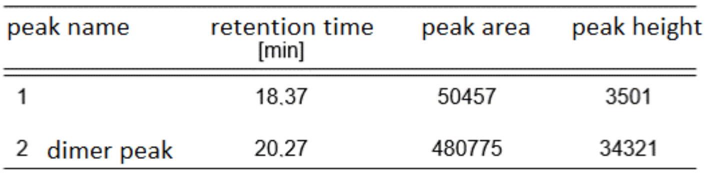

peak name	retention time [min]	peak area	peak height
1	18.37	50457	3501
2 dimer peak	20.27	480775	34321

Figure 8-3: Transfer of the HPLC-MS analysis method to the HPLC analysis. Chromatogram of the reaction of PCA and NAcDAP reacted by laccase from *C. unicolor* at pH 6, recorded at 311 nm. Top: recording of an HPLC-MS analysis, Bottom: Picture of HPLC analysis, including peak integration. Reaction conditions: 5 mM PCA, 1 mM NAcDAP, 0.028 g L^{-1} laccase from *C. unicolor*, 1 mL reaction volume, 10 vol% ethanol, 60 min reaction time, T = 25 °C.

8.4 Example for the analysis of HPLC-MS data

The evaluation method used for analysis of HPLC-MS data is shown using the results of the reaction of PCA and NAcDAP catalyzed by laccase from *C. unicolor* as an example. Initially, background measurements of the one-component systems under consideration were carried out without the addition of laccase. Following, the chromatograms of the pure substances catalyzed by laccase from *C. unicolor* were used for comparison. The aim was to determine which homomolecular products of the pure substances were formed during the reaction with laccase in the absence of an additional reaction partner.

When comparing the two diagrams in Figure 8-4, it can be seen that NAcDAP is not a substrate for laccase from *C. unicolor*, since no products were formed during the reaction with the laccase (shown by the lack of peaks). Only the educt peak at 2.36 min is present in both diagrams, which is surrounded by a peak formed by the buffer used. The peaks at 28.91 min, at 32.55 min and at 40.32 min are device-specific peaks and can be found in all HPLC(-MS) measurements.

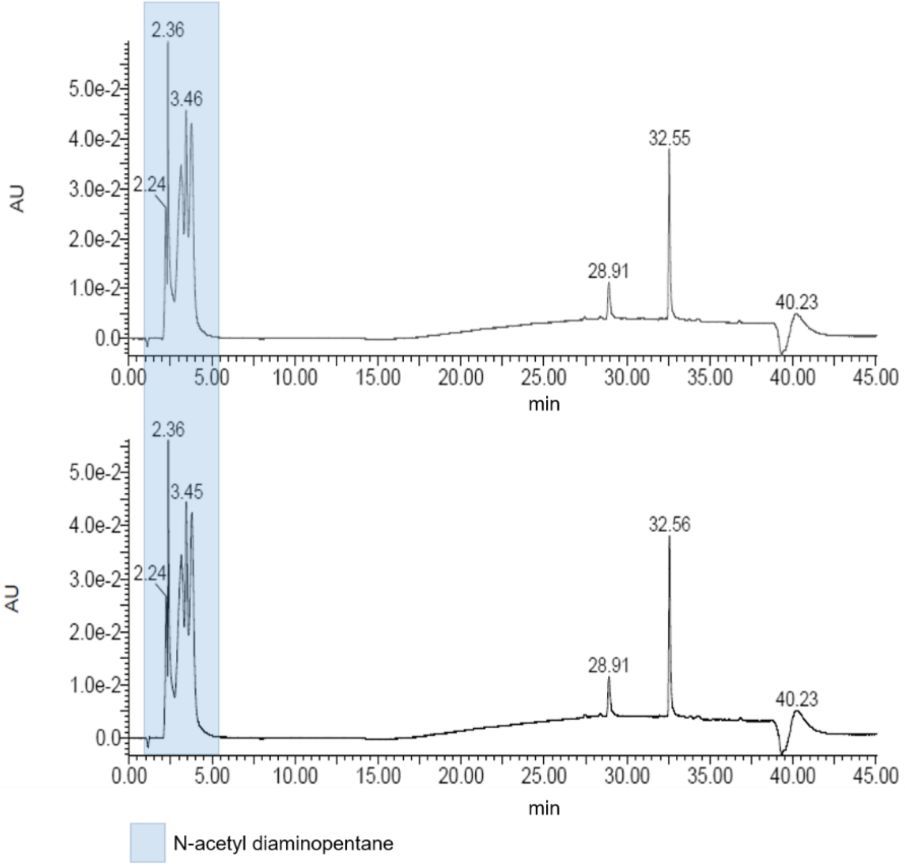

Figure 8-4: Chromatograms of NAcDAP reacted by laccase from *C. unicolor* at pH 5, recorded at 280 nm. Top: pure substance, bottom: reacted by laccase. Reaction conditions: 1 mM NAcDAP, 0.028 g L^{-1} laccase from *C. unicolor*, 1 mL reaction volume, 10 vol% ethanol, 60 min reaction time, T = 25 °C.

In Figure 8-4, the peak of the buffer at 2.24-3.51 min is found again. In addition, the educt peak of PCA at 7.06-7.95 min is clearly visible in the two diagrams. Furthermore, various product peaks during the laccase-catalyzed reaction can be seen in the bottom diagram, whereby it can be seen that the educt peak of PCA has clearly decreased during product formation.

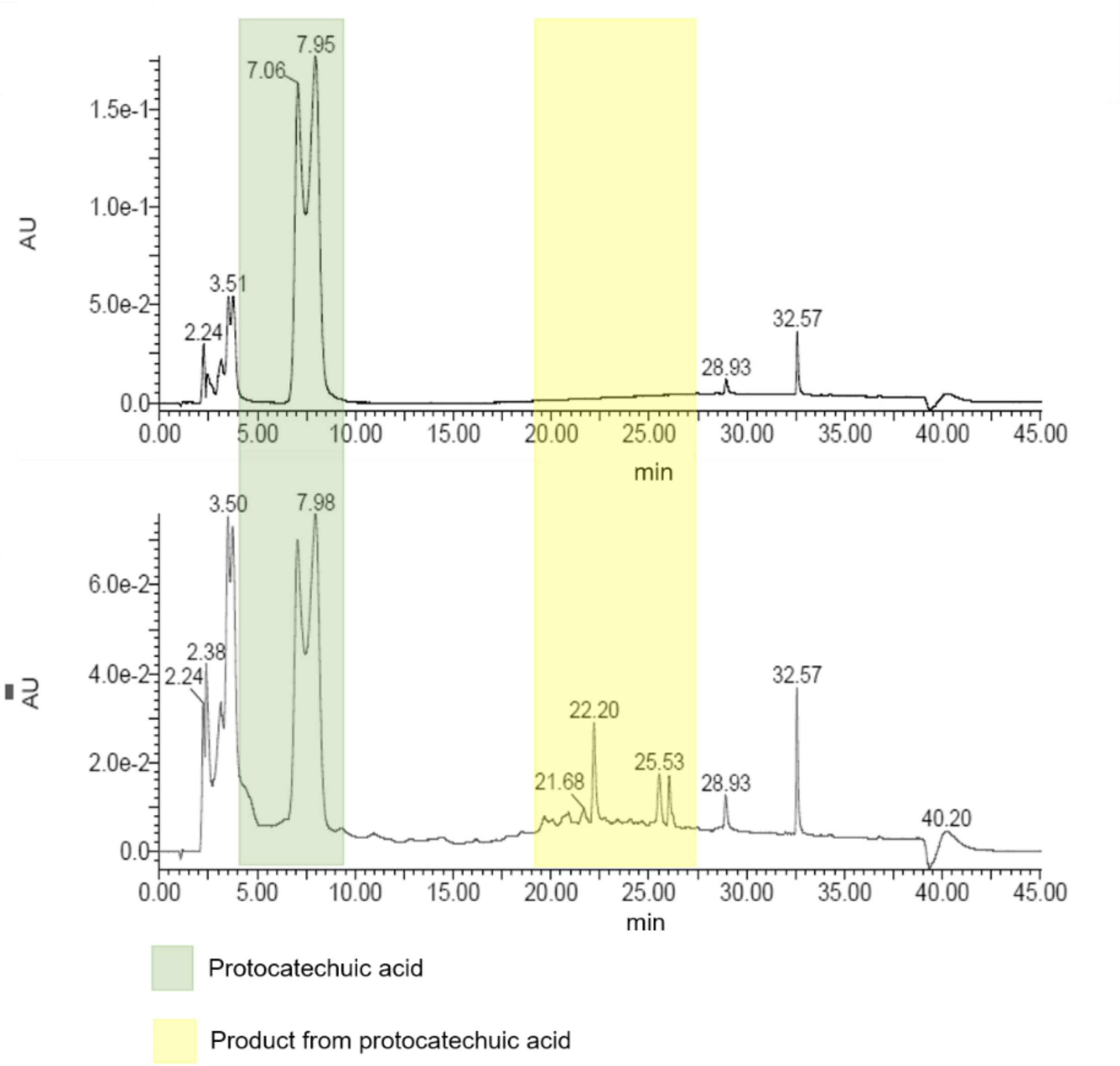

Figure 8-5: Chromatograms of PCA reacted by laccase from *C. unicolor* at pH 5, recorded at 280 nm. Top: pure substance, Bottom: reacted by laccase. Reaction conditions: 5 mM PCA, 0.028 g L^{-1} laccase from *C. unicolor*, 1 mL reaction volume, 10 vol% ethanol, 60 min reaction time, T = 25 °C.

The next step in the HPLC-MS analysis was to compare the product peaks in the reaction of PCA with laccase (see Figure 8-6, top) and the reaction of PCA and NAcDAP with laccase (see Figure 8-6, middle). Since NAcDAP itself is not a substrate for laccase from *C. unicolor*, the reaction of this single component did not need to be further considered. The difference in peak formation in these two diagrams shows the products, which are a polymer from the educts PCA and NAcDAP or parts thereof.

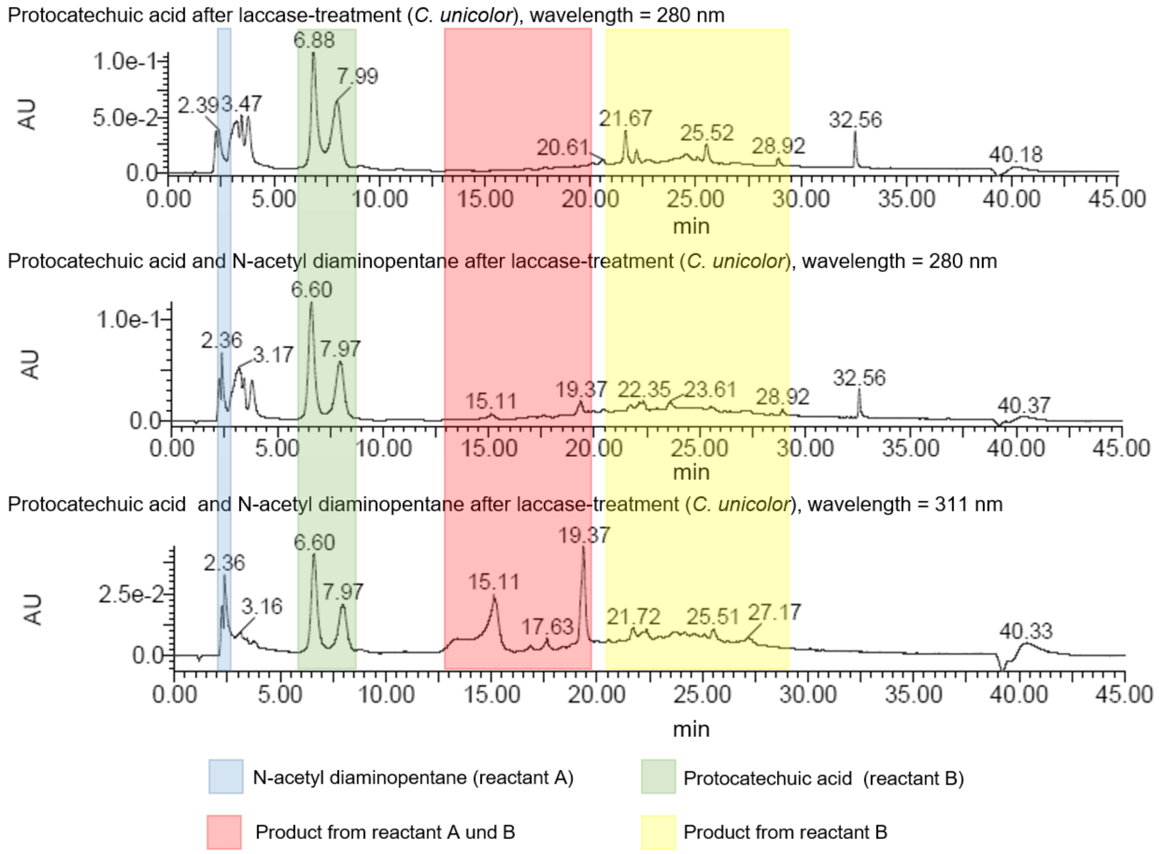

Figure 8-6: Chromatograms of PCA (top) or PCA and NAcDAP (middle and bottom) reacted by laccase from *C. unicolor* at pH 6, recorded at 280 (top and middle) and 311 nm (bottom). Reaction conditions: 5 mM PCA, 1 mM NAcDAP, 0.028 g L^{-1} laccase from *C. unicolor*, 1 mL reaction volume, 10 vol% ethanol, 60 min reaction time, T = 25 °C.

The focus of the analysis was to identify products, that had an m/z ratio corresponding to the sum of the molar masses of the two educts. Here there is a high probability that the desired dimer from the two educts is involved, although a reliable statement can only be made after additional analysis. Higher-molecular polymers were not considered in the analysis, as the m/z ratio alone did not allow any meaningful conclusions to be drawn about the actual composition. Similarly, lower m/z ratios did not play a role in the analysis, since polymers from parts of the educts are also difficult to analyze due to the many possibilities of cleavage.

The expected dimer, which had a m/z ratio of 295 (ESI-) (see Figure 2-9), eluted at 19.37 min (see Figure 8-6, middle) and the UV-vis absorption maximum was 311 nm (see Figure 8-6, bottom). The other peaks at 15.11 min and at 17.63 min showed products with a m/z ratio of 266 and 288 and therefore could not be assigned to the expected dimer.

An analysis was completed by comparing the dimer found with the negative sample (see Figure 8-7).

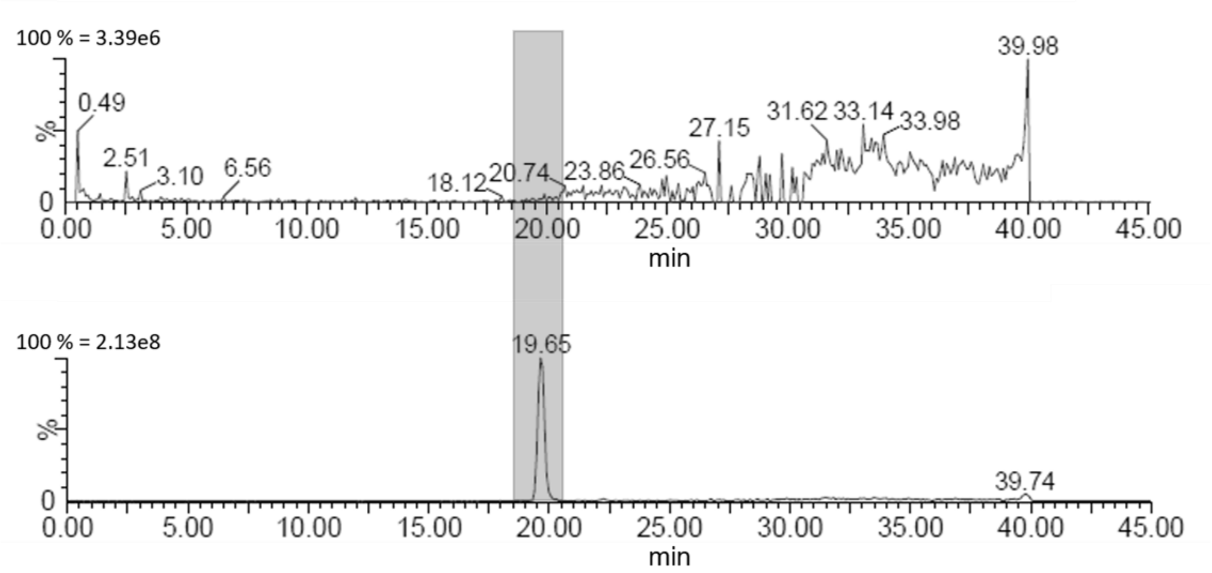

Figure 8-7: Mass trace (m/z = 295, ESI-) of PCA (above) or PCA and NAcDAP (bottom) reacted by laccase from *C. unicolor* at pH 6. Reaction conditions: 5 mM PCA, 1 mM NAcDAP, 0.028 g L^{-1} laccase from *C. unicolor*, 1 mL reaction volume, 10 vol% ethanol, 60 min reaction time, T = 25 °C.

In Figure 8-7 the mass trace at a m/z ratio of 295 (ESI-) is shown from the reaction of PCA by laccase from *C. unicolor* (top) and from the reaction of PCA with NAcDAP by laccase from *C. unicolor* (bottom). The upper diagram shows only a background noise, whereas the lower diagram shows a clear product peak, which proves the existence of the dimer found. Here it is important to note the difference in scaling between the two diagrams with a difference of two powers of ten.

8.5 Experimental design and HPLC-MS results for product optimization

The effect of the pH value, the concentration of the catechol donor, the ethanol concentration, the temperature and the oxygen availability on the product formation was parametrically optimized. Table 8-3 summarizes the first experimental design, consisting of 35 different parameter constellations (Exp. 1 to Exp. 35), whereby three reference experiments were carried out with average parameter values of the influencing variables (pH 5.5, 5.05 mM PCA, 30 vol% ethanol, 22.5 °C and 500 rpm)

Table 8-3: Experimental design and results of the first test series of optimization. ('-': second measurement aborted due to technical problems.)

Name	Ethanol conc. [vol%]	PCA conc. [mM]	pH-value [-]	Tem-peratur [°C]	Shaking speed [rpm]	Product peak 1st measure ment	Product peak 2nd measure ment
Exp. 1	30	5.05	5.5	22.5	500	479468	704196
Exp. 2	30	5.05	5.5	22.5	500	533129	787770
Exp. 3	30	5.05	5.5	22.5	500	456226	685327
Exp. 4	40	1	6	15	0	145823	192241
Exp. 5	50	10	4	15	0	0	0
Exp. 6	30	10	6.5	15	0	1602157	1536007
Exp. 7	10	0.1	7	15	500	0	0
Exp. 8	50	0.1	5	15	500	0	0
Exp. 9	10	10	4	15	1000	0	0
Exp. 10	50	1	4	15	1000	0	0
Exp. 11	10	0.1	7	15	1000	0	0
Exp. 12	50	5	7	15	1000	140390	-
Exp. 13	20	0.1	4	15	1000	0	0
Exp. 14	10	5	6	20	0	864321	968817
Exp. 15	20	1	5	20	0	227814	292471
Exp. 16	40	10	6.5	20	0	1462755	1539850
Exp. 17	30	2	6.5	20	1000	569610	457489
Exp. 18	40	5	5	20	1000	1171901	1604576
Exp. 19	50	0.1	6.5	25	0	0	0
Exp. 20	10	2	4	25	0	0	0
Exp. 21	40	1	4	25	500	0	0
Exp. 22	20	5	6	25	500	1027404	1388306
Exp. 23	30	0.1	7	25	1000	0	0
Exp. 24	40	5	7	30	0	666742	-

Name	Ethanol conc. [vol%]	PCA conc. [mM]	pH-value [-]	Tem-peratur [°C]	Shaking speed [rpm]	Product peak 1st measurement	Product peak 2nd measurement
Exp. 25	10	10	5	30	0	1018820	1008943
Exp. 26	20	0.1	7	30	0	0	0
Exp. 27	50	2	5	30	0	733294	907264
Exp. 28	30	0.1	4	30	0	0	0
Exp. 29	30	2	6.5	30	500	678666	579767
Exp. 30	10	1	6	30	1000	943164	876002
Exp. 31	10	10	7	30	1000	4475084	3705427
Exp. 32	20	10	4	30	1000	0	0
Exp. 33	50	2	7	30	1000	0	0
Exp. 34	50	10	6	30	1000	5872473	6959992
Exp. 35	10	1	6	25	500	480775	459420
Exp. 36	10	1	7	25	500	318990	0

The initial 35 tests were then extended by a second series of 15 tests (Exp. 36 to Exp. 50, see Table 8-4), whereby the three reference tests were also carried out with the parameters already mentioned.

Table 8-4: Experimental design and results of the second test series of optimization. ('-': second measurement aborted due to technical problems.)

Name	Ethanol conc. [vol%]	PCA conc. [mM]	pH-value [-]	Tem-peratur [°C]	Shaking speed [rpm]	Product peak 1st measurement	Product peak 2nd measurement
Exp. 37	10	1	4	15	0	0	0
Exp. 38	20	5	6.5	15	0	879416	1050758
Exp. 39	40	0.1	6	30	1000	0	0
Exp. 40	50	5	5	25	1000	408642	630795
Exp. 41	50	10	7	30	0	666502	684708
Exp. 42	20	10	7	20	500	1267807	1360219
Exp. 43	50	1	6.5	20	500	0	53571
Exp. 44	10	0.1	4	30	1000	0	0
Exp. 45	30	2	7	25	0	230611	173930
Exp. 46	30	2	5	30	500	412662	475054
Exp. 47	40	10	6	15	1000	285567	-
Exp. 48	30	5.05	5.5	25	500	449911	583029
Exp. 49	30	5.05	5.5	25	500	537985	703468
Exp. 50	30	5.05	5.5	25	500	556157	722153

Linear and nonlinear models for the analysis of the relative peak area for dimerization of PCA and NAcDAP and the respective coefficients of determination are shown in Table 2-3. The model parameters pr1 to pr9 are summarized in Table 8-5.

Table 8-5: Model parameters pr1 to pr9 for model #1-#14 (see Table 2-3) for the analysis of the relative peak area for dimerization of PCA and NAcDAP.

Model	pr1	pr2	pr3	pr4	pr5	pr6	pr7	pr8	pr9
#1	0.003	0.057	0.252	0.005	0.000	-1.625			
#2	-0.032	-0.210	-0.043	0.000	0.000	0.506	0.001	0.005	0.039
#3	0.001	-0.078	0.202	0.054	0.000	-1.687	-0.005	-0.005	0.040
#4	0.003	0.057	0.252	0.005	-1.644				
#5	-0.003	0.055	0.101	-0.023	0.000	-0.779	0.000	0.002	0.005
#6	0.008	0.113	0.262	0.035	0.000	-2.261	0.000	0.001	-0.004
#7	0.001	-0.175	0.083	0.000	0.000	-0.415	0.038		
#8	-0.026	-0.130	-0.010	0.014	-0.005	0.001	0.039	-0.003	0.004
#9	-0.001	-0.106	0.114	0.023	-0.896	0.000	0.038	-0.004	-0.001
#10	-0.001	-0.107	0.092	0.017	-0.747	0.000	0.038	-0.003	
#11	-0.001	-0.100	0.092	0.016	-0.751	0.000	0.038	-0.003	-0.001
#12	1.053	7.036	0.411						
#13	1.181	7.016	0.379						
#14	-0.031	-0.207	-0.036	0.000	0.483	0.001	0.038	0.004	

8.6 Erklärung (Declaration)

Hiermit erkläre ich, dass die Dissertation selbst angefertigt wurde und alle benutzten Hilfsmittel in der Arbeit angegeben sind, dass die Dissertation oder Teile davon noch nicht als Prüfungsarbeit für eine staatliche oder andere wissenschaftliche Prüfung eingereicht ist und dass die gleiche oder eine andere Abhandlung nicht bei einem anderen FB oder einer anderen Uni als Dissertation eingereicht wurde.

Ort, Datum

Unterschrift: Charlotte Capitain

Translation:

I hereby declare that the dissertation has been prepared by myself and all the aids used are indicated in the paper, that the dissertation or parts thereof have not yet been submitted as an examination paper for a state or other scientific examination and that the same or another paper has not been submitted to another FB or another university as a dissertation.

8.7 List of author’s peer-reviewed publications

The following list contains the peer-reviewed publications of the author. Parts of this thesis, including the theory, material and methods and results of section 2.3.4 to 2.3.6 as well as the results presented in chapter 3 have been previously published in ‘*Investigation of C-N formation between catechols and chitosan for the formation of a strong, novel adhesive mimicking mussel adhesion*’ [67]. The implementation of the DSC-based method for the detection of biodegradation in complex samples (section 5.3.1 to 5.3.3) has been previously published in ‘*Differential scanning calorimetry for quantification of polymer biodegradability in compost*’ [264].

- **C. Capitain**, S. Wagner, J. Hummel, N. Tippkötter (2020) Investigation of C-N formation between catechols and chitosan for the formation of a strong, novel adhesive mimicking mussel adhesion. In: Waste and Biomass Valorization.
  DOI: 10.1007/s12649-020-01110-5
- **C. Capitain**, J. Ross-Jones, S. Möhring, N. Tippkötter (2020) Differential scanning calorimetry for quantification of polymer biodegradability in compost. In: International Biodeterioration & Biodegradation Bd. 149 (2020), S. 104914.
  DOI: 10.1016/j.ibiod.2020.104914
- T. Teumer, **C. Capitain**, J. Ross-Jones, N. Tippkötter, M. Rädle, F.-J. Methner (2018) In-line Haze Monitoring Using a Spectrally Resolved Back Scattering Sensor. In: BrewingScience 71 (May/June 2018), pp. 49-55. DOI: 10.23763/BrSc18-06teumer
- H. Wagner, **C. Capitain**, K. Richter, M. Nessling, J. Mampel (2016) Engineering bacterial microcompartments with heterologous enzyme cargos. In: Eng. Life Sci.
  DOI: 10.1002/elsc.20160010

8.8 List of supervised seminar papers and theses

A list of seminar papers and theses who contributed to this thesis is provided in Table 8-6.

Table 8-6: List of supervised seminar papers and theses (2016-2019), who have made a contribution to the dissertation.

Student	Type of work	Title
Philipp März	Bachelor thesis	Charakterisierung einer Laccase aus *Cerrena unicolor* und enzymatische Polymerisation von L-DOPA und L-DOPA mit Syringaldehyd.
Jens Weiermüller	Master thesis	Enzymatische Polymerisation von Guaiacyl-Ligninmodellkomponenten mit derivaten der Aminosäure L-DOPA und Diaminolinkern
Max Rech	Bachelor thesis	Aufreinigung und Charakterisierung von ethanolstabilen Laccasen Fermentations-überständen von *Cerrena unicolor*
Anke Frey	Student project	Optimierung der Aminierung von Organosolv-Lignin
Linda Lukeba	Student project	Etablierung einer SEC-Methode für die Analyse von aminierten Lignin und polymerisierten Ligninmodellkomponenten
Andrea Staub	Bachelor thesis	Etablierung von chromatographischen und optischen Verfahren zur Evaluierung der Zweistufen-Reaktion
Martin Paetz	Student project	Funktionalisierung von Lysin-Lignin

8.9 Curriculum Vitae

M.Sc. Charlotte C. Capitain

Education

01/2016 – 03/2021	Doctoral student at University of Kaiserslautern, Department of Bioprocess Engineering, Germany
10/2013 – 09/2015	Master of Science in Industrial Biotechnology at Technical University of Munich, Germany
11/2014 – 07/2015	Master thesis topic: Microbial production of diterpenic compounds in a bioreactor
09/2009 – 07/2013	Bachelor of Science in Biotechnology at Applied University of Mannheim, Germany
11/2012 – 04/2013	Bachelor thesis topic: Heterologous expression and re-programming of microcompartments in *E. coli*

Work experience

01/2016 – 12/2019	Scientific staff at Technical University of Kaiserslautern Tasks: • Microbial production and purification of polyols for food industry (Industry project) • Biodegradation studies of polyurethane containing polymers (Industry project) • Coordinator of the Integrated Research Training Group of the Collaborative Research Centre 926 (MICOS), organising seminars and retreats for doctoral candidates. • Supervising and coordinating of students • Laboratory responsibility • Development of bioanalytical methods (GPC, HPLC, MS, DSC, FT-IR) combined with multivariate data analysis.
07/2013 – 10/2013	Research Assistant at BRAIN Biotech AG in Zwingenberg, Germany Task: Engineering of bacterial microcompartments
09/2011 – 02/2012	Intern at Memorial University of Newfoundland, Canada Task: Preparation of a gene mutant of *S. clavuligerus*
04/2010 – 07/2011	Teaching Assistant at Mannheim University of Applied Sciences Mannheim University of Applied Sciences

Qualifications

Languages:	German (native), English (fluent), Spanish (intermediate), French (intermediate)
Computer Skills	Matlab, Origin, SuperPro Designer, Unscrambler, Adobe InDesign, MS Office, Python